Application of nanoparticles for the development of new antituberculosis therapies

Joana Costa Gouveia

Université de Lille 2 DROIT ET SANTÉ

THESE

Doctorat de l'université Lille 2

Discipline: Immunologie, microbiologie, virologie, parasitologie

Spécialité: Biologie Cellulaire

UTILISATION DE NANOPARTICULES POUR LE DEVELOPPEMENT DE NOUVELLES THERAPIES ANTITUBERCULEUSES

Soutenue publiquement le 1er Décembre 2017 par:

Joana Costa Gouveia

Membres de Jury:

Prof. Ruxandra GREF, Institut des Sciences Moléculaires d'Orsay	Président du jury
Dr. Vivi MIRIAGOU, Hellenic Pasteur Institute	Rapporteur
Dr. Laurent MARSOLLIER, Université d'Angers	Rapporteur
Dr. Alain BAULARD, Institut Pasteur de Lille	Examinateur
Dr. Priscille BRODIN, Institut Pasteur de Lille	Directeur de thèse

Université de Lille 2 DROIT ET SANTÉ

THESIS

PhD Thesis at University of Lille 2

Discipline: Immunology, microbiology, virology, parasitology

Speciality: Cell Biology

APPLICATION OF NANOPARTICLES FOR THE DEVELOPMENT OF NEW ANTITUBERCULOSIS THERAPIES

Public defence on December 1st 2017 by:

Joana Costa Gouveia

Jury Members:

Prof. Ruxandra GREF, Institut des Sciences Moléculaires d'Orsay	Jury President
Dr. Vivi MIRIAGOU, Hellenic Pasteur Institute	Reviewer
Dr. Laurent MARSOLLIER, Université d'Angers	Reviewer
Dr. Alain BAULARD, Institut Pasteur de Lille	Reviewer
Dr. Priscille BRODIN, Institut Pasteur de Lille	PhD Director

Le travail présenté dans cette dissertation été réalisé à Univ. Lille, CNRS, INSERM, CHU Lille, Institut Pasteur de Lille, U1019 - UMR 8204 - CIIL – Centre d'Infection et d'Immunité de Lille, F-59000 Lille, France.

The work presented in this dissertation was performed at Univ. Lille, CNRS, INSERM, CHU Lille, Institut Pasteur de Lille, U1019 - UMR 8204 - CIIL - Center for Infection and Immunity of Lille, F-59000 Lille, France.

Dedicated to the memories of my "Sis" Susana Correia (1989-2017)

I'll never let them dye

"As long as men are free to ask what they must, free to say what they think, free to think what they will, freedom can never be lost and science can never regress."

J. Robert Oppenheimer

ACKNOWLEDGEMENTS / REMERCIEMENTS

This thesis represents a history of personal and professional growth, build with collaboration of many people. To them, I would like to express my affection and gratitude.

I would like to thank Dr. Ruxandra Gref, Dr. Vivi Miriagou, Dr. Laurent Marsollier and Dr. Alain Baulard for having accepted to be members of my PhD jury.

I would like to thank my supervisor, Dr. Priscille Brodin, for kindly accepting me as her PhD student and providing me the great opportunity to work in an excellent laboratory with state of the art equipment.

I am very grateful to all the current and previous members of the CGIM group, Alexandre Vandeputte, Arnaud Machelart, Christophe Queval, Clara Aguilar, Eik Hoffmann, Gaspard Deloison, Isabelle Ricard, Nathalie Deboosere, Ok-Ryul Song, Raffaella Iantomasi, Romain Veyron-Churlet, Vincent Delorme and to the members of Frank Lafont's team, for their strong support and for all the great moments.

A special thanks to Nathalie Deboosere and Arnaud Machelart for writing the french part of this thesis, and for their prompt help, whenever I needed it.

I am very grateful to Rosangela Frita, for her corrections to the introduction of this thesis, for the conversations, suggestions and for being a good friend.

I am also grateful to Luis Solans, Kamel Djaout, Ruben Hartkoorn and Martin Moune for all their support, encouragement and consideration.

I would also like to thank all the members of the Marie Curie Initial Training Network "CycloNHit", in particular to Elisabetta Pancani, with whom I have worked more closely, developing a good friendship.

Last but not least, to my family and friends, for the unconditional support, affection and trust. For being there in all my ups and downs and for giving me the strength and peacefulness to complete this stage.

RESUME

La tuberculose (TB) est un problème de santé mondiale majeur qui est à l'origine de 10.4 millions de nouveaux cas et 1.8 millions de morts en 2015 selon l'Organisation Mondiale de la Santé (OMS). Cette maladie est causée par la bactérie *Mycobacterium tuberculosis* (Mtb) qui infecte principalement les poumons et qui se transmet par l'inhalation d'aérosols contaminés.

Le traitement de TB nécessite la prise quotidienne d'antibiotiques de première ligne pendant 6 mois, dont la mauvaise utilisation peut être à l'origine de l'apparition de souches Mtb multi-résistantes.

La nouvelle stratégie de santé publique de l'OMS, "End TB", vise à réduire de 90 % l'incidence de TB d'ici 2035. Pour y parvenir, il est important de définir de nouvelles approches visant à réduire la durée et la toxicité des traitements et améliorer leur efficacité vis-à-vis des bactéries actives et latentes.

L'approche abordée lors de ma thèse a consisté à utiliser des nanoparticules (NPs) pour développer de nouvelles thérapies antituberculeuses. La bibliographie sur le sujet montre que cela pourrait être une stratégie prometteuse. Nous avons par conséquent étudié quatre applications potentielles des NPs:

1- Vectorisation des médicaments pour les administrer au niveau pulmonaire. L'éthionamide (ETH) est un antibiotique de deuxième ligne utilisé pour le traitement de TB avec des effets secondaires indésirables. L'ETH est une "pro-drogue", qui nécessite une bioactivation par une monooxygenase bactérienne, dont l'efficacité peut être elle-même augmentée par des molécules chimiques appelées "booster". Nous avons étudié l'effet de l'ETH et de booster, co-encapsulés dans des NP de poly-β-cyclodextrine (pCD) biodégradables pour le traitement de TB. Nous avons d'abord évalué leur efficacité *in vitro* sur la croissance extracellulaire et intracellulaire (dans les macrophages) de Mtb grâce à l'utilisation d'un système automatisé de microscopie confocale à haut contenu. Dans les deux essais, nous avons constaté que les médicaments conservaient leur activité après encapsulation et que les NP n'étaient pas cytotoxiques. L'efficacité des NP chargées a ensuite été étudiée *in vivo* chez des souris infectées par voie intranasale. La suspension de NP a été délivrée sous forme d'aérosols directement dans les poumons par voie endotrachéale à l'aide d'un Microsprayer® Aerosolizer. Une réduction significative de la

charge bactérienne dans les poumons de 3-log a été observée après 6 administrations de doses inférieures à celles thérapeutiques.

2- Amélioration de la solubilité et biodisponibilité des antibiotiques. La clofazimine (CLZ) est un antibiotique utilisé dans le traitement de la lèpre et pourrait être, au regard de son efficacité *in vitro* sur les souches de Mtb multi-résistantes, un candidat potentiel pour celui de TB. La CLZ est extrêmement lipophile, gênant ainsi sa solubilité. Dans notre étude, son encapsulation dans des particules de silice nanoporeuses a stabilisé l'état amorphe de la CLZ et a augmenté radicalement sa solubilité. Après encapsulation ou solubilisation dans le diméthylsulfoxyde (DMSO), la CLZ a d'autre part montré une activité antibactérienne similaire sur Mtb.

3- Libération des antibiotiques dans les compartiments intracellulaires. La Vancomycine (VCM) est utilisée pour des applications cliniques comme alternative de la pénicilline dans le traitement de *Staphylococcus aureus* et pourrait être utilisée pour celui de TB. Cependant, comme beaucoup d'antimicrobiens, VCM est incapable d'atteindre les concentrations thérapeutiques optimales à l'intérieur des cellules infectées. L'encapsulation de cet antibiotique à l'intérieur de NP à base de PLGA avec la libération dépendant du pH a amélioré son efficacité contre les bactéries intracellulaires.

4- Activité antimycobacterial Intrinsèque des NPs. Différentes NPs (89 polymeric β-cyclodextrines (pCD), 1 NP mésoporeuses hybrides (NanoMOF) et 1 NP en argent) ont été évaluées *in vitro*. Aucune n'a présenté d'activité antituberculeuse intrinsèque prometteuse.

En conclusion et au regard des options thérapeutiques limitées pour combattre les souches résistantes et de la rareté de solutions innovantes dans le pipeline de découverte de médicament, ces travaux ont montré que les NPs pouvaient constituer une approche antituberculeuse originale.

ABSTRACT

Tuberculosis (TB) is a major problem of global health, responsible for 10.4 million new cases and 1.8 million deaths in 2015 according to the World Health Organization (WHO). This disease is caused by inhalation of small aerosol droplets containing *Mycobacterium tuberculosis* (Mtb), and lungs are usually the major site of infection.

TB can usually be treated with a daily six months course of standard, or first-line, antituberculosis drugs. If first-line drugs are misused, the onset of multidrug-resistant Mtb can occur.

The new WHO global public health strategy "End TB" aims the reduction of TB incidence 90 % by 2035. To reach these ambitious targets, new approaches are urgently needed to get a faster, less harmful and more efficient treatment for active and latent TB.

My thesis focused on the use of nanoparticles (NPs) to develop new antituberculosis therapies. Our review of the literature showed that it could be a promising approach. Here, we investigated four potential uses of the NPs.

1- Nanocarrier for pulmonary delivery of drugs. Ethionamide (ETH) is a second line antibiotic with high toxicity and several adverse side effects. ETH is a prodrug that requires bioactivation by a bacterial monooxygenase, which can be enhanced by chemical molecules named "boosters". We investigated the simultaneous delivery of ETH and boosters coencapsulated in biodegradable poly-β-cyclodextrin (pCD) based NPs by the pulmonary route for the treatment of TB. First, we evaluated the *in vitro* efficacy of the designed formulations on Mtb extracellular growth and intracellular growth inside macrophages using an automated confocal high-content microscopy system. And we found for both assays that the drugs maintained their activity after encapsulation and the pCD were not cytotoxic. Given these promising results, their efficacy was then tested *in vivo*. The NPs suspension, administered directly into mouse lungs by endotracheal way using a Microsprayer® aerosolizer, was proved to be well-tolerated and led to a 3-log decrease of the pulmonary mycobacterial load after 6 administrations and using lower doses than the therapeutic ones.

2- Enhancement of the solubility and the bioavailability of antibiotics. Clofazimine (CLZ) is an antibiotic usually used in a combination therapy for the treatment of leprosy

and could be a potential candidate for the treatment of TB because of its *in vitro* efficacy on resistant Mtb strains. CLZ is extremely lipophilic and has important solubility problem. In our study, its encapsulation in nanoporous silica particles stabilized the amorphous state of CLZ and dramatically increased the drug solubility. On the other hand, CLZ encapsulated in nanoporous silica particles or efficiently dissolved in Dimethyl Sulfoxide (DMSO) showed a similar antibacterial activity on Mtb, validating the assessment of solubility of CLZ by encapsulation.

3- Intracellular delivery of antibiotics. Vancomycin (VCM) is used for clinical applications for nearly 50 years as a penicillin alternative to treat penicillinase-producing strains of *Staphylococcus aureus*. VCM can be used for TB treatment as a repurpose. However, like many antimicrobials, VCM is unable to reach the optimal therapeutic concentrations inside infected cells. Encapsulation of this antibiotic inside Poly (Lactic-co-Glycolic Acid) (PLGA)-based NPs with pH-triggered release enhanced its efficacy against intracellular bacteria.

4- Intrinsic antimycobacterial activity of NPs. Different NPs (89 polymeric β-cyclodextrins (pCD), 1 Nanoporous Metal-Organic Frameworks (NanoMOF), and 1 silver NP) were tested *in vitro* but none presented promising intrinsic antituberculosis activity. Some pCD were slightly active *in vitro* on extracellular Mtb but cytotoxic.

In conclusion, this work demonstrated that nanoparticles can provide a novel antituberculosis approach regarding the limited therapeutic options to fight drug-resistant Mtb and the scarcity of novel antituberculosis drugs in the drug discovery pipeline.

INDEX / SOMMAIRE

LIST OF FIGURES / LISTE DES FIGURES *

*Except manuscripts

LIST OF TABLES / LISTE DES TABLES *

*Except manuscripts

ABBREVIATIONS AND ACRONYMS / ABRÉVIATIONS ET ACRONYMES

ADE	Acoustic Droplet Ejection
AUC	Area Under the Curve
BCG	Bacillus Calmette Guérin
BSL-3	Biosafety Level 3
CD	Cyclodextrin
CFP-10	10 kDa culture filtrate protein
CFU	Colony Forming Units
CLZ	Clofazimine
CYP450	Cytochrome P450
DAPI	4,6-Diamidino-2-Phenylindole
DC	Dendritic Cell
DNA	Deoxyribonucleic acid
DMSO	Dimethyl Sulfoxide
EMB	Ethambutol
ESAT-6	6 kDa early secretory antigenic target
ETH	Ethionamide
ethA	Monooxigenase Ethionamide Activator
ethR	Ethionamide transcriptional Repressor
FDA	U.S. Food & Drug administration
GIT	Gastro Intestinal Tract
GFP	Green fluorescent protein
h	Hour
HIV	Human Immunodeficiency Virus
HTS	High Throughput Screening
IGRA	Interferon-Gamma Released Assays
IL	Interleukin
INH	Isoniazid
iNOS	Inducible Nitric Oxide Synthase
LAM	Lipoarabinomannan
LAMP	Loop-Mediated Isothermal Amplification
LC3	Autophagic marker Light Chain 3
LPA	Line Probe Assay
MDK	Minimum Duration for Killing
MDR	Multidrug-Resistant
MIC	Minimum Inhibitory Concentration
MRSA	Methicillin-resistant *Staphylococcus aureus*
Mtb	*Mycobacterium tuberculosis*

MTBC	*Mycobacterium Tuberculosis* Complex
NAD	Nicotinamide Adenine Dinucleotide
NADPH	Nicotinamide Adenine Dinucleotide Phosphate
NAG	N-Acetylglucosamine
NAM	N-Acetylmuramic acid
NanoMOF	Nanoporous Metal-Organic Frameworks
NDH-2	NADH Dehydrogenase
NK	Natural Killer
NO	Nitric Oxide
NSP	Nanoporous Silica Particles
NTM	Nontuberculous Mycobacteria
OADC	Oleic Albumin Dextrose Catalase
OD	Optical Density
PAMP	Pathogen-Associated Molecular Patterns
PAS	Para-Aminosalysilic acid
pCD	Polymeric β-Cyclodextrins
PCR	Polymerase Chain Reaction
PLA	Poly-Lactic Acid
PLGA	Poly (Lactic-co-Glycolic Acid)
PPD	Tuberculin purified protein derivative
PRR	Pattern Recognition Receptors
PZA	Pyrazinamide
qPCR	Quantitative Polymerase Chain Reaction
RD	Region of Difference
RIF	Rifampicin
rpm	Revolutions Per Minute
RNA	Ribonucleic Acid
RNS	Reactive Nitrogen Species
ROS	Reactive Oxygen Species
SNPs	Single-Nucleotide Polymorphisms
STR	Streptomycin
TB	Tuberculosis
TLR	Toll-Like Receptor
TNF	Tumour Necrosis Factor
TST	Tuberculin Skin Test
WHO	World Health Organization
VCM	Vancomycin
XDR	Extensively Drug-Resistant

1. INTRODUCTION

1.1. Tuberculosis: a permanent challenge

Tuberculosis (TB) has always been present in human populations throughout known human history and it may have killed more people than any other microbial pathogens (Daniel 2006). Over a billion lives were lost to TB in the past 200 years (**Figure 1**) (Paulson 2013).

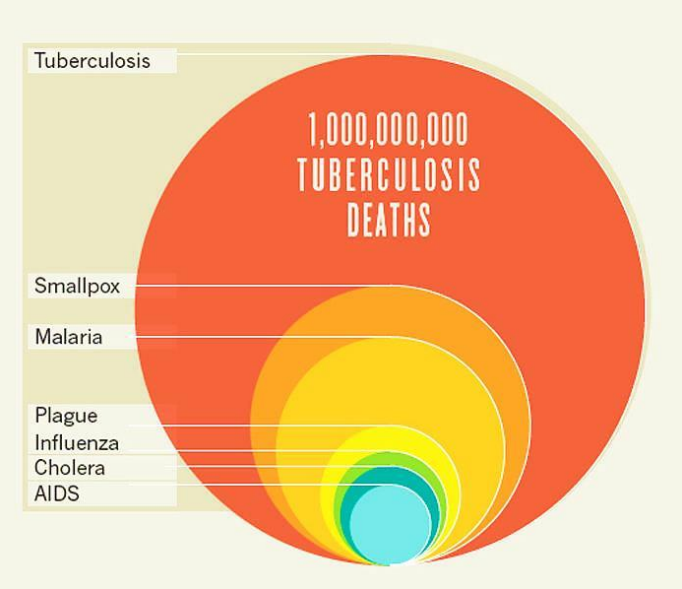

Figure 1 - Number of deaths caused by different infectious diseases during the last 200 years. From (Paulson 2013).

Archaeological evidence and written records describing the disease were found in several ancient civilizations from different geographical regions, showing that TB was widespread in humans since the Neolithic period and has remained so until the present day (Daniel 2006; Barberis, Bragazzi et al. 2017; Donoghue 2017).

During the 18th and 19th centuries, TB, also called white plague, because of the extreme anaemic pallor of those affected, reached epidemic proportions in Europe and caused millions of deaths (Daniel 2006; Barberis, Bragazzi et al. 2017).

TB declined after the late 19th century until the mid-20th most probably as a result of improved socioeconomic conditions and the development of sanatoria for the isolation and treatment of infectious patients (Daniel 2006; Lienhardt, Glaziou et al. 2012). The development of the Bacillus Calmette Guérin (BCG) vaccine (used in humans since 1921) and the discovery of antituberculosis drugs starting in 1944 also contributed for the

decline of global TB incidence (Lienhardt, Glaziou et al. 2012). These developments could have had a much greater impact on control of the disease but regrettably, as the prevalence of the disease declined in developed countries, so did the interest in global disease surveillance and research (Zumla, Mwaba et al. 2009).

TB incidence unexpectedly increased in the late 1980s. Numerous factors were responsible for this including the emergence of the Human Immunodeficiency Virus (HIV), lack of access to antituberculosis drugs, increased immigration from countries where TB is common and the rise and spread of drug-resistant strains (Kamholz 1996).

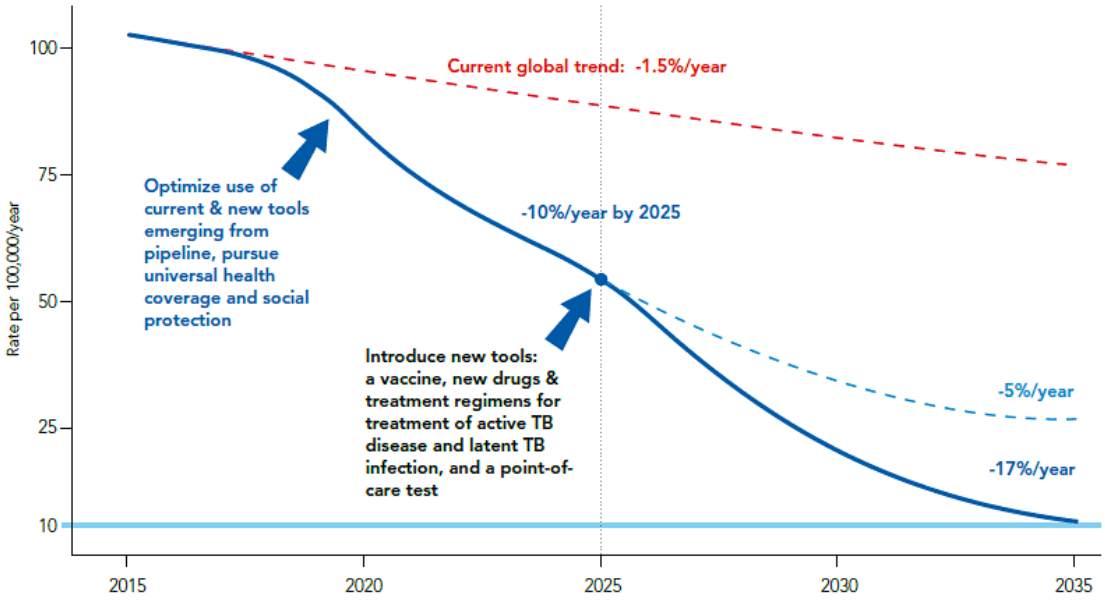

Figure 2- Desired decline in global TB incidence rates to reach the WHO 2035 targets. From (WHO 2017).

In 1993, the World Health Organization (W.H.O.) declared TB a global public health emergency. Since then, it has implemented and scaled-up successive global public health strategies for TB control: the DOTS (Directly Observed Treatment Short course) in 1993, the "Stop TB" strategy in 2006 and the "End TB" strategy in 2014 (Sotgiu, Sulis et al. 2017). The first two WHO strategies successfully contributed to decrease the annual TB incidence rate but not enough to achieve the WHO target: TB elimination by 2050 globally (incidence rate of less than one TB case per million population is referred to as elimination) (Sotgiu, Sulis et al. 2017). The new WHO strategy "End TB" aims to reduce TB deaths by 95 %, to reduce TB incidence to 90 % by 2035 and to ensure that no family is burdened with catastrophic costs due to TB by 2020 (Petersen, Maeurer et al. 2017;

Sotgiu, Sulis et al. 2017). To reach these ambitious targets the annual decline in global TB incidence rates must first accelerate from 1.5 % per year in 2015 to 10 % per year by 2025 (**Figure 2**). To sustain progress beyond 2025 requires the development of new tools such as a new vaccine, safer, more effective and shorter treatment options for active and latent TB and rapid, affordable, diagnostic methods of all forms of drug-susceptible and drug resistant disease (Petersen, Maeurer et al. 2017; Schito, Hanna et al. 2017; Sotgiu, Sulis et al. 2017).

According to the 2016 report on TB research funding trends (T.A.G. 2016), the total funding for TB R&D in 2015 was more than 620 million dollar, with the top donors, the Bill & Melinda Gates Foundation and U.S. National Institute of Allergy and Infectious Diseases giving almost 50 percent of the total funding. This value is far from the 2.9 billion dollar total funding for malaria, in 2015 (W.H.O 2016), and the 1.9 billion dollar total funding for HIV, in 2016 (UNAIDS 2017).

For new tools to be available by 2025 more investments in research and development, as well as on political commitment to implement effective programs to control TB and TB comorbidities are required.

1.1.1. Clinical presentation and diagnostics

Until mid-1800s many believed that TB was a hereditary disease. In 1865 a French military surgeon, Jean Antoine-Villemin, proved the contagious nature of the disease by inoculating a rabbit with “a small amount of purulent liquid from tuberculous cavity” removed at autopsy from a TB victim (Daniel 2006).

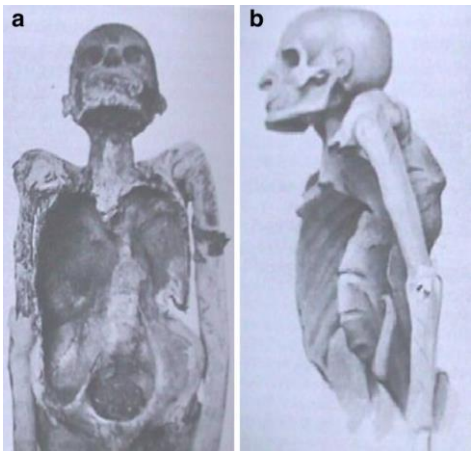

Figure 3 - The remains of Nesparehan, a priest of Amun, in the 21st Dynasty of the Ancient Egypt, typical of Pott's disease. a) big right psoas abcess; b) angular curvature of the spine. From (Said 2014)

TB is transmitted mainly from person to person by small aerosol droplets of 1-5 microns in diameter, expelled by infected hosts, for example by coughing, sneezing or speaking. Those droplets may remain suspended in the air during hours and be posteriorly inhaled by another host. In consequence, TB predominantly affects the lung (85 % of the cases are pulmonary TB) (W.H.O. 2016). Nevertheless, it may access the blood stream and affect other parts of the body such as pleura, lymph nodes (scrofula), abdomen, genitourinary tract, skin, joints, meninges and bones (Pott's disease) (**Figure 3**), and cause extrapulmonary disease (W.H.O. 2014).

The infection with *Mycobacterium tuberculosis* (Mtb), the causative agent of the vast majority of TB cases, may result in extremely different outcomes (**Figure 4**); however, patients are categorized as having either latent TB infection or active TB disease (O'Garra, Redford et al. 2013).

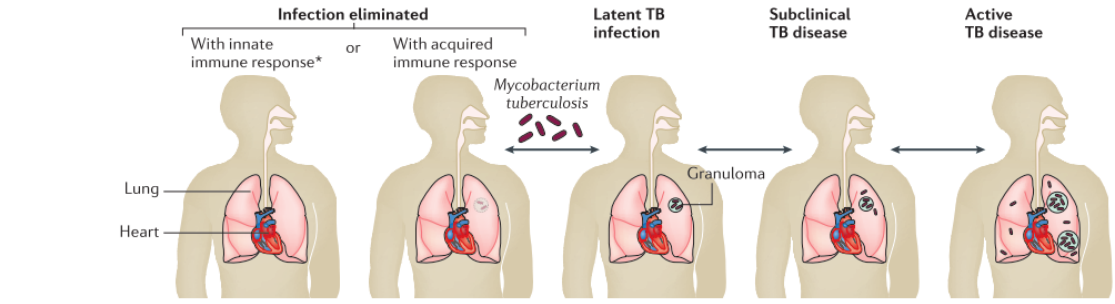

TST	Negative	Positive	Positive	Positive	Usually positive
IGRA	Negative	Positive	Positive	Positive	Usually positive
Culture	Negative	Negative	Negative	Intermittently positive	Positive
Sputum smear	Negative	Negative	Negative	Usually negative	Positive or negative
Infectious	No	No	No	Sporadically	Yes
Symptoms	None	None	None	Mild or none	Mild to severe
Preferred treatment	None	None	Preventive therapy	Multidrug therapy	Multidrug therapy

Figure 4- TB clinical presentations. From (Pai, Behr et al. 2016)

In latent TB, patients remain with no signs or symptoms of the disease (O'Garra, Redford et al. 2013). It is estimated that one third of the human population is latently infected with Mtb. The diagnostic is commonly made by the classic tuberculin skin test (TST) and/or Interferon-Gamma Released Assays (IGRA). These tests measure the response of T cells to Mtb antigens and enable to evaluate if the person has been infected with Mtb (Pai, Denkinger et al. 2014; Fogel 2015; Salgame, Geadas et al. 2015; Pai, Behr et al. 2016).

The TST has been used for TB diagnosis over 100 years (Salgame, Geadas et al. 2015). It is performed by intradermal injection of tuberculin Purified Protein Derivative (PPD), a mixture of antigens present in both Mtb and other mycobacteria. In a person who developed T cell-mediated immunity to these antigens, a delayed-type hypersensitivity skin reaction will occur within 48-72 hours after injection. Interpretation of TST reactions takes into account: the millimetres of induration (swelling), the person's risk of being infected with TB and of progression to disease, if infected (Pai, Denkinger et al. 2014; Fogel 2015; Pai, Behr et al. 2016). TST has the advantage of being a simple and low cost method, for that reason it is widely used. However, it lacks specificity and sensitivity, due to its cross-reaction with BCG and Nontuberculous Mycobacteria (NTM) and false negative responses in immunosuppressed individuals (Pai, Denkinger et al. 2014; Fogel 2015; Pai, Behr et al. 2016).

In the early 2000s IGRA was introduced as immunodiagnostic tool to solve the specificity and sensitivity issues of TST (Pai, Behr et al. 2016). IGRA measures the interferon-γ production of whole blood isolated T-cells *in vitro* upon stimulation with antigens encoded by Region of Difference 1 (RD1) such as Early Secreted Antigenic Target 6 (ESAT-6) and Culture Filtrate Protein 10 (CFP-10). RD1 antigens are more specific than PPD for Mtb because they are not encoded in the genome of any BCG vaccine strains or of most NTM species (Pai, Denkinger et al. 2014; Pai, Behr et al. 2016).

However, positive TST and/or IGRA results are shared by patients who have cleared the infection but retain a strong memory T cell response, those who have developed an adaptive immune response, yet who remain infected by bacteria in a quiescent or latent state ("true" latent infection), and those with subclinical or active TB. On the contrary, individuals that cleared the infection without developing a detectable adaptive immune response or infected individuals with highly localized immune response or insufficient magnitude to be detectable systemically may present negative TST and/or IGRA negative results (Pai, Behr et al. 2016). Thus, none of the currently available testsable to accurately differentiate between different forms of the disease.

The principle signs and symptoms of active TB include fatigue, lack of appetite, weight loss, fever, chest pain and severe coughing with bloody sputum (Pai, Behr et al. 2016). Patients with subclinical TB don't report symptoms but are culture positive.

The first action for the detection of pulmonary TB is generally the chest x-ray. The bacteriological confirmation is additionally performed by microscopic examination, mycobacterial culture of sputum smears and molecular tests (Caulfield and Wengenack ; Pai, Behr et al. 2016). Microscopic examination is able to rapidly detect Mtb using Ziehl-Neelsen staining (also called acid-fast staining). However, only half the number of TB cases are detected with this diagnostic method and it doesn't detect drug-resistance (WHO). Moreover, Ziehl-Neelsen staining cannot distinguish Mtb from other acid-fast bacillus such as *Rhodococcus* spp. and *Nocardia* spp. (Caulfield and Wengenack). Mycobacterial culture of sputum smears has high sensitivity and is able to identify Multidrug Resistant (MDR) Mtb strains simply by using antibiotics during culture. However, growth of Mtb on traditional solid medium requires long time, between 2 to 8 weeks, depending on the initial number of Mtb (Caulfield and Wengenack ; Ryu 2015). The use of liquid media is significantly faster, between 10 to 14 days and is more sensitive for detecting mycobacteria than solid media. There are now automated machines such as the Bactec Mycobacterial Growth Indicator Tube 960 (Becton Dickinson), which enabled early recognition of bacterial growth by using a fluorescent sensor that detects oxygen consumption. However, liquid systems are more prone to contamination by other microorganisms and they do not allow visualization of colony morphology and pigmentation, which is useful for distinguishing colonies of Mtb and of other NTM species (Caulfield and Wengenack ; Ryu 2015).

Molecular methods have been developed over the last two decades and are being increasingly used for detection of Mtb. These tests are highly specific compared to sputum smears and are also rapid; results can be available on the same day (Ryu 2015). Besides detecting the presence of *Mycobacterium tuberculosis* Complex (MTBC) and some NTM, some of these methods allow to detect resistance to antituberculous drugs and identification of the exact bacterial species.

Xpert MTB/RIF (Cepheid) assay is a cartridge based sample preparation with fully automated quantitative Polymerase Chain Reaction (qPCR), targeting different sequence regions of *rpoB* gene with fluorescent probes. The *rpoB* gene encodes the β-subunit of the bacterial RNA polymerase and mutations in this gene are responsible for approximately 96 % of Rifampicin (RIF) resistance (Caulfield and Wengenack). Therefore, xpert MTB/RIF can be a useful diagnostic tool to detect both Mtb and resistance to RIF. However, GeneXpert machine is not widely available yet.

Loop-mediated isothermal amplification (LAMP) is a constant temperature method of amplifying DNA from Mtb in a single step. Unlike Polymerase Chain Reaction (PCR), it does not need a thermal cycler and results can be read with naked eye as fluorescence or turbidity (Dorman 2015).

Line probe assay (LPA) also uses PCR amplification of DNA that codes for resistance to a certain drug. The products are detected as colour bands on a paper strip of nitrocellulose, which contains DNA probes that activate a colorimetric indicator, when bound to target DNA (Dorman 2015). First-line LPA can detect resistance to first-line drugs RIF, Isoniazid (INH) and Ethambutol (EMB). Second-line LPA can detect resistance to second-line drugs such as some fluoroquinolones (ofloxacin and levofloxacin) and all second-line injectables (kanamycin, amikacin, and capreomycin) (Group 2017).

Advances in several diagnostic tools have contributed for the increase of the specificity and sensitivity of TB diagnosis. Nevertheless, the development of new TB diagnostic tools must continue to increase accuracy and to decrease costs and time in order to promote timely initiation of treatment, better treatment outcomes, and, ultimately, ending the TB epidemic.

1.1.2. Pathogenesis of Mtb and phagocytic cells

Pathogenic life cycle of Mtb initiates when small aerosol droplets are expelled by an infected host (**Figure 5**). Once the bacillus is transmitted to a new host and delivered to lower lungs, the immune response to Mtb is initiated. Initial bacterial recognition is made by alveolar macrophages but also neutrophils, monocytes and Dendritic Cells (DCs), through different Pattern Recognition Receptors (PRRs) expressed on the surface of these cells (Ernst 2012; O'Garra, Redford et al. 2013). Of the PRRs, Toll-Like Receptor 2 (TLR2) recognizes the largest number of identified mycobacterial Pathogen-Associated Molecular Patterns (PAMPs), including lipoproteins, phosphatidylinositol mannans and lipomannan (Ernst 2012). This triggers various intracellular signaling cascades that leads to the production of proinflamatory cytokines such as Interleucin 1β (IL-1β), Tumor Necrosis Factor (TNF) and IL-12. This response leads to the recruitment of other immune cells. Neutrophils and monocytes are the first ones arriving, phagocytose additional

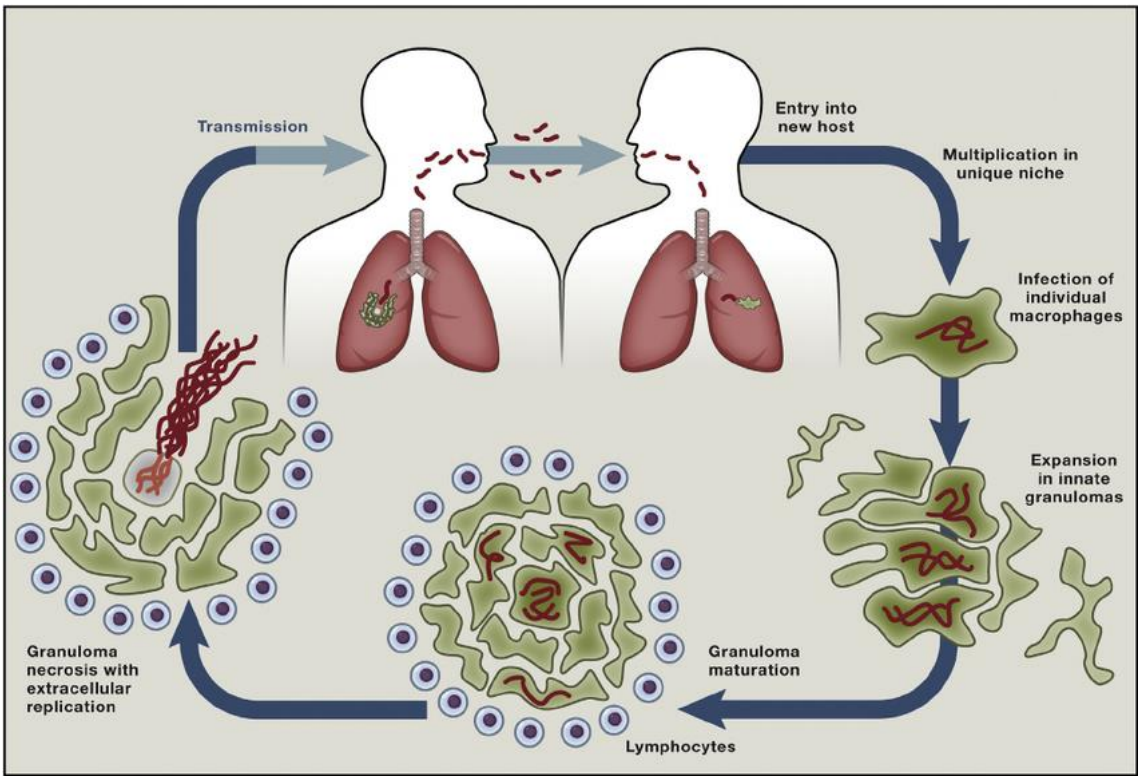

Figure 5 – Pathogenic life cycle of Mtb. From (Cambier, Falkow et al. 2014)

bacteria, secrete more cytokines and chemokines, and begin to organize the early granuloma, the hallmark of this disease.

Mtb recognition leads also to different microbicidal mechanisms, such as the production of toxic effector molecules like Reactive Oxygen Species (ROS) or Reactive Nitrogen Species (RNS) produced by the Inducible Nitric Oxide Synthase (iNOS), phagossome acidification, and apoptosis (Behar, Martin et al. 2011; Kleinnijenhuis, Oosting et al. 2011).

The fate of intracellular mycobacteria can also be influenced by autophagy, a cellular process whereby cytoplasmatic components, including organelles and intracellular pathogens, are sequestered in a double-membrane vesicle called autophagosome and delivered to the lysosome for degradation (Kleinnijenhuis, Oosting et al. 2011; O'Garra, Redford et al. 2013). The activation of autophagy, by IFN-γ for example, leads to phagosome maturation and an increase in its acidification and killing of Mtb (Gutierrez, Master et al. 2004).

DCs also phagocytose Mtb and then migrate to lung-draining lymph nodes to present mycobacterial antigens to naive T lymphocytes. This step is essential for the activation

and differentiation of Mtb antigen-specific T cels and the development of an effective adaptive immune response. Effector T cells arrive to sites of infection and mediate macrophage microbicidal activity through the production of IFN-γ, thus controling Mtb growth (Cooper 2009). If the response is too slow, bacteria grow and reach a point where although a potentially protective response is being expressed, the environment is such that it is not effective (Cooper 2009).

For that reason, Mtb impairs antigen presentation and migration of DCs to the draining lymph-nodes and induction of protective adaptive cellular responses is delayed compared with that of other infections or immunization (Wolf, Linas et al. 2007; Wolf, Desvignes et al. 2008). Initiation of adaptive immunity responses to Mtb is delayed, approximatelly 42 days after infection in humans and 11-14 days in mice (Ernst 2012). In the meantime, Mtb proliferates in the early granulomas by a continual cycle of death of infected macrophages and infection of newly arriving macrophages, by phagocytosis of infected macrophages that have recently undergone apoptosis (Davis and Ramakrishnan 2009).

As granulomas continue to mature, macrophages form an organized aggregate whose membranes become tightly interdigitated like those of epithelial cells (Ramakrishnan 2012). Granuloma macrophages can also fuse into multinucleated giant cells or differentiate into foam cells, which are characterized by lipid accumulation. Many other cell types are also present in the granuloma, such as neutrophils, DCs, Natural Killer (NK) cells, T cells and B cells. Bacteria are most commonly present in the central necrotic areas in which dead and dying macrophages can be seen (**Figure 6**). Over time, there is an increase in fibroblast proliferation around the granuloma, that together with collagen and other extracellular matrix proteins leads to the formation of a fibrous capsule that surround the lesion and prevent bacterial spread (Guirado and Schlesinger 2013).

Mtb can persist for decades within the granuloma structures in a latent state, serving as a reservoir of the bacterium and, if the host becomes immunocompromised, it may lead to disease reactivation. Eventually, bacteria starts to proliferate, leading to increasing accumulation of necrotic debris, or caseum, in the granuloma center, which eventually leads to rupture of the granuloma and bacilli escape into the airways, thus spreading the infection to new tissue and potentially new hosts.

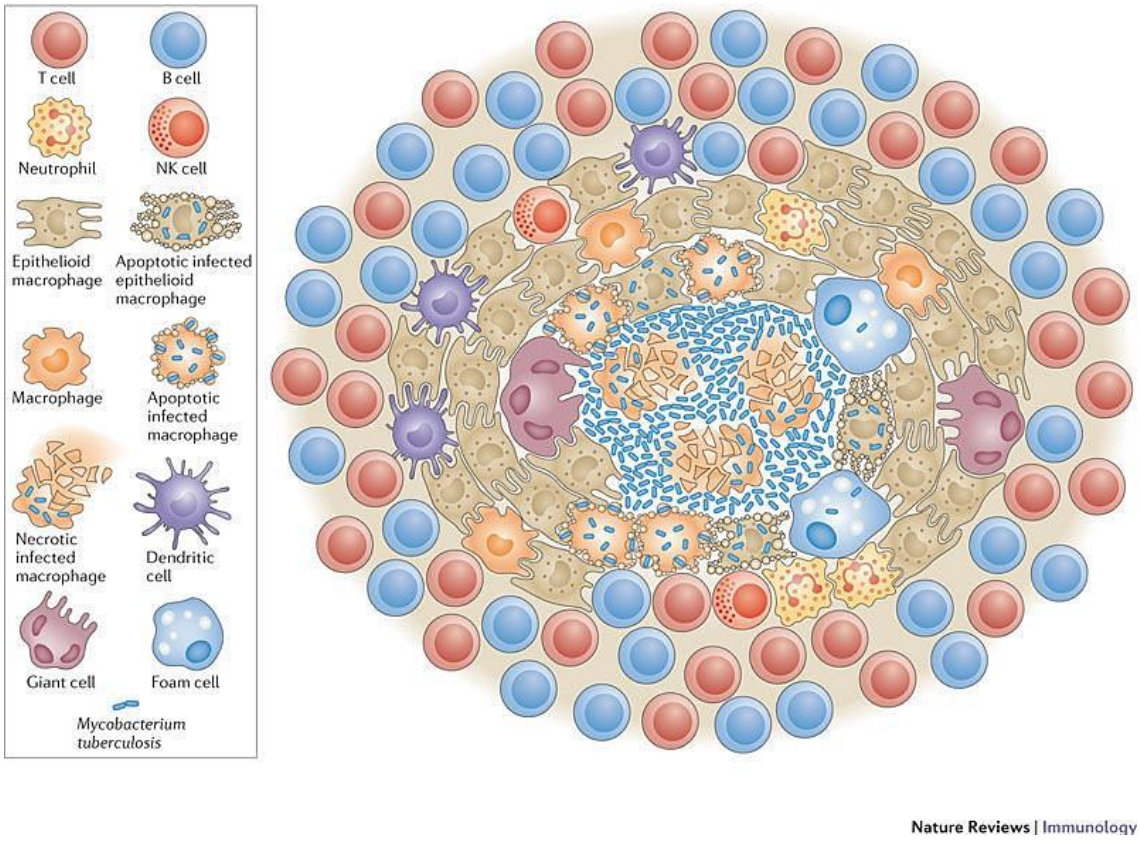

Figure 6 – Structure and cellular constituents of the tuberculous granuloma. From (Ramakrishnan 2012)

Granulomas are generally assumed as protective structures that prevent dissemination of infection and provide a local environment for interaction of cells of the immune system. Indeed, individuals who never showed signs of active TB have evidence of healed granulomas (Cosma, Sherman et al. 2003). However, granuloma is also a place that supports Mtb expansion. Virulent Mtb bacilli evolved multiple virulence mechanisms to rapidly adapt to the hostile environment in the granuloma and manipulate it for their own advantage (Ramakrishnan 2012; Cambier, Falkow et al. 2014).

Mtb evades destruction by preventing phagolysosomal fusion and persisting in the phagosome, reducing acidification of the phagosomal compartment to a pH of around 6.4, still acidic but considerably less hostile than the pH of the lysosome (pH around 4.8), thus adapting to the intracellular environment of the macrophage and creating a niche for survival (O'Garra, Redford et al. 2013; Tan and Russell 2015).

Mtb is also able to modulate host cell metabolism to favor its survival. For example, Mtb is able to induce accumulation of lipid-loaded droplets inside the cell and then use fatty acids and cholesterol as a carbon source (VanderVen, Huang et al. 2016).

Moreover, Mtb possess an important protein secretion system ESX-1 encoded by genes in RD1, which secretes 6 kDa early secretory antigenic target ESAT-6 and 10 kDa culture filtrate protein CFP-10, proteins that play important roles in the bacterial pathogenesis. ESX-1 is required for mycobacterium virulence and its absence attenuates the strain *M. bovis* BCG vaccine (Pym, Brodin et al. 2002). ESX-1 has been shown to induce phagolysosomal rupture and provide cytosolic access to Mtb, which appears to results in cell toxicity and host cell death involving necrosis (Simeone, Bobard et al. 2012; Simeone, Sayes et al. 2015). This releases intracellular bacteria to the extracellular environment, permitting mycobacterial growth and subsequent re-infection. ESX-1 also induces apoptosis of infected cells, most likely through its secreted effector ESAT-6, which appears to promote bacterial proliferation during granuloma formation (Davis and Ramakrishnan 2009).

Understanding the mechanisms used by Mtb to manipulate the host and proliferate may contribute for the development of effective therapeutic and preventive options against TB.

1.1.3. Risk factors

The diversity of clinical manifestations after exposure to Mtb depends upon different environment-, social-, pathogen- and host-specific factors (**Figure 7**).

The strain virulence, the concentration of the bacterial inoculum and the duration of exposure are key determinants of whether infection occurs and increases the risk of progression to active disease (Salgame, Geadas et al. 2015).

Host characteristics such as immunity, genre, age and comorbidities are also related with increased risk of progression to active disease.

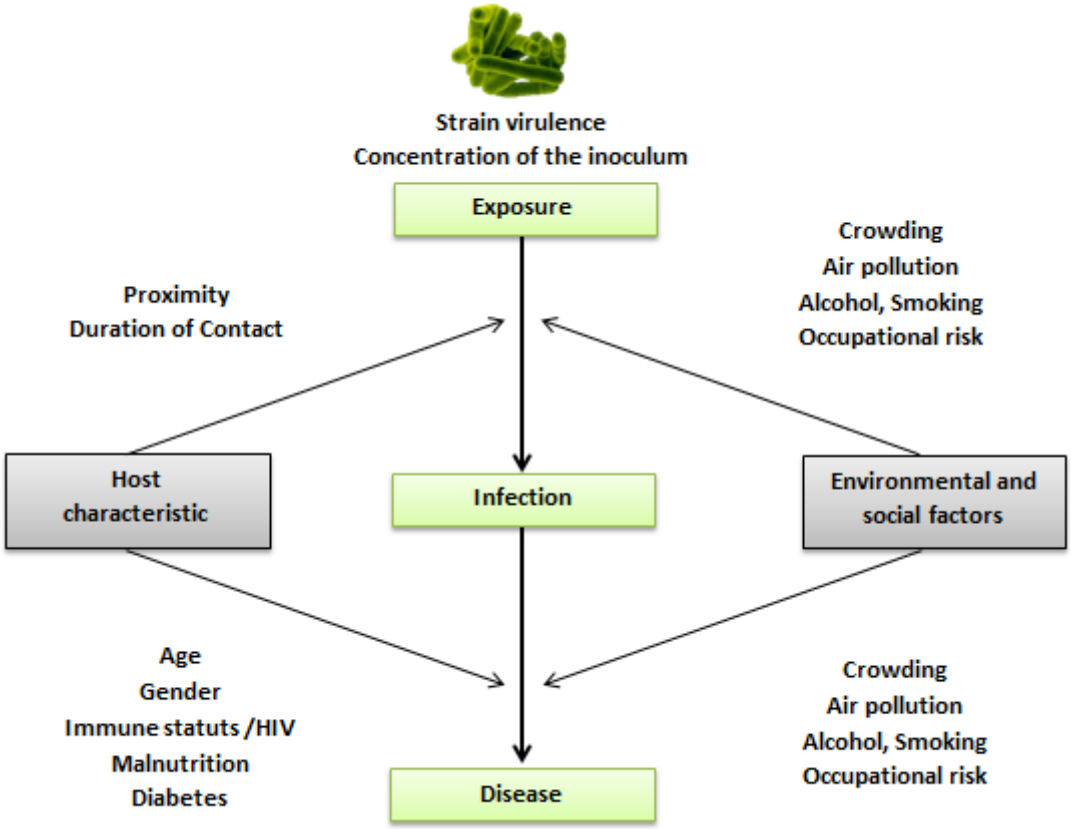

Figure 7 - Risk factors for Mtb.

The HIV infection is the strongest risk factor for TB. In 2015, HIV-infected people accounted for 12 % of all new active TB disease cases and 22 % of all TB-associated deaths (W.H.O. 2016). Indeed, TB is the most prevalent opportunistic disease among people living with HIV, contributing to nearly one third of all its mortality (Tiberi, Carvalho et al. 2017).

Other medical conditions and health-risk behaviours that weaken the immune system are associated with a greater risk of developing TB, such as diabetes mellitus, silicosis, chronic renal failure needing dialysis, immune-suppressive therapy, head and neck cancer, tobacco smoking, alcohol abuse and undernutrition (Dheda, Barry et al. 2016; Pai, Behr et al. 2016).

Highest risk of infection with Mtb is seen among children (0-4 years old) and young adults, from male sex (after adolescence) and individuals with specific genetic polymorphisms (Dheda, Barry et al. 2016). Already in classical Greece the physician Hippocrates (460- 370 BC) recognized the predilection of the disease, at that time called

phthisis (Greek word meaning “consumption”), for young adults: “Phthisis makes its attacks chiefly between the age of eighteen and thirty five” (Daniel 2006).

Latently infected individuals are more susceptible to develop active TB during their lifetime, which is estimated to happen in 5-10 % of the cases (Lin and Flynn 2010; O'Garra, Redford et al. 2013).

Socioeconomic and environmental factors are also shown to increase the susceptibility to infection, including poverty, overcrowding and air pollution.

1.1.4. Epidemiology

“TB will not be eliminated anywhere until it is eliminated everywhere”

Don Enarson.

When anyone not working in the fields of TB science or medicine is asked about the disease, they often recall a debilitated and pallid woman from the mid-20th century coughing blood into a handkerchief. However, TB is not a disease of the past. It is estimated that more than 2 billion people, equally to one third of the world’s population, are infected with Mtb (WHO). Fortunately, most of infections with Mtb (90-95 %) remain

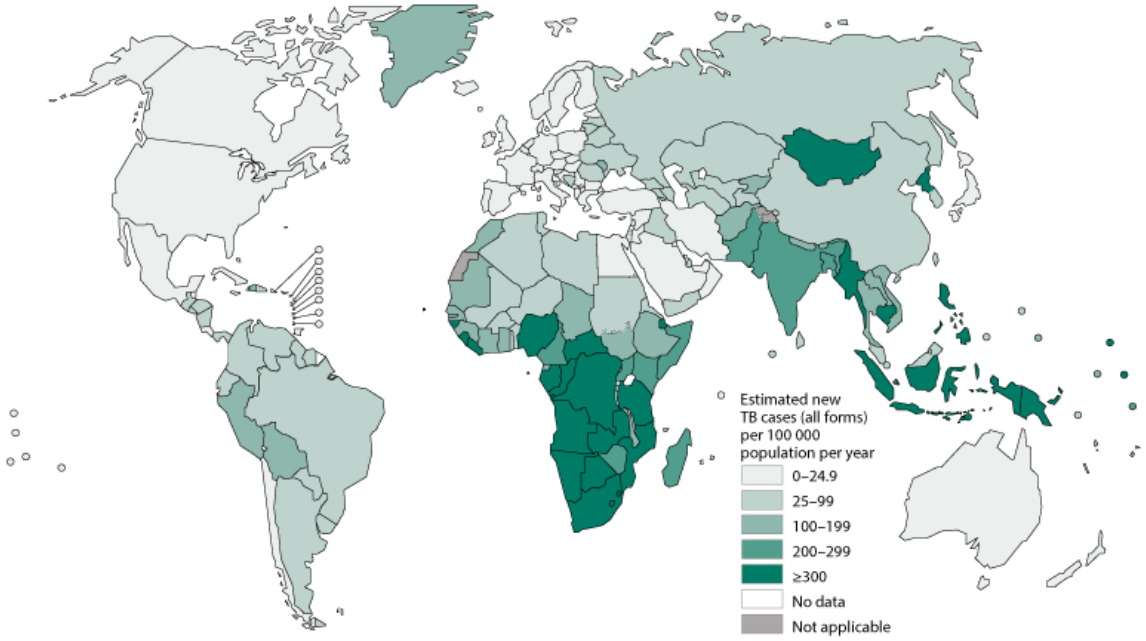

Figure 8- Estimated worldwide TB incidence rates in 2012, as determined by the WHO. From (WHO 2016).

asymptomatic (latent TB) with a 5-10 % lifetime risk of progressing to active TB (Gideon and Flynn 2011; Salgame, Geadas et al. 2015). Even so, TB was one of the top ten causes of death worldwide in 2015, and the number one cause of death from an infectious disease, surpassing HIV and malaria (W.H.O. 2016). According to WHO, in 2015 there were 10.4 million new TB cases worldwide and 1.8 million deaths were caused by this disease, including 0.4 million HIV-associated TB deaths (W.H.O. 2016).

TB epidemiology is heterogeneously distributed worldwide, as shown on the map of estimated TB incidence (**Figure 8**). Most cases are estimated to occur in Asia and Africa (61 % and 26 %, respectively), with the six countries with highest number of incident cases in 2015 (India, Indonesia, China, Nigeria, Pakistan and South Africa) accounting for 60 % of the total number of cases (W.H.O. 2016).

1.1.5. Etiological agent of TB: *Mycobacterium tuberculosis* complex (MTBC)

On March 24th, 1882, Dr. Robert Koch announced the discovery, of Mtb, the etiological agent of TB disease. This important discovery is commemorated each year on March 24th, the World TB Day (Lakhtakia 2014).

Mtb belongs to a group of phylogenetically related species collectively denominated as MTBC, which in addition to Mtb includes other species such as *M. africanum, M. bovis, M. canettii M. avium* and *M. microti* (Comas, Coscolla et al. 2013; Galagan 2014; Brites and Gagneux 2015). All of these species are potential human pathogens; however, the vast majority of the cases of TB in humans are caused by Mtb and *M. africanum* (Brites and Gagneux 2015).

Mycobacterium is a genus of the actinobacteria phylum (gram-positive bacteria with high guanine and cytosine content in DNA). Among *Mycobacterium* genus, Mtb belongs to the slow growth group, with a doubling time of 12-24 h under optimal conditions (Delogu, Sali et al. 2013). Mycobacterial cells are irregular rods of 0.3-0.5 µm in diameter and 1.5-4.0 µm in length (Cook, Berney et al. 2009).

A major feature of mycobacteria is the unusual cell envelope structure, which provides a strong impermeable barrier and plays an important role in the pathogen's

survival and virulence, It is composed of three major structural components: the plasma membrane, the cell wall core and the capsule (Kieser and Rubin 2014) (**Figure 9**).

The plasma membrane consists of a typical lipid bilayer with protein interactions. It is surrounded by long polymers of peptidoglycan, which comprises repeating disaccharide *N*-acetylglucosamine (NAG) and *N*-acetylmuramic acid (NAM) that are cross-linked via short peptide chains attached to the NAM (Kieser and Rubin 2014). The peptidoglycan layer confers rigidity and osmotic stability to the cell wall of mycobacteria as it does to several other gram-positive and gram-negative bacteria (Jankute, Cox et al. 2015).

A layer of arabinogalactan consisting of arabinan disaccharides and galactose monosaccharides surrounds the peptidoglycan layer. Arabinan is bound to long-chain mycolic acids, which form the characteristic hydrophobic thick lipid layer of mycobacteria. This layer constitutes approximately 50 % of mycobacterium dry weight and it is responsible for the resistance to degradation by lysosomal enzymes and by many drugs (Kleinnijenhuis, Oosting et al. 2011).

Glycolipids and porins are also found in the cell wall, as Lipoarabinomannan (LAM), which is anchored to the cell membrane (Brown, Wolf et al. 2015). The arabinan motifs of LAM are further decorated by capping moieties, depending on the mycobacteria species.

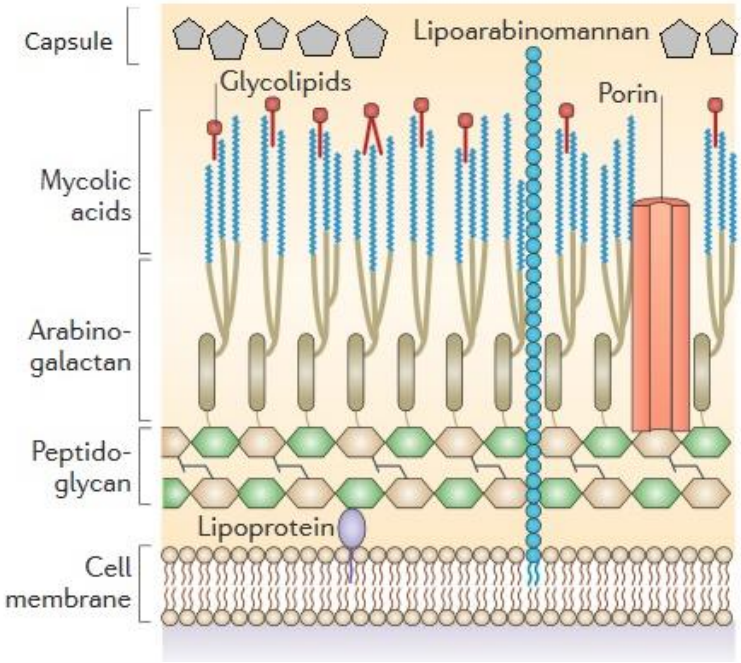

Figure 9- Diagram of the basic components of the mycobacterial cell wall. Adapted from (Brown, Wolf et al. 2015).

In the case of Mtb, LAMs are capped with mannose and are referred to as ManLAMs (Jankute, Cox et al. 2015).

Due to the high density of lipids in the cell wall, mycobacteria resist staining by ordinary methods such as a Gram stain. They are also resistant to acid and alcohol de-colorization and are described as acid-fast bacilli (Kieser and Rubin 2014). A different staining method must be used, namely the Ziehl-Neelsen Stain, a method in which the acid-fast mycobacterium is stained in bright red with carbol fuchsin, combined with phenol. After application of an acid decolorizing solution and a counter stain (methylene blue), non-acid-fast bacteria become blue (Vasanthakumari 2009).

1.1.6. Evolution and genetic diversity within the MTBC

"You have to know the past to understand the present"
Dr. Carl Segan

The ancient association of TB with humanity was initially recognized by observation of the characteristic Pott's disease lesions in the spine of human fossils. However, other pathologies such as brucellosis and chronic inflammation can also cause changes in the bones that can be difficult to distinguish from TB (Donoghue 2017). Moreover, it is estimated that skeletal TB corresponds only to 3-5 % of untreated cases, so only a small fraction of ancient TB infections were detected by simple skeleton observation (Donoghue 2017).

The introduction of molecular diagnostic methods to Paleopathology in the 90s has enabled the specific identification of TB in historical and archaeological specimens. (Donoghue 2017). This advance has expanded our knowledge of the probable origin of the different Mtb lineages and their geographical distribution, which opens up new challenges in the understanding of the evolution of human-pathogen relationships.

The oldest evidence of TB infection in humans comes from ancient human remains from the Neolithic era dating from 9000 years ago (Hershkovitz, Donoghue et al. 2008). Signs of the infection in humans were also found in Egyptian mummies dating back to c. 3000 BC (Zink, Haas et al. 2001).

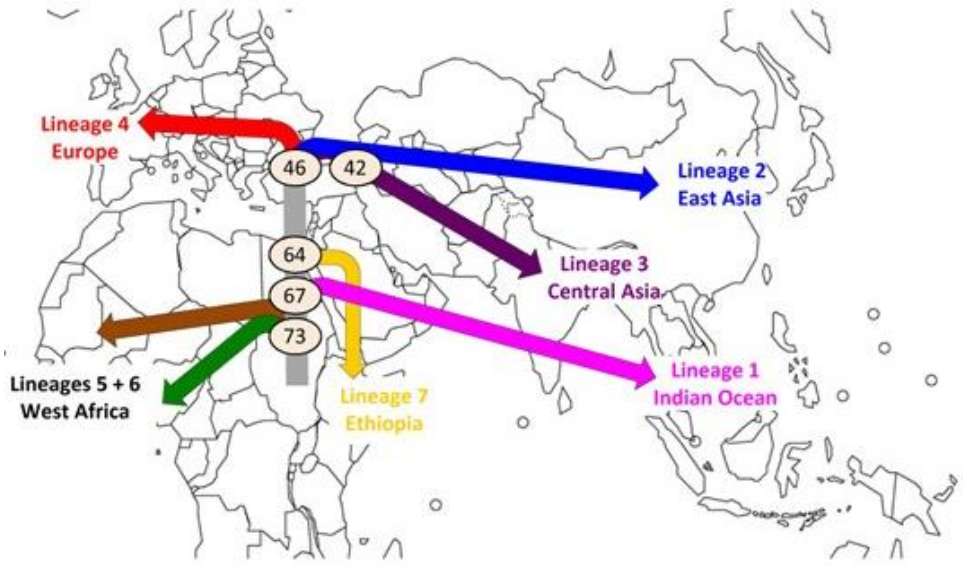

Figure 10 - Map summarizing phylogeographic and dating analyses of MTBC. Major splits are annotated with the median value (in kya) of the dating of the relevant node.

Genomic studies revealed that Mtb has coexisted with human beings in the last 70.000 years (Comas, Coscolla et al. 2013; Brites and Gagneux 2015). During this period, both the pathogen and the host have adapted to each other to increase chances of survival (Comas, Coscolla et al. 2013; Brites and Gagneux 2015). From this evolution, seven different lineages of mycobacteria that constitute the MTBC have arisen (**Figure 10**) (Comas, Coscolla et al. 2013; Galagan 2014; Brites and Gagneux 2015). Each lineage is linked with a specific geographic region, where the bacteria are more often isolated: lineage 1 occurs around the Indian Ocean, lineage 2 is widely distributed in East Asian countries, lineage 3 occurs in Central Asia, lineage 4 has a broad distribution in Europe and America, lineage 5 and 6 are restricted to West Africa and lineage 7 is restricted to Ethiopia (Comas, Coscolla et al. 2013; Brites and Gagneux 2015).

Bacteria of the MTBC have been described as being genetically monomorphic (Sreevatsan, Pan et al. 1997; Ramaswamy, Amin et al. 2000; Comas, Chakravartti et al. 2010; Achtman 2012; Galagan 2014). However, as mentioned above, infection with MTBC strains may result in a wide spectrum of disease outcomes, ranging from clearance to latent or active TB with different severity degrees. Until recently, the different outcomes of Mtb infection were totally attributed to host and environmental factors. Currently, there is increasing evidence that part of TB diversity may result from the heterogeneity of

the bacteria. For instance, studies using MTBC strains from different phylogeographical lineages demonstrated that: (i) strains from the same lineage are more likely to spread among the human population from the same geographic origin (Gagneux, DeRiemer et al. 2006); (ii) different lineages of MTBC have different rates of progression from latent to active TB (de Jong, Hill et al. 2008); (iii) different Mtb strains lead to different macrophage and in vivo immune responses (Portevin, Gagneux et al. 2011; Carmona, Cruz et al. 2013) and that (iv) the modern lineages L2 and L4 have different intracellular growth rates and induce a weaker innate proinflammatory response, when compared to ancient lineages (L1, L5, L6 and L7).

This suggests that the limited genetic diversity existent within the MTBC, impacts different aspects of TB as well as host-pathogen interactions.

1.1.7. Treatment and prophylaxis

Before the discovery of antibiotics, treatment of TB was limited to a regimen of rest and better nutrition. In the late 19th and 20th, the development of sanatoriums contributed to a moderate control of the disease. In these institutions, patients were exposed to high altitude, fresh air, good nutrition, bed rest and sunbathing (**Figure 11**) (Riva 2014). Here, more invasive approaches were also applied, such as lung collapse

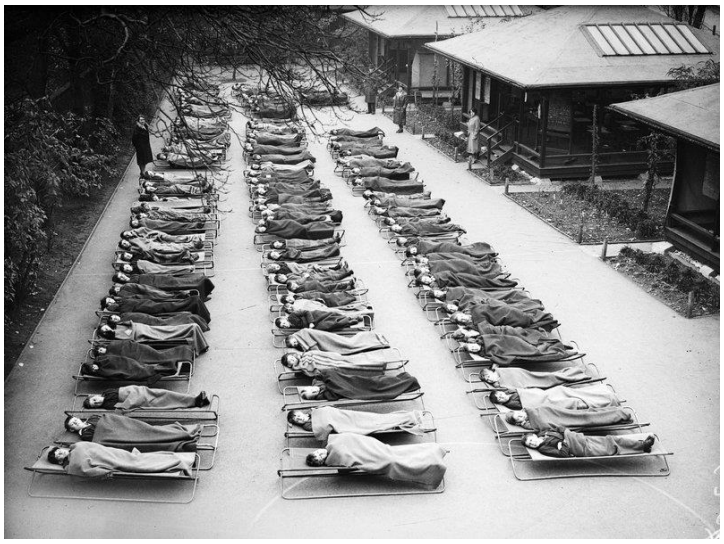

Figure 11 - Children with TB sleep outside at Springfield House Open Air School in London in 1932. Like sanatoriums, these schools offered TB patients a place to receive fresh air and sunshine cure. From (1932).

therapies and surgical resection of disease lung tissue (Riva 2014). It is doubtful whether the sanatorium treatment improved the survival of the patients, but it provided a haven for those healing from TB and it may have helped reducing the spread of the disease.

The introduction of chemotherapy against TB started in 1940s with the discovery of Streptomycin (STR), in 1943, derived from *Streptomyces griseus* **(Figure 12)**. The results were impressive but soon STR resistant mutants began appearing, threatening the success of antibiotic therapy (Kerantzas and Jacobs 2017). Shortly afterwards, Para-Aminosalycilic acid (PAS), a synthetic antimicrobial, was introduced as an oral therapy. In 1948, researchers from the Britain Medical Research Council demonstrated that combined treatment with STR and PAS was superior to each drug alone and prevented the emergence of drug resistance (Z Ahmad 2011; Kerantzas and Jacobs 2017). These results provided the first evidence of the necessity for multiple drugs in treating TB to prevent development of drug resistance.

INH, which remains the most potent drug against actively dividing tubercle bacilli, was discovered and brought into clinical use in 1952. In addition to its potency, INH is remarkably selective for mycobacteria (Chakraborty and Rhee 2015). It was initially

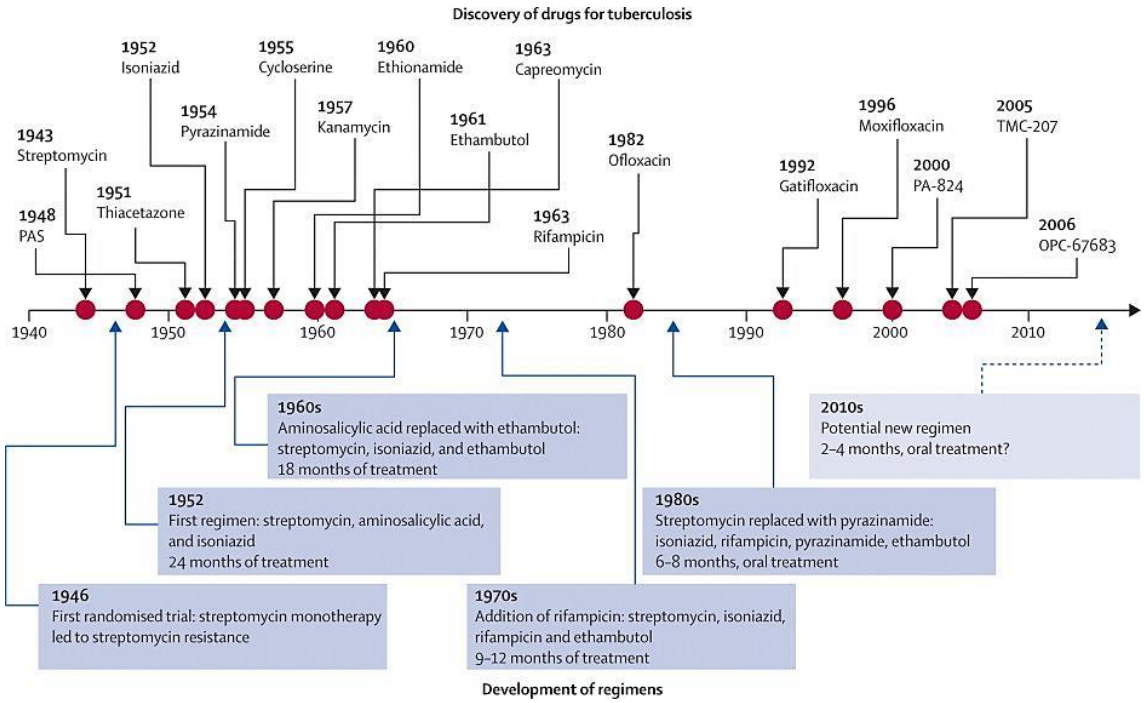

Figure 12 – History of drug discovery and development of treatment regimens for TB. From (Ma, Lienhardt et al. 2010).

thought that INH could be used as monotherapy but, INH resistance subsequently appeared, demonstrating again the importance of combining different drugs for the treatment of TB (Murray, Schraufnagel et al. 2015). The “triple therapy”, combining INH, STR and PAS, was the standard treatment during 15 years (Murray, Schraufnagel et al. 2015).

In 1961 an extensive screening led to the discovery of EMB. This synthetic antibiotic was reported to be as effective as PAS when combined with INH even at a low dose and it was much better tolerated (Murray, Schraufnagel et al. 2015). For that reason, soon it replaced PAS in the standard treatment (Z Ahmad 2011).

The next major advance was the introduction of RIF in 1963, derived from *Amycolatopsis mediterranei* (Z Ahmad 2011). This drug exhibited a spectacular activity and was able to kill dividing and semidormant bacteria, the so called “persisters”, like no other drug (Dobbs and Webb 2017). The addition of RIF to the standard regimen of STR, INH and EMB, in the 1970s, allowed to reduce the length of treatment from 18 months to 9 months and led to improved cure rates (Murray, Schraufnagel et al. 2015). However, it causes an increase of the hepatic Cytochrome P450 (CYP450) oxidase system, decreasing the levels of many other drugs, including many protease inhibitors, a class of antiviral drugs (Dobbs and Webb 2017). Currently, there are no sterilizing drugs that can prevent relapse as effectively as rifamycins, therefore, combining drug therapies in patients co-infected with HIV and Mtb is complex. Rifabutin, another rifamycin, is a less potent inducer of CYP450 and may be used as an alternative to RIF when drug-drug interactions or drug intolerance impedes use of RIF (Dobbs and Webb 2017).

Pyrazinamide (PZA) was also added to the standard regimen allowing a shortening of treatment to 6 months due to its activity against slow-growing and non-replicating organisms (Murray, Schraufnagel et al. 2015).

Currently, the standard therapy for new-cases of drug-susceptible TB has a high success rate of 83 % (W.H.O. 2016) but require taking antibiotics daily during long time. It consists of a combination of the first-line drugs INH and RIF for at least 6 months and PZA and EMB during the first 2 months (Pai, Behr et al. 2016).

Despite the existence of an effective treatment, drug resistance has continued to grow. TB resistant to at least INH and RIF is termed MDR. Extensively Drug-Resistant

(XDR) is defined as MDR with additional resistance to at least one fluoroquinolone (ofloxacin, levofloxacin, gatifloxacin, moxifloxacin) and a second line injectable drug (amikacin, capreomycin, and kanamycin) (W.H.O. 2016).

The treatment of MDR- or XDR-TB is complex, expensive, lengthy, and uses drugs with uncertain efficacy and characterized by high toxicity, which correlates with lower patient adherence and increases the probability of treatment failure and development of even more resistance to antibiotics. Treatment success rate is only 52 % for MDR TB and 28 % for XDR TB (W.H.O. 2016).

According to the new WHO drug classification (2016) (**Table 1**) the treatment of RIF-resistant or MDR-TB should include at least 5 potentially active drugs during the intensive phase: one first-line drug such as PZA and 4 second-line TB-drugs, one from of a later generation fluoroquinolone (moxifloxacin, levofloxacine or gatifloxacine; group A), an injectable aminoglycoside (amikacin, capreomycin, or kanamycin; group B) and at least 2 from group C (Ethionamide (ETH)/protionamide, cycloserine/terizidone, linezolid and Clofazimine (CLZ)). If some of these drugs cannot be used, additional drugs from group D can reinforce the regimen to bring the total to 5 drugs (2016). Group D is divided into 3 subgroups: first-line antituberculosis drugs (D1), the new drugs in confirmatory phase III trials, bedaquiline and delamanid (D2), and other agents of uncertain role in MDR-TB treatment (D3). The recommended duration is 20 months with an intensive phase (with injectable drugs) during the first 8 months (2016).

The 2016 WHO update on MDR-TB treatment guidelines suggests that partial lung resection used alongside a recommended MDR-TB regimen may be considered for the management of MDR- and XDR-TB (2016). However, weak evidence exists confirming that it increases the prognosis, compared to chemotherapy alone.

Also in 2016, WHO has recommended a shorter (9-12 months) MDR-TB treatment regimen with seven drugs, for patients with RIF-resistant or MDR-TB that is not resistant to second-line drugs (2016). The treatment includes 3 drugs (kanamycin, prothionamide, and high-dose INH) for 4–6 months, plus 4 drugs (moxifloxacin, CLZ, PZA, and EMB) given throughout the course of treatment. This new recommendation is expected to benefit the majority of MDR-TB patients; however, an inappropriate use (XDR-TB, for example) may worsen resistance.

Table 1 –WHO recommended antituberculosis drugs and actions.

Drug	Mechanisms of action	Activating enzyme/ Gene target	Group
Isoniazide (P)	Inhibit production of the cell wall component mycolic acid	*katG, inhA*	First-line D1 (high dose)
Rifampicin	Inhibit RNA synthesis	*rpoB*	First-line
Ethambutol	Inhibit production of the cell wall component arabinogalactan	*embB*	First-line D1
Pyrazinamide (P)	Disrupt plasma membrane	*pncA, rpsA*	First-line D1
Rifabutin	Inhibit RNA synthesis	*rpoB*	Alternative to RIF
Levofloxacin	Inhibit DNA gyrase and topoisomerase IV	*gyrA/B*	A
Moxifloxacin	Inhibit DNA gyrase and topoisomerase IV	*gyrA/B*	A
Gatifloxacin	Inhibit DNA gyrase and topoisomerase IV	*gyrA/B*	A
Kanamycin	Inhibit protein synthesis	*rrs*	B
Amikacin	Inhibit protein synthesis	*rrs*	B
Capreomycin	Inhibit protein synthesis	*rrs tlyA*	B
Streptomycin	Disrupt protein synthesis	*rpsL, rrs, gidB*	B
Ethionamide (P)	Inhibit production of the cell wall component mycolic acid	*ethA, inhA*	C
Linezolid R	Disrupt protein synthesis	*23S rRNA, rplC*	C
Clofazimine	Interfere with redox	*Rv0678*	C
Cycloserine	Inhibit production of the cell wall component peptidoglican	*cycA, alrA*	C
Bedaquiline (TMC207)	Inhibits ATP synthase	*atpE*	D2
Delamanid (P)	Inhibit production of the cell wall component mycolic acid	*ddn*	D2
p-aminosalicylic acid	Interfer in the process of folate synthesis	*thyA, folC*	D3
Imipenem plus cilastatin			D3
Meropenem			D3
Amoxicilin plus clavulanate			D3
Thiocetazone			D3

(P): Pro-drug
Known chemical classes are colour coded: **fluoroquinolone**, **rifamycin**, **oxazolidinone**, **nitroimidazole**, **diarylquinoline**, **aminoglycoside**, **cyclic peptide**, **pyridine**, **aminosalicylate**, **riminophenazine.**

The treatment of XDR-TB is designed on the basis of the patient's individual results of drug susceptibility testing and on similar principles to those drawn for MDR-TB.

Not only the development of new drugs is important to eradicate TB, an effective new vaccine is also needed. Despite years of research, no vaccine currently provides reliable protection against pulmonary TB in adults, the most prevalent and contagious form of the disease (Ottenhoff and Kaufmann 2012). Indeed, although many components of the host immune response against MTBC are known, lack of an immune correlate of protection, have been hampering the development of a more effective vaccine (Ottenhoff and Kaufmann 2012).

The current vaccine BCG was introduced in 1921 and remains the only available vaccine against TB (Luca and Mihaescu 2013). It was developed by Calmette and Guérin in the Institute Pasteur of Lille from a live attenuated strain of *M. bovis*, which lost its virulence towards humans after more than 11 years of consequent subcultures (Luca and Mihaescu 2013).

The effectiveness of this vaccine is variable and limited in adulthood pulmonary TB, even though, it is among the most widely administered vaccines, with more than 4 billion doses delivered to date, and it saved a large number of deaths that would otherwise be caused by TB every year. (Ottenhoff and Kaufmann 2012).

No universal BCG vaccination policy exists, and national vaccination schedules vary widely. In France, for example, a country with low prevalence of TB, universal mandatory BCG vaccination of children was suspended in 2007, with a shift to selective vaccination of children living in the Ile-de-France (Paris and suburbs) or French Guyana regions, and children considered by a physician as living in an environment with a high risk of exposure to TB (Lévy-Bruhl D 2007).

BCG vaccine and the existent antituberculosis drugs are clearly insufficient for worldwide TB control and alternative strategies for TB prevention and therapy are urgently needed.

1.1.8. Development of new antituberculosis drugs and regimens

Before a promising new drug is brought to the market it needs to pass through a series of pre-clinical and clinical trials, which is a long (10 or more years), expensive and complex process. In preclinical studies *in vitro* and *in vivo* studies are performed to study the drug's activity, physicochemical properties, pharmacokinetics and toxicity. In the TB field, mouse models are currently the most commonly used (Cooper 2014). During clinical trials, drugs are tested on people in three steps: Phase I trials are performed in 20-100 healthy volunteers to determine safety and dosing; Phase II trials are performed in up to several hundred people with the disease to get an initial idea of efficacy and side effects; Phase III trials evaluate efficacy and monitor adverse reactions in large numbers of patients during long time (1 to 4 years); Phase IV trials are conducted to uncover more information about efficacy, safety and side-effects after being approved by U.S. Food & Drug Administration (FDA) for marketing (FDA).

Development of new antituberculosis drugs should ideally be able to overcome the problems associated with the current regimens, fulfilling a set of requirements that includes a high level of potency to reduce the treatment duration, ability to inhibit new targets, which is crucial for MDR-TB and XDR-TB treatment, good penetration into all tissues where the Mtb resides, have low toxicity profile for use in children and pregnant women, compatibility with antiretroviral therapy, absence of antagonistic activity with existing TB drugs, ease of use, and be active against different physiological states of Mtb, including latency. Alongside with these ideal criteria, other practical aspects are important such as low production costs, compound stability and low rate of spontaneous resistance emergence.

1.1.8.1. New antituberculosis drugs in development (phase III)

After the introduction of RIF in the late 1960s, the war on TB was considered winnable with existent tools and drug development for TB has stagnated for decades (Murray, Schraufnagel et al. 2015). Between 1970 and 2000 only fluoroquinolones were introduced for the treatment of MDR-TB (Hofman, Segers et al. 2016). Resurgence of TB in the late 1980s renewal the interest in finding drugs to eliminate the disease. From 2000 onwards, multiple new antituberculosis drugs are in clinical development (**Figure**

13), the majority of which are incorporated into the TB Drug Accelerator, a programme sponsored by the Bill&Melinda Gates Foundation (Hofman, Segers et al. 2016; Pai, Behr et al. 2016). Two of these drugs, bedaquiline and delamanid, are still in confirmatory phase III trials but have been already conditionally approved in many countries and are now recommended by WHO as an addition to a background treatment for MDR- and XDR-TB, for whom an effective treatment regimen is not available (2016). Based on ongoing trials, these drugs have been proven to be effective in increasing sputum smear and culture conversion, and in improving success rates at the end of treatment, although safety concerns for these drugs, including cardiotoxicity and deaths, remains (Murray, Schraufnagel et al. 2015; Hofman, Segers et al. 2016). Accelerated approval of these drugs indicates the lack of viable alternatives and poor outcomes for patients with MDR- and XDR-TB. Bedaquiline, previously identified as R207910 and then TMC207, is a promising new TB drug discovered in a high-throughput phenotypic screen for compounds active against *M. smegmatis,* and subsequently showed activity against other mycobacteria, including Mtb (Andries, Verhasselt et al. 2005; Chakraborty and Rhee 2015). It is a novel diarylquinolone that works through a new mechanism, inhibiting essential ATP synthase activity of both replicating and dormant mycobacteria. The activity of bedaquiline is specific for mycobacteria, while the Minimum Inhibitory Concentration (MIC) for other prokaryotic and eukaryotic is much higher (Andries, Verhasselt et al. 2005; Hoagland, Liu et al. 2016). Bedaquiline displays potent early and late bactericidal activity and excellent MICs against both drug-sensitive (0.03 µg/mL) and MDR-TB (0.12 µg/mL), as well as outstanding activity in *in vivo* murine models (Andries, Verhasselt et al. 2005). Moreover, the long effective half-life (24 h) (Andries, Verhasselt et al. 2005) may allow the use of bedaquiline for intermittent drug administration when combined with others drugs in the regimen against MDR-TB and XDR-TB. However, its metabolism via the CYP450 system limits its potential use as adjunct to RIF, a potent inducer of CYP450 system (Hoagland, Liu et al. 2016).

The second promising drug, delamanid, formerly called OPC-67683, belongs to the nitroimidazoles, a class of compounds with known activity against protozoan and anaerobic bacterial infections. Delamanid is effective in killing both replicating (aerobic condition) and non-replicating (anaerobic condition) mycobacteria *in vitro* and in the guinea pig TB model (Chen, Hashizume et al. 2017). It inhibits the synthesis of methoxy-

and keto-mycolic acids, crucial components of the cell wall of MTBC, thus its antibacterial

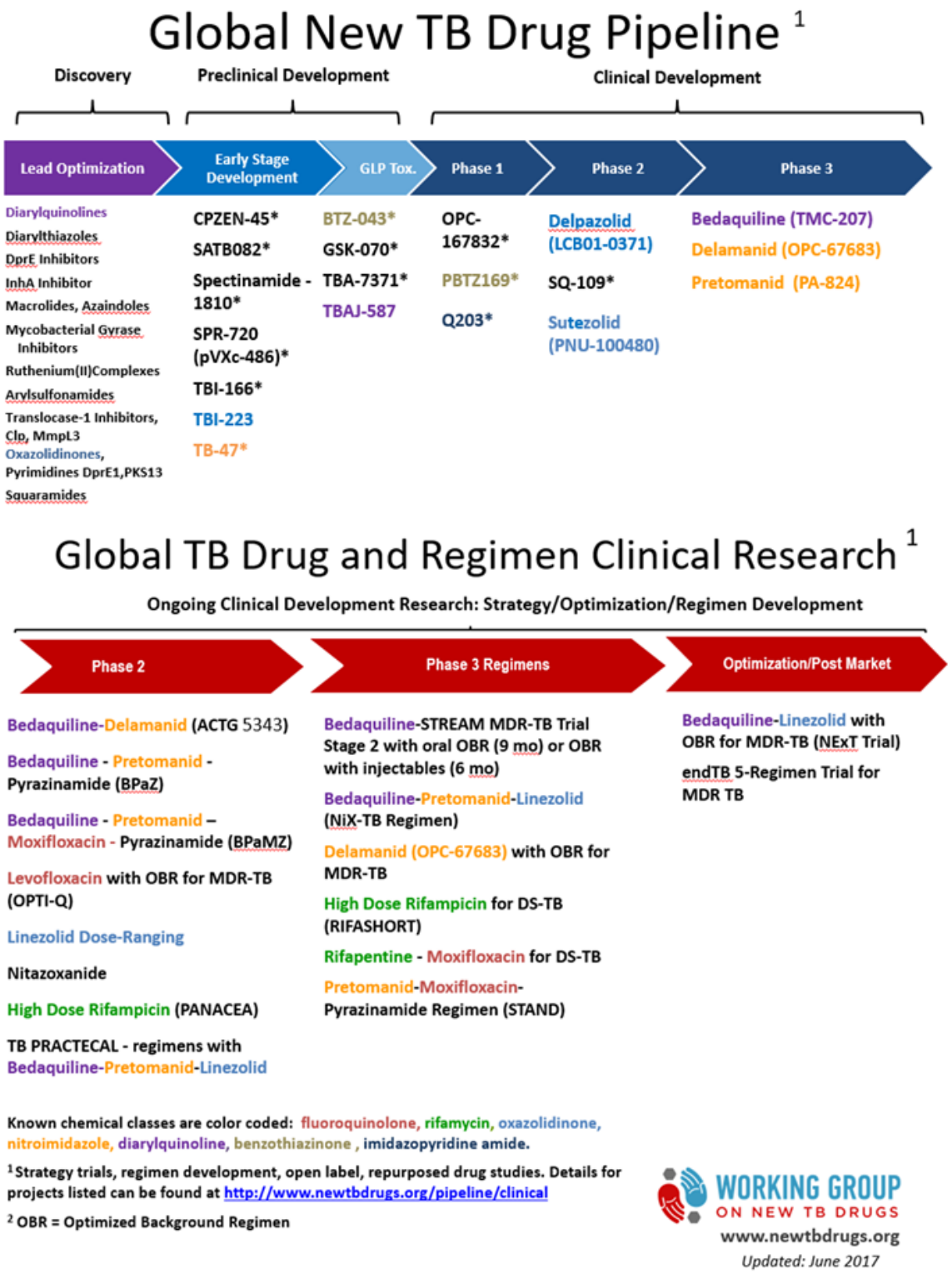

Figure 13 – Global TB new drug pipeline and ongoing clinical development research.

activity is mycobacteria-specific. Unlike INH, delamanid has little effect on α-mycolic acid biosynthesis (Matsumoto, Hashizume et al. 2006). Despite the absence of an effect

on α-mycolic acid, the MICs reported with delamanid with both drug-susceptible and drug-resistant Mtb*, in vitro,* are lower (0.006-0.024 μg/mL) than the ones reported with INH (0.05-0.78 μg/mL) (Matsumoto, Hashizume et al. 2006). As a prodrug, delamanid requires activation possibly mediated via the F420-deazaflavin-dependent nitroreductase (*ddn*) of Mtb.

Pretomanid (PA-824) is another nitroimidazole currently in clinical development (phase III). It also exhibits bactericidal activity against both latent and active TB and it has also shown activity against both drug-sensitive and drug-resistant TB (Stover, Warrener et al. 2000). Similarly to delamanid, pretomanid inhibits the synthesis of methoxy- and keto-mycolic acids in mycobacteria cell wall and requires metabolic activation through *ddn* (Rv3547) (Manjunatha, Boshoff et al. 2006), but MICs reported (0.015-0.25 μg/mL) are higher than delamanid and comparable to INH (Stover, Warrener et al. 2000). Pretomanid also kills non-replicating Mtb by intracellular Nitric Oxide (NO) release, which appears to be crucial for its anaerobic activity through poisoning of cytochrome c oxidase (Singh, Manjunatha et al. 2008). Similarly, delamanid may also induce NO production and this may be responsible for cell killing under non-replicating conditions since mycobacteria do not extensively remodel mycolic acids under anaerobiosis (Boshoff and Barry 2006).

1.1.8.2. Repurposed drugs

Repurposed drugs are antimicrobials that were developed for other diseases, but which have useful antimycobacterial activity. Repurposing is attractive as a drug development strategy since much is already known about approved agents, including their pharmacokinetics and pharmacodynamics features, dosing, safety, tolerability and manufacturing. Even though further studies of drug dosing, safety, drug-drug interactions and efficacy in the context of the long multidrug regimen treatment of TB is needed, repurposing drugs accelerates their entrance in the market of TB drugs (Dheda, Barry et al. 2016). The major drawback of this strategy is the increased risk of emergence of drug resistance as a side effect of previous treatments nonrelated to TB. Several existing antibiotics are now being repurposed for treatment of TB and some of these are listed under WHO drugs (**Table 1**).

Fluoroquinolones are a class of antibiotics frequently used to treat a wide variety of bacterial infections. The main targets are bacterial topoisomerase II (DNA gyrase) and DNA topoisomerase IV, two critical enzymes for bacterial viability (Dheda, Barry et al. 2016). Several members of this class have been used as second-line drugs for the treatment of MDR-TB. Interest of moving fluoroquinolones to the first-line was renewed when it was shown that moxifloxacin instead of INH in the standard regimen could reduce the duration of therapy in a murine model of TB (Nuermberger, Yoshimatsu et al. 2004). However, three trials have demonstrated that regimens including both moxifloxacin and gatifloxacin are not effective in shortening the treatment to 4 months (Gillespie, Crook et al. 2014; Jindani, Harrison et al. 2014; Merle, Fielding et al. 2014). Currently, different moxifloxacin-containing regimens are in clinical trials (**Figure 13**) to improve the treatment of MDR-TB and patients co-infected with TB and HIV. Levofloxacin is also under a phase II clinical study to determine the highest levofloxacin area under the curve (AUC) that is associated with maximal efficacy and acceptable safety/tolerability.

CLZ is an extremely lipophilic riminophenazine antibiotic discovered in the 1950's and used since 1962 in a combination therapy for the treatment of leprosy (Cholo, Steel et al. 2012). It was initially discarded for the treatment of TB possibly because other agents brought on the market at about the same time were more effective and because of some undesirable side-effects such as pigmentation of the skin and gastrointestinal upset (Murray, Schraufnagel et al. 2015). CLZ demonstrated *in vitro* activity against drug-resistant and drug-susceptible Mtb and efficacy against a mouse model of TB (Reddy, Nadadhur et al. 1996). The activity of CLZ was also observed *in vitro* and *in vivo* against Mtb persisters (Xu, Lu et al. 2012) and against latent TB (Zhang, Sala et al. 2012). Moreover, in mouse models, CLZ demonstrated potential to shorten the duration of TB chemotherapy in combination with first-line and second-line drugs (Grosset, Tyagi et al. 2013; Tyagi, Ammerman et al. 2015).

CLZ is now recommended by the WHO to treat MDR-TB as a medicine with "unclear efficacy" (group C). Although the exact mode of action is not completely understood, it appears to act as a prodrug, which is reduced by NADH dehydrogenase (NDH-2), and subsequently after spontaneous reoxidation, liberates ROS (Lechartier and Cole 2015).

Oxazolidinones are antibiotics developed for the treatment of infections caused by resistant gram-positive bacteria, which exert their antimicrobial activity by inhibiting

protein synthesis by binding to the bacterial 23S ribosomal RNA (Dheda, Barry et al. 2016). The first commercially available oxazolidinone, linezolid, is now recommended by WHO to treat patients with MDR-TB (group C). Different studies suggest that linezolid containing chemotherapy for drug-resistant TB may improve treatment success, but patients must be monitored carefully because of significant side effects associated with long treatment (Cox and Ford 2012; Lee, Lee et al. 2012; Sotgiu, Centis et al. 2012; Tang, Yao et al. 2015). Other two oxazolidinones, sutezolid (previously known as PNU-100480) and delpazolid (LCB01-0371), are currently in clinical development phase II, and one oxazolidinone, TBI-223, is in preclinical development.

β-lactams are a class of broad-spectrum antibiotics, consisting of all antibiotic agents that contain a β-lactam ring in their molecular structures. This ring mimics the shape of the terminal D-alanyl-D-alanine peptide sequence that serves as the substrate for cell wall transpeptidases that form covalent bonds between different peptidoglycan chains, during periods of cell growth. The tight binding of these drugs to the transpeptidase active site inhibits the synthesis of the peptidoglycan layer of the bacterial cell wall, resulting in a weakened cell wall that is susceptible to lysis during periods of cell growth. The most important mechanism of bacterial resistance to β-lactam antibiotics is enzymatic inactivation by β-lactamases by cleavage of the β-lactam ring. Mtb possesses a constitutively active broad-spectrum β-lactamase, BlaC, which may justify why β-lactams have received little attention as antituberculosis drugs (Dheda, Barry et al. 2016). However, addition of clavulanate, an irreversible inhibitor of BlaC, enhances β-lactam activity (Hugonnet and Blanchard 2007). Carbapenems, a subclass of β-lactams, such as meropenem, and imipenem, are relatively resistant to hydrolysis by β-lactamases, and thus are active against Mtb *in vitro*, nonetheless their activity is enhanced by the addition of clavulanate (Hugonnet, Tremblay et al. 2009). Combination of carbapenems plus clavulanate showed significantly improved survival in a murine model of TB (Veziris, Truffot et al. 2011), and a systematic review of carbapenem-containing regimens in individuals with MDR- XDR-TB showed to have very good safety and tolerability and treatment efficacy higher than 57 % in five studies with culture conversion rates between 60 % and 94.8 % (Sotgiu, D'Ambrosio et al. 2016). The combination of a carbapenem and penicillin, another subclass of β-lactams, such as amoxicillin might also have synergistic or additive effect *in vitro* (Gonzalo and Drobniewski 2013). A recent phase 2A trial with limited number of patients examined the activity of meropenem, amoxicillin, and

clavulanate combination and showed early bactericidal activity in patients with pulmonary drug-susceptible TB (Diacon, van der Merwe et al. 2016). However, all drugs were administered three times per day, and meropenem requires intravenous administration, which makes this combination impractical in many settings.

1.1.8.3. "Revived" old TB drugs

Many drugs developed during the early days of TB drugs development, are now rarely used because of poor efficacy and associated toxicity.

An innovative approach to make old TB drugs strong again arose from the observation that a significant number of antituberculosis antibiotics are prodrugs that must be bioactivated by mycobacterial enzymes to exert their activity, and that overproduction of the prodrug activator in recombinant mycobacteria increased the sensitivity to the prodrug. This means that the bioactivation is not fully exploited and that only part of the prodrug administered is actually exerting its antimycobacterial effect, living space for optimizing this process.

In particular, Ethionamide (ETH), an old TB drug currently recommended by WHOto treat patients with MDR-TB (group C), is a prodrug that is inactive until activation by the mycobacterial monooxygenase ethionamide activator (ethA) (Baulard, Betts et al. 2000; DeBarber, Mdluli et al. 2000), which first oxidizes ETH to a corresponding S-oxide and further catalyses the covalent addition of Nicotinamide Adenine Dinucleotide (NAD) to ETH, forming the ETH-NAD active adduct (Vannelli, Dykman et al. 2002; Laborde, Deraeve et al. 2016). Similar to INH, after activation, the resultant ETH adduct inhibits an enoyl-acyl carrier protein reductase, InhA, an essential enzyme of Mtb involved in the synthesis of mycolic acids, critical constituents of the mycobacterial cell wall. ETH activation by ethA is negatively regulated by the Ethionamide transcriptional Repressor (ethR), which limits the potency of ETH (Baulard, Betts et al. 2000; DeBarber, Mdluli et al. 2000; Engohang-Ndong, Baillat et al. 2004).

Willand N. *et al.* searched for compounds able to inhibit the DNA-binding function of the repressor ethR, thus boosting the bioactivation of ETH (Willand, Dirie et al. 2009). One of the compounds selected, BDM31343, enabled to reduce the dose of ETH necessary to decrease the pulmonary bacterial load in a Mtb mice model of infection.

Mice were treated 6 days per week, during 3 weeks, with a combination of 50 mg/Kg (body weight) BDM31343 in DMSO given intra-peritoneally twice daily and different concentrations of ETH administered in DMSO orally, once a day. After 3 weeks of treatment, the efficacy obtained with 9 or 27 mg/Kg ETH could be equalled by 3 or 9 mg/Kg of ETH in combination with 100 mg/Kg BDM31343, respectively (Willand, Dirie et al. 2009). These results proved that by using inhibitors of ethR that boost the activation of ETH, it is possible to reduce the dose of ETH, while keeping the same efficacy.

The structure of BDM31343 was further optimized, leading to the development of BDM41906, which presents an increased activity profile, improved physicochemical and pharmacokinetic properties, and microsomal stability (Flipo, Desroses et al. 2012).

Because mycobacterial enzymes that activate prodrugs are not essential for bacterial growth and pathogenesis, the genes that encode them commonly undergo mutations that cause loss of function or attenuation, as observed for the INH-, PZA-, PAS- and ETH-resistant clinical isolates with mutations in *katG* (Zhang, Heym et al. 1992), *pncA* (Scorpio and Zhang 1996), *ribD* (Mathys, Wintjens et al. 2009; Zheng, Rubin et al. 2013) and e*thA* (Baulard, Betts et al. 2000; DeBarber, Mdluli et al. 2000), respectively. In the same way, mutations in *ddn* (Rv3547), a gene encoding an enzyme involved in the bioactivation of the new prodrugs delamanid and pretomanid, are associated with resistance to these drugs (Manjunatha, Boshoff et al. 2006; Matsumoto, Hashizume et al. 2006).

Thus, for the case of ETH, although the use of compounds that inhibit the repressor ethR might proof very efficient to boost the efficacy of ETH against drug-sensitive and MDR bacteria, it would be ineffective against ETH-resistant Mtb strains, mutated in *ethA*.

However, in the process of optimizing the structure of compounds that inhibit the repressor ethR, Blondiaux N. *et al.* unexpectedly found molecules unable to bind to ethR but that were still highly effective in boosting ETH activity against Mtb. Because these compounds had no antibacterial activity *per se*, the authors hypothesized that they may trigger an alternative bioactivation pathway for ETH. Using genome wide transcriptional analysis, the authors found that while BDM41906 induced the transcription of both e*thR* and *ethA*, the new compounds, represented by SMARt-420, induced a distant pair of

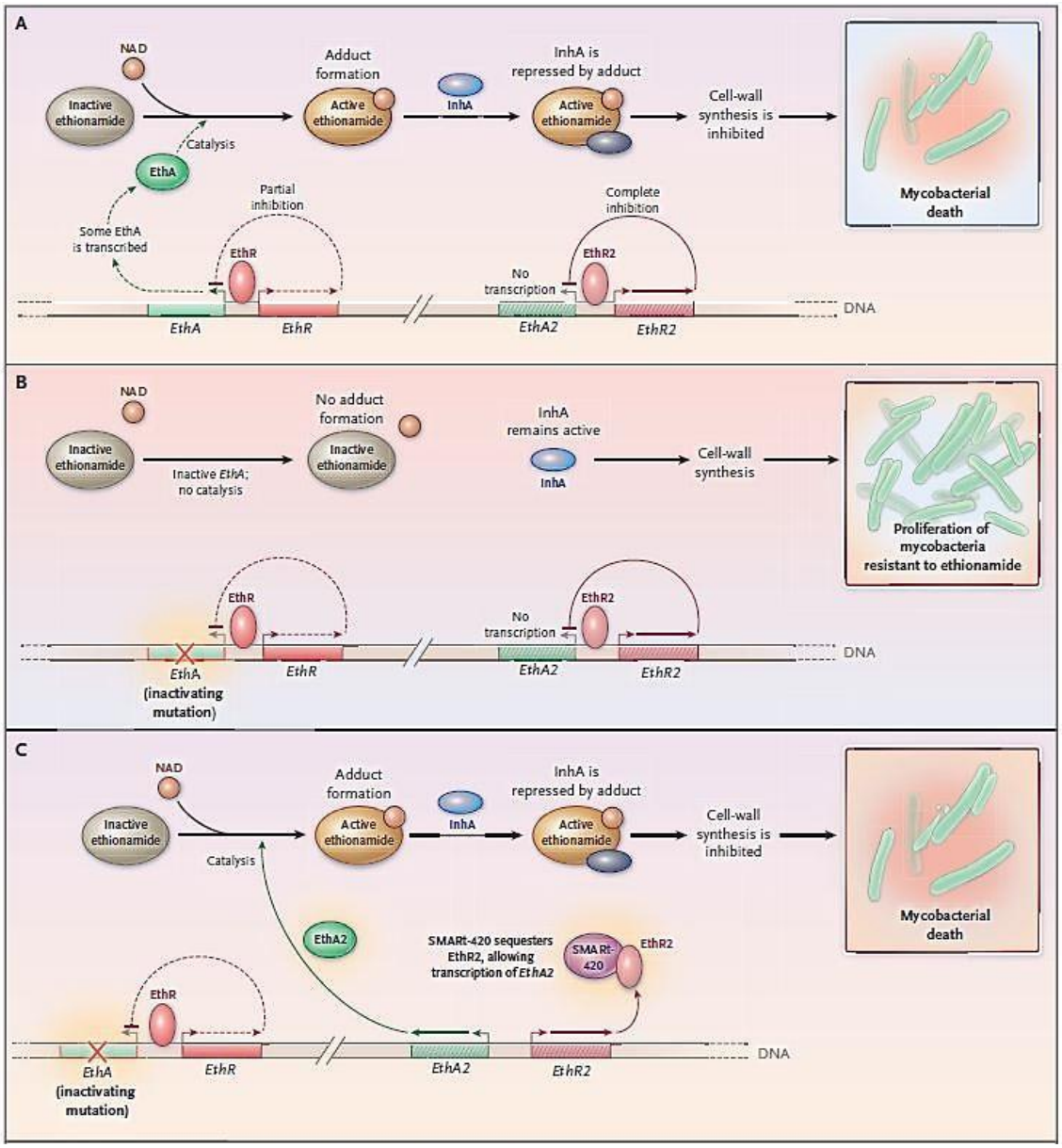

Figure 14 – Alternative activation of ETH with the use of SMARt-420.
A: In susceptible Mtb, transcription of the enzyme ethA is only partially repressed by the transcription factor ethR, allowing some production of ethA and conversion of ETH to the NAD adduct, the active moiety that inhibits cell-wall synthesis; **B:** In ETH-resistant Mtb loss-of-function mutations in the gene encoding ethA results in no activation of the drug; **C**: Normally, ethA2 is completely repressed by ethR2. Adding SMARt-420, blocks the binding of ethR2 to DNA and allows high-level expression of ethA2, thus representing an alternative mechanism for the activation of ETH. From (Rubin 2017).

genes with homology to *ethR* and e*thA*, which they called *ethR2* and *ethA2* (**Figure 14**). Further, they showed that, like the analogous system, ethR2 represses the transcription of ethA2. SMARt-420 by binding to ethR2 inhibits the repression of ethA2, leading to activation of ETH. Treatment of Mtb with SMARt-420 not only increased susceptibility to

ETH but was also highly active against all TB strains tested, including MDR strains mutated in *ethA.*

Therefore, exploring mechanisms of bioactivation is a promising strategy to give new life to old antituberculosis prodrugs, opening perspectives of dose and side effects reduction, and also reverting resistance mechanisms by inducing the activation of the prodrug through alternative pathways.

1.1.9. Mycobacterial resistance, tolerance and persistence to antibiotic treatment

TB pathology is extremely complex and dynamic, varying between patients and within a single individual patient. The spatial and temporal heterogeneity of TB lesions imply that Mtb has to constantly adapt to different stresses created by the local microenvironment. For example, the availability of oxygen and nutrients, the pH and the presence of oxidative stress is different when Mtb is within an extracellular environment in the caseous cavity or when it is in an intracellular environment inside a macrophage, in an early granuloma or in a hypoxic granuloma. Each of these conditions induces mycobacterial metabolic and physiologic adaptations that rise distinct subpopulations with different gene expression profiles, rate of replication, and other functional characteristics (Lenaerts, Barry et al. 2015). This heterogeneity affects the efficacy of antituberculosis chemotherapy that may not be able to act against the different mycobacterial subpopulations and most likely contributes to the long treatment duration and requirement for multi-drug combination.

For example INH, a drug that targets the biosynthesis of the cell wall, is a potent early bactericidal drug, highly active against rapidly dividing bacteria that are producing new cell wall, but it has low activity against bacteria that are maintained in a non-replicating state due to restriction of oxygen (Paramasivan, Sulochana et al. 2005). RIF, a drug that targets RNA polymerase, although not so active at early time points, it is equally active against both replicating and non-replicating bacilli (Paramasivan, Sulochana et al. 2005), probably because of the constant need for RNA production, even when bacteria are not undergoing active replication. On the other side, PZA, a drug that requires low pH to be active, only works against dormant and semi-dormant organisms that reside in an acidic environment, such as the one found within granulomas and in macrophages after

phagosome-lysosomal fusion (Zhang and Mitchison 2003). Thus, the same drug may have different efficacy against the same bacteria in different environments.

The introduction of antituberculosis chemotherapy subjected Mtb to another stress, which forced bacteria to develop adaptation mechanisms such as resistance and tolerance to antibiotic environment.

TB was the first infectious disease in which drug resistance was described, soon after the introduction of STR, in 1948 (Pai, Behr et al. 2016). Resistance is the inherited ability of a microbe to grow at high concentrations of an antibiotic, irrespective of the duration of treatment, and it is quantified by the minimum inhibitory concentration (MIC) of antibiotic that is required to prevent growth. Mtb is considered drug resistant when more than 1 % of bacterial cells grow in the presence of critical drug concentrations (Dheda, Barry et al. 2016). Mtb may be intrinsically resistant to an antibiotic, namely by cell wall impermeability, active efflux, modification of targets, enzymatic degradation or modification of antibiotics and activation of a transcriptional regulator or may acquire resistance by changes in the DNA that usually result from mutations in chromosomal genes encoding drug targets or enabling enzymes and possibly by horizontal gene transfer (Blair, Webber et al. 2015; Nasiri, Haeili et al. 2017) .

When drug-resistant TB results from infection with a drug-resistant strain it is called primary resistance (Dheda, Gumbo et al. 2017). For long time the impact of primary resistance was underappreciated because it was thought that the mutations that lead to resistance produced a fitness cost, and that resistant strains were less virulent or less easily transmitted. However, it is now known that, additional mutations often follow or coincide with drug resistance mutations and can compensate for the deleterious effects caused by the mutation that lead to the resistance. Molecular epidemiology studies in high-burden locations have shown high degrees of strain clustering, which is indicative of transmission (primary resistance) rather than acquisition (secondary resistance), in the majority of known MDR-TB cases and a significant part of XDR-TB cases (Dheda, Gumbo et al. 2017).

When resistance is developed during the treatment course is referred as secondary or acquired resistance. Acquired resistance to antituberculosis drugs is believed to be driven by poor adherence to a long TB therapeutic regimen and programmatic failure, with doses and dosing schedules that lead to suboptimal antibiotic concentrations.

Though, other mechanisms such as pharmacokinetic variability, induction of efflux pumps that transport the drug out of cells, and suboptimal drug penetration into TB lesions are also crucial for the development of drug resistance. Moreover, some bacterial strains have genetic hypermutable backgrounds that have greater propensity to cause acquired drug resistance (Dheda, Gumbo et al. 2017).

Tolerance is the ability, inherited or not, of bacterial cells to survive a transient exposure to antibiotics at concentrations that would otherwise be lethal (Kester and Fortune 2014), which is often achieved by slowing down an essential bacterial process. Dormancy is an extreme case of slow growth that leads to tolerance. Tolerance may be acquired through a genetic mutation or conferred by environmental conditions; for example, poor growth conditions have been shown to increase tolerance to different classes of antibiotics (Brauner, Fridman et al. 2016). Unlike resistance, tolerance applies only to bactericidal antibiotics and not to bacteriostatic antibiotics, as all bacteria are expected to survive transient exposure to bacteriostatic antibiotics since they only arrest growth. Tolerance to an antibiotic is almost insensitive to the concentration and dependent only on the duration of exposure, thus MIC is not informative as a metric to evaluate tolerance. Tolerant bacteria can have the same MIC as non-tolerant bacteria. Brauner, Fridman *et al.*, propose the use of the Minimum Duration for Killing (MDK) as a quantitative indicator of tolerance that can be extracted from a time-kill curve.

The term persistence is used to describe the ability of a subpopulation of a clonal bacterial population to survive exposure to high concentrations of an antibiotic. The "persisters" constitute the less numerous subpopulation (normally less than 1 %) and are killed at a slower rate than the susceptible cells. Persistence may be dependent on time (persisters undergo tolerance) or dependent on concentration (persisters undergo transient overexpression of a resistance factor) (Brauner, Fridman et al. 2016). Persistence is non-heritable, when persistent subpopulation cells are isolated, regrown and re-exposed to the same antibiotic treatment, the same heterogeneous response to the drug will be observed, with the division of the population into persistent and non-persistent subpopulations.

In the clinic, these insights may be useful for the establishment of a more effective therapy, by using inhibitors of resistance or extending the treatment duration, for example.

1.2. Nanotechnology as new tool in TB treatment

A bibliographic review on this subject was published on Drug discovery today.

1.2.1. Revue de la littérature - Résumé

"Comment les nanoparticules peuvent-elles contribuer à la thérapie antituberculeuse?"

Face à la recrudescence des cas de résistance aux antibiotiques, la tuberculose (TB) est un problème de santé mondiale majeur, qui est à l'origine de 10.4 millions de nouveaux cas et 1.8 millions de morts en 2015 selon l'Organisation Mondiale de la Santé (OMS). Cette maladie est causée par la bactérie *Mycobacterium tuberculosis* (Mtb) qui infecte principalement les poumons et qui se transmet par l'inhalation d'aérosols contaminés. Cette mycobactérie est capable de survivre et de se répliquer à l'intérieur des cellules phagocytaires, comme les macrophages pulmonaires.

A l'heure actuelle, le traitement de TB nécessite la prise quotidienne de plusieurs antibiotiques, dits de première ligne, qui sont l'isoniazide (INH), l'éthambutol (EMB), la rifampicine (RIF) et la pyrazinamide (PZA), pendant 6 mois. Une mauvaise utilisation de ces antibiotiques, notamment liée à leurs effets secondaires indésirables, est en partie à l'origine de l'apparition de souches Mtb multi-résistantes (MDR) et nécessite alors l'utilisation d'antibiotiques de seconde ligne pendant 18 à 24 mois. La combinaison de plusieurs antibiotiques est alors associée à des effets secondaires sévères.

De nouveaux médicaments sont nécessaires, mais, en dépit du fait que plusieurs molécules soient en cours d'étude, et certaines d'entre elles en essais cliniques, seules la Bedaquiline et Delamanid ont été approuvées pour le traitement conditionnel de patients atteints de TB résistantes (OMS, 2014 ; OMS, 2013). Dans l'attente de nouvelles molécules, il serait intéressant d'améliorer l'efficacité des traitements existants.

Une stratégie prometteuse consiste à cibler directement Mtb au niveau des macrophages pulmonaires en administrant les composés antituberculeux directement au site d'infection par aérosolisation. De plus, il est indispensable de définir de nouvelles

approches pour réduire la durée et la toxicité des traitements et améliorer leur efficacité vis-à-vis des bactéries actives et latentes.

Ainsi, l'encapsulation de composés antituberculeux dans des nanoparticules (NP) pourrait constituer une approche prometteuse pour le traitement de TB. Les NP sont déjà largement utilisées dans les domaines de l'agro-alimentaire et de la médecine, dont le domaine des maladies infectieuses.

Dans ce contexte, notre travail avait pour principal objectif de présenter une bibliographie exhaustive sur l'utilisation des NP pour le traitement de TB, en croisant toutes les données disponibles de la littérature, afin d'avoir une vue globale sur cette application avant d'envisager de nouveaux développements.

Ainsi, dans cette revue bibliographique, nous avons recensé plusieurs groupes à travers l'Europe (comprenant des universités, des entreprises, des instituts de recherche et des industries pharmaceutiques) qui ont unis leurs forces dans le cadre d'un consortium international pour utiliser les nanotechnologies pour le développement et la mise en œuvre de traitements originaux contre les cas de TB multi-résistante. Ces données montrent essentiellement deux domaines d'application possibles des NP dans le cadre des traitements antituberculeux reposant sur: (i) leurs propriétés antimycobactériennes intrinsèques ; et (ii) leur utilisation comme vecteurs ou « nanocarriers » pour les médicaments antituberculeux connus, de façon à réduire les doses et les effets secondaires associés et permettre leur administration par voie orale ou pulmonaire. Des résultats prometteurs ont été obtenus dans des modèles d'infection *in vitro* et *in vivo* sur l'animal, et ont besoin à présent d'être évaluer en tant que médicament - candidat à l'échelle clinique.

Ce travail bibliographique a été un point de départ extrêmement important pour dégager des pistes de nouvelles approches thérapeutiques antituberculeuses et nous a ainsi conduits à étudier quatre applications potentielles des nanoparticules: utilisées (i) comme nanocarriers pour les antibiotiques pour les administrer au niveau pulmonaire; (ii) pour améliorer la solubilité et la biodisponibilité des antibiotiques; (iii) pour la libération des antibiotiques dans les compartiments intracellulaires; et (iv) leurs propriétés antimycobactériennes intrinsèques.

1.2.2. Literature review

How can nanoparticles contribute to antituberculosis therapy?

Authors list: **Joana Costa-Gouveia**[1], José A. Aínsa[2,3,4], Priscille Brodin[1#], Ainhoa Lucía[2,3,4#]

Affiliations:

1: University of Lille, CNRS, INSERM, University Hospital Center of Lille, Pasteur Institute of Lille, U1019 - UMR 8204 - CIIL - Center for Infection and Immunity of Lille, 59000 Lille, France

2: Departamento de Microbiología (Facultad de Medicina), and BIFI, Universidad de Zaragoza, Zaragoza (Spain);

3: Instituto de Investigación Sanitaria Aragón (IIS-Aragón), Zaragoza (Spain);

4: CIBER de Enfermedades Respiratorias (CIBERES), Instituto de Salud Carlos III, Madrid (Spain)

#Corresponding authors:

Priscille Brodin (priscille.brodin@inserm.fr) Tel :+33 6 79 42 78 53

Ainhoa Lucía (ainhoalq@unizar.es) Tel: +34 876 55 43 45

Keywords: Tuberculosis, nanoparticles, antituberculosis drugs, tuberculosis treatment.

Teaser:

The number of effective drugs to treat TB is limited, the incidence of MDR-TB and XDR-TB is increasing, and developing novel drugs against TB is difficult. Nanoparticles (alone or carrying anti-TB drugs) are interesting alternatives with a potential for therapeutic use in treatment of TB.

Abstract

Therapeutic approaches using nanoparticles are being successfully used in foods and in several fields of medicine, including infectious diseases. Regarding TB treatment, nanoparticles may be a useful strategy for two distinct applications: (i) for their intrinsic antimycobacterial activity; (ii) as vehicles for known antitubercular drugs to allow reduction of dose and drug-associated side effects, and administration via user-friendly administration routes such as pulmonary or oral ones. Promising results were obtained *in vitro* and in animal *M. tuberculosis* models and need now to be translated into clinical drug candidates. Such a prospect may provide an opportunity to the current limited therapeutic options for drug resistant TB and to the scarcity of novel antituberculosis drugs in the drug discovery pipeline.

Introduction

The problem of antibiotic resistance in *Mycobacterium tuberculosis* has been declared a global health emergency by the WHO, which may endanger the control of tuberculosis (TB). Rising cases of multi-drug resistant (MDR) TB and extensively drug resistant (XDR) TB all over the world are increasingly hindering treatment of TB, making mandatory the use of second line drugs (SLDs) [1]. Treatment of MDR-TB is expensive, prolonged (18-24 months) and complex (with at least a combination of 5 drugs that include injectable drugs) and associated with a higher incidence of adverse effects. New drugs are urgently needed, but despite several molecules are being investigated, some of them already in clinical trials, only bedaquiline and delamanid have been approved for conditional treatment of specific MDR-TB patients in the last years **[2,3]**.

It is obvious that besides classical drug discovery strategies, new approaches are urgently needed to get a faster, more efficient and less harmful treatment. For this purpose, nanoparticles (NPs) have been shown since many years to be useful and versatile tools that can be used as antibacterial agents, and also as drug delivery systems, with numerous examples in the literature regarding various antibiotics and antibacterial agents. Nowadays, several groups across Europe including universities, small and medium-sized enterprises, research institutes and pharmaceutical companies join forces together in the frame of research consortiums to apply nanotechnology for the

development and implementation of novel treatments for multidrug resistant pathogens, including MDR- XDR -TB.

Use of NPs as new tools in TB treatment

NPs: characteristics and advantages for TB treatment

Very simply, we could consider a NP as a tiny object measuring less than 1000 nanometers that works as a whole unit (**Fig. 1**, **[9]**). They can be made of very different materials (biodegradable lipids, liposomes, solid-lipid NPs, polymers like poly lactic-co-glycolic acid (PLGA) or polysaccharides like chitosan), and can be produced by different methods, resulting in NPs with different structures and sizes.

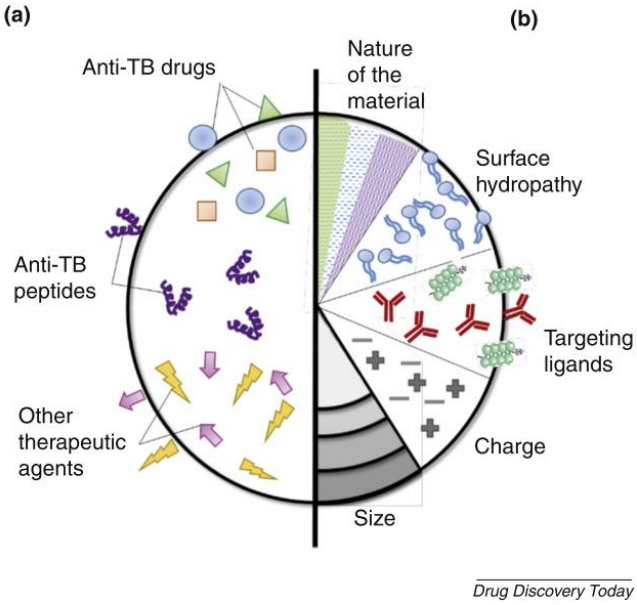

Figure 1. Composition and properties of nanoparticles. (a) Composition of the different types of nanoparticles that have been tested for activity against *M. tuberculosis*, such as those encapsulating first or second-line anti-TB drugs, alone or in combination, as well as other potentially useful particles such as antimicrobial peptides, other therapeutic agents or small DNA fragments. **(b)** The main nanoparticle properties that can influence the uptake, distribution and efficacy of nanoparticle-based therapies are: nature of the polymer, size, surface charge, surface hydropathy, and targeting ligands. Source: Adapted, with permission, from **[9].**

NPs made of inorganic materials show antibacterial activity *per se*. The most common are the metal NPs (such as Ag, Au, Ga, Cu….), which possess unique physical, chemical, electrical, optical, mechanical and magnetic properties, and their antimicrobial effects are well documented **[4-8]**.

One second, and probably the major advantage of nanosized carriers is their use as drug delivery systems owing to their unique physicochemical properties. In general, they are of small size, high surface to volume ratio, and high stability [9]. Normally they can incorporate both lipophilic and hydrophilic drugs (**Fig. 1**, **[9]**), as well as other molecules such as carbohydrates, proteins or lipids to stabilize and functionalize them [6]. In this way, NPs may improve the aqueous solubility of poorly soluble drugs, protect the drugs from degradation and allow a controlled release of the loaded drug, thereby the dose and frequency of administration can be reduced. Additionally, they can be modified to control their biodistribution allowing selective delivery to target organs or tissues **[9]**. For all those characteristics NPs are smart tools for the improvement of pharmacokinetics, solubility, bioavailability, toxicity or pharmacodynamics of drugs.

The development of effective and safe nanotherapeutic methods is particularly relevant in the treatment of drug-resistant tuberculosis, since very long treatments with highly toxic second-line drugs are required for those cases. The properties of NPs could diminish the dose of the drugs used to treat MDR-TB, and direct them to the infected macrophages in the lung, decreasing the toxicity and side effects, and increasing their efficacy. To this end, dedicated NPs have to be developed for each TB drug and optimized for targeting the lungs harboring extracellular as well as intracellular bacteria.

NPs with intrinsic antimycobacterial activity

Metal NPs present antimicrobial activity against a variety of microorganisms, and *M. tuberculosis* is not an exception (**Table 1**).

Silver (Ag) has been used as antibacterial agent for centuries **[10,11]**. Its antimicrobial activity is reported to increase when in the nano-form, which may be due to the ability to enter through cell membranes **[12]**, and nowadays silver NPs (AgNP) are widely used in consumer products such as textiles, disinfectant sprays, antibacterial ointments,

bandages or medical devices **[13]**. AgNPs are reported to have high antibacterial properties against Gram positive and Gram negative bacteria **[11,12,14-17]**.

Table 1. Nanocarriers with antimycobacterial activity.

Material (+load)	Features	Refs
AgNPs	*In vitro* antimycobacterial activity	**[13, 20, 21]**
AgNPs + cationic peptides	Antimycobacterial activity *in vitro* and in infected macrophages	**[22]**
AgNPs	Selection of resistant mutants	**[23]**
GaNPs	More efficacy *in vitro* and *in vivo* than free gallium *In vivo* targeting NPs to the macrophages	**[26]**
AuNPs	*In vitro* antimycobacterial activity	**[27]**
FeNPs + SM	*In vitro* antimycobacterial activity	**[28]**
PAA covered with Fe oxide	Efflux inhibition. Sinergy with RIF, INH and norfloxacin	**[29]**
EWNS	*In vitro* activity	**[33]**

Abbreviations: AgNPs: silver nanoparticles; GaNPs: gallium nanoparticles; AuNPs: gold nanoparticles; FeNPs: iron nanoparticles; SM: streptomycin; PAA: polyacrylic acid; RIF: rifampicin; INH: isoniazid; EWNS: engineered water nano-structures.

Because of that, the specific antimycobacterial activity of AgNPs has been studied, and reported that AgNPs show higher activity against mycobacteria than copper oxide NPs, followed by zinc oxide NPs, with poor antimycobacterial activity for both of them **[13]**.

The synthesis of AgNPs can be done via chemical methods but also physical methods. Concerning the chemical methods, sodium citrate, sodium borohydride, dimethlyformamide are typical compounds used to reduce Ag+ into metallic silver **[18]**. However as for organic NPs, eco-friendly pure methods based on the use of apiin, geraniol and gum kondagogu as reducing agents were also shown successful to produce AgNPs so that the synthesis process of AgNPs is no more an impediment to their development **[19]**. A study showed that AgNPs synthesized by synthetic agents present greater bacterial inhibition **[20]**, although AgNPs synthesized from medicinal plants-derived reducing agents also presents antimycobacterial activity **[21]**. In both studies it is reported that the antimycobacterial activity of AgNPs is higher than that of gold NPs

(AuNPs), and lower than the bimetallic ones (Au-Ag) despite the mechanism of action of each metal is still under investigation.

Other strategies like combining the effect of biogenic-AgNPs and antimicrobial cationic peptides are being investigated **[22]**, and are revealed as a promising antimycobacterial strategy.

Certain types of NPs, like any other antibiotic, may carry the risk of developing resistance. After exposure to AgNPs, Mycobacterium smegmatis populations resistant to AgNPs and AgNO3 were obtained, and they were cross-resistant to antibiotics as well, although no cross-resistance was observed to other inorganic compounds like CuSO4 and ZnSO4 **[23]**. This suggests that general resistance mechanisms such as efflux pumps could be mediating resistance to these materials, which needs to be properly addressed.

Besides its *in vitro* antibacterial properties, AgNPs have been reported to suppress innate responses of monocyte-derived macrophages in response to *M. tuberculosis* infection **[24]**. This ability of NPs to modulate pathogen-induced immune responses must be further taken into account when one wants to fully understand the impact of NPs in in vivo models of infection.

Gallium (Ga) is a metal very similar to iron (Fe), which is essential for the metabolism and growth of *M. tuberculosis*. Substituting Ga for Fe in the active site of enzymes may render them non-functional, and this is a potential approach for novel antituberculous therapy. Gallium has been reported to present antimicrobial activity against mycobacteria **[25]**, showing efficacy in murine tuberculosis models where *M. tuberculosis* CFUs in the lungs, liver, and spleen of mice decreased when they were treated with gallium nitrate. Nanoformulating the gallium, (GaNP), a sustained release of the metal was obtained, achieving a prolonged action. GaNPs were more efficient than free gallium, and the particles could be targeted to the macrophages, where inhibited growth of *M. tuberculosis* for up to 15 days following single drug loading **[26]**.

Although gold (Au) has been reported to be less active against mycobacteria than silver, thiol conjugated gold NPs show high activity against *M. smegmatis* **[27]**.

Covering iron NPs (FeNPs) with a polysaccharide (chitosan) to load in its surface an antibiotic like streptomycin, produces a new type of magnetic nanocomposite with various properties as a potential tool to both diagnose and treat tuberculosis infections

[28]. Similarly, polyacrylic acid (PAA)-coated iron oxide NPs produces an inhibition in the efflux of drugs in *M. smegmatis*, resulting in synergistic effect of these NPs with rifampicin, isoniazid and norfloxacin **[29]**. Remarkably, this only happens when using the stabilized, coated NPs, and not the PAA or iron NPs alone. So a new use of metallic coated NPs as efflux pumps inhibitors can be considered.

All NPs need to be cleared from the body completely in a reasonable time period. Typically after infection, NPs rapidly distribute into various organs, circulate in the blood and are excreted though the urinary system or in the feces. As metals may accumulate in various organs in the body, it is thus important to investigate the renal and fecal-clearance of inorganic NPs when tested in animal models. Whether a NP can pass through the kidney is strongly dependent on their physical properties (size, charge, shape, etc.) **[30]**. A recent study showed that an increase in particle density correlates with a longer retention times in permeable organs for tumor targeting inorganic NPs **[31]**. However, irrespective of particle size and coating, acute oral exposure to AgNP is associated with predominantly fecal elimination and is not associated with accumulation in tissue or toxicity **[32]**. Many researchers now focus their attention to biodegradable nanoparticles.

NPs as vehicles for effective per os delivery

Oral delivery is the most common and convenient form of drug administration (**Fig. 2**). To be effective, the medicines to be taken per os have to resist to the acidic gastric pH, to be soluble, absorbable through the gastrointestinal (GI) mucus barrier and maintain therapeutic levels in the target organs **[34]**. In this sense, formulations of TB drugs with NPs are being developed to increase their bioavailability, protect the drugs from degradation and release them in a time- and location-controlled manner.

Orally administered NPs must cross the GI mucus barrier, which in vivo has a considerable hydrophobic character due to the presence of lipids. Due to their nature and characteristics, lipid and hydrophobic polymer based NPs are the two dominant types of nanocarriers used for oral drug delivery **[35]**. But in addition to hydrophobicity/hydrophilicity, other characteristics like mucoadhesion, NP surface charge, or particle size are also important parameters to optimize for efficient oral drug delivery **[36]** and to improve absorption of the nanosystems in the GI tract.

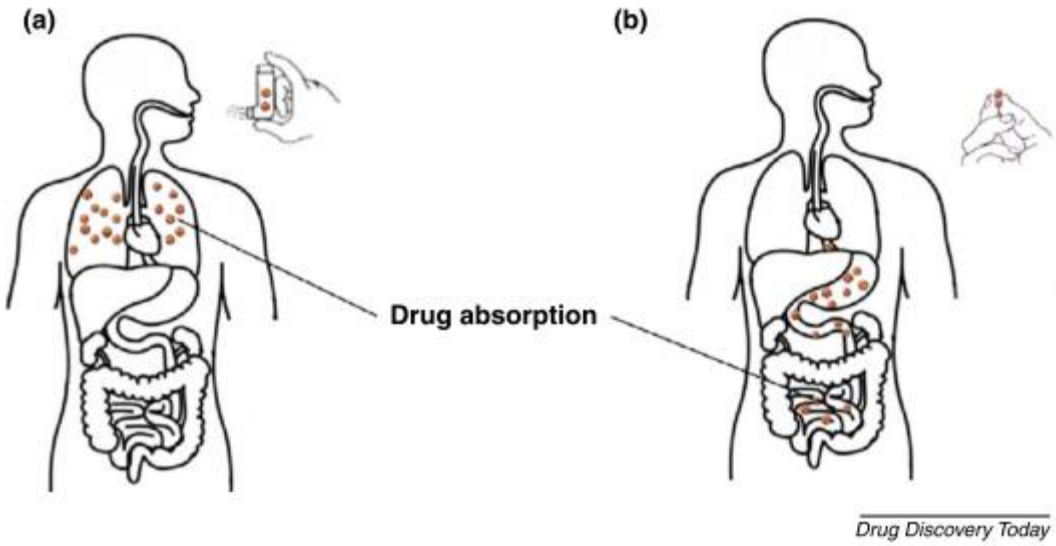

Figure 2. Drug delivery systems for antituberculosis nanoparticles. Whereas pulmonary delivery **(a)** drives nanoparticles directly to the infected organ, the lungs, it is still challenging and requires use of nebulizers or inhalers. Delivery via oral administration **(b)** is simpler but it may encounter difficulties due to stability at acidic pH, absorption in the gastrointestinal tract, etc.

Several NPs have been already reported to be potent carriers for oral administration of antitubercular drugs and the resulting formulations were tested in animal models of TB infection (**Table 2**). As one example, polymeric PLG (poly (lactide-co-glycolide)) loaded with first line drugs [RIF, INH, PZA and EMB], drug levels were maintained 4-5 days in plasma, and 7-9 days in the organs. For this combination of drugs in PLG NPs, 5 oral doses given every 10 days was sufficient

Table 2. Nanocarriers as antimycobacterial drug delivery systems.

	Drug	Nanocarrier	Achievement	Refs
Oral delivery	RIF/INH/PZA/EMB	PLG	Extend drug levels in plasma and lungs Decrease doses in mice and guinea pigs	[38-40]
	RIF/INH/PZA	WGA coated PLG	Improve absorption Decrease doses in guinea pigs	[35] [41]
	ECO/MOXI	WGA coated PLG	Decrease doses in mice	[42]
	LEVO	PLGA	Sustained release and increase level of drugs in the organs	[43]
	SM	PLG	Oral delivery of an injectable drug Increase bioavailability in mice	[44]
	SM	chitosan	Oral delivery of an injectable drug with same efficacy	[45]
	RIF	gelatin	Better biodistribution and higher blood levels in mice	[46]
Pulmonar delivery	INH/RIF	chitosan	Improve *in vitro* and *in vivo* efficacy	[53-55]
	RIF	solid-lipid NPs	Higher RIF levels into alveolvar macrophages *vs* epithelial cells	[56]

Abbreviations: RIF: rifampicin; INH: isoniazid; PZA: pyrazinamide; EMB: ethambutol; PLG: poly (lactide-co-glycolide); WGA: Wheat germ agglutinin; ECO: econazol; MOXI: moxifloxacin; LEVO: levofloxacin; PLGA: poly lactic-co-glycolic acid; SM: streptomycin.

and as efficient in clearing TB infection as 46 daily doses of free drug in mice **[37,38]** or guinea pigs **[39]**. These PLG NPs were able to sterilize the lungs, liver, spleen and also in the meninges **[40]** and this was attributed to improved pharmacokinetics and bioavailability of the drugs upon encapsulation. Further functionalization of these PLG NPs with lectin contributed to improve the relative bioavailability of the drugs. In particular, wheat germ agglutinin (WGA) was used to model NPs in order to improve the absorption because it targets N-acetyl-D-glucosamine and sialic acid, both found ubiquitously throughout the GI tract **[34]**. WGA-coated PLG-NPs were loaded with RIF, INH and PZA, and were administered to guinea pigs through the oral/aerosol route in 3 doses every 15 days. After the treatment, CFUs could not be detected, which is a result comparable with 45 doses of oral free drugs **[41]**. The same type of material has been used to encapsulate other drugs like econazol and moxifloxacin with similar therapeutic

results after oral delivery in mice **[42]**. Another example worth to mention is the use of PLGA for the encapsulation of levofloxacin with promising results in terms of sustained release and levels of the drug in the organs **[43]**.

As said before, oral administration of drugs is usually the best option for treatments and especially for long treatments as for TB therapy. Patients would more likely comply with the treatment if it could be taken per os rather through painful intravenous injections. With that objective, PLGs have been used to encapsulate the injectable drug streptomycin **[44]**. Results in mice reveal 21-fold increase in the bioavailability with respect to the intramuscularly injected streptomycin. In this case, 8 weekly doses are comparable to 24 injections of free streptomycin. Same drug has been loaded in another type of carrier, the polysaccharide chitosan. These particles led to a reduction of one log in growth of bacilli, being as effective as injected streptomycin in aqueous solution at the same concentration **[45]**.

Gelatin nanocarriers are good candidates for the oral delivery as well, due to their biocompatibility, biodegradability, low antigenicity, low cost, and ease of their parenteral use. They have been formulated to vehicle rifampicin, resulting in a better biodistribution and higher blood levels of the drug, which lead to a reduction of the CFUs in lungs and spleen with respect to free rifampicin in mice **[46]**.

Research is still widely active to improve oral administration of the drugs: lipidic and polymeric are the most widely used nanocarriers and more recently polymer-lipid hybrid systems are being investigated **[35]**. These latter show a better drug encapsulation, a modulated drug release, and improved cellular uptake with respect to non-hybrid systems.

We mainly focus here on the use of NPs for drug delivery, but it is worth to mention that similar particles are investigated for the development of vaccines against TB. Oral route was used to administer guar gum NPs loaded with Ag85A **[47]**. The formulation was shown to protect the antigen from the gastric environment, and deliver it to the intestinal region. Moreover, in vivo data indicated that the system induced a strong mucosal as well as systemic immune response, suggesting that it can be utilized for oral delivery of vaccines.

NPs as carriers for pulmonary delivery

Lungs are the primary site for *M. tuberculosis* infection. Upon inhalation of contaminated aerosols, *M. tuberculosis* is deposited in the lungs and is taken up by phagocytic cells, such as macrophages. During active TB, the bacteria replicate actively within granuloma that are multicellular complex structures that the TB drugs must reach **[48]**. Most systemically administered drugs present poor pulmonary distribution and need to be administered in high doses to treat pulmonary TB **[49]**.

Stemming from the successful results obtained for the administration of antibiotics via the pulmonary route for the treatment of pulmonary infections in cystic fibrosis patients since several decades, pulmonary administration of antitubercular drugs has started to be investigated **[50]**. Inhalable antibiotics can be easily self-administered using appropriate devices (**Fig. 2**). The use of this route of administration allows maximal drug delivery to the target site of infection, decrease in drug interactions in the gastrointestinal tract and escaping the hepatic first-pass metabolism **[49,51,52]**. Drugs delivered via pulmonary administration may also produce systemic effects. Lungs have a large surface area covered by a thin epithelium and high perfusion rates, allowing the transport of drug molecules into the systemic circulation **[51]**. As a consequence, drugs administered in the lungs could be detected in various other organs (liver, spleen and kidney) for up to 24 hours after nebulization **[53]**. In particular, chitosan NPs was studied for its ability to increase lung retention and residence time of antibacterial compounds **[54]**. Encapsulation of isoniazid in chitosan NPs improve the efficacy of the parent drug against an *in vitro* model of M. avium infection **[55]** and a mice model of *M. tuberculosis* infection **[53]**.

Another important feature of NPs is that they can increase the selectivity for phagocytic cells, where *M. tuberculosis* usually resides. For instance, higher quantities of rifampicin-loaded solid lipid NPs were delivered of rifampicin into alveolar macrophages **[56]**.

In addition, NPs may act as adjuvants enhancing the immune response. Conjugation of Ag85B antigen with pluronic-stabilized poly(propylene sulphide) NPs proved to improve antigen-specific CD4+ and CD8+ T cell activation when administered in combination with the adjuvant CpG via the pulmonary route **[57]**. They observed that NP-Ag85B and CpG administered via the pulmonary route led to enhanced immune responses and increased the protection of mice against TB, comparing with soluble

Ag85B with CpG and to formulation delivered via the intradermal route. These findings highlight the potential of NP-based formulations delivered through the pulmonary route for the development of novel TB vaccines.

To explore the advantages of lung delivery, inhaled drugs have to be deposited in the deep respiratory airways, where *M. tuberculosis* is normally found. Many parameters influence this deposition, in particular the size, shape, porosity, density, electrostatic charge and aerodynamic diameter of the particles administered **[58]**. For this reason, it is important to study the particles characteristics to evaluate their potential for pulmonary delivery **[59]**. Particles larger than 5 μm undergo deposition in the oropharyngeal region by inertial impaction and they are consequently swallowed **[51,60]**. The optimal particle size for deposition in lower airways after inhalation is commonly accepted to be in the range of 1-3 μm, while particles smaller than 1 μm are believed to be exhaled **[51,60]**. However, studies in the area of environmental toxicology showed that particles smaller than 1 μm are also likely to be deposited in deep lungs by diffusion **[61]**. To render small NPs suitable for deep lung delivery in inhalable dry powder formulations **[62]**, NPs loaded drugs could be further encapsulated in larger microparticles of size ranging from 1 to 5 μm. Alternatively, microparticles in solution may disaggregate in NPs **[63]**.

Besides considering the characteristics of the particles, one should take into account the characteristics of the inhaler device in order to produce an appropriate aerosol. Inhalable liquid formulations are administered using nebulizers and pressurized metered dose inhalers (pMDIs). Nebulizers are particularly useful when high pulmonary doses are required and when the patient is unable to coordinate or achieve flow rates necessary for the use of other inhalation systems **[64]**. PMDIs are the most popular inhaled drug-delivery systems however they are limited by small dose sizes. Inhalable dry powder formulations are administered using dry powder inhalers (DPIs). These formulations are generally more stable than inhalable liquid formulations and usually do not require refrigeration, being therefore suitable for the warm climates normally found in the developing countries where TB is prevalent **[50]**.

In experimental animals the use of nebulizers has several limitations such as imprecision due to the difficulty of measuring the amounts of inhaled drugs and the use of pMDIs or DPIs is not possible since it requires the cooperation of the patient. There are also exposure systems such as whole-body chamber and nose-only chamber for exposing

single or multiple animals to the aerosol. Nose-only chamber has the advantage of minimizing dermal exposure. However, in both systems, there may be loss of materials in the devices before being inhaled. **[65]**. To circumvent that, pulmonary delivery can be performed by intratracheal delivery using a PennCentury MicroSprayer (for inhalable liquids) or a dry powder insufflator **[66]**. In this case, a precise volume of compound is directly sprayed in the lungs.

The use of nano- and microparticles for the development of inhalable antitubercular therapies and vaccines is a promising strategy to fight TB. However, more studies are necessary to evaluate the long-term toxicity of the particles and the effect of excipients used and to discover if this kind of treatment can be used as exclusive therapy or as a combination with the conventional oral therapy.

Functionalization of NPs surface for targeting intracellular *M. tuberculosis*

Macrophages are a major habitat for *M. tuberculosis* to reside in the host for years. Thus, to kill *M. tuberculosis*, one should target these cells and once internalized, the drug should reach the phagosome. NPs offer a promising platform for passively target macrophages by exploiting particle size and administration route. Additionally, there are active strategies to increase the phagocytosis of NPs by macrophages. In this case, the surface of the NP is modified by attaching targeting ligands that bind to molecules specific for the target cells. In fact, macrophages express a broad range of receptors on their surface that mediate recognition and bacterium endocytosis, and that can be targeted by nanocarriers with appropriate ligands (**Table 3**).

The mannose receptor is among the most commonly used for this purpose, since the receptors to this ligand are mainly expressed by macrophages for the recognition of conserved motifs on pathogens. For example, treatment of mannosylated gelatin NPs lead to lower CFUs in the lungs of *M. tuberculosis* infected mice in comparison to treatment of non-mannosylated gelatin particles and free drug **[67]**. As another example, a higher uptake in alveolar macrophages was found for mannosylated cationic nanostructured lipid carriers in comparison with non-mannosylated particles **[68]**. The coupling of loaded-NPs with other sugars, such as lactose, was also reported to enhance

Table 3: Functionalized nanocarriers for antimycobacterial drug delivery

Coating	Drug	Nanocarrier	Achievement	Refs
Mannose	INH	gelatin	Reduce bacteria in TB infected mice Reduce hepatotoxicity of the drug	**[67]**
Mannose	RIF	Cationic lipids	Higher uptake efficiency by alveolar macrophages	**[68]**
Lactose	RIF	PLGA	Increase lung uptake	**[69]**
PEG	MOXI	PLGA	Prolonged blood circulation	**[70]**
Mycolic acids	INH	PLGA	Uptake increase and fusion with lysosomes containing mycobacteria	**[71]**

Abbreviations: INH: isoniazid; RIF: rifampicin; PLGA: poly lactic-co-glycolic acid; PEG: poly ethylene glycol; MOXI: moxifloxacin.

the lung uptake of the drug and particles, in comparison with non-coupled particles and free drug **[69]**.

Surface coating with polyethylene glycol (PEG) is also part of the active targeting strategies. In this case, it inhibits the recognition and phagocytosis by macrophages, prolonging the blood circulation of the drug-loaded NP and decreasing the requirement of repetitive doses **[70]**.

Recently, mycobacterial cell wall mycolic acids were exploited as targeting ligands for drug-encapsulating poly lactic-co-glycolic acid polymer (PLGA) NPs **[71]**. The inclusion of mycolic acids in the nanocarrier resulted on a significant increase in the uptake of NPs and a higher frequency of fusion of NPs-containing phagolysosomes with mycobacterium-containing phagolysosomes **[71]**.

Conclusion and future perspectives

In summary, TB treatment may benefit from the advantages of NPs for several reasons: first, there is a limited number of drugs available for XDR- MDR-TB, many of them presenting important toxicity issues; second, drug resistance is increasing and hence complicating the treatment; and third, although novel drugs have been made available in the last decades, this seems insufficient for coping with the growing

incidence of the disease and the increasing drug resistance of the microorganisms causing these diseases.

When searching for alternative therapeutic approaches to treat TB, we should consider the use of NPs as a promising and worthwhile option, given the lessons we have learnt with fungal infections and amphotericin B liposomal formulations. Indeed, from the nineties, nanoformulations of amphotericin B (a powerful antifungal drug, but having severe toxic side effects) are available **[72]**. These are based on liposomal NPs, and indeed have been successful in retaining drug activity while reducing considerably their toxic effects.

Nanotechnology-mediated drug delivery systems offer many solutions for potential therapeutic agents but they may also offer a variety of challenges for the industrial production of such medicines, mainly the development and regulatory approval costs. However, these difficulties tend to decrease when more products enter in the market and more advanced production methods are developed, a field of study which is currently progressing **[73]**. In addition, it would be of great interest to further develop nanocarriers totally devoid of organic solvents, surfactants and other potentially toxic compounds, not only for their synthesis, but also during the encapsulation steps. Finally, these systems are likely to improve the life quality of the patients and to reduce the overall future health care costs if they reduce the frequency and duration of the treatment, so that the cost-benefit-ratio is favorable.

The long duration of the TB treatment makes drug toxicity more relevant than for other short-term microbial infections, hence NPs could help in reducing doses, targeting specifically infected tissues and organs (mostly the lungs in pulmonary TB, the most frequent form of *M. tuberculosis* disease), and reducing toxicity issues. The cases described in this review have shown a wide diversity of NPs, containing or not additional drugs, having important antimycobacterial activity. These are a solid starting point, a promising guarantee, for thinking of a new future when treating TB, MDR-TB and/or XDR-TB with NPs could come true. If we ask ourselves, how can nanoparticles contribute to antituberculosis therapy, just think of the case of amphotericin B and you will get the answer: hope.

The European community has recently committed to support this area of research through the financing of several research consortia like CycloN-Hit, FORMAMP and NAREB. This very likely that exciting results will come out in the next coming years.

Acknowledgements

The Universidad de Zaragoza is a partner in the European funded consortium NAREB (Nanotherapeutics against resistant emerging bacterial pathogens) (FP7 grant 604237).

Pasteur Institute of Lille is a partner in the European ITN Network “CycloN Hit” (FP7-PEOPLE-2013 n° 608407) and the ANR-TB-NANO (ANR-14-CE08-0017). P. Brodin is recipient of ERC-STG INTRACELLTB Grant n° 260901. Both teams acknowledge support from the More Medicines for Tuberculosis (MM4TB) consortium (Grant n°260872). We thank Ruxandra Gref and Arnaud Machelart for critical reading of the manuscript.

Conflicts of interest

The authors declare that they have no competing financial interest.

References

1 WHO. (2016) Global Tuberculosis Report 2016.

2 WHO. (2014) The use of delamanid in the treatment of multidrug-resistant tuberculosis.

3 WHO. (2013) Interim guidance on the use of bedaquiline to treat MDR-TB.

4 Morones, J.R. et al. (2005) The bactericidal effect of silver nanoparticles. Nanotechnology 16 (10), 2346-2353

5 Ruparelia, J.P. et al. (2008) Strain specificity in antimicrobial activity of silver and copper nanoparticles. Acta Biomater 4 (3), 707-716

6 Veerapandian, M. and Yun, K. (2011) Functionalization of biomolecules on nanoparticles: specialized for antibacterial applications. Appl Microbiol Biotechnol 90 (5), 1655-1667

7 Hajipour, M.J. et al. (2012) Antibacterial properties of nanoparticles. Trends Biotechnol 30 (10), 499-511

8 Bondarenko, O. et al. (2012) Sub-toxic effects of CuO nanoparticles on bacteria: kinetics, role of Cu ions and possible mechanisms of action. Environ Pollut 169, 81-89

9 Griffiths, G. et al. (2010) Nanobead-based interventions for the treatment and prevention of tuberculosis. Nat Rev Microbiol 8 (11), 827-834

10 Morones-Ramirez, J.R. et al. (2013) Silver enhances antibiotic activity against gram-negative bacteria. Sci Transl Med 5 (190), 190ra181

11 Rai, M. et al. (2009) Silver nanoparticles as a new generation of antimicrobials. Biotechnol Adv 27 (1), 76-83

12 Choi, O. et al. (2008) The inhibitory effects of silver nanoparticles, silver ions, and silver chloride colloids on microbial growth. Water Res 42 (12), 3066-3074

13 Donnellan, S. et al. (2016) A rapid screening assay for identifying mycobacteria targeted nanoparticle antibiotics. Nanotoxicology, 1-9

14 Gnanadhas, D.P. et al. (2013) Interaction of silver nanoparticles with serum proteins affects their antimicrobial activity in vivo. Antimicrob Agents Chemother 57 (10), 4945-4955

15 Saeb, A.T. et al. (2014) Production of silver nanoparticles with strong and stable antimicrobial activity against highly pathogenic and multidrug resistant bacteria. ScientificWorldJournal 2014, 704708

16 Yuan, Z. et al. (2013) Interaction of silver nanoparticles with pure nitrifying bacteria. Chemosphere 90 (4), 1404-1411

17 Sharma, V.K. et al. (2009) Silver nanoparticles: green synthesis and their antimicrobial activities. Adv Colloid Interface Sci 145 (1-2), 83-96

18 Iravani, S. et al. (2014) Synthesis of silver nanoparticles: chemical, physical and biological methods. Res Pharm Sci 9 (6), 385-406

19 Kora, A.J. et al. (2012) Size-controlled green synthesis of silver nanoparticles mediated by gum ghatti (Anogeissus latifolia) and its biological activity. Organic and Medicinal Chemistry Letters 2, 17-17

20 Singh, R. et al. (2015) Chemical and biological metal nanoparticles as antimycobacterial agents: A comparative study. Int J Antimicrob Agents 46 (2), 183-188

21 Singh, R. et al. (2016) Phytogenic silver, gold, and bimetallic nanoparticles as novel antitubercular agents. Int J Nanomedicine 11, 1889-1897

22 Mohanty, S. et al. (2013) Cationic antimicrobial peptides and biogenic silver nanoparticles kill mycobacteria without eliciting DNA damage and cytotoxicity in mouse macrophages. Antimicrob Agents Chemother 57 (8), 3688-3698

23 Larimer, C. et al. (2014) Mutation of environmental mycobacteria to resist silver nanoparticles also confers resistance to a common antibiotic. Biometals 27 (4), 695-702

24 Sarkar, S. et al. (2015) Modulation of Human Macrophage Responses to Mycobacterium tuberculosis by Silver Nanoparticles of Different Size and Surface Modification. PLoS One 10 (11), e0143077

25 Olakanmi, O. et al. (2013) Gallium nitrate is efficacious in murine models of tuberculosis and inhibits key bacterial Fe-dependent enzymes. Antimicrob Agents Chemother 57 (12), 6074-6080

26 Narayanasamy, P. et al. (2015) Prolonged-acting, multi-targeting gallium nanoparticles potently inhibit growth of both HIV and mycobacteria in co-infected human macrophages. Sci Rep 5, 8824

27 Gifford, J.C. et al. (2014) Thiol-modified gold nanoparticles for the inhibition of Mycobacterium smegmatis. Chem Commun (Camb) 50 (100), 15860-15863

28 El Zowalaty, M.E. et al. (2015) The ability of streptomycin-loaded chitosan-coated magnetic nanocomposites to possess antimicrobial and antituberculosis activities. Int J Nanomedicine 10, 3269-3274

29 Padwal, P. et al. (2014) Polyacrylic acid-coated iron oxide nanoparticles for targeting drug resistance in mycobacteria. Langmuir 30 (50), 15266-15276

30 Liu, J. et al. (2013) Renal clearable inorganic nanoparticles: a new frontier of bionanotechnology. Materials Today 16 (12), 477-486

31 Tang, S. et al. (2016) Tailoring Renal Clearance and Tumor Targeting of Ultrasmall Metal Nanoparticles with Particle Density. Angewandte Chemie International Edition 55 (52), 16039-16043

32 Bergin, I.L. et al. (2016) Effects of particle size and coating on toxicologic parameters, fecal elimination kinetics and tissue distribution of acutely ingested silver nanoparticles in a mouse model. Nanotoxicology 10 (3), 352-360

33 Pyrgiotakis, G. et al. (2014) Mycobacteria inactivation using Engineered Water Nanostructures (EWNS). Nanomedicine 10 (6), 1175-1183

34 Ensign, L.M. et al. (2012) Oral drug delivery with polymeric nanoparticles: the gastrointestinal mucus barriers. Adv Drug Deliv Rev 64 (6), 557-570

35 Rao, S. and Prestidge, C.A. (2016) Polymer-lipid hybrid systems: merging the benefits of polymeric and lipid-based nanocarriers to improve oral drug delivery. Expert Opin Drug Deliv 13 (5), 691-707

36 Desai, M.P. et al. (1996) Gastrointestinal uptake of biodegradable microparticles: effect of particle size. Pharm Res 13 (12), 1838-1845

37 Pandey, R. et al. (2006) Oral poly(lactide-co-glycolide) nanoparticle based antituberculosis drug delivery: toxicological and chemotherapeutic implications. Indian J Exp Biol 44 (6), 459-467

38 Pandey, R. et al. (2006) Chemotherapeutic efficacy of nanoparticle encapsulated antitubercular drugs. Drug Deliv 13 (4), 287-294

39 Johnson, C.M. et al. (2005) Oral therapy using nanoparticle-encapsulated antituberculosis drugs in guinea pigs infected with Mycobacterium tuberculosis. Antimicrob Agents Chemother 49 (10), 4335-4338

40 Pandey, R. and Khuller, G.K. (2006) Oral nanoparticle-based antituberculosis drug delivery to the brain in an experimental model. J Antimicrob Chemother 57 (6), 1146-1152

41 Sharma, A. et al. (2004) Lectin-functionalized poly (lactide-co-glycolide) nanoparticles as oral/aerosolized antitubercular drug carriers for treatment of tuberculosis. J Antimicrob Chemother 54 (4), 761-766

42 Ahmad, Z. et al. (2008) Novel chemotherapy for tuberculosis: chemotherapeutic potential of econazole- and moxifloxacin-loaded PLG nanoparticles. Int J Antimicrob Agents 31 (2), 142-146

43 Kumar, G. et al. (2012) Optimization, *in vitro*-in vivo evaluation, and short-term tolerability of novel levofloxacin-loaded PLGA nanoparticle formulation. J Pharm Sci 101 (6), 2165-2176

44 Pandey, R. and Khuller, G.K. (2007) Nanoparticle-based oral drug delivery system for an injectable antibiotic - streptomycin. Evaluation in a murine tuberculosis model. Chemotherapy 53 (6), 437-441

45 Lu, E. et al. (2009) Preparation of aminoglycoside-loaded chitosan nanoparticles using dextran sulphate as a counterion. J Microencapsul 26 (4), 346-354

46 Saraogi, G.K. et al. (2010) Gelatin nanocarriers as potential vectors for effective management of tuberculosis. Int J Pharm 385 (1-2), 143-149

47 Kaur, M. et al. (2015) Development and characterization of guar gum nanoparticles for oral immunization against tuberculosis. Drug Deliv 22 (3), 328-334

48 (2016) Global Tuberculosis Report 2016 WHO

49 Hickey, A.J. et al. (2015) Inhaled drug treatment for tuberculosis: Past progress and future prospects. J Control Release

50 Hanif, S.N. and Garcia-Contreras, L. (2012) Pharmaceutical aerosols for the treatment and prevention of tuberculosis. Front Cell Infect Microbiol 2, 118

51 Mehanna, M.M. et al. (2014) Respirable nanocarriers as a promising strategy for antitubercular drug delivery. J Control Release 187, 183-197

52 Pham, D.D. et al. (2015) Pulmonary drug delivery systems for tuberculosis treatment. Int J Pharm 478 (2), 517-529

53 Garg, T. et al. (2016) Inhalable chitosan nanoparticles as antitubercular drug carriers for an effective treatment of tuberculosis. Artif Cells Nanomed Biotechnol 44 (3), 997-1001

54 Andrade, F. et al. (2011) Chitosan formulations as carriers for therapeutic proteins. Curr Drug Discov Technol 8 (3), 157-172

55 Pourshahab, P.S. et al. (2011) Preparation and characterization of spray dried inhalable powders containing chitosan nanoparticles for pulmonary delivery of isoniazid. J Microencapsul 28 (7), 605-613

56 Chuan, J. et al. (2013) Enhanced rifampicin delivery to alveolar macrophages by solid lipid nanoparticles. Journal of Nanoparticle Research 15 (5), 1-9

57 Ballester, M. et al. (2011) Nanoparticle conjugation and pulmonary delivery enhance the protective efficacy of Ag85B and CpG against tuberculosis. Vaccine 29 (40), 6959-6966

58 Costa, A. et al. (2016) The formulation of nanomedicines for treating tuberculosis. Adv Drug Deliv Rev 102, 102-115

59 Abdulla, J.M. et al. (2010) Rehydrated lyophilized rifampicin-loaded mPEG-DSPE formulations for nebulization. AAPS PharmSciTech 11 (2), 663-671

60 Andrade, F. et al. (2013) Nanotechnology and pulmonary delivery to overcome resistance in infectious diseases. Adv Drug Deliv Rev 65 (13-14), 1816-1827

61 Carvalho, T.C. et al. (2011) Influence of particle size on regional lung deposition--what evidence is there? Int J Pharm 406 (1-2), 1-10

62 Weber, S. et al. (2014) Solid Lipid Nanoparticles (SLN) and Nanostructured Lipid Carriers (NLC) for pulmonary application: a review of the state of the art. Eur J Pharm Biopharm 86 (1), 7-22

63 Vadakkan, M.V. et al. (2013) Dry powder cationic lipopolymeric nanomicelle inhalation for targeted delivery of antitubercular drug to alveolar macrophage. Int J Nanomedicine 8, 2871-2885

64 Chan, J.G. et al. (2014) Advances in device and formulation technologies for pulmonary drug delivery. AAPS PharmSciTech 15 (4), 882-897

65 Wong, B.A. (2007) Inhalation exposure systems: design, methods and operation. Toxicol Pathol 35 (1), 3-14

66 Misra, A. et al. (2011) Inhaled drug therapy for treatment of tuberculosis. Tuberculosis (Edinb) 91 (1), 71-81

67 Saraogi, G.K. et al. (2011) Mannosylated gelatin nanoparticles bearing isoniazid for effective management of tuberculosis. J Drug Target 19 (3), 219-227

68 Song, X. et al. (2015) Rifampicin loaded mannosylated cationic nanostructured lipid carriers for alveolar macrophage-specific delivery. Pharm Res 32 (5), 1741-1751

69 Jain, S.K. et al. (2010) Lactose-Conjugated PLGA Nanoparticles for Enhanced Delivery of Rifampicin to the Lung for Effective Treatment of Pulmonary Tuberculosis. PDA J Pharm Sci Technol 64 (3), 278-287

70 Mustafa, S. et al. (2016) Effect of PEG and water-soluble chitosan coating on moxifloxacin-loaded PLGA long-circulating nanoparticles. Drug Deliv Transl Res

71 Lemmer, Y. et al. (2015) Mycolic acids, a promising mycobacterial ligand for targeting of nanoencapsulated drugs in tuberculosis. J Control Release 211, 94-104

72 Voltan, A.R. et al. (2016) Fungal diseases: could nanostructured drug delivery systems be a novel paradigm for therapy? Int J Nanomedicine 11, 3715-3730

73 Elahian, F. et al. (2016) High-throughput bioaccumulation, biotransformation, and production of silver and selenium nanoparticles using genetically engineered Pichia pastoris. Nanomedicine: Nanotechnology, Biology and Medicine

2. OBJECTIVES / OBJECTIFS

Les thérapies actuelles échouent souvent à cause de concentration insuffisante de médicament au niveau des sites d'infection et de leur métabolisme et excrétion rapide. De plus, les voies d'administration de certains antibiotiques sont limitées et spécifiques, en raison de leurs caractéristiques de solubilité et de stabilité.

En collaboration avec les différents partenaires du réseau de formation innovante "CycloN-Hit" constitué dans le cadre du programme européen d'Actions Marie Curie, cette thèse visait à développer des nanoparticules (NP) pour surmonter les problèmes précédemment mentionnés. Le but principal de cette thèse était d'étudier l'utilisation de nanoparticules comme nanocarriers pour administrer les antibiotiques directement au niveau des poumons, et améliorer la solubilité et la biodisponibilité, ainsi que la pénétration intracellulaire des antibiotiques.

Cette thèse avait également pour objectif d'explorer l'activité anti-mycobacterienne intrinsèque des NP.

Atteindre ces buts était important pour développer un nouveau concept de thérapie antibiotique contre TB capable d'atteindre l'agent pathogène dans sa niche de réplication et à combattre ainsi efficacement les cas de tuberculose (TB) sensibles et résistants aux antibiotiques.

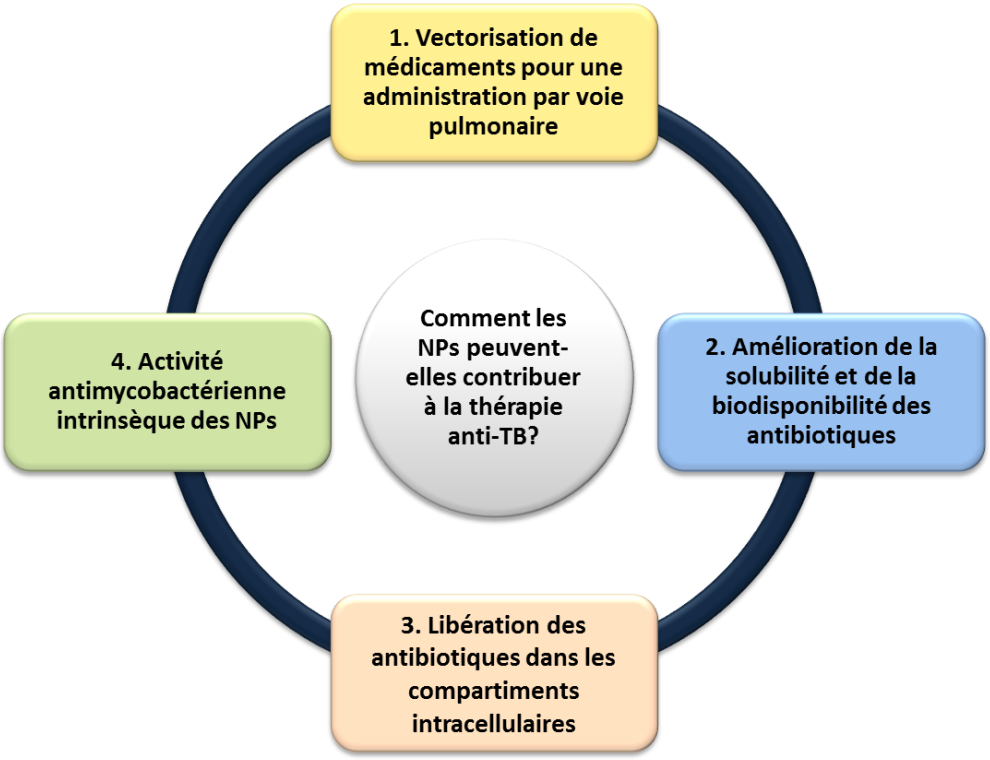

Current therapies often fail because of insufficient drug concentration in the infected areas and fast drug metabolism and excretion. Moreover, some drugs are limited to be used by specific administration routes due to their solubility characteristics and stability inappropriate for other administration routes.

In active collaboration with different partners from the European Union Marie Curie Initial Training Network "CycloN-Hit", this thesis aimed to develop nanoparticles (NPs) to overcome the problems mentioned above. Therefore, the main goals of this thesis were to investigate the use of nanoparticles as nanocarriers:

I. For pulmonary delivery of drugs.
II. To enhance solubility and bioavailability of antibiotics.
III. To improve antibiotic intracellular penetration.

Additionally, this thesis also aimed to:

IV. Explore the intrinsic antimycobacterial activity of NPs.

Addressing these goals will be important to develop a new concept of drug therapy to efficiently combat drug-susceptible and drug-resistant tuberculosis (TB), able to chase the pathogen from its hideout and thus paving the way for the development of new therapeutics means against TB.

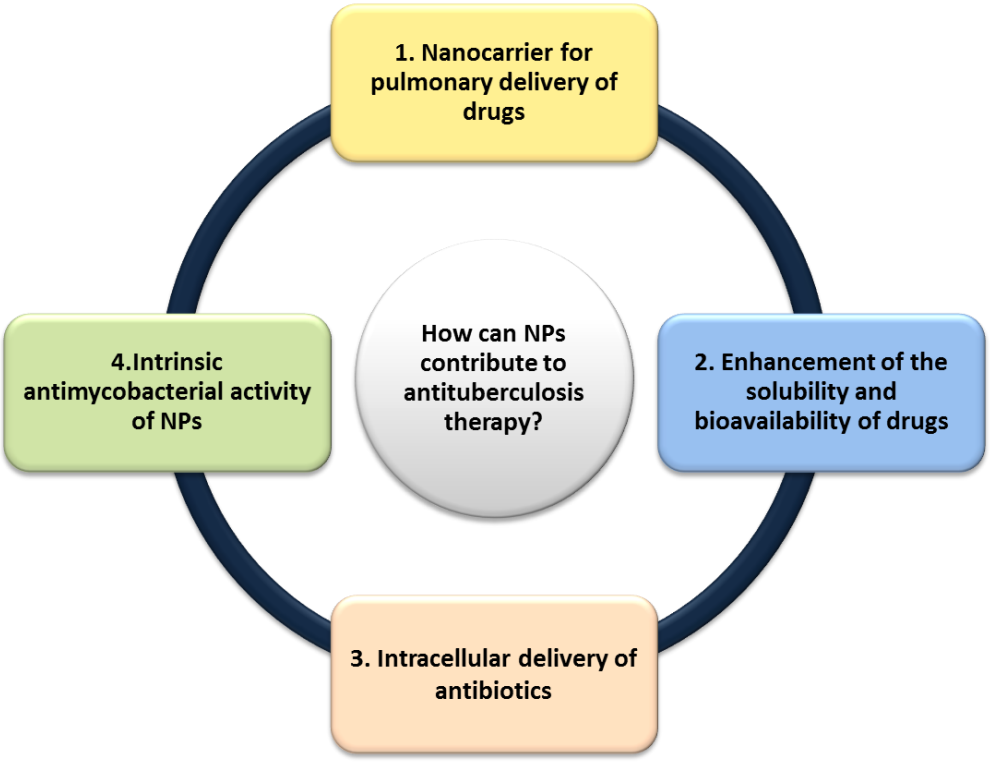

3. CHAPTER I

Nanocarrier for pulmonary delivery of drugs

Vectorisation de médicaments pour une administration par voie pulmonaire

3.1. Résumé article 1: “Thérapie de combinaison pour le traitement de tuberculose: administration pulmonaire d'éthionamide et d'un booster encapsulés dans des nanoparticules”

L'éthionamide (ETH) est le principal antibiotique de seconde ligne utilisé pour le traitement antituberculeux, mais il est à l’origine d’effets secondaires sévères.

L’ETH est une “pro-drogue”, qui nécessite une bioactivation par la bactérie Mtb (via la monooxygenase bactérienne ethA). Chez Mtb, l’expression d’ethA est inhibée par une autre enzyme ethR, responsable d’une diminution de la transformation de la prodrogue (Baulard, Betts et al. 2000). Des molécules ligands, appelées “booster”, ont été récemment développées (Willand, Dirie et al. 2009). Ces boosters sont capables d’inhiber l’action d’ethR et ainsi d’augmenter l’expression d’ethA et la métabolisation de la prodrogue (Blondiaux, Moune et al. 2017).

L’utilisation de ces molécules permet d’une part de diminuer la dose utilisée de l’ETH, réduisant ainsi la toxicité du traitement, et améliore d’autre part fortement son efficacité vis-à-vis des souches résistantes (Bivas-Benita, Ottenhoff et al. 2005). Leur utilisation offre ainsi de nouvelles perspectives pour combattre les cas de TB résistants aux médicaments existants.

Pour augmenter l’efficacité du traitement, une autre stratégie consiste à cibler Mtb principalement localisé dans les macrophages pulmonaires et à favoriser l’entrée les composés antituberculeux sous forme d’aérosols directement dans les poumons. Au vue des données bibliographiques, l’encapsulation de composés antituberculeux dans des nanoparticules (NP) constitue une approche prometteuse (Costa, Pinheiro et al. 2016).

Dans cette étude, nous avons évalué l’effet de l’ETH et du booster BDM41906 (Flipo, Desroses et al. 2012) ([ETH:Booster]) co-encapsulés dans des NP et administrés directement dans les poumons, pour le traitement de TB.

Différents types de NP ont été préalablement sélectionnés sur la base des données bibliographiques: (i) les NP à base de copolymères d’acide poly(lactique-*co*-glycolique) (PLGA) biodégradables et d’acide poly(lactique) (PLA), pour lesquelles une biocompatibilité et la biodégradabilité étaient bien documentées ; et (ii) les NP de poly-β-cyclodextrine (pCD), présentaient également une biocompatibilté chez l’homme bien établie et l’avantage d’être bien tolérée *in vivo* grâce notamment au procédé

d'encapsulation utilisé (dite « verte »), ne nécessitant pas l'utilisation de solvants organiques (Gref, Amiel et al. 2006; Zuckerman, Gritli et al. 2014).

Nos collaborateurs ont co-encapsulé les 2 composés dans ces différentes NP et caractérisés celles-ci d'un point de vue de la taille et de l'efficacité de l'incorporation de [ETH:Booster]. Cette encapsulation nous a permis d'une part de nous aguerrir des obstacles majeurs liés à la cristallisation de l'ETH et la faible solubilité du booster dans l'eau. De façon intéressante, les NP de poly-β-cyclodextrine (pCD) permettent notamment l'incorporation en une seule étape de [ETH:Booster].

Pour étudier l'efficacité de différentes formulations de [ETH:Booster] co-encapsulés contre Mtb, nous avons réalisé au sein de notre laboratoire 2 essais phénotypiques, qui consistaient à comparer l'effet de NP chargées, des NP vides et du couple [ETH:Booster] non encapsulés, sur la croissance (i) extracellulaire et (ii) intracellulaire de *Mycobacterium tuberculosis* (dans des macrophages murins infectés par Mtb*)*, grâce à l'utilisation d'un système de microscopie confocale à haut contenu automatisé (OPERA-PerkinElmer). Dans les deux essais, nous avons constaté que les médicaments conservaient leur activité après encapsulation et que les NP n'étaient pas cytotoxiques.

Les NP de poly-β-cyclodextrine (pCD) ont été choisies pour la suite de notre étude *in vivo*.

Nous avons étudié l'efficacité de ces NP chargées de [ETH:Booster] *in vivo* chez des souris infectées avec Mtb par voie intranasale. La suspension de NP a été délivrée sous forme d'aérosols directement dans les poumons par voie endotrachéale à l'aide d'un Microsprayer® Aerosolizer. Une réduction significative de la charge bactérienne dans les poumons de 3 log a été observée après 6 administrations de doses inférieures à celles thérapeutiques.

En conclusion, nous avons proposé une approche thérapeutique originale combinant l'utilisation de molécules boosters et de nanotechnologies pour améliorer les traitements existants de la tuberculose.

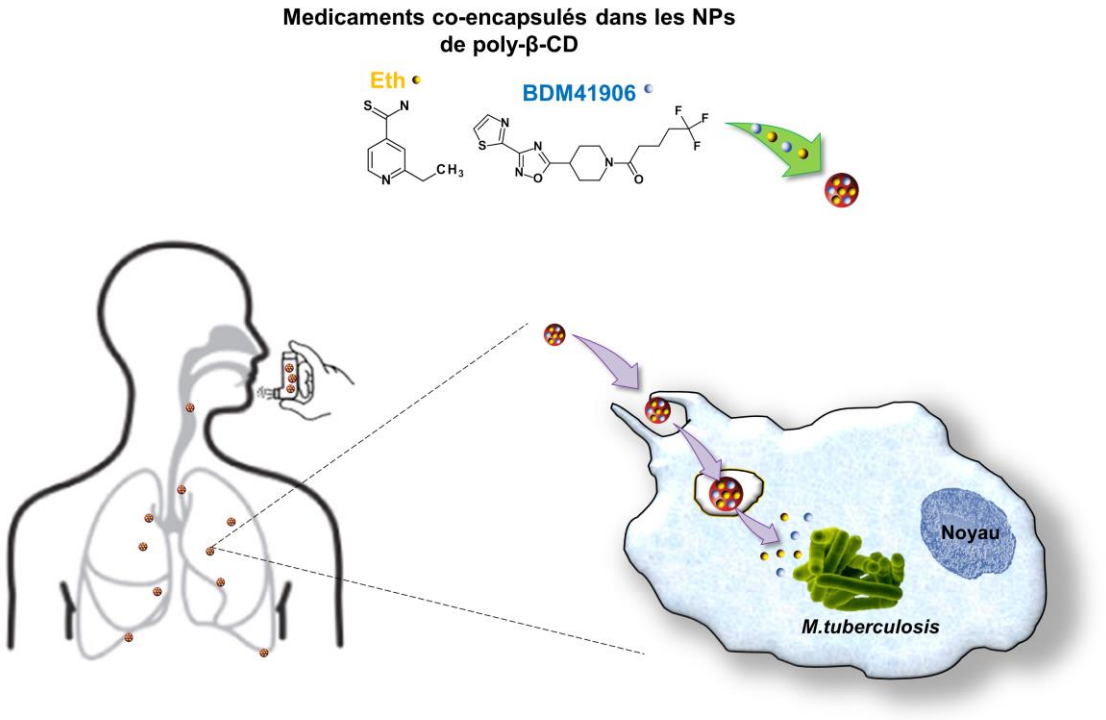

Figure de résumé: Administration pulmonaire de nanoparticules de poly-β-cyclodextrines chargées avec l'ethionamide et un de ses boosters (BDM41906) dans des macrophages infectés avec Mtb.

3.2. Summary article 1: "Combination therapy for tuberculosis treatment: pulmonary administration of ethionamide and booster co-loaded nanoparticles"

Our objective was to develop nanoparticulate carriers for a more adapted treatment of tuberculosis (TB), a leading infection cause of death worldwide. The use of Ethionamide (ETH), the main second line antituberculosis drug, is hampered by low oral bioavailability and the onset of severe side effects. It has been demonstrated that the current clinical outcome of TB could be improved by the recently discovered "Booster" molecules, which strongly increase the efficacy of ETH. However, the administration of the synergic [ETH:Booster] pair is very challenging, as the two molecules possess completely different physico-chemical properties and biodistributions. Moreover, ETH has a strong tendency to crystallize in aqueous media.

To achieve the objective of drug co-administration, we simultaneously co-encapsulated ETH and Booster in nanoparticles able to be administered by pulmonary route, to reach the main site of TB infection in the lungs. To do so, various encapsulation strategies and nanocarriers were considered. Drugs were incorporated in biodegradable polymeric β-cyclodextrin (pCD) nanoparticles. Advantageously, encapsulation in the CD-based nanoparticles enabled circumventing the bottlenecks inherent to the strong tendency of ETH to crystallize and poor solubility of Booster, without using any organic solvent in the encapsulation process.

We report for the first time the use of an automated confocal high content screening platform to study the effect of drug-loaded nanoparticles on *M. tuberculosis* infected cells. The drugs maintained their activity after incorporation in the nanocarriers.

Given these satisfactory results, drug-loaded nanoparticles were further investigated for their antituberculosis property in an *in vivo* model of infection. Nanoparticles based on CDs, which showed the best physiochemical characteristics, were selected for these studies.

The nanoparticles co-loaded with ETH and Booster were administered *in vivo* via pulmonary route in mice that have been priory challenged with *M. tuberculosis*. Compared to untreated mice, the treatment with CD nanoparticles containing the drug combination lead to a significant decrease of the pulmonary bacterial load. Noteworthy, the results were achieved with only three administrations. This study paves the way for a future use of CD-nanoparticles for the delivery of the synergic [ETH:Booster] pair to

infected lungs. Our approach could be used as a supplement to the standard treatment to content the *M. tuberculosis* pulmonary manifestations of the disease and to prevent its dissemination. It may be also considered useful for prevention use for healthy people in contact with TB patients, in order to contain an initial lung infection avoiding the toxicity often associated with oral drug administrations.

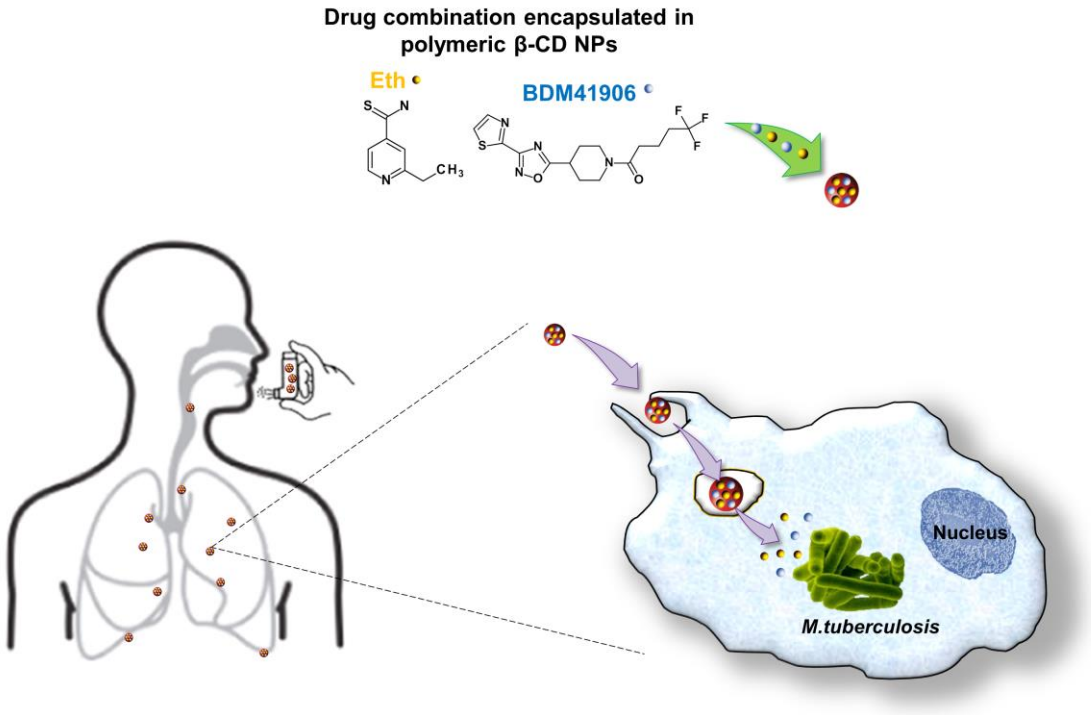

Graphical abstract: Pulmonary delivery of polymeric β-cyclodextrin nanoparticles loaded with ethionamide and one of its boosters (BDM41906) into the Mtb-infected macrophages in the lungs.

SCIENTIFIC REPORTS

OPEN

Combination therapy for tuberculosis treatment: pulmonary administration of ethionamide and booster co-loaded nanoparticles

Received: 14 March 2017
Accepted: 24 May 2017
Published online: 14 July 2017

Joana Costa-Gouveia[1], Elisabetta Pancani[2], Samuel Jouny[1], Arnaud Machelart[1], Vincent Delorme[1], Giuseppina Salzano[2], Raffaella Iantomasi[1], Catherine Piveteau[3], Christophe J. Queval[1], Ok-Ryul Song[1], Marion Flipo[3], Benoit Deprez[3], Jean-Paul Saint-André[4], José Hureaux[4], Laleh Majlessi[5], Nicolas Willand[3], Alain Baulard[1], Priscille Brodin[1] & Ruxandra Gref[2]

Tuberculosis (TB) is a leading infectious cause of death worldwide. The use of ethionamide (ETH), a main second line anti-TB drug, is hampered by its severe side effects. Recently discovered "booster" molecules strongly increase the ETH efficacy, opening new perspectives to improve the current clinical outcome of drug-resistant TB. To investigate the simultaneous delivery of ETH and its booster BDM41906 in the lungs, we co-encapsulated these compounds in biodegradable polymeric nanoparticles (NPs), overcoming the bottlenecks inherent to the strong tendency of ETH to crystallize and the limited water solubility of this Booster. The efficacy of the designed formulations was evaluated in TB infected macrophages using an automated confocal high-content screening platform, showing that the drugs maintained their activity after incorporation in NPs. Among tested formulations, "green" β-cyclodextrin (pCD) based NPs displayed the best physico-chemical characteristics and were selected for *in vivo* studies. The NPs suspension, administered directly into mouse lungs using a Microsprayer®, was proved to be well-tolerated and led to a 3-log decrease of the pulmonary mycobacterial load after 6 administrations as compared to untreated mice. This study paves the way for a future use of pCD NPs for the pulmonary delivery of the [ETH:Booster] pair in TB chemotherapy.

Despite the development of modern medicine, tuberculosis (TB) is still a major health problem. About one-third of the world's population is infected with *Mycobacterium tuberculosis*, the bacterium that causes TB. According to WHO, 10.4 million people had active TB and 1.8 million people died of TB in 2015[1]. Lungs are the primary site for *M. tuberculosis* infection. When a patient with active TB sneezes, coughs or spits, the droplets containing bacteria can be inhaled by surrounding people who can become infected. *M. tuberculosis* is a facultative intracellular bacterium, able to survive and multiply inside phagocytes such as macrophages by subverting the effector functions of these important innate immune cells. *M. tuberculosis* can persist in the host in a dormant state for a long period of time so that the risk of reactivation, even decades after infection, exists[2].

TB can usually be treated with a daily six months course of standard, or first-line, anti-TB drugs. If first-line drugs are misused or mismanaged, the onset of multidrug-resistant TB (MDR-TB) can occur. MDR-TB is defined as TB caused by strains that are resistant to at least isoniazid (INH) and rifampicin (RIF), two powerful first-line anti-TB drugs. MDR-TB takes up to two years of chemotherapy with second-line drugs such as ethionamide

[1]Univ. Lille, CNRS, INSERM, CHU Lille, Institut Pasteur de Lille, U1019 - UMR 8204 - CIIL - Center for Infection and Immunity of Lille, F-59000, Lille, France. [2]University of Paris-Sud, University Paris-Saclay, CNRS, UMR 8214 - Institute for Molecular Sciences of Orsay (ISMO), 91405, Orsay, France. [3]Univ. Lille, INSERM, Institut Pasteur de Lille, U1177 - Drugs and Molecules for living Systems, F-59000, Lille, France. [4]University Hospital Center of Angers, 49000, Angers, France. [5]Pathogénomique Mycobactérienne Intégrée, Département de Génomes et Génétique, Institut Pasteur, Paris, France. Joana Costa-Gouveia and Elisabetta Pancani contributed equally to this work. Benoit Deprez, Nicolas Willand, Priscille Brodin and Ruxandra Gref jointly supervised this work. Correspondence and requests for materials should be addressed to P.B. (email: priscille.brodin@inserm.fr) or R.G. (email: ruxandra.gref@u-psud.fr)

(ETH), fluoroquinolones or aminoglycosides, which are less effective and/or induce more severe side effects than the first-line drugs[3].

Despite its usefulness, ETH exhibits reduced *in vivo* half-life and high toxicity[4]. To achieve an effective serum concentration of ETH through oral administration, doses of at least 500 mg are required[5]. However, adherence to such doses is difficult for the patients because of adverse side effects occurring mainly in the gastrointestinal tract and in the liver[4].

ETH is a prodrug that requires bioactivation. This process is mediated by the bacterial monooxygenase EthA, which is under the control of the transcriptional repressor EthR. The relative low level of ETH bioactivation by EthA is largely responsible for the low sensitivity of *M. tuberculosis* to this antibiotic[6,7]. Recently, molecules inducing conformational changes in EthR, leading to the inhibition of its repressor function, have been discovered[8]. These molecules were found to considerably enhance the activity of ETH and were called "ETH boosters" or more simply "boosters". It was observed in a TB-infected mouse model that the intraperitoneal administration of a booster in combination with an oral administration of ETH significantly increased the antimycobacterial activity of ETH, as compared with the single drug at the same dose[8].

As lungs are the major site of *M. tuberculosis* infection, administration by the pulmonary route could be a valid strategy to improve the efficacy of the [ETH:booster] pair. This strategy could provide higher drug concentrations at the target site and less systemic side effects as compared to other administration routes[9–11]. Some examples are described with other anti-TB drugs such as RIF, INH and pyrazinamide (PZA), encapsulated in poly(D,L-lactic-co-glycolic acid) (PLGA)[12] or alginate[13] nanoparticles (NPs). In the guinea pig TB preclinical model, only few administrations of aerosolized NPs were required to reach the same effects as those obtained with free anti-TB drugs delivered daily by oral route. Nowadays, intrapulmonary aerosol delivery of anti-TB drugs is considered as a promising alternative strategy able to reduce at the same time doses, dose frequency and systemic side effects[14].

In this context, we questioned whether the [ETH:booster] pair could be administered directly to the lungs by means of engineered NPs[15]. The use of NPs to effectively solubilise a variety of poorly soluble pharmaceutical agents, including antibiotics, is currently at the forefront of drug delivery research. However, the efficient incorporation of these molecules has to overcome technological barriers. For instance, booster molecules do not have sufficient water solubility for *in vivo* efficacy (below mg/mL)[16] and have low affinity for most of the biodegradable materials used to prepare NPs. ETH was already encapsulated in colloidal systems[17], microparticles[18,19] and PLGA NPs[20]. However, the strong tendency of ETH to crystallize in aqueous environments as well as in biological fluids makes its incorporation in a nanocarrier particularly difficult[20]. To address the challenges related to the co-encapsulation of ETH with the booster BDM41906[16] (hereby referred to as Booster), we considered investigating NPs made of biodegradable PLGA and poly(lactic acid) (PLA) copolymers and NPs of polymeric β-cyclodextrins (pCD).

PLA and PLGA (co)polymers are the most employed materials to formulate NPs because of their well-documented biocompatibility and biodegradability. Already approved by the Food and Drug Administration (FDA), they form a versatile family allowing to tune the NPs encapsulation and release properties according to their chemical composition (glycolic/lactic acid ratio) and their molecular weight (MW).

Cyclodextrins (CDs) are a family of biocompatible cyclic oligosaccharides made of α-D-glucopyranose units joined through $\alpha(1 \rightarrow 4)$ linkages in a circular way to form a ring with a hydrophilic exterior and a hydrophobic cavity, in which many active agents can be hosted. For example, hydroxypropyl β-CD were used to solubilize the Booster, in order to assess the pharmacokinetic profile of this drug[16]. Many CD-based derivatives are widely used as delivery systems for their well-established biocompatibility in humans, due to their low toxicity and absence of immune stimulation even at high dosage[21–23]. Advantageously, polymeric CD (pCD) NPs were well-tolerated *in vivo* and were found to efficiently incorporate a series of active molecules without the need of organic solvents[24–28].

In all cases, the NPs developed here were characterized by colloidal sizes, narrow size distributions and high incorporation efficiencies of the [ETH:Booster] pair. Interestingly, the pCD NPs allowed for an efficient one-step incorporation of both ETH and Booster by a "green" procedure, meaning without using any organic solvent.

To investigate the efficacy of drug-loaded NPs against *M. tuberculosis*, we used two phenotypic assays that are disease-relevant and amenable to high-throughput. The first one is a photometer-based assay relying on the monitoring of fluorescence from green fluorescence protein (GFP)-expressing *M. tuberculosis* strain. The second is an image-based model that allows the multi-parametric quantification of *M. tuberculosis* replication inside its favourite niche, the macrophage. The latter high-content imaging method has now been successfully implemented in several laboratories for drug discovery purpose[29–33]. Indeed there is more and more consensus that this technology is as reliable as CFU counting for the quantification of bacterial load and moreover, it has the advantage of giving additional information on the cytotoxicity of the studied compounds, which is here of main importance for testing NP formulations.

In vitro studies on *M. tuberculosis* H37Rv in axenic conditions as well as in infected RAW 264.7 macrophages showed that the treatment with the developed NPs containing [ETH:Booster] pair was as potent as that with free [ETH:Booster] pair solubilized in organic solvents. Among tested formulations, the pCD NPs displayed the best physicochemical characteristics and were thus selected for *in vivo* studies. For the first time, they were shown here not significantly modify the composition of lungs immune cell subsets after repeated pulmonary administration of high doses in uninfected mice. Then developed pCD NPs loaded with [ETH:Booster] were administered *via* the endotracheal route to the lungs of *M. tuberculosis*-infected mice using a Microsprayer® device, which enables the delivery of a precise volume of compound[34]. The formulation was able to reduce the mycobacterial load using subtherapeutic doses in a short course of infection model. With a two weeks treatment, the mycobacterial load was drastically decreased by 3-logs as compared to the non-treated animals.

Formulation	Size distribution (PCS)		ETH Content		Booster Content	
	Mean diameter (nm ± SE)	PdI	DL (wt% ± SD)	EE (wt% ± SD)	DL (wt% ± SD)	EE (wt% ± SD)
PLA NPs	254 ± 4	0.054	—	—	—	—
PLA NPs [ETH]	267 ± 3	0.074	38 ± 2	77 ± 5	—	—
PLA NPs [ETH:Booster]	274 ± 4	0.090	36 ± 4	76 ± 5	26 ± 3	51 ± 8
PLA NPs [Booster]	277 ± 5	0.075	—	—	23 ± 2	46 ± 2

Table 1. Main characteristics of empty and drug-loaded PLA NPs made of P4 by nanoemulsion. NPs mean hydrodynamic diameters were determined by PCS and are reported as Mean diameter (Z average nm ± standard error) and Polydispersity Index (PdI). ETH and Booster drug loading (DL) and encapsulation efficiency (EE) were determined by LC-MS-MS and RP-HPLC (the data are mean values ± standard deviation).

Results and Discussion

To address the challenge of treating *in vivo M. tuberculosis* with the [ETH:booster] pair, biodegradable PLA and PLGA NPs and "green" pCD NPs were studied here for their ability to circumvent the bottlenecks related to the limited water solubility of the booster (below mg/mL) and the strong ETH tendency to crystalize. The booster used in this study was the recently developed booster BDM41906[16] (hereby referred to as Booster).

Biodegradable PLA/PLGA NPs. In the first part of the study, a series of PLA/PLGA NPs containing [ETH:Booster] were prepared by nanoprecipitation, a simple one-step encapsulation method. Briefly, a dimethyl sulfoxide (DMSO) solution of PLA or PLGA and drug(s) was precipitated in injectable water leading instantaneously to the production of NPs without the need of any surfactant. DMSO was chosen because, among the pharmaceutically acceptable organic solvents, it is the only common solvent for ETH, Booster and polymers. Immediately after pouring the organic solution in water, monodisperse NPs with a mean diameter of around 170 ± 10 nm were obtained. Remarkably, the NPs mean diameter was stable upon storage at room temperature for up to 5 months with only less than 5% size variation (Supplementary Fig. S1).

The major challenge was to avoid ETH crystallization during NPs storage. Whatever the (co)polymers and the experimental conditions used, the highest ETH loadings obtained without crystallization were only about 11 weight percent (wt%) (for details see Supplementary Figs S2 and S3, Section I). Unfortunately, co-incorporation of Booster in the NPs further decreased the ETH drug loading (DL) (see Supplementary Information, Section I).

A similar strong tendency of a drug to form crystals has been previously observed by Layre *et al.*[35], when encapsulating busulfan in biodegradable poly(alkyl cyanoacrylate) NPs. The busulfan free crystals in the NPs suspensions were extremely difficult to be removed. The study highlighted the challenges related to the encapsulation and consequent delivery of crystalline drugs *in vivo*[36]. Therefore, to simultaneously avoid ETH crystallization and to increase the [ETH:Booster] DL, an alternative method for the preparation of PLA NPs was investigated. PLA NPs made of P4 were prepared by nanoemulsion method using polyvinyl alcohol (PVA) as surfactant.

A dramatic increase of the ETH loading efficiency was observed as compared to the nanoprecipitation method (Table 1). In particular an ETH DL of 38 ± 2 wt% corresponding to an encapsulation efficiency (EE) of 77 ± 5 wt% was found.

Remarkably, ETH and Booster could be well co-incorporated in the same NPs. PLA NPs were characterized by an EE of ETH and Booster of 76 ± 5 wt% and 51 ± 8 wt%, respectively (Table 1). Interestingly, the presence of both drugs in the formulation did not significantly influence the mean diameter of the NPs (Table 1). The NPs size distribution was evaluated by using three independent techniques: photon correlation spectroscopy (PCS), NP tracking analysis (NTA) and transmission electron microscopy (TEM). The NPs mean diameter using PCS, employing dynamic light scattering (DLS) technique, ranged from 254 to 277 nm (Table 1). Polydispersity index (PdI) was less than 0.1, indicating the formation of monodisperse NPs. The Zeta Potential (ZP) of the different formulations was −5 ± 0.5 mV, for both drug loaded or unloaded NPs.

The second method, NTA, has the main advantage of tracking NPs individually in their Brownian motion but it needs a high dilution of NPs suspensions. It can determine at the same time the hydrodynamic diameter of NPs and their concentration in various media[37] (Supplementary video S1). The mean diameter of PLA NPs determined by NTA ranged from 171 to 180 nm and the NPs concentrations were of around 1×10^9 particles/mL (after dilution by a factor of 10,000) with no significant differences between NPs loaded or not with drug(s). These values are smaller than the ones obtained by PCS (Supplementary Table S1). The mean diameters obtained by PCS are often overestimated, due to the presence of aggregates or to the fact that the largest NPs scatter more light than the smaller ones[38,39]. In this study, NTA was the most adapted technique to estimate the average hydrodynamic diameters by individually tracking the NPs in suspension, while DLS was a sensitive and adapted method for stability studies showing that no aggregates could be detected in PLA NPs prepared by nanoemulsion.

Furthermore, in order to get more in-depth information about the size and the morphology of the NPs, cryogenic TEM (cryo-TEM) analysis was performed (Fig. 1). Typical images of [ETH:Booster]-loaded PLA NPs (Fig. 1) showed spherical shapes and homogenous structures. The morphology of the NPs was not influenced by the presence of the drugs.

Besides, a statistical evaluation of the size distribution was performed on more than 2,000 NPs, showing a mean diameter of about 100 nm ± 50 nm (Supplementary Table S1). The mean diameter obtained by cryo-TEM was significantly lower from the ones obtained by both NTA and PCS (Supplementary Table S1). Indeed, the diameters determined by cryo-TEM correspond to the dry diameter of the NPs, without taking into account the hydrated PVA shell which is flattened during the observations[40,41]. Indeed, it has been reported that PLA

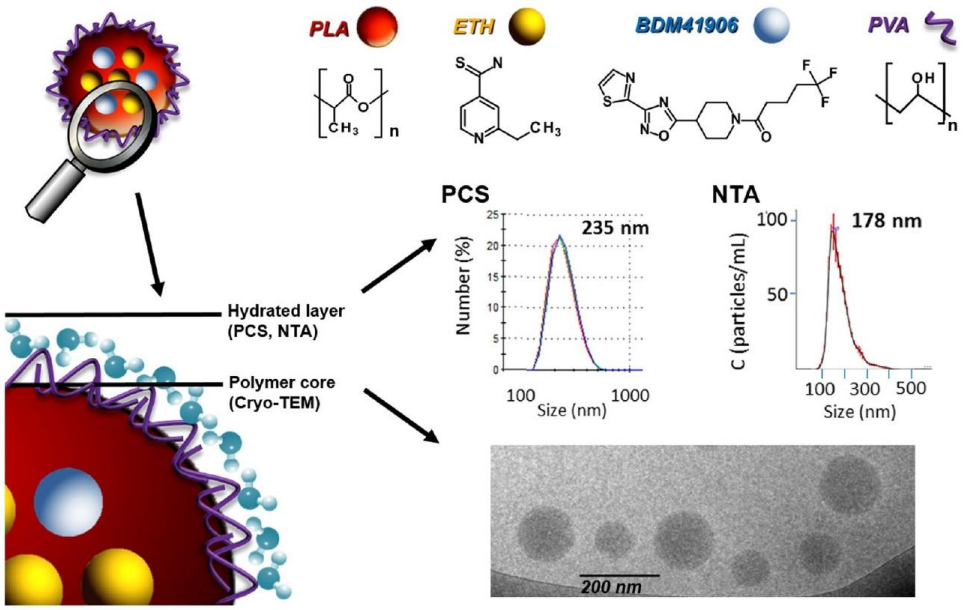

Figure 1. Chemical structure of PLA NPs components (nanoemulsion technique) and characterization of NPs mean diameter using three independent methods, PCS (number average data), NTA and Cryo-TEM. Typical example of NPs encapsulating [ETH:Booster]. Schematical representation of PLA NPs structure and components. Cryo-TEM allows determining the dry diameter (polymer core), whereas PCS and NTA allow measuring the hydrodynamic diameter (Polymer core + hydrated layer).

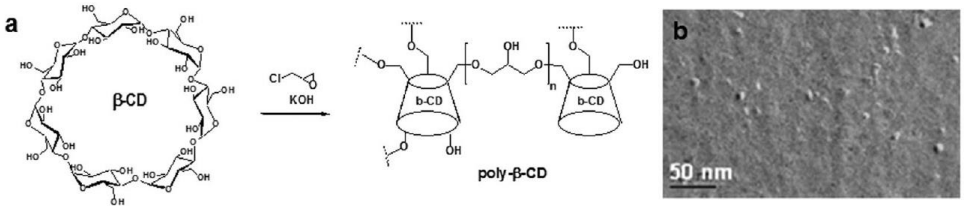

Figure 2. Nanoparticles made of pCD. (**a**) Polymerisation of β-CD with epichlorohydrin leading to the formation of cross-linked poly(2-hydroxy-1,3-propylenedioxy)-polycyclodextrin polymer (pCD) and (**b**) TEM image after freeze fracture of pCD NPs (mean size around 10 nm).

and PLGA NPs possess a hydrated PVA shell of several nm thickness. This could explain the difference of around 70 nm in sizes found between the mean diameter obtained by NTA and the one obtained by cryo-TEM (Supplementary Table S1).

The different methods used to evaluate the NPs size distribution are summarized in Fig. 1, highlighting the importance of using multiple and complementary techniques to fully characterize the NPs systems[42]. The preparation of PLA NPs by nanoemulsion proved to be particularly advantageous for the co-encapsulation of the [ETH:Booster] pair as compared to nanoprecipitation. Both methods led to the formation of NP suspensions stable upon storage in terms of size and PdI (Supplementary Fig. S4). However ETH crystallisation could not be totally avoided even by the nanoemulsion method as the formation of tiny crystals was observed during storage.

"Green" pCD-based NPs containing [ETH:Booster] pair. To overcome the technological challenge of completely avoiding ETH crystallisation, a different approach was attempted by encapsulating this drug at a molecular level. To this end the use of polymeric CDs was particularly appealing. NPs made of cross-linked poly (2-hydroxy-1,3-propylenedioxy)-polycyclodextrin polymer (pCD) were prepared according to previous reports[28] by polymerization of β-CD with epichlorohydrin in alkaline medium (Fig. 2a). We report here for the first time their use to co-encapsulate drugs, together with their pulmonary application.

TEM micrographs after freeze-fracture revealed spherical shapes and diameters of around 10 nm (Fig. 2b). However, DLS and NTA methods were inappropriate to characterize the pCD NPs because of their small sizes. Remarkably, the pCD NPs could be concentrated up to 200 mg/mL without aggregation and were able to soak out both ETH and Booster from their aqueous solutions in the absence of organic solvents. This is a major advantage

as compared to PLA and PLGA NPs, which could not be concentrated without aggregation to more than 5 mg/mL and for which ETH and Booster incorporation requires the use of organic solvents.

The aqueous solubility of both drugs was enhanced as a function of the pCD concentration. In the absence of pCD, the aqueous solubility of ETH determined by high performance liquid chromatography (HPLC) was found to be only 0.48 mg/mL. After 2 days of incubation at room temperature with pCD NPs at a concentration of 50 mg/mL, the apparent solubility of ETH was considerably increased to 1.5 ± 0.2 mg/mL, because of the affinity of the lipophilic drug molecules for the hydrophobic microenvironment of the pCD NPs. Furthermore, ETH solubility was found to be proportional with the pCD NPs concentration. For example, pCD NPs at a concentration of 200 mg/mL increased by 10 fold the apparent solubility of ETH to 4.9 ± 0.6 mg/mL.

Moreover, pCD NPs were highly efficient to incorporate the slightly water-soluble Booster. In particular, pCD NPs at a concentration of 200 mg/ml were able to incorporate up to 5 mg/mL of both ETH and Booster. It is worth mentioning that in order to solubilise the same amount of ETH, a mixture of DMSO: water containing as high as 40–50 vol% DMSO is needed. This elevated amount of organic solvent is incompatible with an *in vivo* administration.

In all cases, pCD NPs containing ETH alone or in combination with Booster were stable upon storage without the presence of any aggregates and/or the formation of ETH crystals (for further details see Supplementary Information - Section I). These results highlight the interest of this "green" strategy based on confining both drugs in a molecular form inside the NPs, totally avoiding the risks related to the use of organic solvents. Indeed, insoluble drugs were shown to readily accommodate in the hydrophobic CD cavities as well as in the confined micro-domains in the crosslinked pCD NPs without crystallization[25].

Efficacy of the NPs containing [ETH:Booster] pair against *M. tuberculosis* replication in phenotypic extracellular and intracellular assays. PLA NPs prepared by nanoemulsion and pCDs NPs that contain [ETH:Booster] pair were then investigated for their activity against *M. tuberculosis* replication. To monitor the activity, we used two phenotypic assays[29,43] that rely on the use of a fluorescent strain of *M. tuberculosis* H37Rv (H37Rv-GFP) and RAW 267.4 macrophages. Briefly, a series of two-fold dilutions of [ETH:Booster] NPs were first performed and 5 µL of each dilution added into a 384-well microplate. It is worth noting that with this method, both ETH and Booster are diluted simultaneously. For DMSO vehicle controls (ETH and Booster) different volumes of solution were transferred using a nanoliter acoustic dispenser and backfilled with DMSO to 500nL, allowing the use of a minimum volume of DMSO that is toxic above 1% final concentration. To obtain the same volume for [ETH:Booster] NPs and [ETH:Booster] DMSO diluted samples, cell medium was added up to 5 µL in the latter ones. Then, 45 µL of PBS-washed H37Rv-GFP bacteria were added alone for the extracellular test and 45 µL of the same bacteria that were previously incubated with RAW 267.4 macrophages for 2 hours were added for the intracellular test. After 5 days incubation at 37 °C, 5% CO_2, the amount of bacteria was quantified by acquisition of the GFP-fluorescence signal on a multimode reader for the extracellular assay and by confocal fluorescence microscopy and automated image-analysis for the intracellular assay (Fig. 3a, Supplementary Fig. S5).

For both assays and each of the combinations, dose-response curves for the different parameters were generated after normalization on DMSO-negative and INH-positive control (Fig. 3b and Fig. 4). For the image-based assay, the intracellular bacteria area was used as a correlate of intracellular growth, while the total cell number is an indicator of the cytotoxicity of the compounds (Fig. 3b). All samples, free-DMSO and encapsulated ETH and [ETH:Booster] pair showed a dose-dependent inhibition and there was no cytotoxicity for any of the samples. For both assays, the results were then further summarized as the concentration of ETH required to inhibit 50% of the bacterial growth (IC_{50}) (Table 2).

As expected, the IC_{50} for [ETH:Booster] pair was lower than that of ETH alone in DMSO conditions and within the range of our previous report given the variability of the assay[16]. Next, the ETH that has been formulated in PLA NPs and pCDs NPs was as potent as the ETH solubilised in DMSO, clearly demonstrating that the encapsulation of ETH was not affecting its efficiency against *M. tuberculosis* replication. Finally, the [ETH:Booster] pair had a two-fold increased effect in both assays compared to the parent ETH thus indicating that a synergic [ETH:Booster] combination can be efficiently reached. Also we verified that empty PLA NPs and pCD NPs had no effect on intracellular bacteria *per se* (Supplementary Fig. S6). Therefore the inhibitory effect of loaded NPs was only due to the effective delivery of their payload of ETH and Booster. These results also demonstrate the lack of toxicity of both empty and loaded NPs (Supplementary Fig. S6b, Fig. 3b).

Effect of NPs containing [ETH:Booster] pair via endotracheal aerosol administration against a short-course *M. tuberculosis* challenge. Given the satisfactory results mentioned above, we decided to investigate the antitubercular properties of the NPs in an *in vivo* model of TB infection. To this end, the NPs co-loaded with ETH and Booster were administered to infected mice via pulmonary administration.

Different devices, such as whole body exposure chamber, head and nose-only exposure systems, deposition by tracheotomy and Microsprayer® have been evaluated to administer NPs directly in the lungs of *M. tuberculosis* infected mice[34,44,45]. The currently available systems for pulmonary administration in small animals have several limitations such as imprecisions due to the difficulty of measuring the amount of inhaled drugs, delivery of low fraction of the administered drug or invasive surgery[44,45]. Stemming from these considerations, the choice of the appropriate delivery device is of outmost importance. The Microsprayer® device appeared as the most reliable device for precise pulmonary administration to rodents as it has been shown that up to $89 \pm 10\%$ of the administered dose was efficiently delivered to mouse lungs[46–48]. Moreover, the use of Microsprayer® was shown to allow an efficient bilateral distribution of the NPs in the lungs[49]. However, not all drug formulations are compatible with this delivery system. Loaded PLA NPs presented a high tendency to be retained by the Microsprayer® and the ETH content from each spray was highly variable, compromising the study of their *in vivo* efficacy.

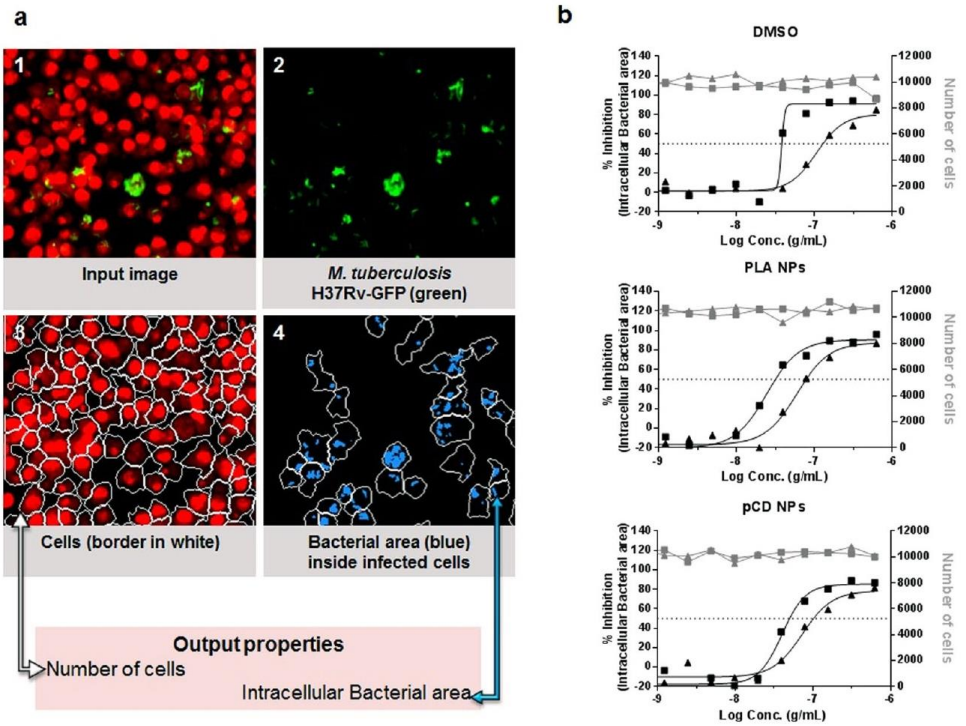

Figure 3. Intracellular antitubercular activity. (**a**) Scheme representing image-based analysis method performed with the image-analysis software Columbus 2.5.1 (PerkinElmer). **1**. Input image: cell nuclei and cell cytoplasm were stained with the DNA dye Syto60 and detected in the red channel; *M. tuberculosis* H37Rv-GFP was detected in the green channel. **2**. *M. tuberculosis* H37Rv-GFP detected in the green channel. **3**. Cells detection in the red channel. The estimated cell limit is represented in white. **4**. Bacterial area detected inside the cells area is represented in blue. Data related to the area of cells was detected in the red channel and data related to the bacterial area was detected in the green channel. (**b**) % of inhibition of intracellular bacterial area (black points) and number of cells (grey points) obtained with ETH (solid triangle) and [ETH:Booster] (solid square) in DMSO, PLA NPs and pCD NPs. Data presented corresponds to one representative experiment of three experiments.

On the contrary, the pCD NPs could be efficiently and reproducibly administered *in vivo* using the Microsprayer®. Indeed, the average amount of pCD NPs suspension (50.9 ± 0.2 mg) delivered by the Microsprayer® was very close to the expected one (52.0 ± 0.2 mg). The weight of each spray was constant, fully reproducible and the standard deviation was low. Remarkably, 98 ± 0.7 wt % of the NPs suspension was recovered after the passage though the Microsprayer®. In addition, the drug loading of pCD NPs was determined by HPLC before and after the passage through the device. For instance, for a suspension of 100 mg/mL of pCD NPs loaded with 2 mg of ETH a recovery of $99 \pm 4\%$ was obtained.

Although as already mentioned CDs are considered biocompatible, few data are available on their pulmonary toxicity. Prior early studies assessed the bronchial responsiveness, airway inflammation and histological changes upon the administration of CDs in animals *via* the pulmonary route[50,51]. These studies revealed only minor toxicity in lungs, which prompted us to study the composition of the immune cell subsets in mouse lungs following Microsprayer® administration of pCD NPs. Thus, uninfected mice were repeatedly given with aerosolized water ("vehicle") or NPs during a period of time up to two weeks (Fig. 5a). This is the first time that high doses of pCD NPs were repeatedly administered into mouse lungs. After treatment, the potential toxicity of pCD NPs endotracheal administration was studied by analyzing the mouse body weight, lung histology and cell recruitment (Fig. 5b,c,d). Body weight was maintained during the treatment and no difference was observed for eosinophils, neutrophils and dendritic cells between the group "vehicle" and the groups that received the treatment during 1 or 2 weeks. Both the histology and the flow cytometry analyses pointed out an increase in CD4 T-cell infiltrates, which could be correlated to what has been previously reported for other CDs derivatives[51]. Also, a mild increase in the number of the alveolar macrophages was noticed upon treatment. Altogether, these results suggested that repeated treatment does not result in major modification of the composition of the immune cell subsets.

Subsequently, the ability of the pCD NPs co-encapsulating the [ETH:Booster] pair to reduce the pulmonary mycobacterial load was investigated in a mouse model of acute *M. tuberculosis* infection. Seven days after infection, mice received 3 doses of pCD containing [ETH:Booster] pair at 10 mg/kg for each drug by endotracheal aerosol administration using the Microsprayer® every 2 days. It is important to point out that free drugs could not be administered by the same way as controls because their solubilisation requires the use of organic solvents,

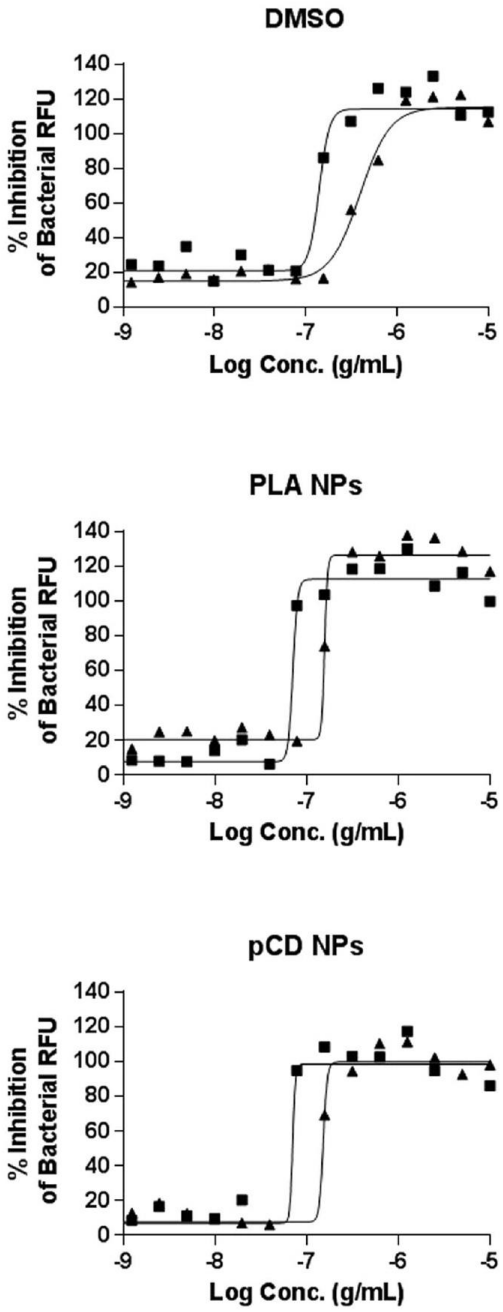

Figure 4. Extracellular antitubercular activity. % of inhibition on bacterial RFU obtained with ETH (solid triangle) and [ETH:Booster] (solid square) in DMSO, PLA NPs and pCD NPs. Data presented correspond to one representative experiment of three experiments.

incompatible with pulmonary administration. Indeed, as previously shown, up to 40–50 vol% DMSO in water is needed to solubilise equivalent amounts of drugs.

For this reason, the water-soluble first-line INH was used as control. Compared to untreated mice, the administration of the drug loaded pCD NPs lead to a significant decrease ($p < 0.01$) of the pulmonary bacterial load, determined as the average number of colony forming units (CFU) (Fig. 6a). These data show that it was possible to obtain an antibacterial effect using just 3 doses of the [ETH:Booster] pair within a one week administration.

To investigate whether a longer course of treatment could lead to a greater efficacy, mice were treated with a regimen of 6 doses given over a two-week time course. As expected for this acute phase of the *M. tuberculosis*

Formulation		Extracellular assay *IC50 (μg/mL) ± SD*	Intracellular assay *IC50 (μg/mL) ± SD*
Controls (DMSO)	ETH	0.30 ± 0.10	0.11 ± 0.01
	[ETH:Booster]	0.11 ± 0.06	0.06 ± 0.02
PLA NPs (Nanoemulsion)	PLA::ETH	0.12 ± 0.04	0.09 ± 0.05
	PLA::[ETH:Booster]	0.06 ± 0.02	0.04 ± 0.02
pCD NPs	pCD::ETH	0.13 ± 0.04	0.06 ± 0.01
	pCD::[ETH:Booster]	0.06 ± 0.02	0.04 ± 0.01

Table 2. Efficiency of the different formulations against *M. tuberculosis* H37Rv-GFP extracellular or intramacrophage replication. Results, expressed as concentration of ETH required to inhibit 50% of the bacterial growth in μg/mL (IC_{50}), were calculated by nonlinear regression analysis using the equation for a sigmoidal dose-response curve with variable slope using the GraphPad Prism 5.0 software. Results are shown as the mean ± standard deviation of three independent experiments.

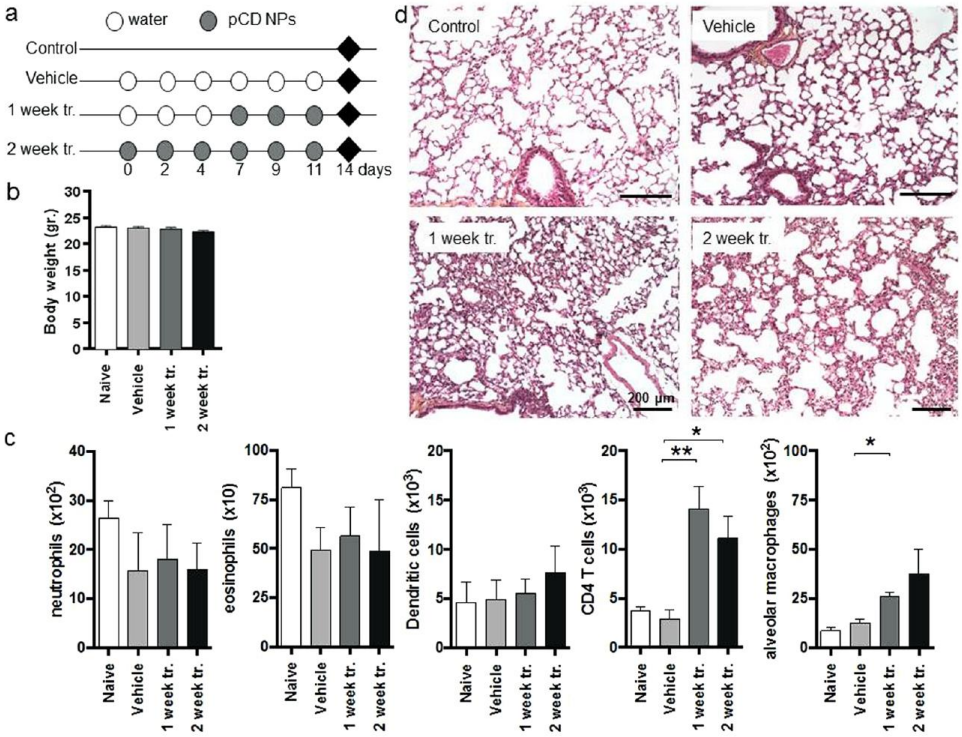

Figure 5. Impact of pCDs NPs administration on pulmonary homeostasis in mouse. (**a**) Protocol. Water (Vehicle) or nanoparticles were administered to mice via the endotracheal route during one (1 week tr.) or two weeks (2 week tr.); ♦ = mice euthanasia. (**b**) Body weight of mice after each treatment. (**c**) Analysis of the recruitment of immune cells in the lungs parenchyma by flow cytometry. The data represent the number of selected cells on 500,000 events; To define the different cells populations we used the following phenotypes: neutrophils ($CD11b^+GR1^+$), eosinophils ($F4/80^+SiglecF^+$), CD4 T cells ($CD3^+CD4^+$), alveolar macrophages ($CD11c^+F4/80^+$) and dendritic cells ($CD11b^+CD11c^+$); the Data are mean values ± standard deviation of one representative experiment of two independent experiments; *$p < 0.1$, **$p < 0.01$. (**d**) After treatment, lungs were analysed by histology (H-E staining, scale bar: 200 μm).

infection, the bacterial load for the control group increased, reaching 10^9 CFUs (in comparison to one week treatment, 10^7 CFUs) (Fig. 6a,b). Lungs from the mice that were treated with 6 doses of the [ETH:Booster] pCD NPs had a mean value of 5×10^5 CFUs, which indicates a dramatic (3-logs) improvement in the efficacy of the formulation compared to three doses only. Corroborating with the massive decrease in the mycobacterial load, the lungs that received [ETH:Booster] pCD NPs displayed much less cell infiltrates than control animals (Fig. 6c). Moreover, the reduction of bacterial load in the lungs was much higher when ETH was co-encapsulated with the Booster ($p < 0.001$) than when ETH was administered alone ($p < 0.1$) (Fig. 6b). Noteworthy, when the formulation containing [ETH:Booster] was given by oral gavage using the same regimen (i.e. 6 doses every 2 days),

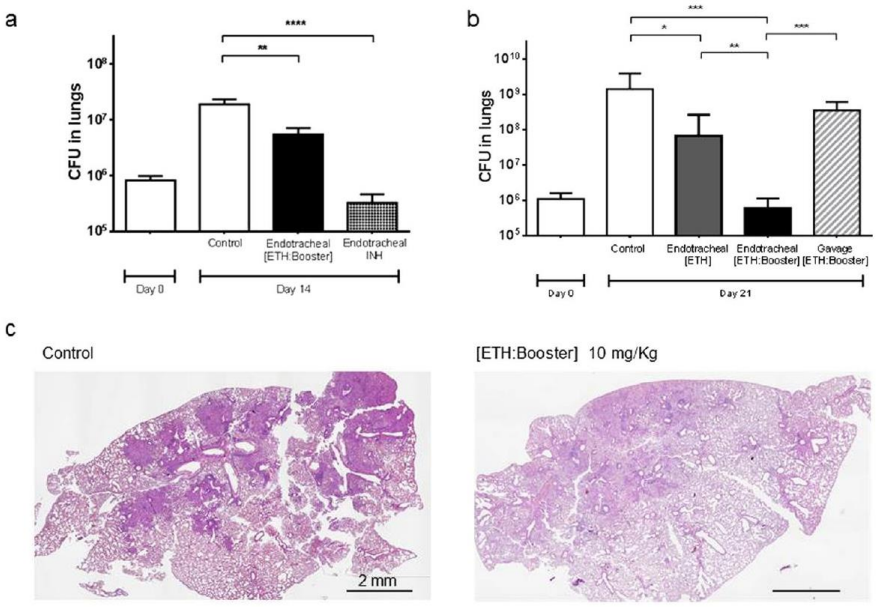

Figure 6. Effect of [ETH:Booster] loaded pCD NPs in a mouse model of *M. tuberculosis* infection. Intranasal infection was performed with *M. tuberculosis* H37Rv. (**a**) After 7 days mice were aerosolized endotracheally either with isoniazid (INH, 25 mg/Kg) as positive control or drug loaded nanoparticles (10 mg/Kg) three times during one week. At day 14 post-infection, mice were euthanized and CFU in the lungs were determined. Control: non-treated *M. tuberculosis* infected mice. Data are mean values ± standard deviation of one representative experiment of three independent experiments; $^{**}p < 0.01$, $^{***}p < 0.001$. (**b–d**) After 7 days mice were aerosolized with drug loaded nanoparticles or received drug loaded nanoparticles by gavage six times during two weeks. At day 21 post-infection, mice were euthanized and lung infection was analysed by CFU determination and by histology (H-E staining, scale bar: 2 mm). Control: non-treated *M. tuberculosis* infected mice. Data are mean values ± standard deviation; $^{*}p < 0.1$, $^{**}p < 0.01$, $^{***}p < 0.001$.

the mycobacterial load in the lungs was similar as the one from non-treated controls, clearly demonstrating the benefit of using the pulmonary route for ETH and Booster co-loaded nanoparticles delivery (Fig. 6b).

Moreover, it is worth mentioning that the effect obtained in the present work with the administration of ETH:Booster 3 times/week during 2 weeks via the endotracheal route is equivalent to the one observed previously upon a daily, 6 days/week administration of ETH by gavage during 3 weeks[8]. Because it drastically reduces the dose and the frequency of the treatment, the present approach has the potential to diminish the systemic side effects of ETH.

The pulmonary delivery of pCD NPs effectively encapsulating the [ETH:Booster] pair could be a promising strategy to improve the standard therapeutic protocol in humans leading to a decrease of the typical daily dose (from 500 mg orally) of ETH[5].

Conclusions

The [ETH:Booster] pair was co-encapsulated in biodegradable polymeric NPs overcoming the bottlenecks inherent to the strong tendency of ETH to crystallize and the limited water solubility of Booster. Advantageously, pCD NPs effectively prevented ETH crystallization both during encapsulation and NPs storage. For the first time, an automated confocal high-content screening platform was used to evaluate the efficacy of the NPs on *M. tuberculosis* infected cells. Noticeably, the drugs maintained their activity after incorporation in NPs.

Among the formulations developed, pCD NPs displayed the best physicochemical properties for the simultaneous delivery of [ETH:Booster] pair in the lungs.

Moreover, pCD NPs were demonstrated not to induce main modifications of the composition of the immune cell subsets following repeated administrations at high doses *in vivo*. The treatment with 6 doses of pCD NPs containing the drug combination, led to a 3 log decrease in lungs CFU in comparison to untreated animals. Noticeably, when administering the same doses by gavage no antibacterial effect could be observed.

The pulmonary administration to animals is very challenging, as the experimental protocols have to take into account the limitations of the available tools and methods. On the other hand, the pulmonary administration in humans (metered dose inhaler) does not deal with the technical limitations related to the delivery of NP formulations in rodents, as the commercial devices allow self-administration without stress or pain.

These findings suggest further *in vivo* investigations of the developed pCD formulation. In the future, our "green" incorporation strategy could be used as a supplement to the standard treatment to contain the *M. tuberculosis* pulmonary manifestations and to prevent its dissemination.

Moreover, given the fact that the current regimen for TB consists in a cocktail of four drugs, the approach used here could be extended to the encapsulation of more than two drugs, simplifying the treatment, decreasing the systemic side effects and increasing the patients' compliance to limit drug misuse.

Materials and Methods

Chemicals. PLGA 75:25 acid terminated (P1) (MW: 37–84 KDa, 10P002), PLGA 50:50 ester terminated (P2) (MW: 70–100 KDa, 10P016) and PLGA 50:50 acid terminated (P3) (MW: 5–20 KDa, 10P019) were kindly provided by PCAS (Expansorb, Aramon, France). PLA ester terminated (P4) (MW:10–18 kDa), PVA (87–90% hydrolysed), DMSO-99.5%, ETH and amikacin were all purchased from Sigma-Aldrich. Injectable water was purchased from Cooper (Melun, France). The solvents were of analytic grade.

The Booster named BDM41906 (5,5,5-Trifluoro-1-[4-(3-thiazol-2-yl-1,2,4-oxadiazol-5-yl)piperidin-1-yl] pentan-1-one) was synthesized as previously described[16].

β-CD was kindly supplied by Roquette, Lestrem, France. pCD NPs of around 10 nm were produced as previously described[28,52] by crosslinking β-CD under strongly alkaline conditions with epichlorohydrin (EP). Briefly, 100 g of anhydrous β-CD were solubilized overnight in 160 mL of NaOH 33% w/w solution. After adding 81.52 g of EP the reaction was stopped using acetone in the vicinity of the gelation point. The β-CD NPs, recovered by ultrafiltration followed by freeze-drying, contained 70% w/w β-CD, as determined by ^{1}H NMR spectroscopy.

Nanoparticle preparation. *Nanoprecipitation.* Encapsulation of ETH in PLA and PLGA NPs was carried out adapting a previously reported procedure[53]. Briefly, 0.4 mL of DMSO solution containing 10 mg polymer (PLA or PLGA) and ETH (0.5 to 7 mg) were poured drop by drop in 7 mL of injectable water under magnetic stirring. In the case of co-encapsulation, 3 mg of Booster were added to the DMSO solution.

Nano-emulsion. Preparation of PLA NPs was carried out as previously reported by Kumar *et al*. with slight modifications[20]. Briefly, 10 mg of ETH were solubilized in 0.2 mL of MeOH and mixed to 1.5 mL of a dichloromethane (DCM) solution containing 20 mg of PLA and 10 mg of Booster. This organic phase was poured into 4 mL of injectable water containing 0.5% w/v PVA and vortexed for 20 seconds. The resulting emulsion was sonicated 1.5 min and the solvents were evaporated under gentle magnetic stirring.

Drug encapsulation in "green" pCD NPs. Encapsulation of ETH and Booster in pCD NPs was carried on without using any organic solvent, by mixing for at least 4 hours the NP suspensions with the drug powders.

Nanoparticle characterization. *Size measurement by PCS and Zeta Potential measurement.* The average hydrodynamic diameter of the NPs was determined at 25 °C with an equilibration time of 60 s using a Malvern Zetasizer® (Nano ZS90, Malvern Instruments S.A., Worcestershire, UK). Dilutions with injectable water were done according to ISO 22412 and experiments were performed in triplicate. Mean diameters were reported as Z Average (nm) ± SE (Standard Error - with a PdI lower than 0.1) or as number mean diameter (nm) ± SD (Standard Deviation). The NPs mean diameters were monitored up to three months of storage at 25 °C. The NPs ZP was measured in KCl 1 mM by Malvern Zetasizer©.

Size measurement by NTA and concentration quantification. The mean hydrodynamic diameter and concentration of the NPs were measured at 25 °C by NTA (NanoSight LM10, Malvern Instruments S.A., Worcestershire, UK). NPs prepared by nanoprecipitation were diluted 2,000 times and the ones made by nanoemulsion 10,000 times. Each sample was measured 5 times for 60 seconds. Results were reported as mean diameter ± SD.

Cryo-TEM. 5 µl of NPs suspensions were deposited onto a 200 mesh copper grid and flash-frozen in liquid ethane cooled down at liquid nitrogen temperature. Cryo-TEM images were acquired on a JEOL 2200FS energy-filtered (20 eV) field emission gun electron microscope operating at 200 kV. Several thousands of images were automatically acquired for each NPs formulation to obtain representative results.

Drug(s) dosage. To determine the amounts of both drugs effectively incorporated in the PLA/PLGA NPs, the suspensions of drug-loaded NPs were centrifuged at 17,000 g for 15 minutes. Aliquots of the supernatants were withdrawn to assess the quantity of non-encapsulated drug (indirect estimation). The NPs pellet was dissolved in DMSO and dosed (direct estimation of the encapsulated drug). In the case of drug-loaded pCD NPs, excess non-encapsulated drug was removed by centrifugation, followed by NP dilution in DMSO and/or acetonitrile/water.

All the samples were dosed by liquid chromatography-mass spectrometry (LC-MS-MS) and reverse-phase HPLC (RP-HPLC) (For details see S.I. – Section III).

The DL can be defined as the mass fraction of a NP that is composed of drug, while the EE can be considered as the fraction of drug effectively encapsulated into the NPs compared with the amount that was used to prepare the NPs[20,54]. The DL and EE were calculated as shown in equation 1 and 2, respectively.

$$DL\ (\%) = \frac{(mg\ of\ encapsulated\ drug^{*})}{(mg\ of\ polymer)} \times 100 \quad (1)$$

$$EE\ (\%) = \frac{(mg\ of\ encapsulated\ drug^{*})}{(mg\ of\ drug\ initially\ added\ to\ the\ formulation)} \times 100 \quad (2)$$

[*The amount of encapsulated drug has been calculated with a direct or indirect estimation, depending on the sample fraction considered].

Bacteria and macrophages. *M. tuberculosis* H37Rv strain (ATCC-27294) constitutively expressing the green fluorescent protein (H37Rv-GFP) was used as a reporter for the replication assay. Bacteria were cultured at 37 °C for 16 days in complete 7H9 medium containing 0.5% glycerol (50405, Euromedex), 10% Middlebrook oleic acid-albumin-dextrose-catalase (OADC, 211886, Becton Dickinson), 0.05% Tween 80 (2002A, Euromedex) and 50 µg/mL hygromycin B (10687010, Invitrogen). In the day of the experiment, *M. tuberculosis* were washed with D-PBS Ca- Mg- (14190169, LifeTechnologies) 3 times with centrifugation at 5,000 RPM for 5 minutes and centrifuged at 700 RPM for 2 minutes to remove clumped bacteria. Bacteria were resuspended in RPMI-1640 + glutamax (61870044, LifeTechnologies) containing 10% heat inactivated fetal bovine serum (FBS) (10270106, Gibco) and titrated by measuring the optical density at 600 nm.

Mouse macrophage RAW 264.7 (ATCC # TIB-71) were maintained at 37 °C in RPMI-1640 + glutamax containing 10% FBS and were passed 3 times per week and used before passage number 7. Macrophages were harvested by using Versene (15040033, LifeTechnologies).

Assay plate preparation. ETH, BDM41906 and INH were diluted in DMSO (34943, Sigma-Aldrich) to 10 mg/mL and were dispensed in Echo-qualified 384-well low dead volume source plates (Labcyte). Echo 550 Series Liquid Handler (Labcyte) was used to transfer precise volumes between 5 and 500 nL from the Echo-qualified plate to the 384-well clear-bottom polystyrene assay plates (781091, Greiner Bio-One) by using sound waves. All the samples were backfilled with DMSO until 500 nL. Prior to addition of cells, 4.5 µL of cell medium were dispensed in the Echo-dispensed wells.

NPs loaded with ETH or with the [ETH:Booster] pair were diluted in water to 0.2 mg/mL of ETH. 2-fold serial dilutions of the mother solution in a final volume of 100 µL were performed in sterile MilliQ water in a 384 deep well "diamond plate" (P-384-120SQ-C-S, Axygen) in order to obtain a dose-response curve. Posteriorly, 5 µL of the NPs were dispensed in the 384-well assay plates.

***M. tuberculosis* replication phenotypic assays.** Bacteria were diluted at 2×10^6 bacteria/mL using complete 7H9 medium and 45 µL/well of bacterial suspension were added in 384-well assay plates. After 5 days incubation at 37 °C, 5% CO_2, extracellular plates were read using a fluorescence reader (Victor X3, Perkin Elmer) at excitation/emission of 485/535 nm for 0.1 seconds/well with a small emission aperture and CW-lamp energy of 50,000. The read-out, relative fluorescence units (RFU), versus the ETH concentration was then plotted using GraphPad Prism 5.0 software and the concentration required to inhibit 50% of the bacterial replication (IC_{50}) was calculated by nonlinear regression analysis using the equation for a sigmoidal dose-response curve with variable slope.

For intracellular assay, bacteria were mixed with RAW 264.7 macrophages to prepare a suspension at 5×10^5 cells/mL and 1×10^6 bacteria/mL (multiplicity of infection 2) in RPMI-1640 + glutamax containing 10% FBS. After 2 hours of infection at 37 °C with shaking (120 RPM), infected cells were washed with RPMI-1640 + glutamax containing 10% FBS by centrifugation at 1,100 RPM for 5 minutes. The remaining extracellular bacilli from the infected cell suspension were killed by a 1 hour 50 µg/mL amikacin (A2324-5G, Sigma) treatment and then washed twice with RPMI-1640 + glutamax containing 10% FBS. Finally, 45 µL/well of cellular suspension was added in the 384-well assay plate and incubated during 5 days at 37 °C, 5% CO_2. Macrophages were then stained with 5 µM Syto 60 (S11342, Molecular probes) dye for 1 hour, followed by plate sealing, imaging acquisition and data analysis.

Confocal images were recorded on an automated fluorescent ultra-high-throughput microscope Opera (Perkin Elmer) (For details see S.I. – Section III). A series of 6 pictures at the center of each well were taken and each image was then analysed using Columbus system version 2.5.1 as previously described[43] to extract the intracellular bacterial area and the number of cells. The intracellular bacterial area was normalized with the negative control DMSO (0% inhibition) and the positive control INH at a concentration of 1 µg/mL (100% inhibition) by converting it into a percentage of bacterial replication inhibition (% inhibition). % inhibition was calculated as shown in the equation 3:

$$\%\ inhibition = \left(1 - \frac{\text{Test bacterial area} - \text{INH bacterial area}}{\text{DMSO bacterial area} - \text{INH bacterial area}}\right) \times 100 \quad (3)$$

For each compound, a plot of % inhibition versus the ETH concentration was determined with GraphPad Prism 5.0 software and the IC_{50} was calculated in the same way as in the extracellular assay.

***In vivo* experiments.** 6-week old Balb/C female mice were purchased from Janvier (Le Genest-Saint-Isle, France) and were maintained in the animal house facility of the Pasteur Institute of Lille, France (Agreement B59-350009). The project received ethical approval by French Committee on Animal Experimentation and the Ministry of Education and Research (00579.01 approved on December 2nd 2015) and all experiments were performed in accordance with relevant guidelines and regulations.

Lung histology. Infected or uninfected 8-week-old mice were divided in groups and endotracheally administered with water (vehicle) or pCD NPs (Figs 5a and 6).

At the determined end-point mice were euthanized, lungs were harvested and soaked in 4% formaldehyde (10% formalin solution, neutral buffered, HT501128, Sigma-Aldrich) for 24 hours, before being embedded in paraffin. Tissues were sliced with microtome and 5 µm sections were stained with Hematoxylin-Eosin (H-E) for light microscopy examination for anatomopathology.

Flow cytometry. Harvested lungs were cut into small pieces and incubated for 1 hour at 37 °C with a mix of DNAse I (100 µg/ml, Sigma-Aldrich) and collagenase (1.6 mg/ml, Roche) 400 U/ml. Lung cells were washed and filtered before being incubated with saturating doses of purified 2.4G2 (anti-mouse Fc receptor, ATCC) in 200 µl PBS 0.2% BSA 0.02% NaN3 (FACS buffer) for 20 minutes at 4 °C to prevent antibody binding on the Fc receptor. Various fluorescent mAb combinations in FACS buffer were used to stain $3–5 \times 10^6$ cells. Acquisitions were done on FACScanto II cytofluorometer (Becton Dickinson) with the following mAbs from BD Biosciences: Fluorescein (FITC)-coupled HL3 (anti-CD11c), FITC-coupled 145-2C11 (anti-CD3), APC-coupled RB6-8C5 (anti-GR1), phycoérythrine (PE)-coupled RM4-5 (anti-CD4), PE-coupled E50-2440 (anti-SIGLEC-F), APC-coupled BM8 (anti-F4/80). APC-eF780-coupled M1/70 (antiCD11b) were purchased from eBiosciences and fixable viability dye eFluor 506 (eBiosciences) was used to gate viable cells.

Efficacy studies. 8-week-old mice (4 mice *per* group) were inoculated with *M. tuberculosis* H37Rv via the intranasal route to reach 10^6 bacteria in the lungs at day 0. NPs or INH were administered to mice using a Microsprayer® (MicroSprayer® Aerosolizer – Model IA-1C-M and FMJ-250 High Pressure Syringe, Penn Century Inc., Wyndmoor, PA). For the 1-week treatment and the 2-week treatment, administrations were performed on day 7, 9, 11 and on day 7, 9, 11, 14, 16, 18 respectively. The body weight of mice was monitored after each treatment (Fig. 5b). To assess the reproducibility of NPs administration through the MicroSprayer®, the delivered doses of NP suspensions were collected in glass vials after each spray and were accurately weighed. Then the amount of the delivered drug was quantified by HPLC as already described.

The protocol to administer the NPs in mice was adapted from a previously reported one[55]. Briefly, mice were placed in isoflurane chamber (Aerrane®, Baxter SAS, France). Each mouse was placed on the back on a platform (Mouse Intubation Platform – Model MIP, Penn Century Inc., Wyndmoor, PA) with isoflurane mask and hanging on its teeth. The tongue was pulled out by a tweezer and a laryngoscope (Small Animal Laryngoscope for mouse – Model LS-2-M, Penn Century Inc., Wyndmoor, PA) was used to see the trachea and to enable the aerosolization of 50 µL of NP suspensions inside the lungs.

At day 14 or 21, mice were euthanized and lungs were homogenized with MM300 bead beater (Retsch) and eight ten-fold serial dilutions were plated onto 7H11 agar plates supplemented with 10% OADC. CFUs were determined after a three-weeks growth. Represented data are mean values ± standard deviation of one representative experiment of three independent experiments. Results for each independent experiment were summarized in Supplementary Table S2. Statistics were performed using Student's t-test and one-way ANOVA analysis. Same p-values for *in vivo* experiments were obtained with the two tests. $*p < 0.1$, $**p < 0.01$,$***p < 0.001$.

References

1. Global tuberculosis report 2016 (WHO 2016).
2. O'Garra, A. *et al*. The immune response in tuberculosis. *Annu Rev Immunol* **31**, 475–527, doi:10.1146/annurev-immunol-032712-095939 (2013).
3. Gandhi, N. R. *et al*. Multidrug-resistant and extensively drug-resistant tuberculosis: a threat to global control of tuberculosis. *Lancet* **375**, 1830–1843, doi:10.1016/S0140-6736(10)60410-2 (2010).
4. Ethionamide. *Tuberculosis* **88**, 106–108, doi:10.1016/s1472-9792(08)70009-x.
5. Zhu, M. *et al*. Population pharmacokinetics of ethionamide in patients with tuberculosis. *Tuberculosis (Edinb)* **82**, 91–96 (2002).
6. Baulard, A. R. *et al*. Activation of the pro-drug ethionamide is regulated in mycobacteria. *Journal of Biological Chemistry* **275**, 28326–28331 (2000).
7. Vannelli, T. A., Dykman, A. & de Montellano, P. R. O. The antituberculosis drug ethionamide is activated by a flavoprotein monooxygenase. *J. Biol. Chem.* **277**, 12824–12829 (2002).
8. Willand, N. *et al*. Synthetic EthR inhibitors boost antituberculous activity of ethionamide. *Nat. Med.* **15**, 537–544 (2009).
9. Mehanna, M. M., Mohyeldin, S. M. & Elgindy, N. A. Respirable nanocarriers as a promising strategy for antitubercular drug delivery. *J Control Release* **187**, 183–197, doi:10.1016/j.jconrel.2014.05.038 (2014).
10. Pham, D. D., Fattal, E. & Tsapis, N. Pulmonary drug delivery systems for tuberculosis treatment. *Int J Pharm* **478**, 517–529, doi:10.1016/j.ijpharm.2014.12.009 (2015).
11. Hickey, A. J., Durham, P. G., Dharmadhikari, A. & Nardell, E. A. Inhaled drug treatment for tuberculosis: Past progress and future prospects. *J Control Release*. doi:10.1016/j.jconrel.2015.11.018 (2015).
12. Pandey, R. *et al*. Poly (DL-lactide-co-glycolide) nanoparticle-based inhalable sustained drug delivery system for experimental tuberculosis. *J Antimicrob Chemother* **52**, 981–986, doi:10.1093/jac/dkg477 (2003).
13. Ahmad, Z., Sharma, S. & Khuller, G. K. Inhalable alginate nanoparticles as antitubercular drug carriers against experimental tuberculosis. *Int J Antimicrob Agents* **26**, 298–303 (2005).
14. Bivas-Benita, M., Ottenhoff, T. H., Junginger, H. E. & Borchard, G. Pulmonary DNA vaccination: concepts, possibilities and perspectives. *J Control Release* **107**, 1–29 (2005).
15. Costa, A. *et al*. The formulation of nanomedicines for treating tuberculosis. *Adv Drug Deliv Rev* **102**, 102–115 (2016).
16. Flipo, M. *et al*. Ethionamide boosters. 2. Combining bioisosteric replacement and structure-based drug design to solve pharmacokinetic issues in a series of potent 1, 2, 4-oxadiazole EthR inhibitors. *J. Med. Chem.* **55**, 68–83 (2011).
17. Lopes, E., Pohlmann, A. R., Bassani, V. & Guterres, S. S. Polymeric colloidal systems containing ethionamide: preparation and physico-chemical characterization. *Pharmazie* **55**, 527–530 (2000).
18. Bhanushali, C. J., Zidan, A. S., Rahman, Z. & Habib, M. J. Ion-pair chromatography for simultaneous analysis of ethionamide and pyrazinamide from their porous microparticles. *Aaps Pharmscitech* **14**, 1313–1320, doi:10.1208/s12249-013-0025-3 (2013).
19. Vale, N. *et al*. New times, new trends for ethionamide: *In vitro* evaluation of drug-loaded thermally carbonized porous silicon microparticles. *Eur J Pharm Biopharm* **81**, 314–323, doi:10.1016/j.ejpb.2012.02.017 (2012).

20. Kumar, G. *et al*. *In vitro* physicochemical characterization and short term *in vivo* tolerability study of ethionamide loaded PLGA nanoparticles: potentially effective agent for multidrug resistant tuberculosis. *J Microencapsul* **28**, 717–728, doi:10.3109/02652048.2011.615948 (2011).
21. Davis, M. E. & Brewster, M. E. Cyclodextrin-based pharmaceutics: past, present and future. *Nat Rev Drug Discov* **3**, 1023–1035, doi:10.1038/nrd1576 (2004).
22. Committee for Human Medicinal Products (CHMP) Background review for cyclodextrins used as excipients. *European Medecines Agency* (2014).
23. Stella, V. J. & He, Q. Cyclodextrins. *Toxicol Pathol* **36**, 30–42, doi:10.1177/0192623307310945 (2008).
24. Zuckerman, J. E. *et al*. Correlating animal and human phase Ia/Ib clinical data with CALAA-01, a targeted, polymer-based nanoparticle containing siRNA. *Proc Natl Acad Sci USA* **111**, 11449–11454, doi:10.1073/pnas.1411393111 (2014).
25. Daoud-Mahammed, S. *et al*. Cyclodextrin and polysaccharide-based nanogels: entrapment of two hydrophobic molecules, benzophenone and tamoxifen. *Biomacromolecules* **10**, 547–554, doi:10.1021/bm801206f (2009).
26. Daoud-Mahammed, S. *et al*. Self-assembling cyclodextrin based hydrogels for the sustained delivery of hydrophobic drugs. *J Biomed Mater Res A* **86**, 736–748, doi:10.1002/jbm.a.31674 (2008).
27. Davis, M. E. *et al*. Evidence of RNAi in humans from systemically administered siRNA via targeted nanoparticles. *Nature* **464**, 1067–1070 (2010).
28. Gref, R. *et al*. New self-assembled nanogels based on host-guest interactions: characterization and drug loading. *J Control Release* **111**, 316–324, doi:10.1016/j.jconrel.2005.12.025 (2006).
29. Christophe, T., Ewann, F., Jeon, H. K., Cechetto, J. & Brodin, P. High-content imaging of Mycobacterium tuberculosis-infected macrophages: an *in vitro* model for tuberculosis drug discovery. *Future Med Chem* **2**, 1283–1293, doi:10.4155/fmc.10.223 (2010).
30. Christophe, T. *et al*. High content screening identifies decaprenyl-phosphoribose 2′ epimerase as a target for intracellular antimycobacterial inhibitors. *PLoS Pathog* **5**, e1000645, doi:10.1371/journal.ppat.1000645 (2009).
31. Queval, C. J. *et al*. STAT3 Represses Nitric Oxide Synthesis in Human Macrophages upon Mycobacterium tuberculosis Infection. *Sci Rep* **6**, 29297 (2016).
32. Sorrentino, F. *et al*. Development of an Intracellular Screen for New Compounds Able To Inhibit Mycobacterium tuberculosis Growth in Human Macrophages. *Antimicrob Agents Chemother* **60**, 640–645 (2015).
33. Stanley, S. A. *et al*. Identification of host-targeted small molecules that restrict intracellular Mycobacterium tuberculosis growth. *PLoS Pathog* **10**, e1003946 (2014).
34. Costa-Gouveia, J., Ainsa, J. A., Brodin, P. & Lucia, A. How can nanoparticles contribute to antituberculosis therapy? *Drug Discov Today* (2017).
35. Layre, A. M. *et al*. Busulfan loading into poly(alkyl cyanoacrylate) nanoparticles: physico-chemistry and molecular modeling. *J Biomed Mater Res B Appl Biomater* **79**, 254–262, doi:10.1002/jbm.b.30536 (2006).
36. Bouligand, J. *et al*. Busulphan-loaded long-circulating nanospheres, a very attractive challenge for both galenists and pharmacologists. *J Microencapsul* **24**, 715–730 (2007).
37. Filipe, V. *et al*. Fluorescence single particle tracking for the characterization of submicron protein aggregates in biological fluids and complex formulations. *Pharm Res* **28**, 1112–1120, doi:10.1007/s11095-011-0374-0 (2011).
38. Filipe, V., Hawe, A. & Jiskoot, W. Critical evaluation of Nanoparticle Tracking Analysis (NTA) by NanoSight for the measurement of nanoparticles and protein aggregates. *Pharm Res* **27**, 796–810, doi:10.1007/s11095-010-0073-2 (2010).
39. Li, Y., Lubchenko, V. & Vekilov, P. G. The use of dynamic light scattering and brownian microscopy to characterize protein aggregation. *Rev Sci Instrum* **82**, 053106, doi:10.1063/1.3592581 (2011).
40. Zambaux, M. F., Bonneaux, F., Gref, R., Dellacherie, E. & Vigneron, C. Preparation and characterization of protein C-loaded PLA nanoparticles. *J Control Release* **60**, 179–188 (1999).
41. Zambaux, M. F. *et al*. Influence of experimental parameters on the characteristics of poly(lactic acid) nanoparticles prepared by a double emulsion method. *J Control Release* **50**, 31–40 (1998).
42. Kumar, G., Shafiq, N. & Malhotra, S. Drug-loaded PLGA nanoparticles for oral administration: fundamental issues and challenges ahead. *Crit Rev Ther Drug Carrier Syst* **29**, 149–182 (2012).
43. Queval, C. J. *et al*. A microscopic phenotypic assay for the quantification of intracellular mycobacteria adapted for high-throughput/high-content screening. *J Vis Exp* e51114, doi:10.3791/51114 (2014).
44. Guillon, A. *et al*. Pulmonary delivery of dry powders to rats: tolerability limits of an intra-tracheal administration model. *Int J Pharm* **434**, 481–487 (2012).
45. Wong, B. A. Inhalation exposure systems: design, methods and operation. *Toxicol Pathol* **35**, 3–14 (2007).
46. Maillet, A. *et al*. The airways, a novel route for delivering monoclonal antibodies to treat lung tumors. *Pharm Res* **28**, 2147–2156, doi:10.1007/s11095-011-0442-5 (2011).
47. Chandenier, J. *et al*. The utility of a nebulised intra-tracheal rat model of invasive pulmonary aspergillosis. *Mycoses* **52**, 239–245 (2009).
48. Gagnadoux, F. *et al*. Aerosol delivery of chemotherapy in an orthotopic model of lung cancer. *The European respiratory journal* **26**, 657–661, doi:10.1183/09031936.05.00017305 (2005).
49. Aragao-Santiago, L. *et al*. Compared *in vivo* toxicity in mice of lung delivered biodegradable and non-biodegradable nanoparticles. *Nanotoxicology* **10**, 292–302, doi:10.3109/17435390.2015.1054908 (2016).
50. Cabral Marques, H. M., Hadgraft, J., Kellaway, I. W. & Taylor, G. Studies of cyclodextrin inclusion complexes. IV. *The pulmonary absorption of salbutamol from a complex with 2-hydroxypropyl-β-cyclodextrin in rabbits. Int J Pharm* **77**, 303–307 (1991).
51. Evrard, B. *et al*. Cyclodextrins as a potential carrier in drug nebulization. *J Control Release* **96**, 403–410 (2004).
52. Othman, M. *et al*. A comprehensive study of the spontaneous formation of nanoassemblies in water by a "lock-and-key" interaction between two associative polymers. *J Colloid Interface Sci* **354**, 517–527 (2011).
53. Bilati, U., Allémann, E. & Doelker, E. Nanoprecipitation versus emulsion-based techniques for the encapsulation of proteins into biodegradable nanoparticles and process-related stability issues. *Aaps Pharmscitech* **6**, E594–E604 (2005).
54. Ankrum, J. A. *et al*. Engineering cells with intracellular agent–loaded microparticles to control cell phenotype. *Nat. Protocols* **9**, 233–245, doi:10.1038/nprot.2014.002 (2014).
55. Bivas-Benita, M., Zwier, R., Junginger, H. E. & Borchard, G. Non-invasive pulmonary aerosol delivery in mice by the endotracheal route. *Eur J Pharm Biopharm* **61**, 214–218 (2005).

Acknowledgements

We gratefully acknowledge Eik Hoffmann, Helene Bauderlique, Nathalie Deboosere, Isabelle Ricard, Rosangela Frita, Grant Kiely, Alexandre Vandeputte, Gaspard Deloison, Quentin Pascal and Laurent Marsollier for technical assistance and image analysis. We acknowledge the PICT-IBiSA, Frank Lafont and Antonino Bongiovanni from BiCEL for providing access to microscopy equipment. We thank Michel Terray (Malvern Instruments) for helpful discussions. Financial support for this work was provided by the European Community (CycloN Hit Grant no 608407, ERC-STG INTRACELLTB Grant no 260901), the Agence Nationale de la Recherche (ANR-10-EQPX-04-01, ANR-14-CE08-0017, ANR-14-CE14-0027-01, the Feder (12001407 (D-AL) Equipex Imaginex BioMed) and the Region Nord Pas de Calais (convention no 12000080).

Author Contributions

The author(s) have made the following declarations about their contributions: Conceived and designed the experiments: J.C.G., E.P., S.J., A.M., A.B., J.H., R.G., P.B. Performed the experiments: J.C.G., E.P., S.J., A.M., J.P.S., A.B., R.G., P.B. Contributed reagents/materials/analysis tools: J.C.G., E.P., S.J., A.M., V.D., G.S., R.I., C.Q., O.R.S., C.P., N.W., M.F., B.D., J.P.S., J.H., R.G., A.B., P.B. Performed data analysis: J.C.G., E.P., S.J., A.M., V.D., G.S., R.I., L.M., N.W., R.G., A.B., P.B. Wrote the paper: J.C.G., E.P., S.J., A.M., R.G., P.B.

Additional Information

Supplementary information accompanies this paper at doi:10.1038/s41598-017-05453-3

Competing Interests: The authors declare that they have no competing interests.

Publisher's note: Springer Nature remains neutral with regard to jurisdictional claims in published maps and institutional affiliations.

3.4. Article 1 – Supplementary Information

Section I - Nanoparticles development

PLA/PLGA NPs – Nanoprecipitation method

Several PLA and PLGA polymers were employed to prepare the nanoparticles by nanoprecipitation (P1, P2, P3, P4, see materials and method section). In all cases the formulated NPs were remarkably stable upon storage up to 5 months, with less than 5 % size variation. The size variation over a period of 1 month is shown in the Supplementary Fig. S1.

Interestingly no difference in the size evolution of NPs was shown between the formulation stored at room temperature or in the refrigerator (4°C).

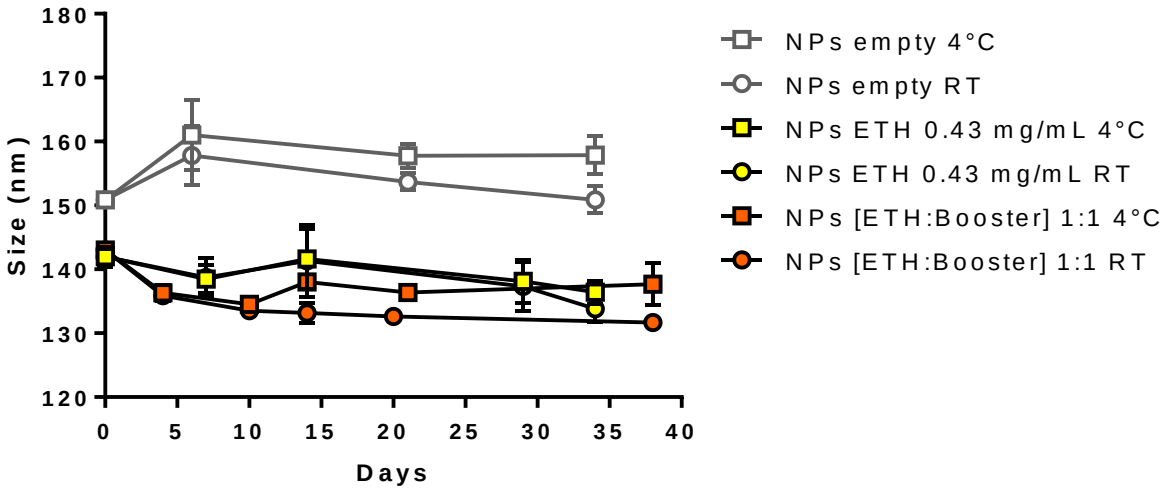

Supplementary Figure S15 – Stability of nanoparticles obtained by nanoprecipitation method over a period of 1 month (measured by DLS). The graph shows size stability of nanoparticles (charged or not) over 1 month. RT: storage at room temperature, 4°C: storage in the refrigerator.

The first attempt of formulation has been performed using P1 (1.43 mg/mL polymer in suspension). The encapsulation of Ethionamide (ETH) alone was studied by trying to encapsulate increasing concentrations of this drug (from 0.07 to 0.71 mg/mL). The results are shown in the Supplementary Fig. S2.

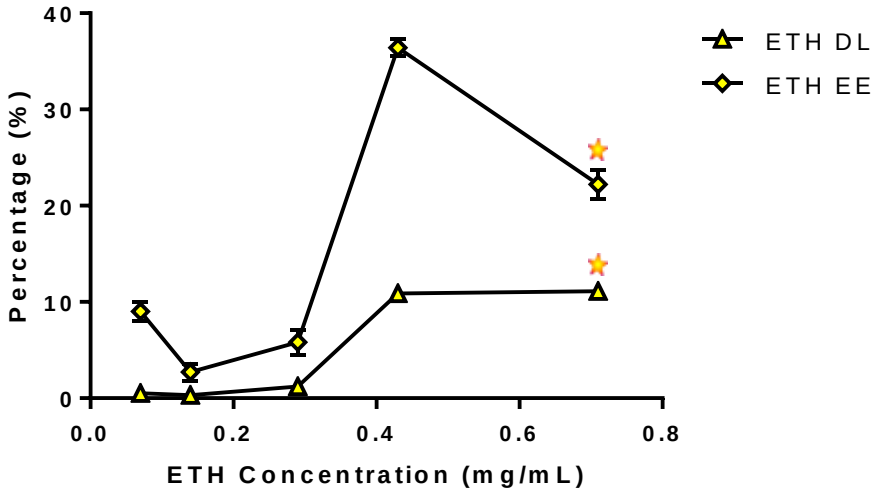

Supplementary Figure S16 – Effect of increasing ETH concentration on EE% and DL% of nanoparticles formulated by nanoprecipitation with P1. The yellow star (★) represents the formation of ETH crystals few days after nanoparticles preparation (ETH concentration of 0.71 mg/mL).

Formulations up to an ETH concentration of 0.43 mg/mL were completely stable. In these conditions the highest achieved drug loading (DL) and encapsulation efficiency (EE) were 11 wt % and 36 wt %, respectively. Unfortunately, raising the amount of ETH to 0.71 mg/mL in the attempt to further increase DL and EE, the DL resulted unchanged and the encapsulation efficiencies decreased to 22 % (Supplementary Fig. S2). Moreover, increasing ETH amounts in the NP preparation procedure lead to the formation of drug crystals which progressively grew in the suspension media until being seen with the naked eye, few days after NP preparation (Supplementary Fig. S3).

Supplementary Fig. S3 shows the decreasing of DL and EE (P1 and ETH concentration of 0.71 mg/mL) during the first 8 days after NPs formulation. The formation of crystals was observed after 5 days and corresponds to a further decrease in NPs DL and EE.

ETH crystallisation in P1 NPs was avoided only at ETH concentrations below 0.71 mg/mL, which is insufficient for *in vivo* applications. Attempts to concentrate the NPs suspensions failed because of a strong aggregation in the absence of protective surfactants.

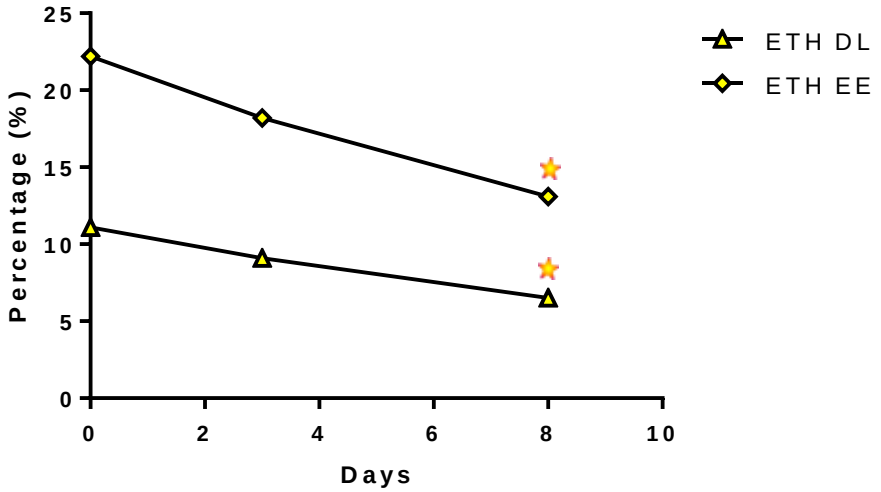

Supplementary Figure S17 - DL% and EE% decrease during storage. DL and EE decreased during first days of storage leading to the formation of crystals at the bottom of the flask (represented by the yellow star ★ in the figure) and to a decrease of both DL and EE.

In an additional attempt to increase both DL and EE, a series of PLA and PLGA copolymers were used, with different molecular weights and compositions (P2, P3 and P4). In all cases, aggregation or drug crystallization occurred. Better results in terms of DL and EE (24 wt % and 34 wt %) were obtained with P3 and an ETH concentration of 1 mg/mL. However, crystallisation occurred after 5 days as for the other polymers. Moreover, co-encapsulating Booster did not improve ETH loading, as it was found that Booster had stronger affinity for the polymeric NP than ETH. As an example, at the ratios [ETH:Booster] [1:0.1] and [1:1], ETH DL were lower than 2 wt %. Interestingly Booster DL and EE during coencapsulation were significantly higher than ETH ones (9 % and 29 % wt respectively, for ratio [1:1]) showing a higher affinity of the Booster for the polymeric matrix.

PLA NPs – Nanoemulsion method

To address the challenge of coencapsulating ETH and Booster, a second method based on the formation of an emulsion, stabilized with polyvinyl alcohol (PVA), a

surfactant approved for pulmonary administration, was set up using P4 (see material and methods section).

An extensive study on mean diameter of PLA NPs obtained by nanoemulsion has been performed using the 3 independent methods: PCS, NTA and cryo-TEM (see main text). The results show the importance of the use of different techniques to truly characterise nanoparticulate systems. Results are reported in Supplementary Table S1. It's interesting to point out that no significant difference in the diameter of NPs has been found between empty PLA NPs and drug-loaded PLA NPs.

Supplementary Table S2 - Main characteristics of empty and drug-loaded NPs made of P4 by the nanoemulsion method. NP mean hydrodynamic diameters were determined by PCS and NTA. Nanoparticles dry diameter was determined by cryo-TEM and nanoparticle concentration was obtained by NTA. Concentration results given were obtained after 10,000 times dilution of each sample as prescribed to fit the instrument requirements and to allow the particle to move freely according to their Brownian motions.

Formulation	Mean diameter					Concentration
	D PCS Z Average (nm ± SE)	PdI PCS	D PCS Number (nm ± SE)	D NTA (nm± SD)	Cryo-TEM	NTA (particle/mL)
NPs	254 ± 4	0.054	220 ± 10	176 ± 45	110 ± 50	$1.01x10^9$
NPs [ETH]	267 ± 3	0.074	226 ± 10	176 ± 48	100 ± 40	$0.88x10^9$
NPs [ETH:Booster] [1:0.1]	258 ± 3	0.058	223 ± 10	180 ± 51	100 ± 50	$1.03x10^9$
NPs [ETH:Booster] [1:1]	274 ± 4	0.090	235 ± 11	178 ± 52	100 ± 50	$0.89x10^9$
NPs [Booster]	277 ± 5	0.075	238 ± 11	171 ± 49	120 ± 55	$0.91x10^9$

NPs formulated with the nanoprecipitation method were remarkably stable upon storage more than 5 months, with less than 10 % size variation and a PdI still lower than 0.1. The size variation over a period of 1 month is shown in the Supplementary Fig. S4

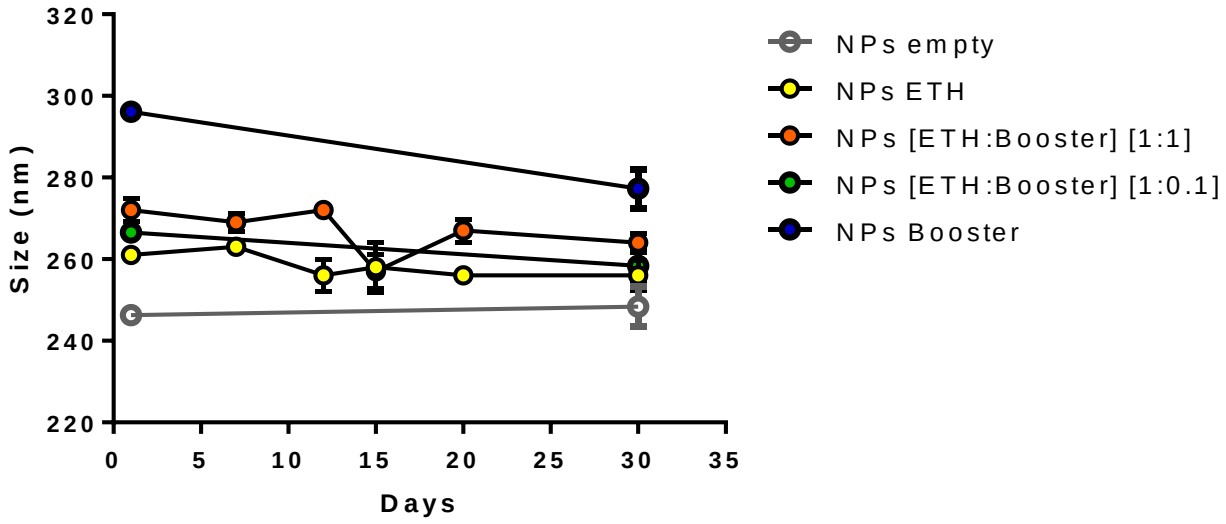

Supplementary Figure S4 – Stability of NPs obtained by nanoemulsion over a period of 1 month. No crystallization was observed during storage and no significant size or polydispersity changes (DLS) were found.

Section II - Phenotypic extracellular and intracellular assays

To investigate the efficacy of drug-loaded NPs against *M. tuberculosis,* we used two phenotypic assays that are disease-relevant and amenable to high-throughput. The first one is a simple assay relying on the monitoring of fluorescence from a strain of *M. tuberculosis* that expresses the green fluorescence protein using a microplate photometer. The second is an image-based model that allows the multi-parametric quantification of *M. tuberculosis* replication inside its favourite niche, the macrophage. The dedicated protocol used for image analysis with the Columbus software is given in Supplementary S5 below.

Input Image	**Stack Processing :** Individual **Flatfield Correction :** None		
Find Nuclei	**Channel :** Exp1Cam3 **ROI :** None	**Method :** B Common Threshold : 0.5 Area : > 15 µm² Split Factor : 5 Individual Threshold : 0.55 Contrast : > 0.2	Output Population : Nuclei
Select Population (5)	**Population :** Nuclei	**Method :** Common Filters Remove Border Objects Region : Nucleus	Output Population : Nuclei 2
Calculate Intensity Properties (2)	**Channel :** Exp1Cam3 **Population :** Nuclei 2 **Region :** Nucleus	**Method :** Standard Mean	Output Properties : Intensity Nucleus Exp1Cam3
Select Population (3)	**Population :** Nuclei 2	**Method :** Filter by Property Intensity Nucleus Exp1Cam3 Mean : > 200	Output Population : Nuclei 2 Selected
Find Cytoplasm	**Channel :** Exp1Cam3 **Nuclei :** Nuclei 2 Selected	**Method :** A Individual Threshold : 0.15	
Find Spots	**Channel :** Exp1Cam2 **ROI :** Nuclei 2 Selected **Region :** Cell	**Method :** B Detection Sensitivity : 0.55 Splitting Coefficient : 1 Calculate Spot Properties	Output Population : Spots
Calculate Intensity Properties	**Channel :** Exp1Cam2 **Population :** Spots **Region :** Spot	**Method :** Standard Mean	Output Properties : Intensity Spot Exp1Cam2
Select Population	**Population :** Spots	**Method :** Filter by Property Intensity Spot Exp1Cam2 Mean : > 150 Spot Contrast : > 0.2 Boolean Operations : F1 and F2	Output Population : Bacteria
Calculate Morphology Properties (2)	**Population :** Bacteria **Region :** Spot	**Method :** Standard Area	Output Properties : Bacteria
Define Results	**Method :** List of Outputs **Population : Nuclei 2 Selected** Number of Objects **Population : Bacteria** Bacteria Area [µm²] : Sum		

Supplementary Figure S5- Columbus script used for image analysis. Two colour-images were analysed. The red recorded on the channel "Exp1Cam3" was used for the nucleus and cytoplasm detection. The green recorded on the channel "Exp1Cam2" was used to detect the bacteria. ROI: Region of interest.

In Supplementary Fig. S6 we point out that the % of inhibition in the presence of empty PLA and empty pCD is negligible (close to zero) independently from the concentration of the NPs, both in the intra- and extracellular assay. These results show that the antibacterial effect observed is due to the presence of ETH and Booster released from the nanoparticles since the unloaded nanoparticles were not able to impair bacterial replication.

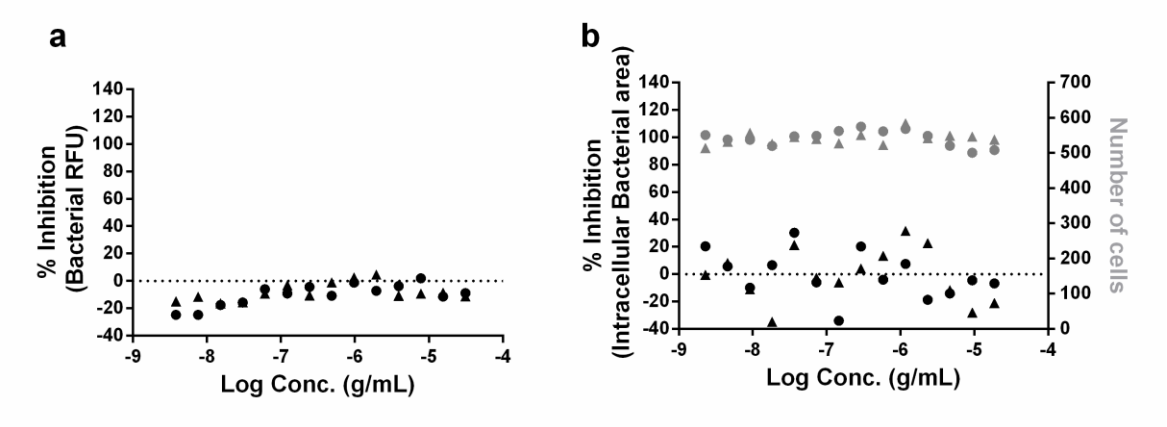

Supplementary Figure S6- Effect of empty NPs on intra- and extra-cellular assay. (a) % of inhibition of bacterial RFU obtained with empty PLA made by the nanoemulsion method (solid circle) and with empty pCD (solid triangle). **(b)** % of inhibition of intracellular bacterial area (black points) and number of cells (grey points) obtained with empty PLA made by the nanoemulsion method (solid circle) and with empty pCD (solid triangle).

Section III - Detailed Materials and methods

Compounds and drugs used

PLGA 75:25 acid terminated (P1) (MW: 37-84 KDa, 10P002), PLGA 50:50 ester terminated (P2) (MW: 70-100 KDa, 10P016) and PLGA 50:50 acid terminated (P3) (MW: 5-20 KDa, 10P019) were kindly provided by PCAS (Expansorb, Aramon, France). PLA ester terminated (P4) (MW =10-18 kDa), PVA (87-90% hydrolyzed), DMSO-99.5%, ETH and amikacin were all purchased from Sigma-Aldrich. Injectable water was purchased from Cooper (Melun, France). Dichloromethane (DCM-Analar Normapur stabilized with about 0.002% of 2-methyl-2-butene) and MeOH were from Prolabo (Fontenay-sous-Bois, France). KCl (99%) was purchased from Alfa Aesar (Karlsruhe, Germany).

The Booster named BDM41906 (5,5,5-Trifluoro-1-[4-(3-thiazol-2-yl-1,2,4-oxadiazol-5-yl)piperidin-1-yl] pentan-1-one) was synthesized as previously described (Flipo, Desroses et al. 2011).

β-CD was kindly supplied by Roquette, Lestrem, France. pCD NPs of around 10 nm were produced as previously described (Gref, Amiel et al. 2006; Othman, Bouchemal et al. 2011) by crosslinking β-CD under strongly alkaline conditions with epichlorohydrin

(EP). Briefly, 100 g of anhydrous β-CD was solubilized overnight in 160 mL of NaOH 33% w/w solution. Then, 81.52 g of EP was rapidly added and the reaction was stopped in the vicinity of the gelation point by addition of acetone. The β-CD NPs, recovered by ultrafiltration followed by freeze-drying, contained 70% w/w β-CD, as determined by ^{1}H NMR spectroscopy.

Nanoparticle preparation

Nanoprecipitation: encapsulation of ETH in PLA and PLGA NPs was carried out adapting a previously reported procedure (Bilati, Allémann et al. 2005). Briefly, 0.4 mL of DMSO solution containing 10 mg polymer (PLA or PLGA) and ETH (0.5 to 7 mg) were poured drop by drop in 7 mL of injectable water under magnetic stirring. In the case of co-encapsulation, 3 mg (ratio 10:10) or 0.3 mg of Booster (ratio 10:1) were added to the DMSO solution.

Nano-emulsion: preparation of PLA NPs was carried out as previously reported by Kumar et al. with slight modifications (Kumar, Malhotra et al. 2011). Briefly, 10 mg of ETH were solubilized in 0.2 mL of MeOH and mixed to 1.5 mL of a dichloromethane (DCM) solution containing 20 mg of P4 in DCM. For the co-encapsulation of the synergic drugs pair, 10 mg of Booster, in case of 10:10 ratio, or 1 mg of Booster, in case of 10:1 ratio, were solubilized in the solution of PLA in DCM. Control empty NPs were prepared in the same conditions, except that the drugs were not added.

The organic phase was poured into 4 mL of an aqueous phase (injectable water) containing 0.5% w/v PVA and emulsified 20 seconds (vortex). The mixture was then sonicated (Sonopuls HD 2070, BANDELIN electronic GmbH & Co, Berlin, Germany) at 20% power for 1.5 min, stopping the procedure each 30 seconds to avoid the overheating and for 30 additional seconds to 10%. The resulting emulsion was left uncapped under magnetic stirring, checking the weight of the flask to monitor the evaporation of the organic solvents, until complete evaporation of DMC and MeOH.

Drug encapsulation in “green” pCD NPs: encapsulation of ETH and Booster in pCD NPs was carried on without using any organic solvent, by mixing for at least 4 hours the NP suspensions with the drug powders.

Nanoparticle characterization

Size measurement by PCS and Zeta Potential measurement

The average hydrodynamic diameter of the NPs was determined at 25°C, in triplicate, with an equilibration time of 60 s, using a Malvern Zetasizer® (Nano ZS90, Malvern Instruments S.A., Worcestershire, UK). For the measurement of method 1 formulations, Samples were analyzed without performing any dilution (method 1) and with 1:10 and 1:100 dilutions in injectable water (as prescribed by ISO 22412) in the case of method 2. No significant differences were noticed in the hydrodynamic diameter of the two dilutions. All autocorrelation functions have an intercept with amplitude equal to 0.9 or higher. Mean diameters were reported as Z Average (nm) ±SE (Standard Error - with a Polydispersity Index lower than 0.1) or as number mean diameter (nm) ±SD (Standard Deviation).

The stability of the NPs prepared by nanoprecipitation and nanoemulsion was assessed at RT (25°C-storage conditions). The NPs mean diameters were monitored up to three months of storage at 25°C via DLS size measurements. (see Supplementary Fig. S1 and S5)

Also the Zeta Potential (ZP) of nanoparticles was measured in KCl 1Mm by Malvern Zetasizer©. Each sample was diluted 100 times and 1,000 times in KCl 1mM. Results are reported as ZP (mV) ± SD.

Size measurement by NTA and concentration quantification

Mean hydrodynamic diameter and concentration of the NPs were measured 5 times for 60 seconds at 25°C by NTA (NanoSight LM10, Malvern Instruments S.A., Worcestershire, UK, equipped with a 565 nm filter and a NanoSight syringe pump). NPs prepared by nanoprecipitation were diluted 2,000 times and the ones made by nanoemulsion 10000 times. Results are reported as Mean diameter ± SD.

Cryogenic transmission electron microscopy (cryo-TEM)

5 µl of NPs suspensions (diluted 4 times in water) were deposited onto a 200 mesh holey copper grid (Ted Pella Inc.) and flash-frozen in liquid ethane cooled down at liquid nitrogen temperature. Cryo-TEM images were acquired on a JEOL 2200FS energy-filtered

(20eV) field emission gun electron microscope operating at 200 kV using a Gatan ssCCD 2048 × 2048 pixels. Several thousands of images were automatically acquired for each NP formulation to obtain representative results.

Drug sample preparation for drug(s) dosage

To determine the amounts of ETH and Booster incorporated in PLGA NPs, 500 µL of NP suspensions were centrifuged at 17,000g for 15 minutes. Then, 200 µL of the supernatant were withdrawn to assess the quantity of non-encapsulated drug (indirect estimation). The NPs pellet was dissolved in 250 µL DMSO and dosed (direct estimation of the encapsulated drug). For the pCD NPs, aliquots of pCD NPs containing drug(s) were centrifuged at 5000 rpm for 10 min to remove unloaded drug(s). The supernatant containing the pCD NPs was then diluted with DMSO (1:1 volume ratio) and dosed by HPLC after dilution in DMSO and/or with acetonitrile/water 45/55 v/v.

All the samples were dosed by liquid chromatography-mass spectrometry (LC-MS-MS) and reverse phase HPLC (RP-HPLC). For LC-MS-MS analysis, a Waters Acquity I Class – Xevo TQD system using an Acquitity BEH C18 column (50x2.1mm, 1.7 µm) at 40°C was used. The mobile phase at a flow of 600 µL/min was composed by two solvents: ammonium acetate 10 mM (Solvent A, spontaneous pH) and acetonitrile (CH_3CN) with 0,1% HCOOH (Solvent B) (UPLC gradient of B= 0% at time 0.98% from minute 2.00 to 2.50 then 0% from minute 2.60) and its flow was 600 µL/min.

Samples were prepared by diluting them 100 times in MeOH and then 100 times in a solution of MeOH containing the internal standards, then 1 µL of each sample was injected in the system.

The RP-HPLC analysis were performed after dilution with the mixture acetonitrile/water 45/55 v/v using a Agilent HPLC system (Agilent 1100 Series) equipped with a C18 column (Kinetex 5u C18, 100 A, Phenomenex, and UV detector at λ = 280 nm. The chromatographic conditions were as follows: solvent A 0.1% Trifluoroacetic Acid (TFA) in water and solvent B 0.1% TFA in acetonitrile; 0–2 min: 0%–20% B, 2–6 min: 20%–45% B, 6–10 min: 45%-75% B, 10–15 min: 75%–0%. Flow rate: 1.0 mL/min at room temperature.

In all cases, R^2 values for both ETH and Booster were higher than 0.99. From the obtained data the DL and EE were calculated as shown in equation 1 and 2, respectively. The DL can be defined as the mass fraction of a NP that is composed of drug, while the EE can be considered as the fraction of drug effectively encapsulated into the NPs compared with the amount that was initially added during the particles preparation (Kumar, Malhotra et al. 2011; Ankrum, Miranda et al. 2014).

$$DL(\%) = \frac{(mg\ of\ encapsulated\ drug^{**})}{(mg\ of\ polymer)} \times 100 \quad (1)$$

$$EE(\%) = \frac{(mg\ of\ encapsulated\ drug^{**})}{(mg\ of\ drug\ initially\ added\ to\ the\ formulation)} \times 100 \quad (2)$$

[***The amount of encapsulated drug has been calculated with a direct or indirect estimation, depending on the sample fraction considered]*

Bacteria and macrophages

M. tuberculosis H37Rv strain constitutively expressing the green fluorescent protein (H37Rv-GFP) was used as a reporter for the replication assay. Bacteria were cultured at 37 °C for 16 days in complete 7H9 medium containing 0.5 % glycerol (50405, Euromedex), 10% Middelbrook oleic acid-albumin-dextrose-catalase (OADC) (211886, Becton Dickinson), 0.05% Tween 80 (2002A, Euromedex) and 50 µg/mL hygromycin B (10687010, Invitrogen). In the day of the experiment, *M. tuberculosis* were washed with D-PBS Ca-Mg- (14190169, LifeTechnologies) 3 times with centrifugation at 5,000 RPM for 5 minutes and centrifuged at 700 RPM for 2 minutes to remove clumped bacteria. Bacteria were resuspended in RPMI-1640 + glutamax (61870044, LifeTechnologies) containing 10 % heat inactivated fetal bovine serum (FBS) (10270106, Gibco) and titrated by measuring the optical density at 600 nm.

Mouse macrophage RAW 264.7 (ATCC # TIB-71) were maintained at 37°C in RPMI-1640 + glutamax containing 10% FBS and were passed 3 times per week and used before passage number 7. Macrophages were harvested by using Versene (15040033, LifeTechnologies).

Assay plate preparation

ETH, BDM41906 and INH were diluted in DMSO (34943, Sigma-Aldrich) to 10 mg/mL and were dispensed in Echo-qualified 384-well low dead volume source plates (Labcyte). Echo 550 Series Liquid Handler (Labcyte) was used to transfer precise volumes between 5 and 500 nL from the Echo-qualified plate to the 384-well clear-bottom polystyrene assay plates (78198, Greiner Bio-One) by using sound waves. All the conditions were backfilled with DMSO until 500 nL. Prior to addition of cells, 4.5 µL of cell medium were dispensed in the Echo-dispensed wells.

NPs loaded with ETH or with the [ETH:Booster] pair were diluted in water to 0.2 mg/mL of ETH. 2-fold serial dilutions of the mother solution in a final volume of 100 µL were performed in sterile MilliQ water in a 384 deep well "diamond plate" (P-384-120SQ-C-S, Axygen) in order to obtain a dose-response curve. Posteriorly, 5 µL of the NPs were dispensed in the 384-well assay plates.

Extracellular *in vitro* assay

Bacteria were diluted at 2×10^6 bacteria/mL using complete 7H9 medium and 45 µL/well of bacterial suspension were added in 384-well assay plates. After 5 days incubation at 37°C, 5% CO_2, extracellular plates were read using a fluorescence reader (Victor X3, Perkin Elmer) at excitation/emission of 485/535 nm for 0.1 seconds/well with a small emission aperture and CW-lamp energy of 50,000. The read-out, relative fluorescence units (RFU), versus the ETH concentration was then plotted using GraphPad Prism 5.0 software and the concentration required to inhibit 50% of the bacterial replication (IC_{50}) was calculated by nonlinear regression analysis using the equation for a sigmoidal dose-response curve with variable slope.

Intramacrophage *in vitro* assay

For intracellular assay, bacteria were mixed with RAW 264.7 macrophages to prepare a suspension at 5×10^5 cells/mL and 1×10^6 bacteria/mL (multiplicity of infection 2) in RPMI-1640 + glutamax containing 10% FBS. After 2 hours of infection at 37°C with shaking (120 rpm), infected cells were washed with RPMI-1640 + glutamax containing

10% FBS by centrifugation at 1,100 rpm for 5 minutes. The remaining extracellular bacilli from the infected cell suspension were killed by a 1 hour 50 μg/mL amykacin (A2324-5G, Sigma) treatment and then washed twice with RPMI-1640 + glutamax containing 10% FBS. Finally, 45 μL/well of cellular suspension was added in the 384-well assay plate and incubated during 5 days at 37°C, 5% CO_2. Macrophages were then stained with 5 μM Syto 60 (S11342, Molecular probes) dye for 1 hour, followed by plate sealing, imaging acquisition and data analysis.

Image acquisition

Confocal images were recorded on an automated fluorescent ultra-high-throughput microscope Opera (Perkin Elmer). This microscope is based on an inverted microscope architecture that allows imaging of cells cultivated in 96- or 384-well microplates. Images were acquired with a 20X- water immersion objective (NA 0.70). A double laser excitation (488-nm and 640-nm) and dedicated dichroic mirrors were used to record green fluorescence of mycobacteria and red fluorescence of the macrophages on two different cameras, respectively. A series of 6 pictures at the center of each well were taken and each image was then analyzed using Columbus system version 2.5.1 as previously described (Queval, Song et al. 2014) to extract the bacterial area and the number of cells.

Intramacrophage assay data analysis

Bacterial area was normalized with the negative control DMSO (0% inhibition) and the positive control INH at a concentration of 1 μg/mL (100 % inhibition) by converting it into a percentage of bacterial replication inhibition (% inhibition). % inhibition was calculated by the formula:

$$\%\ inhibition = \left(1 - \frac{\text{Test bacterial area} - \text{INH bacterial area}}{\text{DMSO bacterial area} - \text{INH bacterial area}}\right) \times 100$$

This formula was used to normalize the “test bacterial area” from different experiments, in order to decrease potential bias in the results due to differences in the % of infection and bacterial growth between experiments. For each compound, a plot of %

inhibition versus the ETH concentration was determined with GraphPad Prism 5.0 software and the IC_{50} was calculated in the same way as in the extracellular assay.

***In vivo* efficacy**

6-week old Balb/C female mice were purchased from Janvier (Le Genest-Saint-Isle, France) and were maintained in the animal house facility of the Pasteur Institute of Lille, France (Agreement B59-350009). The project (reference 00579.01) received ethic approval.

Toxicology studies

Sixteen uninfected 8-week mice were divided in four groups and endotracheally administered with water (vehicle) or pCD NPs over a period of 2 weeks (Fig 5a).

At day 14 mice were sacrificed, lungs were harvested and soaked in 4% formaldehyde (10% formalin solution, neutral buffered, HT501128, Sigma-Aldrich) for 24 hours, before being embedded in paraffin. Tissues were sliced with microtome and 5 µm sections were stained with Hematoxylin-Eosin (H-E) for light microscopy examination by an anatomopathologist. For flow cytometry analysis, lung were harvested, cut into small pieces and incubated for 1 hour at 37°C with a mix of DNAse I (100 µg/ml, , Sigma-Aldrich) and collagenase (1.6 mg/ml, Roche) 400 U/ml. Lung cells were washed and filtered before being incubated with saturating doses of purified 2.4G2 (anti-mouse Fc receptor, ATCC) in 200 µl PBS 0.2 % BSA 0.02 % NaN3 (FACS buffer) for 20 minutes at 4°C to prevent antibody binding on the Fc receptor. Various fluorescent mAb combinations in FACS buffer were used to stain 3-5x106 cells. Acquisitions were done on FACScantoII cytofluorometer (Becton Dickinson) with the following mAbs from BD Biosciences: Fluorescein (FITC)-coupled HL3 (anti-CD11c), FITC-coupled 145-2C11 (anti-CD3), APC-coupled RB6-8C5 (anti-GR1), phycoérythrine (PE)-coupled RM4-5 (anti-CD4), PE-coupled E50-2440 (anti-SIGLEC-F), APC-coupled BM8 (anti-F4/80). APC-eF780-coupled M1/70 (antiCD11b) was purchased from eBiosciences and fixable viability dye eFluor 506 (eBiosciences) was used to gate viable cells.

Efficacy studies

8-week mice (4 mice per group) were inoculated with *M. tuberculosis* H37Rv via the intranasal route to 10^6 bacteria in the lungs at day 0. On day 7, 9 and 11 after infection, NPs or INH were administered to mice using a Microsprayer® (MicroSprayer® Aerosolizer – Model IA-1C-M and FMJ-250 High Pressure Syringe, Penn Century Inc., Wyndmoor, PA). For the 1-week treatment and the 2-week treatment, administrations were on day 7, 9, 11 and on day 7, 9, 11, 14, 16, 18 respectively. To assess the reproducibility of NPs administration through the MicroSprayer®, the delivered doses of NP suspensions were collected in glass vials after each spray and were accurately weighted. Then the amount of the delivered drug was quantified by HPLC as already described.

The protocol to administer the NPs in mice was adapted from a previously reported one (Bivas-Benita, Zwier et al. 2005). Briefly, mice were placed in isoflurane chamber (Aerrane®, Baxter SAS, France). Then, one mouse was placed on the back on a platform (Mouse Intubation Platform – Model MIP, Penn Century Inc., Wyndmoor, PA) with isoflurane mask and hanging on its teeth. The tongue was pulled out by a tweezer and a laryngoscope (Small Animal Laryngoscope for mouse – Model LS-2-M, Penn Century Inc., Wyndmoor, PA) was used to see the trachea and 50µL of suspensions were delivered inside the lung allowing to aerosolize 50 µL suspensions inside the lungs. At day 14 or 21, mice were sacrificed and lungs were homogenized with MM300 bead beater (Retsch) and eight ten-fold serial dilutions were plated onto 7H11 agar plates supplemented with 10% OADC. CFUs were determined after a three-week growth. Statistics were performed using Student's t-test and one-way ANOVA analysis. Same p-values for in vivo experiments were obtained with the two tests. *: $p<0.1$, **: $p<0.01$,***: $p<0.001$.

Supplementary Video S1 – NTA video of a NP suspension obtained by nanoemulsion. NTA allows tracking each NP individually to determine its mean hydrodynamic diameter and the concentration of the sample. Indeed, the Nanosight instrument is able to track the Brownian motion of NPs, in order to determine its diffusion coefficient (D_t) and consequently calculate, using Stokes-Einstein equation the sphere-equivalent hydrodynamic diameter. The NP suspensions were diluted by a factor of 10^4 to fit the instrument requirements and to allow the particle to move freely

according to their Brownian motion. More than 2000 NPs are followed in each experiment.

References

1 Flipo, M. *et al.* Ethionamide boosters. 2. Combining bioisosteric replacement and structure-based drug design to solve pharmacokinetic issues in a series of potent 1, 2, 4-oxadiazole EthR inhibitors. *Journal of medicinal chemistry* **55**, 68-83 (2011).

2 Gref, R. *et al.* New self-assembled nanogels based on host-guest interactions: characterization and drug loading. *J Control Release* **111**, 316-324, doi:10.1016/j.jconrel.2005.12.025 (2006).

3 Othman, M. *et al.* A comprehensive study of the spontaneous formation of nanoassemblies in water by a "lock-and-key" interaction between two associative polymers. *J Colloid Interface Sci* **354**, 517-527 (2011).

4 Bilati, U., Allémann, E. & Doelker, E. Nanoprecipitation versus emulsion-based techniques for the encapsulation of proteins into biodegradable nanoparticles and process-related stability issues. *Aaps Pharmscitech* **6**, E594-E604 (2005).

5 Kumar, G. *et al.* In vitro physicochemical characterization and short term in vivo tolerability study of ethionamide loaded PLGA nanoparticles: potentially effective agent for multidrug resistant tuberculosis. *J Microencapsul* **28**, 717-728, doi:10.3109/02652048.2011.615948 (2011).

6 Ankrum, J. A. *et al.* Engineering cells with intracellular agent–loaded microparticles to control cell phenotype. *Nat. Protocols* **9**, 233-245, doi:10.1038/nprot.2014.002 (2014).

7 Queval, C. J. *et al.* A microscopic phenotypic assay for the quantification of intracellular mycobacteria adapted for high-throughput/high-content screening. *J Vis Exp*, e51114, doi:10.3791/51114 (2014).

8 Bivas-Benita, M., Zwier, R., Junginger, H. E. & Borchard, G. Non-invasive pulmonary aerosol delivery in mice by the endotracheal route. *Eur J Pharm Biopharm* **61**, 214-218 (2005).

4. CHAPTER II

Enhancement of the solubility and the bioavailability of antibiotics

Amélioration de la solubilité et de la biodisponibilité des antibiotiques

4.1. Résumé article 2: “Encapsulation de la Clofazimine dans des particules de silice nanoporeuses pour le traitement oral de *M. tuberculosis* résistant aux antibiotiques”

La propagation mondiale de micro-organismes résistants aux antibiotiques constitue une menace majeure pour la santé publique mondiale. Et malgré la prise de conscience de cette menace au cours des 30 dernières années, aucun nouveau type d'antibiotiques n’a été jusqu’alors développé par l’industrie pharmaceutique, suite aux échecs coûteux de développement de nouvelles thérapies de traitement à court terme (Nathan 2004). L’utilisation de nouveaux excipients pour reformuler des antibiotiques existants pourrait alors permettre de développer de nouvelles thérapies en améliorant leur efficacité et leur performance.

Ainsi l’utilisation d’antibiotiques déjà utilisés pour le traitement d’autres maladies, et pour lesquels aucune résistance bactérienne n’a été observée, pourrait constituer une stratégie pertinente pour accélérer le développement de nouvelles formulations thérapeutiques, et notamment pour la lutte contre la tuberculose multi-résistante et latente.

Par exemple, la Clofazimine (CLZ), un antibiotique découvert au cours des années 1950 et utilisé dans le traitement de la lèpre, pourrait être un candidat potentiel pour le traitement de la tuberculose (TB). L’efficacité de CLZ a déjà été montrée *in vitro* sur des souches de *Mycobacterium tuberculosis* multi-résistantes, avec une fréquence extrêmement basse de résistance à cet antibiotique (Yawalkar and Vischer 1979; Reddy, O'Sullivan et al. 1999). Cependant, son utilisation pour le traitement de TB n’a pas été envisagée jusqu'à présent, en raison de la variabilité de son activité thérapeutique observée dans différents modèles animaux (Van Rensburg, Anderson et al. 1997; Mukherjee, Rich et al. 2004; Van Deun, Maug et al. 2010; Cholo, Steel et al. 2012). De plus, son administration par voie orale chez l’homme a également montré des concentrations d’antibiotique inadaptées et une dose totale dans le plasma insuffisante pour obtenir une activité bactéricide contre *M. tuberculosis* (O'Connor, O'Sullivan et al. 1995; Janulionis, Sofer et al. 2004).

Néanmoins, les dernières données *in vitro* ont ravivé notre intérêt pour son utilisation pour le traitement de cas de TB multi-résistantes.

D’autre part, des formulations basées sur l’utilisation des nanotechnologies pour la délivrance d'antibiotiques se sont avérées efficaces *in vitro* et *in vivo* pour traiter ou prévenir d’autres maladies infectieuses (Huh and Kwon 2011; Semiramoth, Di Meo et al. 2012; Abed and Couvreur 2014; Song, Ahmad Nor et al. 2016; Wang, Wang et al. 2016). Mais le développement de produits pharmaceutiques basés sur l’utilisation de nanocarriers a été jusqu’alors entravée par des aspects réglementaires et la pénurie de connaissances relatives à l'effet biologique, la toxicité et la sécurité à long terme du matériel de transport utilisé (Crist, Grossman et al. 2013). Dans ce contexte, les particules à base de silice nanoporeuses (PSN) semblaient constituer des vecteurs attrayants pour l’administration d’antibiotiques par voie orale, de par leurs propriétés chimiques (Mamaeva, Sahlgren et al. 2013). Les PSN sont constituées de dioxyde de silicium amorphe (SiO2) chimiquement semblable au silicium colloidal couramment utilisé comme excipient dans l’agro-alimentaire et dans de nombreuses formulations à visée pharmaceutique (capsules, suspensions et comprimés par voie orale; préparations transdermiques, rectales et vaginales). L'Agence de protection de l'environnement (EPA) a notamment montré son absence de toxicité pour l'administration orale.

Sur la base de ces données bibliographiques intéressantes, notre étude a consisté à développer une nouvelle formulation de CLZ basée sur l’utilisation d’un nanocarrier pour améliorer la pharmacocinétique de CLZ et s’attaquer aux infections de TB multi-résistantes.

Dans des études précédentes, nos collaborateurs avaient montré que l'encapsulation de molécules pharmaceutiques à l'intérieur de la structure nano-poreuse des particules stabilisait les molécules dans leur forme amorphe, en améliorant leur solubilité et leur biodisponibilité (Xia, Zhou et al. 2012; Xia, Pethe et al. 2014).

Au vue de ces résultats prometteurs, le but de ce travail était d’encapsuler CLZ dans des particules de silice nanoporeuses, dans le but d’augmenter sa solubilité pour améliorer sa biodisponibilité dans des formulations destinées à une administration orale. Une sélection de particules de silice poreuses, se différenciant par leur taille, et la taille et le volume des pores, ont été étudiées.

Nos collaborateurs se sont chargés de la caractérisation physico-chimique de CLZ encapsulée dans les différentes PSN, ainsi que d’étudier sa stabilité après encapsulation, sa solubilité dans un milieu mimant le fluide gastrique, ainsi que sa toxicité et sa

perméabilité dans des cellules intestinales modèles. Dans notre étude, l'utilisation de particules de silice nanoporeuses a permis de stabiliser l'état amorphe de CLZ (pendant plus de 6 mois) et d'augmenter jusqu'à 20 fois la solubilité de l'antibiotique dans le liquide gastrique modèle, la vitesse de dissolution étant fonction de la morphologie et de la texture des PSN utilisées.

Dans notre laboratoire, nous avons étudié l'effet *in vitro* de différentes PSN sur des macrophages modèles infectés par Mtb. L'effet des PSN chargées, des PSN vides et de l'antibiotique non encapsulé sur la croissance intracellulaire de Mtb ont été évalués par utilisation d'un système de microscopie confocale à haut contenu automatisé (OPERA-PerkinElmer). Les résultats ont montré de façon intéressante que l'encapsulation de CLZ dans des PSN avait amélioré considérablement la solubilité de CLZ et sa perméabilité cellulaire, en atteignant des concentrations antimicrobiennes efficaces sur Mtb dans des macrophages infectés.

Pour la première fois, nous avons réussi avec succès à reformuler CLZ dans des PSN. Cette étude montre que l'utilisation de CLZ, un antibiotique bien connu et commercialisé pour le traitement d'autres maladies, combinée à un mode d'administration basé sur l'utilisation de nanotechnologies, peut constituer une stratégie pertinente et originale pour s'attaquer aux infections de TB résistantes aux antibiotiques.

4.2. Summary article 2: "Clofazimine encapsulation in nanoporous silica particles for the oral treatment of antibiotic resistant *M. tuberculosis*"

The worldwide spread of antibiotic-resistant microorganisms is no longer a prediction for the future, but it is now a major threat to worldwide public health. Despite the increasing awareness to this threat, over the last 30 years, no major new types of antibiotics have been developed by pharmaceutical companies mainly due to the persistent costly failure to discover novel antibiotics for short-term treatment therapies (Nathan 2004). The use of novel advanced excipients to reformulate existing antibiotic drugs allows the development of new therapies to enhance their efficacy and improve their performance.

Thus, the use of existing antibiotics already used in other diseases treatment, that have not acquired bacterial resistance, can offer a route to speed up the development time for new therapeutic formulations.

Clofazimine (CLZ), for example, is an antibiotic discovered in the 1950s currently used for the treatment of leprosy, can be a potential candidate to the tuberculosis (TB) treatment. The CLZ efficiency was already shown *in vitro* against *Mycobacterium tuberculosis* multi-resistant strains, with extremely low frequency of drug resistance to the antibiotic (Yawalkar and Vischer 1979; Reddy, O'Sullivan et al. 1999). However, the use for TB treatment has not been considered so far, due to the variability of the therapeutic activity observed in different animal models (Van Rensburg, Anderson et al. 1997; Mukherjee, Rich et al. 2004; Van Deun, Maug et al. 2010; Cholo, Steel et al. 2012). Furthermore, oral administration in humans showed inadequate peak drug concentrations and insufficient total dose in plasma to obtain bactericidal activity against *M. tuberculosis* (O'Connor, O'Sullivan et al. 1995; Janulionis, Sofer et al. 2004).

Nevertheless, the promising *in vitro* data have rekindled our interest in its use for multi-resistant TB treatment.

Nanotechnology based formulation for the delivery of antibiotics that have proven effective *in vitro* and *in vivo* for treating or preventing infectious diseases (Huh and Kwon 2011; Semiramoth, Di Meo et al. 2012; Abed and Couvreur 2014; Song, Ahmad Nor et al. 2016; Wang, Wang et al. 2016). However, development of pharmaceutical products using nanocarriers has been hindered due to regulatory issues and limited long-term safety and

toxicity data (Crist, Grossman et al. 2013). In this context, nanoporous silica particles (NSPs) have emerged as an attractive excipient with desirable properties for the delivery of oral drugs (Mamaeva, Sahlgren et al. 2013). NSPs are composed by amorphous SiO2 and analytically indistinguishable from colloidal SiO2, which has generally recognized as safe status from the US FDA for use its use in food and as an excipient for many dosage forms (oral capsules, suspensions and tablets; transdermal, rectal and vaginal preparations). The Environmental Protection Agency (EPA) has determined amorphous silica to show no toxicity by oral administration and therefore is exempt from requirement of tolerance status.

Based on this interesting bibliographic data, our work consisted in the development of a new formulation of CLZ using nanocarriers to improve the CLZ pharmacokinetics and fight multi-resistant TB.

In previous studies, our collaborators have shown that the encapsulation of pharmaceutical molecules inside the nanoporous structure, stabilized the molecules in their amorphous form, improving their solubility and bioavailability (Xia, Zhou et al. 2012; Xia, Pethe et al. 2014).

Motivated by this finding, the aim of this work was to encapsulate CLZ into NSPs in order enhance its solubility to improve its bioavailability in oral dosage formulations. A selection of different porous silica particles were used, differing in particle size, pore size and pore volume.

Our collaborators were in charge of the physicochemical characterization of the CLZ encapsulated in the NSP, as well as to study its stability after encapsulation, its solubility, toxicity and permeability in intestinal cells models. In our study, the use of silica nanoporous allowed to stabilize the amorphous state of CLZ (for more than 6 months) and to increase up to 20 times the solubility of the antibiotic in the model gastric fluid, the rate of dissolution being a function of the morphology and texture of the NSPs used.

In our laboratory, we studied the *in vitro* effect of different NSPs in macrophages models infected with *M. tuberculosis*. The effect of the loaded NSP, empty NSP and the non-encapsulated antibiotic in the intracellular *M. tuberculosis* replication was evaluated by the utilization of an automated confocal high content screening (OPERA-PerkinElmer).

The results showed that the CLZ encapsulation in the NSP had considerably improved the solubility and cell permeability of the CLZ, achieving effective antimicrobial concentrations in TB-infected macrophages.

For the first time, we were able to reformulate CLZ in NSP. This work shows that the use of CLZ, a well-known marketed antibiotic for treatment of other diseases, combined with an administration mode based in nanotechnologies, can be a pertinent strategy to fight drug-resistant TB.

4.3. Article 2

Clofazimine encapsulation in mesoporous silica particles for the oral treatment of antibiotic resistant *M. tuberculosis* infections

Authors list: Sabrina Valetti**,[1,2,] Xin Xia[1], **Joana Costa-Gouveia**[3], Priscille Brodin[3], Marie Françoise Bernet-Camard[4], Margareta Andersson[1] & Adam Feiler*[1,5]

Affiliations:

1: Nanologica AB, SE-151 36 Södertälje, Sweden

2: Biofilms – Research Center for Biointerfaces, Department of Biomedical Sciences, Faculty of Health & Sciences, Malmö University, Sweden

3: Univ. Lille, CNRS, INSERM, CHU Lille, Institut Pasteur deLille, U1019 – UMR 8204 – CIIL – Center for Infection & Immunity of Lille, F-59000 Lille, France

4: EA4043 Unité BactériesPathogènes et Santé (UBaPS), Univ. Paris-Sud, Université Paris-Saclay, 92296, Châtenay-Malabry Cedex, France

5: Surface and Corrosion Science, KTH Royal Institute of Technology, SE-100 44 Stockholm, Sweden

*Author for correspondence: adam@nanologica.com

**Author for correspondence: sabrina.valetti@outlook.com

Keywords: amorphous • Caco-2 cells • clofazimine • drug carrier • HPLC • intramacrophage • *in vitro* assay • nanoporous silica particles • oral drug delivery • tuberculosis

Structured abstract

Aims: First extensive reformulation of clofazimine (CLZ) in nanoporous silica particles (NSPs) for tackling antibiotic-resistant tuberculosis (TB) infections.

Materials & methods: Solid-state characterization of several CLZ-encapsulated NSP formulations was followed by *in vitro* drug solubility, Caco-2 intestinal cells drug permeability and TB antibacterial activity.

Results: NSPs stabilize the amorphous state of CLZ (shelf stability >6 months) and dramatically increase the drug solubility in simulated gastric fluid (up to 20-fold) with different dissolution kinetics depending on the NSPs used. CLZ encapsulation in NSP substantially enhances the permeation through model intestinal cell layer, achieving effective antimicrobial concentrations in TB-infected macrophages.

Conclusion: Promising results toward refurbishment of an approved marketed drug for a different indication suitable for oral anti-TB formulation.

Introduction

The worldwide spread of antibiotic-resistant microorganisms is no longer a prediction for the future, but it is now a major threat to worldwide public health.(WHO 2015) Currently, three of the top ten causes of death worldwide are from infectious diseases. In 2013, there were around 480 000 new cases of multidrug-resistant tuberculosis (MDR-TB) and extensively drug-resistant tuberculosis (XDR-TB) identified in 100 countries.(WHO 2015) The antibiotic therapy is the pillar of the modern medicine, enabling routine medical and surgical procedures to be effective and successful with the protection of antimicrobial treatment.(Nathan and Cars 2014) However, unconstrained overprescription, misuse and poor patient adherence to the treatment regimen has caused the systematic and uncontrolled evolution of drug-resistant bacteria. Despite the increasing awareness to this threat, over the last 30 years, no major new types of antibiotics have been developed by pharmaceutical companies mainly due to the persistent, costly failure to discover novel antibiotics for short-term treatment therapies.(Nathan 2004) The cost for development of antibiotic therapy, which necessarily needs to be produced in high volumes and sold at a low price, and for a short

treatment regimen does not induce commercial incentive for pharmaceutical companies. A solution that can synergistically improve and expedite the pharmaceutical development of antibiotics is to use novel advanced excipients to reformulate existing antibiotic drugs to enhance their efficacy and improve their performance. Refurbishment of clinically tested pharmaceutical drugs that have not acquired bacterial resistance offers a route to dramatically speed up the development time for new therapeutic formulations.

In this context, clofazimine (CLZ), has great potential as a candidate for the treatment of human tuberculosis (TB).(Cholo, Steel et al. 2012) CLZ is an extremely lipophilic riminophenazine antibiotic, used today in a combination therapy for the treatment of leprosy, marketed under the trade name Lamprene. CLZ was discovered in the 1950s and originally investigated as an anti-TB drug. It is impressively active *in vitro* against MDR/XDR strains with extremely low frequency of drug resistance and good safety profile.(Yawalkar and Vischer 1979; Browne, Harman et al. 1981; Reddy, O'Sullivan et al. 1999; van Ingen, Simons et al. 2010) However, its use to treat human TB has, so far, been hampered mainly because of its inconsistent therapeutic activity in various animal models.(Van Rensburg, Anderson et al. 1997; Mukherjee, Rich et al. 2004; Van Deun, Maug et al. 2010; Cholo, Steel et al. 2012) Oral administration in humans showed inadequate peak drug concentrations and insufficient total dose in plasma to obtain bactericidal activity against *M. tuberculosis*. (O'Connor, O'Sullivan et al. 1995; Janulionis, Sofer et al. 2004) The unfavorable oral pharmacokinetics of CLZ is well-known in leprosy treatment, where a study of daily administration of dosages of 100, 300 or 400 mg CLZ resulted in average plasma levels of 0.7, 1.0 and 1.41 mg/L, respectively.(Yawalkar and Vischer 1979) The intestinal adsorption of CLZ is low due to its poor solubility in the gastro intestinal tract (GIT) and the majority of the unabsorbed CLZ is largely excreted unchanged in the feces.(Cholo, Steel et al. 2012)

Nonetheless the promising *in vitro* data and focus on improved pharmaceutical formulations to offer a defense against the acute need to tackle TB infection has rekindled interest in novel drug delivery carriers that can improve the CLZ pharmacokinetic profile for its use in MDR- and XDR-TB. There are a few examples of nanotechnology-based formulation for the delivery of antibiotics that have proven effective *in vitro* and *in vivo* for treating or preventing infectious diseases.(Huh and Kwon 2011; Semiramoth, Di Meo et al. 2012; Abed and Couvreur 2014) However, despite

enormous expectation surrounding the nanomedicine field, rapid translation from research into clinically approved products is hindered due to regulatory issues and limited long-term safety and toxicity data.(Bawa 2013; Crist, Grossman et al. 2013). The anticipated rapid adoption of nanotechnology-based formulation has suffered from the paucity of knowledge relating to the biological effect of carrier materials with unknown, but potentially adverse side effects, from the carrier material at the nanometer size range. In this context, mesoporous silica-based particles (NSPs) have emerged as an attractive excipient with desirable properties for the delivery of oral drugs.(Mamaeva, Sahlgren et al. 2013) NSPs comprise pure amorphous silicon dioxide (SiO_2), and analytically indistinguishable from colloidal silicon dioxide, which has Generally Regarded As Safe status from the US FDA (Food and Drug Authority) for use its use in food and as an excipient for many dosage forms (oral capsules, suspensions, and tablets; transdermal, rectal, and vaginal preparations). The Environmental Protection Agency has determined amorphous silica to show no toxicity by oral administration and therefore is exempt from requirement of tolerance status.(Agency September 1991)

Our previous studies *in vitro* and *in vivo* have demonstrated how the encapsulation and confinement of pharmaceutical drug molecules inside the internal nanoporous structure of the NSP stabilize the molecule in its amorphous form, leading to enhanced solubility and bioavailability.(Xia, Zhou et al. 2012; Kjellman, Xia et al. 2014; Xia, Pethe et al. 2014) Motivated by this finding, the aim of this work was to encapsulate CLZ into NSPs in order enhance its solubility to improve its bioavailability in oral dosage formulations. A selection of different porous silica particles were used, differing in particle size, pore size and pore volume. A full physicochemical characterization of the CLZ encapsulated in the NSP, *in vitro* dissolution in simulated gastric fluid (SGF) and intestinal permeation as well as the antimicrobial activity in TB-infected macrophages were performed in order to investigate the potential benefit in refurbishment CLZ in oral TB treatment.

1. Materials and methods

1.1. Materials

CLZ was purchased from Santa Cruz Biotechnology (Heidelberg, Germany). FaSSIF-V2 Powder was purchased from Biorelevant (London, UK). Buffers and consumables for cell

culture were purchased from Dominique Dutscher SAS (Brumath Cedex, France), VWR (Fontenay-sous-Bois cedex, France) and Thermo Fisher (Illkirch, France). Syringe filters from VWR. Solvents and chemicals were supplied from Sigma Aldrich (Tyreso, Sweden) or VWR (Stockholm, Sweden).

1.2. Synthesis of mesoporous silica particles

Four different NSPs were used in the current investigation with different particle size and morphology and different pore sizes and surface areas. Two of the NSPs were synthesized via molecular templating methods according to previously described procedures: NFM-1[28], SBA-15 [29]. The molecular templated synthesis route generates particles with a sharp single pore size matching that of the templating molecule. Details on the synthesis protocols are described in the supplementary material. The other two porous particles were synthesized in a sol-gel process via spraying of a silica precursor to produce spherical particles with a reasonably narrow particle size range 5–20 microns. The porosity arises in these particles during the condensation and drying of the silica gel which yields a broader pore size compared to the templated synthesis route. The surface area, pore volume and pore size is strongly influenced by condensation conditions and can be easily varied in order to produce a variety of particles with differing textual properties.

1.3. Material characterization

Low angle X-ray diffraction measurements to investigate the pore structure of NSPs were performed on a Panalytical PRO MPD diffractometer in transmission mode using a focusing mirror and Cu-K α radiation, with samples spread on mylar films.

Nitrogen adsorption-desorption isotherm (Micromeritics Tristar II 3020-Apparatus, Norcross, GA, USA) was used to investigate the porosity of empty silica particles (before drug loading). All samples were degassed at 200 °C for 3 hours under nitrogen gas flow. The surface area was calculated by the Brunauer-Emmett-Teller equation in the relative pressure range between 0.05 and 0.2 [30]. The pore diameters and pore volumes were calculated according to BJH Barrett-Joyner-Halenda adsorption model.

Scanning electron microscopy images were obtained using a JSM-7401F scanning electron microscope (JEOL Ltd.,Tokyo, Japan) operating at 1 kV. The materials were investigated in their native state, that is, without gold coating.

Thermogravimetric analysis (TGA) was used to measure the amount of drug loaded in the silica carriers using the instrument model TGA 209 (NETZSCH) operating with a temperature ramp between 20 and 990ºC and a heating rate of 20°C/min. The plug-in gas atmosphere was dry air. The sample weights varied from 3 mg to 10 mg. As control, CLZ (pure drug crystals) was also analyzed.

Differential scanning calorimetry (DSC) (Q204, NETZSCH) was used to determine if there was crystallinity in the loaded samples which is observed as a phase transition during melting. The loaded samples (3 – 4 mg) were added in pierced aluminum pan (NETZSCH), and heated from 40 to 200 or 300ºC at a rate of 10ºC min-1. An empty pan was used to calibrate the temperature scale and the enthalpy response. As control, calcined silica particles before drug loading, CLZ (pure drugs – crystals), CLZ evaporated after acetone solution and physical mixtures comprising CLZ and NSPs without loading procedure were analyzed.

1.4. Loading of Clofazimine into Mesoporous Silica

CLZ was loaded into NSPs by incipient wetness impregnation followed by solvent evaporation, since it is practical for laboratory-scale control of the loading amount. In brief, a concentrated solution of the drug (5 mg/mL) in acetone was mixed under gentle stirring at room temperature for 2 hours with NSPs previously dried at 120°C under vacuum for 3h in order to remove residual humidity in the pores. The solvent was removed by rotary evaporation (100 rpm) under reduced pressure at 40°C until complete evaporation of solvent. The powder was then dried overnight in air. The drug/silica wt% was varied from 5% to 50% in order to investigate the maximum loading capacity of each of the silica particles.

1.5. Drug release and drug dissolution experiments

The *in vitro* release kinetics of the pure drug and drug-loaded NSP was conducted in SGF (0.01 HCl, 0.25 % NaCl, 0.1% SDS) (pH 2) at 37ºC, with stirring rate 50 rpm. The conditions were chosen to provide the closest simulation of in vivo conditions, while

using the simple pharmacopeia dissolution apparatus. The equivalent amount of drug was used in pure drug and drug-loaded NSP formulation and chosen to be 50mg since this is used in clinical applications. At each time point, aliquots of 1-2 mL were collected and filtered with a hydrophilic syringe filter (polyethersulfone: 0.45 µm) in order to avoid interference from the particles and/or drug crystals. Due to the extreme lipophilic nature of CLZ, which may alter the accuracy of the standard curve for analysis in a UV-visible spectrometer, the release profile was evaluated by HPLC-UV method (see section below). All release experiments showed good reproducibility.

1.6. Cell and bacterial culture

Human intestinal cell lines Caco-2 was established from the parental human colonic adenocarcinoma cell line [31], and maintained as recommended. Briefly, the Caco-2 cells were cultured in DMEM (25mM glucose) supplemented with 15% heat-inactivated (30 min, 56°C) fetal calf serum (Boehringer, Mannheim, Germany) and 1% nonessential amino acids (Life Technologies, Villebon sur Yvette, France). Cells were passaged weekly using trypsin-EDTA. The culture medium was changed daily. Caco-2 cells were maintained in a humid atmosphere at 37 °C with 10% CO2 and used between passage 51 and 57 after thawing.

Mouse macrophage RAW 264.7 (ATCC # TIB-71) were maintained at 37°C in RPMI-1640 + glutamax containing 10% fetal bovine serum (FBS) and were passed 3 three-times per week and used before passage number 7. Macrophages were harvested by using Versene (15040033, LifeTechnologies).

M. tuberculosis H37Rv strain constitutively expressing the Green Fluorescent Protein (GFP) was used as a reporter for the replication assay. Bacteria were cultured at 37°C for 16 days in complete 7H9 medium containing 0.5% glycerol (50405, Euromedex, Souffelweyersheim, France), 10% middelbrook OADC enrichment (211886, Becton Dickinson, Le Pont-de-Claix, France), 0.05% Tween 80 (2002A, Euromedex) and 50 µg/mL hygromycin B (10687010, Invitrogen, ThermoFisher, Illkirch, France). On the day of the experiment, *M. tuberculosis* were washed with Dulbecco's phosphate-buffered saline Ca-Mg- (14190169, LifeTechnologies) three-times with centrifugation at 5000 rpm for 5 min and centrifuged at 700 rpm for 2 min to remove clumped bacteria. Bacteria were resuspended in RPMI-1640 + GlutaMAX (61870044, Life Technologies) containing 10%

heat-inactivated FBS (Gibco, ThermoFisher, Illkirch, France) and titrated by measuring the optical density at 600 nm.

1.7. Cellular and transport media

For the permeation study, the Fasted State Simulated Intestinal Fluid V2 (FaSSIF-V2) transport media was chosen as the apical buffer in order to have a biorelevant medium simulating intestine fluid that was not toxic for the Caco-2 cells [32, 33]. The basolateral buffer was DMEM (without phenol red) supplemented with 1% of bovine serum albumin (BSA) (Sigma Aldrich, France) to increase the recovery of lipophilic compound and allow a correlation between absorption in Caco-2 cells and absorbed fraction in human intestinal lining [34].

For each transport experiment, the FaSSIF-V2 media was freshly prepared dissolving FaSSIF-V2 powder in half of the volume of FaSSIF-V2 DMEM-maleate buffer. After complete dissolution of the powder, the rest of the FaSSIF-V2 DMEM-maleate buffer was added and the medium left to stand at room temperature for 1hour (FaSSIF-V2 final concentration: 1.79g/L). The FaSSIF-V2 DMEM-maleate was prepared as follows: NaOH (0.3475 g), maleic acid (0.5575 g) and NaCl (1.0025 g) were dissolved in 0.225 L of DMEM. The pH was adjusted to 6.5 and made up to a volume of 0.25 L with DMEM. The FaSSIF-V2 DMEM-maleate buffer was sterilized with Vacuum Filter/Storage Systems, Sterile, Corning® (VWR, Fontenay-sous-Bois cedex, France) and kept in the fridge until used. The final composition of the biorelevant transport media are given in Supplementary Table S1.

1.8. Caco-2 cell viability assay

The 3-(4,5-dimethylythiazol-2-yl)-2,5-diphenyltetrazolium bromide (MTT, Merck Millipore, Darmstadt, Germany) assay was used for determining cytotoxicity on the Caco-2 cell line. The MTT assay quantifies mitochondrial dehydrogenase activity as a measure of cell viability [35]. Caco-2 cells were seeded at a density of 2.5 ×104 cells per well in TPP® tissue culture plates 96-well plate (Dominique Dutscher, France) over a week in order to achieve the 100% of confluence and simulated the monolayer permeability. Cells were then treated with series of concentrations of CLZ (serial dilutions from a concentrated ethanolic solution) or NSP. After 6 hours of incubation, the medium was

replaced with 0,05 mg/mL solution of MTT reagent in free-serum DMEM medium for 24 hours. The culture medium was further removed and replaced by 200 µL of dimethyl sulfoxide (DMSO), in order to dissolve the formazan crystals.

The absorbance of the solubilized dye was measured spectrophotometrically with a microplate reader (GENios, TECAN XFLUOR4) at 550 nm. The percentage of viable cells for each treatment was calculated from the ratio of the absorbance of each well containing the treated cells versus the average absorbance of the control wells (i.e., Ethanol- or growth medium-treated cells). All experiments were conducted at least in triplicate.

1.9. Caco-2 intestinal permeation

Caco-2 cells were seeded in Transwell-6 insert 24mm, TC Treated PET Membrane. (Fisher, France) at a density of 4.5 X 105 cells/well and then incubated for 21-28 days for differentiation. Medium was changed every 2 days in both compartments. The cellular polarization and differentiation of Caco-2 monolayer was determined by measuring the transepithelial electrical resistance (TEER) using an epithelial voltmeter (EVOM2). The shorter electrode was inserted in the apical side and longer electrode in the basolateral side. Care was taken that the electrode did not touch the cell monolayer and/or the plastic. Based on the literature, a resistance reading of 50-400Ω cm2 was considered as indicative of a confluent Caco-2 monolayer with tight junctions. Caco-2 monolayers were rinsed one time with the apical and basolateral buffers before permeation experiments. The intestinal permeation experiments through Caco-2 monolayers was designed in order to assess a possible tool to forecast in vivo performance of oral solid dosage forms. To this end, the permeation test was performed with CLZ after dissolution in SGF. Briefly, 1.5 mM of CLZ and NLAB-Silica-CLZ formulations were incubated in SGF at 37ºC, rpm 75. After 1 hour (average gastric emptying time in fasted state), aliquots (16.67 µL) were diluted to 2.5 mL with the FaSSIF-V2 transport media and then this solution was transferred in the apical compartment of the Transwell. At the same time, 2.8 mL of DMEM (without phenol red) with 1% of BSA was put in the basolateral side. The permeation experiments were performed from apical to basolateral direction. At each endpoint, aliquots (200 uL) from the basolateral side was taken and replaced with the same amount of fresh basolateral buffer in order to keep the volume constant. Aliquots were extracted in MeOH (800 uL) and then centrifuged at 14000 rpm for 20 min.

Recovery test was performed in order to investigate the best procedure for CLZ extraction in presence of BSA. Samples were stored at -18ºC until HPLC analysis. At the end of the experiment, the integrity of the Caco-2 monolayer was evaluated by measuring the TEER and the transport of sodium fluorescein (1 mg/ml). When a TEER change was recorded more than the 20% of the initial value, the TEER recovery was tested after overnight incubation in cell culture medium. Sodium fluorescein concentration in the basolateral side was measured by UV spectrophotometry at 490 nm. The TEER change measured was transient and reversible and the sodium fluorescein transport was under 0.6% h-1cm-1[36]. These data suggested the integrity of the cellular monolayer. Results were expressed as cumulative transport as a function of the time. Experiments were done in triplicate.

The permeability coefficient (Papp) and accumulated insulin (%) across the Caco-2 monolayer was calculated according to Equations 1 & 2, as previously reported in literature [37].

$$Papp = (\Delta Q/\Delta t)/(C0 \times A) \quad (1)$$

$$Accumulated\ insulin\ \% = 100 \times Q/(0.5 \times C0) \quad (2)$$

where *ΔQ/Δt* (in ng/s) indicates the linear apparent rate of mass appearing on the basolateral side of the cell monolayer, Q (in ng) indicates the accumulated mass on the basolateral side of the cell monolayer, C0 (in ng/ml) is the initial concentration of drug on the apical side of the monolayer and A (in cm2) is the sur- face area of the well..

1.10. HPLC-UV method for detection and quantification of CLZ

Quantification of CLZ was made with Agilent 1100 HPLC system comprising a model G1312. A binary gradient pump with degasser (model G1322A), autosampler (model G1367A), thermostated column compartment (model G1316A) and a diode array UV/Visible detector (model G1315B). Data collection was made using Chemstation rev. B.01.03 (Agilent, Kista, Sweden).

For the analysis of Caco-2 intestinal permeation a suitable isocratic method was developed using a 3.0×50 mm column containing 3 µm 100Å C18 functionalised silica (type L1 according to the USP classification, Nanologica AB, Södertälje, Sweden). Mobile

phase A consisted of HPLC quality water with 0.05% trifluoroacetic acid (Merck, Uvasol for spectroscopy) and mobile phase B was acetonitrile (BDH Prolabo, HiPerSolv Chromanorm for HPLC, gradient grade supplied from VWR, Stockholm, Sweden). Mobile phases A and B were mixed 50/50 by the pump. The flow rate was 0.7 ml/min and the column was thermostatted at +40°C. A detection wavelength of 286 nm was used and the injection volume was 100µl. This large volume, which was needed to achieve the required detection limits, could be injected without peak distortions by careful choice of the dilution solvents. Standard solutions in the concentration range 0.01–0.5 µg/ml were prepared in methanol (BDH Prolabo, HiPerSolv Chromanorm for HPLC, gradient grade) and diluted 800 µl + 200 µl DMEM before analysis. Samples taken from the cell experiments were likewise diluted 200 µl + 800 µl methanol during sample work-up so the final mixtures contained the same proportions of organic solvent/water. The detection limit (signal-to-noise ratio =3) was 11 nM calculated for the undiluted Caco-2 cell sample solutions.

For the analysis of CLZ in drug release and dissolution experiment a slightly different method was used. The same mobile phases were used but the column was a 4.6×50 mm column containing 3 µm 100Å C18 functionalised silica (type L1 according to the USP classification, Nanologica AB) and the flow rate was 1.5 ml/min. The injection volume was 5 µl. Standard solutions in the concentration range 1 – 100 µg/ml were prepared in methanol and diluted 500 µl +500 µl 0.01 M HCl with 0.2% NaCl and 0.1% SDS. Samples taken from the dissolution experiments were likewise diluted 500 µl + 500 µl methanol during sample work-up so the final mixtures contained the same proportions of organic solvent/water.

1.11. Effect on M. tuberculosis infected RAW 264.7 macrophages

NFM-1 and CLZ-encapsulated NFM-1 were dispersed in water to concentrations of 3.9mg/mL and 4.2 mg/mL, respectively. Sixteen twofold serial dilutions of the mother solution were performed in MilliQ water in a 384 deepwell “diamond plate” (P-384-120SQ-C-S, Axygen, Thermo Fisher, Illkirch, France) in order to obtain a dose-response curve. CLZ was dissolved in DMSO (34943, Sigma-Aldrich) to 3 mg/mL and was dispensed in Echo-qualified 384-well low dead volume source plates (Labcyte, France). Volumes between 5 and 500 nL of CLZ were transferred to the assay plate using an Echo 550 Series Liquid Handler (Labcyte) and posteriorly were backfilled with DMSO until 500 nl. Prior to

addition of cells, 4.5µL of cell medium were dispensed in those wells. Intramacrophage bacterial replication was assessed following procedures reported previously.(Queval, Song et al. 2014) Briefly, bacteria were mixed with RAW 264.7 macrophages to prepare a suspension at 5×10^5 cells/mL and 1×10^6 bacteria/mL (multiplicity of infection 2) in RPMI-1640 + GlutaMAX containing 10% FBS. After 2h of infection at 37°C with shaking (120 rpm), infected cells were washed with RPMI-1640 + GlutaMAX containing 10% FBS by centrifugation at 1100 rpm for 5 min. The remaining extracellular bacilli from the infected cells suspension were killed by a 1h 50 µg/mL amikacin (A2324-5G, Sigma) treatment and then washed twice with RPMI-1640 + GlutaMAX containing FBS. Finally, 45 µL/well of cellular suspension was added in the 384-well assay plate and incubated during 5 days at 37°C, 5% CO_2. Macrophages were then stained with 5 µM Syto 60 (S11342, Molecular probes, Thermo Fisher, Illkirch, France) dye for 1h followed by plate sealing.(Queval, Song et al. 2014)

Results and discussion

Nanoporous particles with different particle morphologies & pore texture were investigated for CLZ encapsulation

Several types of NSPs have been studied as oral delivery carrier for CLZ. The particles in this study were all in the micron-size range, as distinct from nanometer-sized nanoporous particles, which are more commonly used in the academic literature. Particles larger than 2-3 µm are unadsorbed in the GIT whilst they are localized in the Peyer's patches.(Florence 2005; Gaumet, Gurny et al. 2009) Therefore, micron-sized particles are of optimal size for drug carriers for gastrointestinal drug release with minimum risk of systemic uptake and distribution. Amorphous silica is significantly soluble only at elevated pH (above pH 10) and is therefore excreted largely unchanged in feces.

In previous studies, we have shown that different morphologies, textural and structural characteristics of the NSP have significant influence on the drug dissolution properties.(Xia, Zhou et al. 2012; Kjellman, Xia et al. 2014; Xia, Pethe et al. 2014). In this study we have used spherical shaped particle (ASP277 and ASP734), rod-type (SBA-15) and aggregated pseudo-spherical morphologies for NFM-1 (Figure 1).

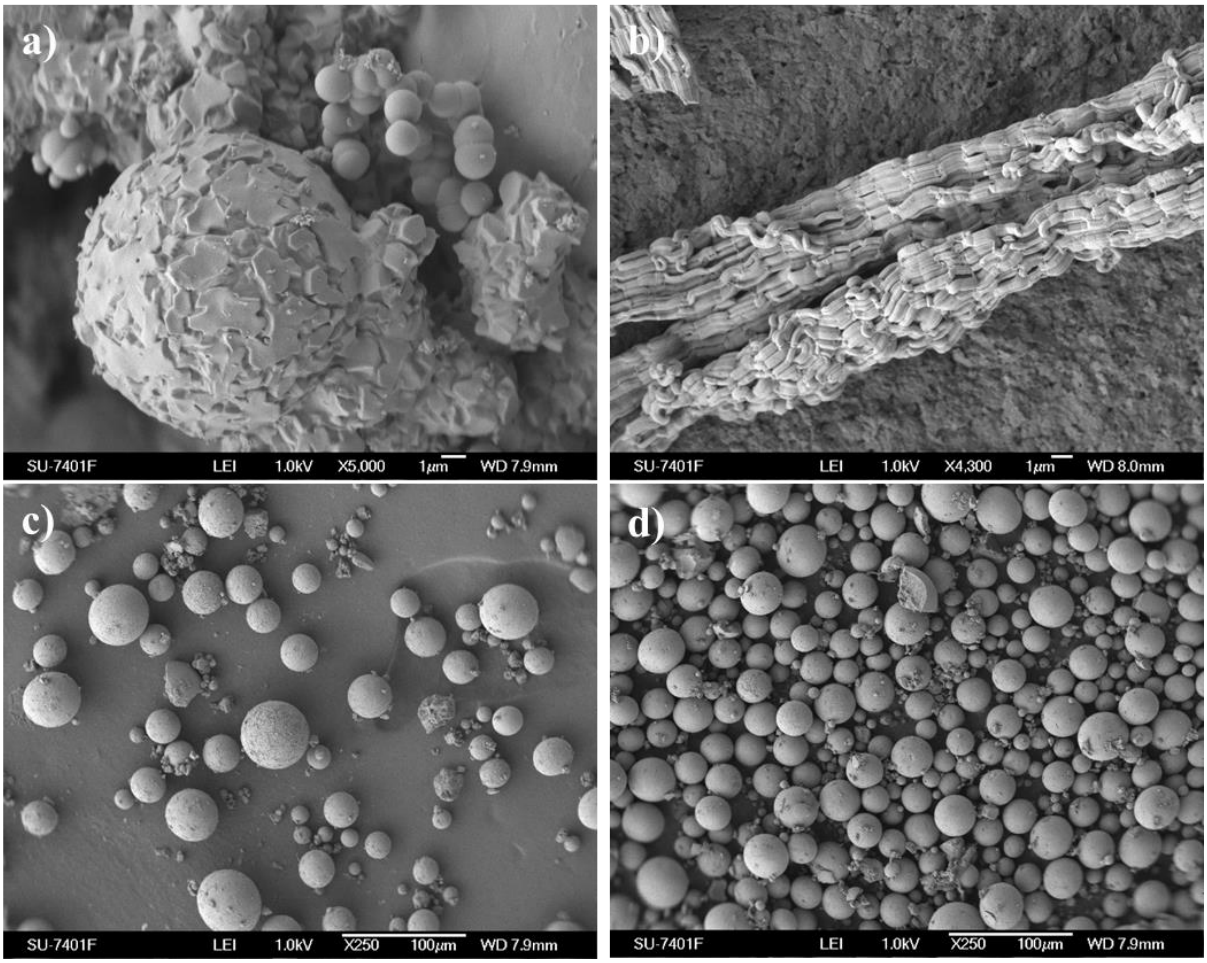

Figure 1 - Scanning electron microscopy images of the mesoporous silica particles: a) NFM-1, b) SBA-15, c) ASP277 and d) ASP734

The periodicity of the internal pore structure of nanoporous silica materials was investigated using low angle x-ray diffraction (Figure 2). Both NFM-1 and SBA-15 possesses a 2D hexagonal network (space group: p6mm) of cylindrical pores. Both samples showed nanoscale peaks and unit cell parameters that are consistent with previously published data. (Atluri, Hedin et al. 2009; Kjellman, Xia et al. 2014) The NFM-1 XRD (x-ray diffraction) peak showed a rather broad peak at 2.5 2 θ, which is influenced by the morphology of the particles with spherical morphology. (Atluri, Hedin et al. 2009; Kjellman, Xia et al. 2014) The pore size was determined to be 23,7 Å for NFM-1 and 62,9 Å for SBA-15 according to the Brunauer–Emmett–Telle analysis (Table 1).

The ASP277 and ASP734 particles showed a smooth curve in the low angle pattern with no distinguishing features, consistent with the expected result from a non-ordered porous structure with a nonuniform pore size.

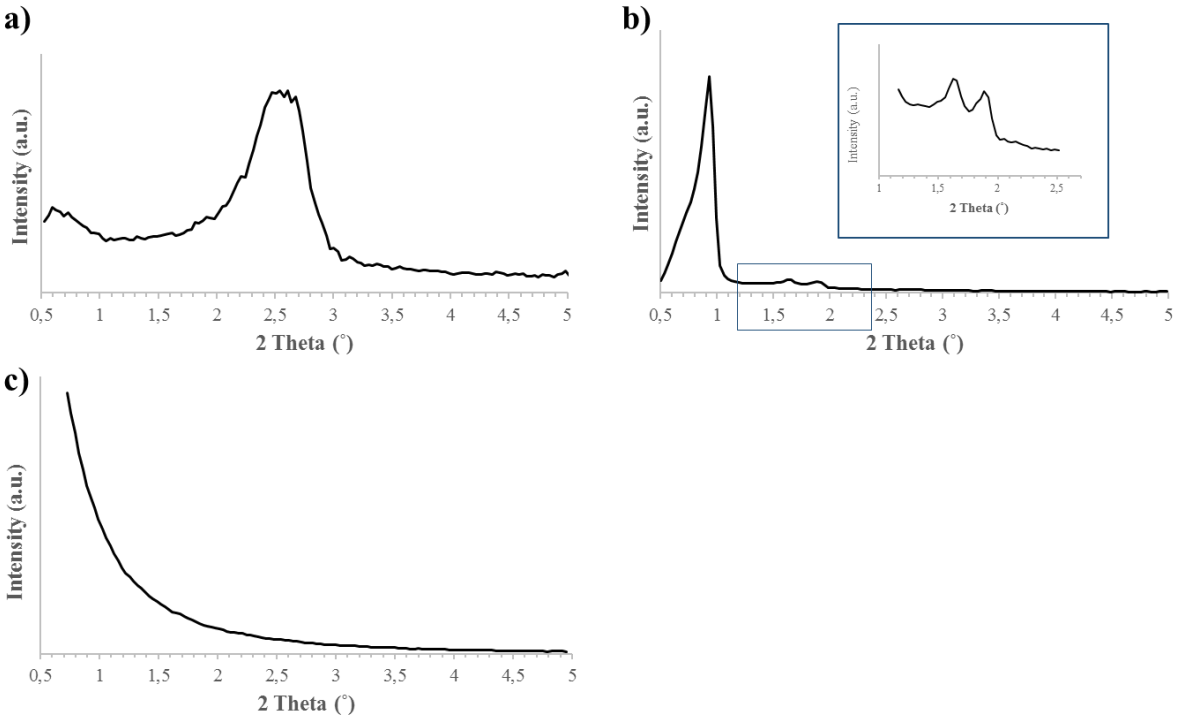

Figure 2 - Low angle X-ray diffraction patterns of a) NFM-1; b) SBA-15; c) typical pattern for ASP277 and ASP734.

Table 1 compares the physical characteristics of the different particles measured using nitrogen sorption. Although NFM-1 and ASP734 show similar surface area (around 750 m^2g^{-1}), the pore interconnectivity is different since NFM-1 has small pore size and low pore volume, whilst ASP734 has both large average pore size and high pore volume. Among the particles, ASP277 presents the highest average pore size (28.40 nm) with the lowest surface area (277 m^2g^{-1}), while SBA-15 presents intermediate values of pore size/volume and surface area. Together, these NSPs represent a wide range of external particle morphology, internal structure and porosity.

Sample	Average pore width (nm)	BET Surface Area ($m^2 g^{-1}$)	Pore volume (cm^3/g)
NFM-1	2.37 small	770.34 high	0.4294 low
SBA-15	6.29 medium	600.23 medium	0.763 medium
ASP277	28.40 high	277.27 low	1.563 high
ASP734	14.29 medium	733.89 high	1.914 high

Table 1 - Surface areas calculated by Brunauer–Emmett–Teller (BET), pore diameters and pore volumes according to Barrett-Joyner-Halenda adsorption model.

NSPs stabilize CLZ in the amorphous form

CLZ was encapsulated in the internal nanopores of the NSP by wet impregnation followed by solvent evaporation. Acetone was chosen as the solvent because of its high volatility and ability to dissolve CLZ (solubility 5 mg/mL). Interestingly, the deep red color of CLZ was visible during encapsulation in the NSP which was readily observed under a light microscope making it easy to verify drug loading in the particles (Supplementary Figure 1). The final amount of CLZ encapsulated in the NSP was determined by TGA which is a standard method commonly used for measuring adsorbed mass in these studies. (Atluri, Hedin et al. 2009; Kjellman, Xia et al. 2014) The change in mass due to decomposition of the organic pay load (i.e;, CLZ) inside the inorganic NSP was in the temperature range between 150 and 900 °C (Supplementary Figure 2). The TGA curves of CLZ-loaded NSPs were similar to the CLZ free drug suggesting that the thermal decomposition of CLZ takes place irrespective of whether or not it is encapsulated in NSP. The physical properties of CLZ encapsulated in the NSP and its degree of crystallinity/amorphous ware investigated by differential scanning calorimetry (DSC). The results show that all the NSPs were able to completely suppress the phase change of CLZ yielding an amorphous form of CLZ encapsulated in the particles (Figure 3). The drug loading capacity while maintaining CLZ in the amorphous form was similar for all the NSP

(from 11% to 17% wt%). The slight dip in the curve observed around 100 ºC is also present in the DSC curves of the empty particles without CLZ encapsulation (Supplementary Figure 3) and is attributed to surface-bound water content present in the NSP.(Kjellman, Xia et al. 2014; Xia, Pethe et al. 2014) In order to confirm that amorphous state of CLZ was due to the encapsulation in the NSP and not just from the solvent evaporation treatment, CLZ was evaporated from acetone solution without the presence of NSP. Furthermore, physical mixtures comprising CLZ and NSPs were also investigated. In all cases, clear melting phase transition were observed, confirming that CLZ recrystallizes during evaporation from acetone if not confined in the NSP pores. The observed stabilized amorphous form of CLZ is consistent with model of suppression of crystallization (Prasad and Lele 1994; Rengarajan, Enke et al. 2008), in which drug confinement in nanopores below a critical pore diameter (d*) reduces the crystallization kinetics due to unfavourable free energy balance. Typically, molecules confined to pores below three-times their molecular size are inhibited from recrystallizing. A recent study on CLZ crystals revealed a triclinic configuration with two molecules per unit cell with dimension 10.507 x 12.852 x 9.601 Å and volume of 1204.01 $Å^3$.(Keswani, Baik et al. 2015) The predicted polar surface area of CLZ is 39.99 $Å^2$(drugbank). This suggests that CLZ encapsulated in pores of NFM-1 with an average pore diameter of 24 Å will be confined to an amorphous form.

Poor physicochemical stability of amorphous drugs is a major challenge in the development of pharmaceutical products.(Serajuddin 1999) Remarkably, encapsulation of CLZ in the NSP particles in this study provided a stabilized amorphous form, which was stable for over 6 months stored at room temperature (Supplementary Figure 4). This is a crucial feature of the nanoporosity of the NSP which gives a unique and distinct advantage of NSP in comparison to other methods for preparing amorphous drug formulations, such as hot melt extrusion and spray drying.

Different porosity of the NSPs affects the drug release kinetics

To evaluate if the amorphous CLZ-NSP formulations had benefit for oral drug administration, the dissolution kinetics of CLZ in SGF was investigate using USP Apparatus 2 (Paddle Apparatus). A concentration of 50mg was used as it represents a conventional tablet dose. The dissolution of CLZ in SGF represents the fate of a typical oral drugs, where drugs usually first undergo dissolution in the gastric environment. CLZ

encapsulated inside NSPs resulted in significant increase in dissolution rate compared with the free CLZ (in either crystalline form as received or after solvent evaporation from acetone) (Figure 4).

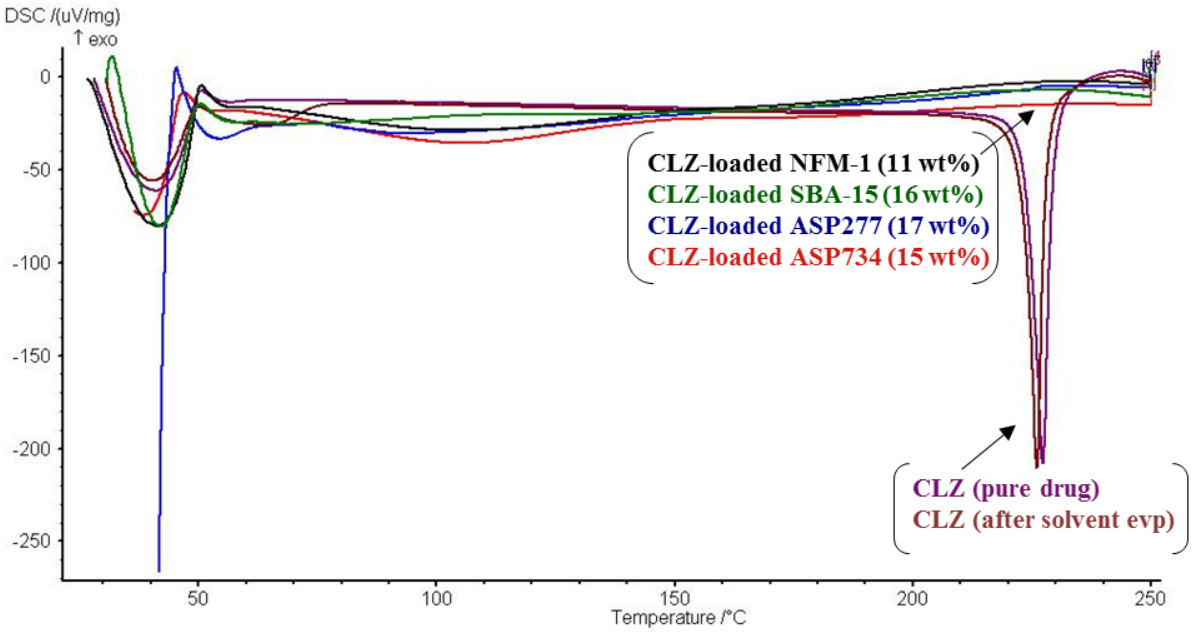

Figure 3 - Solid-state characterization by differential scanning calorimetry of CLZ (crystals – pure drug), CLZ after acetone evaporation, CLZ with NSP as physical mixture (pm) and CLZ-loaded NSPs. In the physical mixtures, CLZ was solubilized in CLZ: Clofazimine; NSP: Nanoporous silica particle.acetone and mixed with NSP (with similar % wt to the respective CLZ-loaded NSP sample) without loading procedure.

In the case of CLZ-encapsulated in ASP734 a dramatic enhancement in dissolution (area under the curve) of approximately of 20-fold was observed in comparison to the CLZ as free drug. The dissolution kinetics were significantly different depending on the NSP particle used. This is due to the intrinsic properties of the nanoporous particles (pore size, surface area and geometry) which influence the release kinetics of the drug, and offers the potential for tuneable drug release profile from different NSP compared to other methods to stabilize the amorphous form. Our previous work on the subject (Xia, Zhou et al. 2012; Kjellman, Xia et al. 2014) showed that pore size and the presence of microporosity could drastically affect the release kinetics. The release profile of the CLZ-loaded NSPs suggest that, in this case also, the surface area plays an important role in the dissolution kinetics. For instance, ASP734 (medium pore size, high surface area) resulted in the fastest dissolution kinetics followed by SBA-15 (medium pore size, medium surface

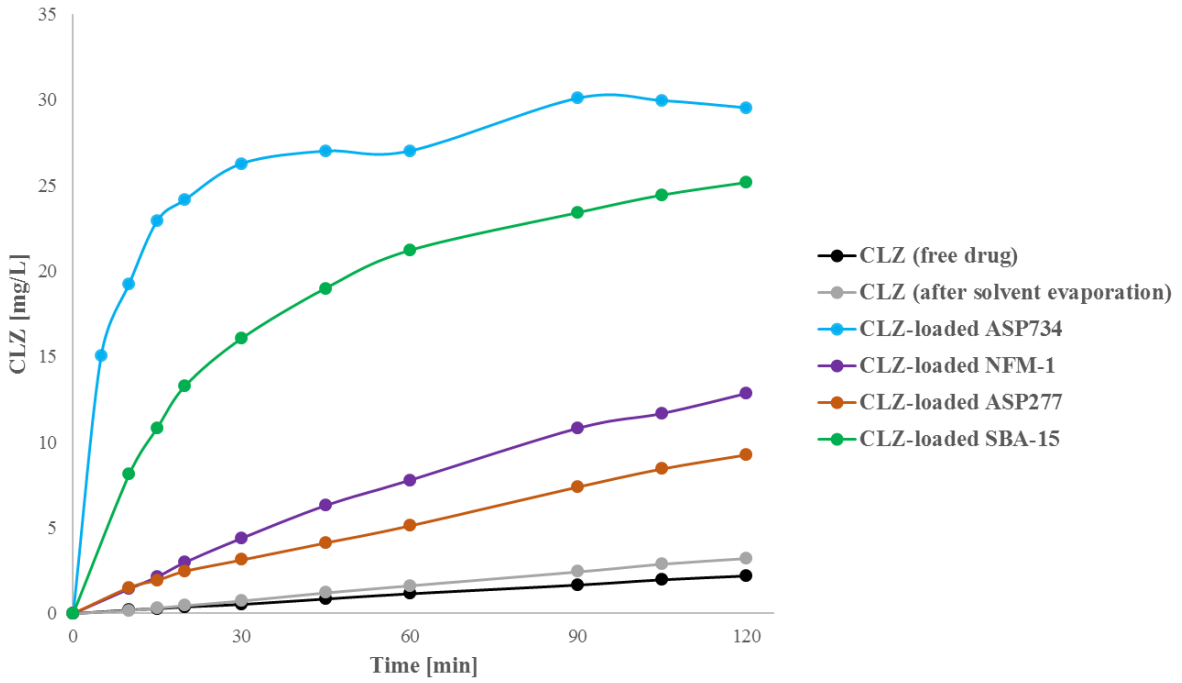

Figure 4 - Dissolution release profile in simulated gastric fluid of clofazimine and clofazimine-loaded nanoporous silica particles. Experiment was made in triplicate. Figure shows the typical release profile. CLZ: Clofazimine.

area). Small (NFM-1) or large (ASP277) pore sizes resulted in slower kinetic release profile. Slower release kinetics from particles with narrow pores (of the order of a few nm's) can be rationalized from slower diffusion kinetics within the pores. In contrast, the slower diffusion kinetics of drug molecules from the particles with larger pores has been observed previously and may result, rather counter-intuitively, from formation of ultra-fine crystals in the pores due to the local concentration exceeding the crystallization saturation concentration. Formation of crystals will shift the equilibrium conditions and hinder the dissolution rate.

NSPs enhance CLZ permeability through human Caco-2 intestinal cells

In order to simulate drug uptake via oral administration, aliquots from the dissolution of CLZ in SGF were incubated with human intestinal Caco-2 monolayer and the concentration of drug transported through the monolayer was investigated. Caco-2 cell monolayers are routinely used in drug development protocols to assess intestinal drug permeability and are accepted as a surrogate for human intestinal permeability measurements by the FDA.(Bergstrom, Holm et al. 2014)

Intestinal *in vitro* permeation studies are usually performed in saline solution such as Hanks' balanced salt solutions despite the fact that the physicochemical and biochemical properties are very different from the intestinal fluid.(Lind, Jacobsen et al. 2007; Antoine, Pellequer et al. 2015) Here, in order to improve the *in vitro/in vivo* correlation, we used the FaSSIF-V2 biomimetic fluid, for which, the composition has been recently revised to predict *in-vitro* dissolutions of oral dosage forms (Markopoulos, Thoenen et al. 2014),(Porter, Trevaskis et al. 2007) and does not affect the integrity of Caco-2 monolayer, in contrast to Fed State Simulated Intestinal Fluid.(Ingels, Deferme et al. 2002) The addition of 1% BSA in the basolateral compartment was found to be important to prevent adsorption of the lipophilic CLZ on the plastic of the Transwell in order to measure the drug concentration. The parameters chosen for the residence time and drug concentration were aligned to obtain the best correlation between absorption of lipophilic compounds in Caco-2 cells and absorbed fraction in humans.(Fossati, Dechaume et al. 2008) All the experiments were performed in a CLZ concentration range with good cell viability according to cell cytotoxicity test (Supplementary Figure 5). It is important to note that the silica particles do not induce cytotoxicity on the intestinal cells. Moreover, change in the TEER was transient and reversible and the sodium fluorescein transport showed that no cellular damage occurred. As shown in Figure 5, CLZ-loaded NSP formulations dramatically increased the intestinal permeation in comparison to the CLZ as free drug, which was below the detection limit (10^{-10} g/ml). The data indicates a slightly higher permeability is achieved from the CLZ-loaded in ASP734 which showed more rapid dissolution kinetics in comparison to the slower release profile from CLZ-loaded in NFM-1. However, this difference is not statistically significant in the experimental setting used. Over a time period of 2 – 3h the release profile from the NFM-1 shows a linear permeation profile with a similar equilibrium concentration being reached compared to the ASP734 particles (Figure 4). The concentration of CLZ in the basolateral component was in the range of 0.01-10 µg/ml with an average concentration of 0.1-1 µg/ml detected after 180 mins through dissolution from NFM-1.

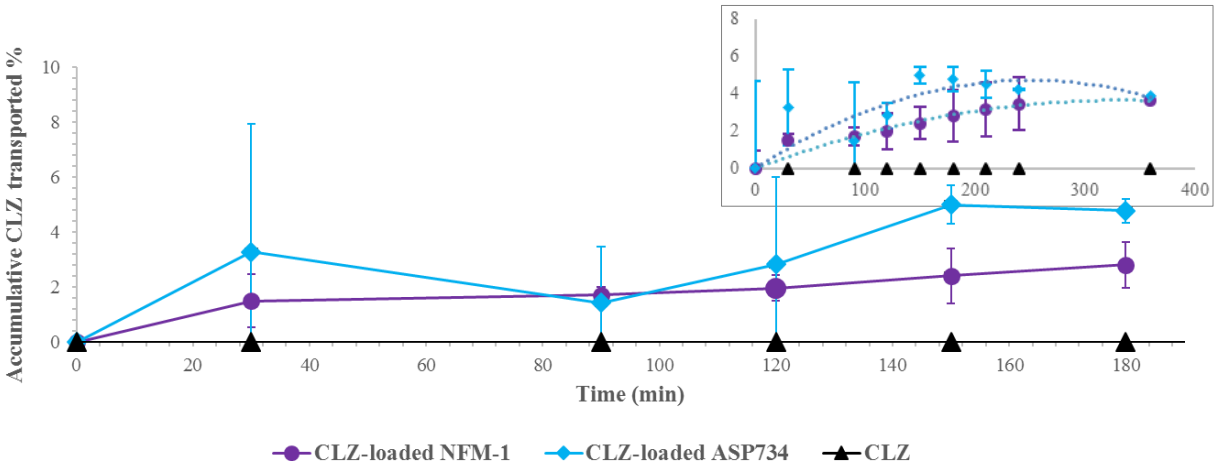

Figure 5 - Intestinal permeability test. Accumulative amount of clofazimine transported through Caco-2 cell monolayer from the apical to the basolateral side as a function of time. The insert shows extended permeation study for 360 min. Results are expressed as mean ± standard deviation (n = 3). In the graph, the 0% of accumulative clofazimine transported is referred to the limit of detection of the HPLC technique (<0.237%). CLZ: Clofazimine.

Reformulation of CLZ in NFM-1 enhances solubility to reach its antimicrobial concentration.

The *in vitro* dissolution kinetics and subsequent Caco-2 permeability measurements provide strong support that *in vivo* CLZ oral bioavailability can be enhanced by encapsulation in NSP. In order to evaluate if NSP-CLZ formulation lead to enhanced antibacterial effect, we investigated the antimicrobial activity of CLZ on *M. tuberculosis* infected RAW macrophages. The NFM-1 particles were chosen for formulation of CLZ since they showed a good reproducibility in the dissolution and permeation studies and, as we have reported previously, shown to provide enhanced bioavailability and pH-independent solubility of lipophilic drugs. TB-infected macrophages were exposed to a 10^5 fold dilution series of CLZ dissolved from NFM-1 particles. Since CLZ as the free drug is virtually insoluble in aqueous conditions it was not possible to conduct a control experiment with dissolved CLZ in aqueous solution. Instead CLZ was dissolved in DMSO in which it is fully soluble. As such, this control served as a comparison to a fully soluble, 100% bioavailability, of CLZ. As shown in Figure 6 (bottom), there is a clear antibacterial effect of CLZ on *M. tuberculosis* with a marked antibacterial effect at concentrations in the range 10^{-7} g/mL to 10^{-6} g/mL. The dose response curves for CLZ dissolved in DMSO and that released from NFM-1 particles showed very similar concentration dependency.

The antibacterial concentration of CLZ achieved by dissolution from NFM-1 in aqueous conditions matches the MIC obtained from a fully dissolved concentration in solvent. The MIC observed is in this study is in very good agreement with very recent results from a multi-lab study using a 7H9 broth microdilution method to establish MICs of several first-line and second-line TB drugs. (Kaniga, Cirillo et al. 2016) The MIC of CLZ was determined to be in the range: 0.03-0.25 µg/ml. It is important to recall that the concentration of CLZ measured in the basolateral medium in the permeation studies was of the order of 0.1-1 µg/mL from NFM-1. Therefore, the enhanced permeation of CLZ by encapsulation in NSP leads to a concentration range up to an order of magnitude higher than the CLZ MIC. This significant result indicates that the formulation of CLZ in NSP can lead to an enhanced permeation of CLZ to achieve the MIC after a single dose.

As a control, in order to verify that the observed bacterial inhibition of CLZ was due to antibacterial action and not simply because of cell toxicity, the macrophage cell viability was measured. In Figure 6 (top), the number of viable cells was counted and visualized for each group of treatment. Notably, the unloaded NFM-1 particles and CLZ encapsulated in NFM-1 did not present cytotoxicity at any concentrations tested,

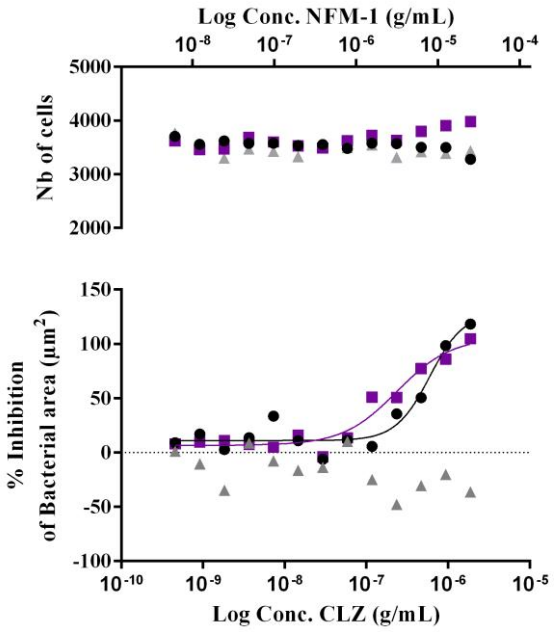

Figure 6 - Number of viable macrophage cells (top) and bacterial area (bottom) after treatment with CLZ dissolved in DMSO (black circle), empty NMF-1 (gray triangle) or CLZ encapsulated in NFM-1 (purple square) in the intramacrophage *in vitro* assay. Experiment was done in triplicate. CLZ: Clofazimine.

validating the good biocompatible profile. In summary, the new CLZ formulation in NSPs offers an innovative and simple formulation that achieves CLZ permeation at concentrations reaching the MIC of the drug. In this context, *in vivo* pharmacokinetic studies are ongoing in our laboratory to investigate the bioavailability enhancement of CLZ in NSP and assess its clinical relevance.

Conclusion

CLZ, a potent multitarget lipophilic riminophenazine antibiotic, was successfully reformulated for the first time in NSPs. NSPs were able to stabilize the amorphous state of CLZ (with a shelf-stability 6 months and more) and dramatically increase the drug solubility in SGF (up to 20-fold). The morphology and the texture of the NSP influenced the dissolution kinetics. Permeation studies through Caco-2 intestinal cells vindicate that the CLZ-encapsulated NSP formulations can substantially enhance the permeation through the GIT. When incubated with TB-infected macrophage, CLZ released from NSP formulation in aqueous conditions showed the same antibacterial effect compared to CLZ dissolved in DMSO, whilst CLZ as free drug was insoluble. The CLZ concentration (dissolved from NFM-1), after permeation through Caco-2 monolayer was up to an order of magnitude higher than the MIC. CLZ-encapsulated NSP present a new and simple refurbishment of a well-known marketed antibiotic for a new indication in the treatment of antibiotic-resistant *M. tuberculosis* infections. Moreover, the NSP carrier is already generally recognized as safe for oral administration, and is demonstrated here to show no cell cytotoxicity, making this study of particular relevance in context of poor antibiotic pipeline with a rekindled interest for a refurbishment of well-known clinically approved drugs.

Executive summary

- This work presents a new, simple and effective refurbishment of a well-known marketed antibiotic in a drug delivery system which is generally recognized as safe for oral administration. This is of particular relevance in the current context of ‘postantibiotic era’ and worldwide spread antibiotic-resistant microorganisms.

- Clofazimine (CLZ) was formulated for the first time in nanoporous silica particles
- CLZ was stabilized in its amorphous state with 6-month shelf stability.
- CLZ's solubility was increased by 20-fold in simulated gastric fluid.
- Nanoporous silica particle's morphology and texture influence the dissolution kinetics.
- CLZ released into aqueous media from nanoporous silica particles showed the same antibacterial effect as CLZ dissolved in organic solvents, while CLZ alone is insoluble in water.
- CLZ's permeation through the GIT was enhanced to levels of concentration range above the MIC on Mycobacterium tuberculosis.

References

1. Fact sheet N°194 - Antimicrobial resistance. www.who.int.
2. Fact sheet January 2017 - The top 10 causes of death. http://www.who.int/mediacentre/factsheets/fs310/en/.
3. Nathan C, Cars O. Antibiotic Resistance — Problems, Progress, and Prospects. *New England Journal of Medicine* 371(19), 1761-1763 (2014).
4. Nathan C. Antibiotics at the crossroads. *Nature* 431(7011), 899-902 (2004).
5. Cholo MC, Steel HC, Fourie PB, Germishuizen WA, Anderson R. Clofazimine: current status and future prospects. *J Antimicrob Chemother* 67(2), 290-298 (2012).
6. Reddy VM, O'sullivan JF, Gangadharam PR. Antimycobacterial activities of riminophenazines. *J Antimicrob Chemother* 43(5), 615-623 (1999).

7. Van Ingen J, Simons S, De Zwaan R *et al*. Comparative study on genotypic and phenotypic second-line drug resistance testing of Mycobacterium tuberculosis complex isolates. *J Clin Microbiol* 48(8), 2749-2753 (2010).

8. Browne SG, Harman DJ, Waudby H, Mcdougall AC. Clofazimine (Lamprene, B663) in the treatment of lepromatous leprosy in the United Kingdom. A 12 year review of 31 cases, 1966-1978. *Int J Lepr Other Mycobact Dis* 49(2), 167-176 (1981).

9. Yawalkar SJ, Vischer W. Lamprene (clofazimine) in leprosy. Basic information. *Lepr Rev* 50(2), 135-144 (1979).

10. Van Deun A, Maug AK, Salim MA *et al*. Short, highly effective, and inexpensive standardized treatment of multidrug-resistant tuberculosis. *Am J Respir Crit Care Med* 182(5), 684-692 (2010).

11. Van Rensburg CE, Anderson R, O'sullivan JF. Riminophenazine compounds: pharmacology and anti-neoplastic potential. *Crit Rev Oncol Hematol* 25(1), 55-67 (1997).

12. Mukherjee JS, Rich ML, Socci AR *et al*. Programmes and principles in treatment of multidrug-resistant tuberculosis. *Lancet* 363(9407), 474-481 (2004).

13. Janulionis E, Sofer C, Song H-Y, Wallis RS. Lack of Activity of Orally Administered Clofazimine against Intracellular Mycobacterium tuberculosis in Whole-Blood Culture. *Antimicrobial Agents and Chemotherapy* 48(8), 3133-3135 (2004).

14. O'connor R, O'sullivan JF, O'kennedy R. The pharmacology, metabolism, and chemistry of clofazimine. *Drug Metab Rev* 27(4), 591-614 (1995).

15. Huh AJ, Kwon YJ. "Nanoantibiotics": a new paradigm for treating infectious diseases using nanomaterials in the antibiotics resistant era. *J Control Release* 156(2), 128-145 (2011).

16. Abed N, Couvreur P. Nanocarriers for antibiotics: a promising solution to treat intracellular bacterial infections. *Int J Antimicrob Agents* 43(6), 485-496 (2014).

17. Semiramoth N, Di Meo C, Zouhiri F *et al*. Self-assembled squalenoylated penicillin bioconjugates: an original approach for the treatment of intracellular infections. *ACS Nano* 6(5), 3820-3831 (2012).

18. Song H, Ahmad Nor Y, Yu M et al. Silica nanopollens enhance adhesion for long-term bacterial inhibition. J. Am. Chem. Soc. 138(20), 6455–6462 (2016).

19. Wang Y, Nor YA, Song H et al. Small-sized and largepore dendritic mesoporous silica nanoparticles enhance antimicrobial enzyme delivery. J. Mater. Chem. B 4(15), 2646–2653 (2016).

20. Crist RM, Grossman JH, Patri AK *et al*. Common pitfalls in nanotechnology: lessons learned from NCI's Nanotechnology Characterization Laboratory*. Integrative Biology* 5(1), 66-73 (2013).

21. Bawa R. FDA and Nanotech: Baby Steps Lead to Regulatory Uncertainty. In: *Bio-Nanotechnology*, (Ed.^(Eds).Blackwell Publishing Ltd. 720-732 (2013).

22. Mamaeva V, Sahlgren C, Linden M. Mesoporous silica nanoparticles in medicine--recent advances*. Adv Drug Deliv Rev* 65(5), 689-702 (2013).

23. Abbaraju PL, Meka AK, Jambhrunkar S et al. Floating tablets from mesoporous silica nanoparticles. J. Mater. Chem. B 2(47), 8298–8302 (2014).

24. Agency USEP. Pesticides And Toxic Substances (7508W). (738-F-9 1-107), (September 1991). https://www3.epa.gov

25. Xia X, Pethe K, Kim R *et al*. Encapsulation of Anti-Tuberculosis Drugs within Mesoporous Silica and Intracellular Antibacterial Activities*. Nanomaterials* 4(3), 813 (2014).

26. Xia X, Zhou C, Ballell L, Garcia-Bennett AE. In vivo enhancement in bioavailability of atazanavir in the presence of proton-pump inhibitors using mesoporous materials*. ChemMedChem* 7(1), 43-48 (2012).

27. Kjellman T, Xia X, Alfredsson V, Garcia-Bennett AE. Influence of microporosity in SBA-15 on the release properties of anticancer drug dasatinib*. Journal of Materials Chemistry B* 2(32), 5265-5271 (2014).

28. Atluri R, Hedin N, Garcia-Bennett AE. Nonsurfactant supramolecular synthesis of ordered mesoporous silica*. J Am Chem Soc* 131(9), 3189-3191 (2009).

29. Zhao D, Feng J, Huo Q *et al*. Triblock copolymer syntheses of mesoporous silica with periodic 50 to 300 angstrom pores. *Science* 279(5350), 548-552 (1998).

30. Brunauer S, Emmett PH, Teller E. Adsorption of Gases in Multimolecular Layers. *Journal of the American Chemical Society* 60(2), 309-319 (1938).

31. Fogh J, Fogh JM, Orfeo T. One hundred and twenty-seven cultured human tumor cell lines producing tumors in nude mice. *J Natl Cancer Inst* 59(1), 221-226 (1977).

32. Markopoulos C, Thoenen F, Preisig D *et al*. Biorelevant media for transport experiments in the Caco-2 model to evaluate drug absorption in the fasted and the fed state and their usefulness. *Eur J Pharm Biopharm* 86(3), 438-448 (2014).

33. Antoine D, Pellequer Y, Tempesta C *et al*. Biorelevant media resistant co-culture model mimicking permeability of human intestine. *Int J Pharm* 481(1-2), 27-36 (2015).

34. Fossati L, Dechaume R, Hardillier E *et al*. Use of simulated intestinal fluid for Caco-2 permeability assay of lipophilic drugs. *International Journal of Pharmaceutics* 360(1–2), 148-155 (2008).

35. Van Meerloo J, Kaspers GL, Cloos J. Cell Sensitivity Assays: The MTT Assay. In: *Cancer Cell Culture*, Cree IA (Ed.^(Eds).Humana Press 237-245 (2011).

36. Mellaerts R, Mols R, Kayaert P *et al*. Ordered mesoporous silica induces pH-independent supersaturation of the basic low solubility compound itraconazole resulting in enhanced transepithelial transport. *Int J Pharm* 357(1-2), 169-179 (2008).

37. Li P, Tan A, Prestidge CA, Nielsen HM, Müllertz A. Self-nanoemulsifying drug delivery systems for oral insulin delivery: *In vitro* and in vivo evaluations of enteric coating and drug loading. *International Journal of Pharmaceutics* 477(1–2), 390-398 (2014).

38. Queval CJ, Song OR, Delorme V *et al*. A microscopic phenotypic assay for the quantification of intracellular mycobacteria adapted for high-throughput/high-content screening. *J Vis Exp* (83), e51114 (2014).

39. Florence AT. Nanoparticle uptake by the oral route: Fulfilling its potential? *Drug Discov Today Technol* 2(1), 75-81 (2005).

40. Gaumet M, Gurny R, Delie F. Localization and quantification of biodegradable particles in an intestinal cell model: the influence of particle size. *Eur J Pharm Sci* 36(4-5), 465-473 (2009).

41. Zhou C, Garcia-Bennett AE. Release of folic acid in mesoporous NFM-1 silica. J. Nanosci. Nanotechnol. 10(11), 7398–7401 (2010).

42. Jambhrunkar S, Qu Z, Popat A, Karmakar S, Xu C, Yu C.Modulating *in vitro* release and solubility of griseofulvin using functionalized mesoporous silica nanoparticles. J. Colloid Interface Sci. 434, 218–225 (2014).

43. Prasad BR, Lele S. Stabilization of the amorphous phase inside carbon nanotubes: Solidification in a constrained geometry. *Philosophical Magazine Letters* 70(6), 357-361 (1994).

44. Rengarajan GT, Enke D, Steinhart M, Beiner M. Stabilization of the amorphous state of pharmaceuticals in nanopores. *Journal of Materials Chemistry* 18(22), 2537-2539 (2008).

45. Keswani RK, Baik J, Yeomans L *et al*. Chemical Analysis of Drug Biocrystals: A Role for Counterion Transport Pathways in Intracellular Drug Disposition. *Mol Pharm* 12(7), 2528-2536 (2015).

46. Drugbank Clofazimine. www.drugbank.ca/drugs/DB00845

47. Serajuddin AT. Solid dispersion of poorly water-soluble drugs: early promises, subsequent problems, and recent breakthroughs. *J Pharm Sci* 88(10), 1058-1066 (1999).

48. Bergstrom CA, Holm R, Jorgensen SA *et al*. Early pharmaceutical profiling to predict oral drug absorption: current status and unmet needs. *Eur J Pharm Sci* 57 173-199 (2014).

49. Lind ML, Jacobsen J, Holm R, Mullertz A. Development of simulated intestinal fluids containing nutrients as transport media in the Caco-2 cell culture model:

assessment of cell viability, monolayer integrity and transport of a poorly aqueous soluble drug and a substrate of efflux mechanisms. *Eur J Pharm Sci* 32(4-5), 261-270 (2007).

50. Porter CJ, Trevaskis NL, Charman WN. Lipids and lipid-based formulations: optimizing the oral delivery of lipophilic drugs. *Nat Rev Drug Discov* 6(3), 231-248 (2007).

51. Markopoulos C, Andreas CJ, Vertzoni M, Dressman J, Reppas C. In-vitro simulation of luminal conditions for evaluation of performance of oral drug products: Choosing the appropriate test media. *Eur J Pharm Biopharm* 93 173-182 (2015).

52. Ingels F, Deferme S, Destexhe E, Oth M, Van Den Mooter G, Augustijns P. Simulated intestinal fluid as transport medium in the Caco-2 cell culture model. *Int J Pharm* 232(1-2), 183-192 (2002).

53. Kaniga K, Cirillo DM, Hoffner S *et al*. A Multi-Laboratory, Multi-Country Study to Determine Minimal Inhibitory Concentration Quality Control Ranges for PhenotypicDrug-Susceptibility Testing of Selected First-Line Anti-TB Drugs, Second-Line Injectables, Fluoroquinolones, Clofazimine and Linezolid. *J Clin Microbiol* (2016).

5. CHAPTER III

Intracellular delivery of antibiotics

Libération des antibiotiques dans les compartiments intracellulaires

5.1. Résumé article 3: “L'utilisation de nanocarriers à base de PLGA améliore l'efficacité de la Vancomycine contre *Mycobacterium tuberculosis* intracellulaire”

Face à la nécessité de définir de nouvelles stratégies pour améliorer l’efficacité des traitements contre les souches multirésistantes de TB, l’utilisation d'antibiotiques approuvés pour le traitement d'autres maladies est une alternative intéressante pour améliorer le développement de nouveaux traitements antituberculeux (Dheda, Barry et al. 2016).

La Vancomycine (VCM), un antibiotique de référence utilisé depuis des décennies comme alternative de la pénicilline pour le traitement des souches de *Staphylococcus aureus* Methicillin-résistantes *(*MRSA) (Chua and Howden 2009), avait montré une activité bactéricide sur des cultures axéniques de bactéries Mtb (Collins and Uttley 1988; Provvedi, Boldrin et al. 2009; Dinesh, Sharma et al. 2013; Schoonmaker, Bishai et al. 2014; Soetaert, Rens et al. 2015; Rens, Laval et al. 2016). Ces données nous ont permis d’envisager son utilisation comme nouvelle stratégie pour le traitement de TB, sachant également qu’aucune donnée concernant l’efficacité de cet antibiotique vis-à-vis de Mtb intracellulaires n’était jusqu’alors disponible.

Au vue des échecs cliniques liés à la faible pénétration intracellulaire de cet antibiotique précédemment décrits (Lamer, de Beco et al. 1993; Kollef 2007; Lehar, Pillow et al. 2015), VCM serait ainsi incapable d'accéder aux macrophages infectés pour atteindre les concentrations thérapeutiques optimales dans les niches intracellulaires de Mtb. En revanche, les cellules phagocytaires sont bien connues pour leur capacité à internaliser les nanoparticules (NP) contenant des médicaments (Pelgrift and Friedman 2013; Ladaviere and Gref 2015; Costa-Gouveia, Ainsa et al. 2017; Costa-Gouveia, Pancani et al. 2017). Ainsi, l'utilisation de nanocarriers capables de pénétrer dans des cellules infectées pour y libérer un antibiotique actif et atteindre ainsi les agents pathogènes, est une stratégie prometteuse pour surmonter la faible capacité de VCM à entrer dans les cellules.

Dans le cadre de notre étude, plusieurs critères ont été préalablement fixés, de façon à choisir un nanocarrier adapté pour favoriser un effet intracellulaire de VCM. Ces nanoparticules devaient ainsi: i) avoir un diamètre moyen inférieur à un micron pour être

efficacement phagocytés par les macrophages infectés ; ii) permettre d'encapsuler plus de 10 % de VCM par NP ; iii) libérer l'antibiotique de manière contrôlée dans les compartiments intracellulaires ; iv) être préparée par une méthode simple avec une utilisation minimale d'excipients ; et v) être stable durant le stockage.

Dans d'autres études, VCM avait été incorporée dans des liposomes et délivrée dans les macrophages (Ma, Shang et al. 2011; Pumerantz, Muppidi et al. 2011; Sande, Sanchez et al. 2012; Surewaard, Deniset et al. 2016), mais avec de faibles efficacités d'encapsulation (< 20 % VCM) . Des nanoparticules à base de polymères d'acide poly(lactique-*co*-glycolique) (PLGA) ou de chitosan ont également été utilisées, mais une faible quantité de VCM avait pu être encapsulée (4–6 % poids) à cause des propriétés hydrophobes de l'antibiotique (Hu, Fang et al. 2015). Plus récemment (Pei, Mohamed et al. 2017), VCM a été encapsulée dans différentes NP à base de PLGA, d'un polymère de polyéthylène glycol -PLGA ou d'un dérivé de chitosan. De façon intéressante, les NP de 500–1000 nm, et contenant jusqu'à 9.5 % VCM (poids), ainsi générées, étaient capables de libérer l'antibiotique de manière dépendante de la valeur de pH. En revanche, la méthode de préparation était complexe et exigeait l'utilisation de quantités précises de plusieurs ingrédients.

Dans notre étude, nous proposons d'encapsuler VCM dans des nanoparticules (NP) à base PLGA, dans le but de stabiliser VCM et de délivrer l'antibiotique directement dans les macrophages infectés.

Nos collaborateurs ont caractérisé les nanoparticules ainsi obtenues et montré par cryomicroscopie électronique de transmission (cryo-TEM) de grandes inclusions dans les NP contenant vraisemblablement l'antibiotique. La préparation des NP a permis de charger jusqu'à 14.5 % (poids) de VCM par NP. Ces NP ont pu être conservées plus de trois mois sans diminution significative de la quantité d'antibiotique encapsulée. Et de façon intéressante, il a été montré que VCM était libérée à pH 5.5, mais pas à pH neutre, ni dans les milieux de culture de cellule.

Au sein de notre laboratoire, nous avons étudié l'effet *in vitro* de VCM encapsulée ou non sur la croissance intracellulaire de Mtb dans des macrophages murins infectés. L'utilisation de la microscopie confocale (système de microscopie confocale à haut contenu automatisé OPERA-PerkinElmer) nous a permis de montrer que les NP étaient efficacement phagocytées par les macrophages infectés. 73 et 99 % des cellules

contenaient des NP après une incubation de 2 et 24 heures, respectivement. Et, alors que VCM présente une faible stabilité dans les milieux biologiques, le traitement avec VCM encapsulée dans ce type de NP a été 5 fois plus efficace sur les bactéries Mtb intracellulaires qu'un traitement avec l'antibiotique libre. L'encapsulation de cet antibiotique à l'intérieur de NP à base de PLGA a donc amélioré 5 fois l'efficacité de l'antibiotique.

En conclusion, l'encapsulation de VCM dans des NPs à base de PLGA pourrait constituer une nouvelle application dans le traitement de TB.

Ces nouvelles données montrent également la capacité des NP à base de PLGA à encapsuler de quantité importante d'antibiotique et nous permet d'envisager de poursuivre une autre étude qui visera à encapsuler des combinaisons synergiques de VCM et d'autres antibiotiques, et notamment avec des inhibiteurs de la synthèse des lipides mycobactériens qui ont déjà montré un effet synergique potentiel (Soetaert, Rens et al. 2015; Rens, Laval et al. 2016).

Ce travail devrait contribuer au développement de nouvelles thérapies antituberculeuses efficaces et améliorer le traitement actuel pour d'autres maladies infectieuses causées par des bactéries Gram positives.

5.2. Summary article 3: "PLGA engineered polymeric nanocarriers improve the efficacy of vancomycin against intracellular *Mycobacterium tuberculosis* "

Tuberculosis (TB), which is mainly caused by *Mycobacterium tuberculosis* (Mtb), is still killing 1.8 million people annually. Although the TB death rate has decreased, the emergence of multidrug-resistant (MDR) and extensively drug-resistant (XDR) infections is highly worrisome. Nowadays, the lack of effective alternatives for the treatment of TB makes the repurpose of known drugs such as vancomycin (VCM) an attractive strategy. Indeed, recent studies highlight the potential of VCM, alone or in combination with other drugs, to treat MDR-TB.

However, like many antimicrobials, VCM is unable to access infected cells to reach the optimal therapeutic concentrations within the intracellular replicative niches. In contrast, phagocyte cells are well known for their ability to internalize drug-loaded NPs. Thus, the use of engineered nanocarriers able to readily penetrate infected cells to release their active drug cargo in the vicinity of intracellular pathogens appears as a promising strategy to overcome the poor ability of VCM to bypass membranes.

Here we show the potential of engineered nanoparticles (NPs) loaded with VCM to kill Mtb H37Rv strain in mouse macrophage RAW 264.7 cell line. A thorough optimization of the NP preparation procedure enabled the formation of NPs of around 320 nm including large aqueous compartments with entrapped VCM. Drug loadings reached 14.5 wt%, overpassing the ones reported so far in the literature. Despite their simple preparation method, easy to be scaled-up, the NPs possessed desired features for intracellular drug delivery, including a pH-triggered release.

Noteworthy, it was shown that the NPs were efficiently taken up by infected cells. For instance, after 5 h incubation with the NPs, 99 % of the macrophages contained particles. Confocal microscopy enabled to ascertain that the NPs were inside the cells and were not just adsorbed on their surface. NPs acted as "Trojan horses" massively penetrating inside the macrophages and possibly delivering their drug cargo because of the lower pH in the endosomes. As a result, the activity of entrapped VCM was around 5 times higher than that of free VCM.

With further studies, we believe that these VCM-loaded NPs could find potential applications for TB treatment.

5.3. Article 3

PLGA engineered polymeric nanocarriers improve the efficacy of vancomycin against intracellular *Mycobacterium tuberculosis*

Running Head: PLGA-encapsulated vancomycin against *M. tuberculosis*

List of Authors: Joana Costa-Gouveia[1#], Giuseppina Salzano[2#], Mario Menendez-Miranda[2], Eik Hoffmann[1], Nathalie Deboosere[1], Didier Desmaële[3], Priscille Brodin[1*&], Ruxandra Gref[2*&]

[1]Univ. Lille, CNRS, INSERM, CHU Lille, Institut Pasteur de Lille, U1019 - UMR 8204 - CIIL - Center for Infection and Immunity of Lille, Lille, France

[2]University of Paris Sud, University Paris-Saclay, CNRS, UMR 8214 - Institute for Molecular Sciences of Orsay (ISMO), Orsay, France

[3]University of Paris-Sud, University Paris-Saclay, CNRS, UMR 8612 – Institute Galien, Châtenay Malabry, France

[#]Equally contributing first authors

*corresponding authors: Brodin, Priscille (priscille.brodin@inserm.fr), Gref, Ruxandra, (ruxandra.gref@u-psud.fr)

[&]co-senior authors

Keywords: *Mycobacterium tuberculosis*, tuberculosis, vancomycin, PLGA, nanoparticles, nanocarrier system, antimicrobial drug delivery, intracellular pathogenic bacteria

Abstract

Tuberculosis (TB), which is mainly caused by *Mycobacterium tuberculosis (*Mtb*)*, is still killing 1.8 million people annually in the world. There is a growing trend to discover new alternatives to fight drug-resistant TB. Repurposing already approved antibiotics used for other diseases is an attractive drug development strategy. In this context, vancomycin (VCM), the gold-standard treatment of MRSA, was incorporated in nanoparticles (NPs) in an attempt to protect and deliver it to infected macrophages. Here we show a simple NP preparation method enabling to load up to 14.5 wt% VCM in PLGA NPs of around 320 nm. The NPs contained large internal compartments in which the drug was presumably located. They could be stored over three months without significant drug release. Interestingly, VCM was released at pH 5.5 and not at neutral pH nor in cell culture media. NPs were efficiently taken up by infected macrophages and after 2 and 24h incubation, 73 and 99 % of the cells contained NPs, respectively. Confocal microscopy enabled to ascertain that the NPs were located inside the cells and not only on their surface. *In vitro* studies on Mtb H37Rv infected RAW264.7 macrophages showed that the treatment with VCM-PLGA NPs was 5 times more effective than free drug. With further studies, the VCM-PLGA NPs could find potential application for TB treatment.

Introduction

Tuberculosis (TB), which is mainly caused by *Mycobacterium tuberculosis (*Mtb*)*, is still killing 1.8 million people annually in the world (1). Although the TB death rate has decreased, the emergence of multidrug-resistant (MDR) and extensively drug-resistant (XDR) infections is highly worrisome. As in some regions such as Eastern Europe, the percentage of XDR-TB cases increased, there is a growing concern to discover new potent drugs to fight MDR-and XDR-TB.

Repurposing “old” drugs used for other diseases is an attractive drug development strategy since much is already known about approved agents, accelerating their entrance in the market of TB drugs (2).

Vancomycin (VCM) is a glycopeptide antibiotic molecule able to form a hydrogen bond with the terminal D-alanyl-D-alanine moieties during peptidoglycan biosynthesis, thereby

preventing bacterial cell wall backbone synthesis. It has been the treatment of choice for serious infections caused by methicillin-resistant *Staphylococcus Aureus* (MRSA) for decades (3). Due to its efficiency in treating MDR infectious agents and the lack of other therapeutic options for the treatment of MRSA, its use has been reserved to serious infections not treatable with any other antibiotics in order to prevent development of resistant strains.

Currently, although VCM remains the gold-standard treatment of MRSA, new alternative antimicrobials are available and VCM-resistant *S. aureus* strains are emerging (4, 5). Repurposing VCM for the treatment of TB is considered nowadays a valid and interesting strategy supported by studies showing the activity of VCM against axenic Mtb cultures (6–11), but this antibiotic was never tested against intracellular Mtb.

Some factors affect VCM clinical activity, such as poor bioavailability, protein binding (≤50 %) (12) and poor intracellular penetration.

Indeed, like many antimicrobials, VCM is unable to access infected cells to reach the optimal therapeutic concentrations within the intracellular replicative niches of Mtb. Clinical failures with this drug were mainly attributed to its poor intracellular penetration (13–16). In contrast, phagocyte cells are well known for their ability to internalize drug-loaded NPs (17–20). Thus, the use of engineered nanocarriers able to readily penetrate infected cells to release their active drug cargo in the vicinity of intracellular pathogens could be a promising strategy to overcome the poor ability of VCM to bypass membranes.

An efficient VCM nanocarrier should: i) have mean diameter lower than one micron to be efficiently taken up by infected macrophages; ii) possess loadings higher than 10 wt% and good entrapment efficiencies; iii) release the drug in a controlled manner in the intracellular compartments; iv) be prepared by a straightforward method with a minimal use of excipients and v) be stable upon storage. Indeed, as VCM is a relatively expensive drug, entrapment efficiencies should be increased to reduce production costs. Similarly, VCM loadings should be maximized to avoid the use of large quantities of excipients which could cause adverse side effects. Ideally, materials with known safety profiles should be used.

VCM was incorporated in liposomes for its delivery to macrophages(21–24). However the entrapment efficiencies were low (less than 20%) (21–23). Polymeric poly (lactic-co-glycolic acid) (PLGA) NPs or chitosan NPs have also been used to encapsulate VCM, but the loadings (amount of VCM/NP) was low (4–6 wt%) in reason of the high hydrophilicity of the drug (25, 26). Of note, VCM was loaded in NPs of around 200 nm made of a poly(ethylene glycol) -poly(L-histidine)- PLGA (PEG-PLH-PLGA) copolymer designed to shield nontarget interactions at pH 7.4 but bind avidly to bacteria in acidic conditions (27). More recently (28), VCM was entrapped in composite NPs made of PLGA, a diblock poly(ethylene glycol) (PEG)-PLGA copolymer, Eudragit and a chitosan derivative. Interestingly, the NPs with sizes in the range of 500–1000 nm and containing up to 9.5 wt% VCM were able to release the drug in a pH-dependent manner. However, the preparation method is sophisticated and requires the use of several ingredients added in precise amounts.

Here we show a simple method enabling to load up to 14.5 wt% VCM in PLGA NPs.

By optimizing the preparation procedure, the release of the drug could be controlled and was found to be pH-dependent, with almost no release at neutral pH and fast delivery at pH 5.5 and not. Noteworthy, the pH-controlled release could be achieved by using only PLGA copolymers, avoiding the use of pH-responsive ones. The NPs were taken up by infected macrophages. The VCM loaded NPs were tested *in vitro* and demonstrated their ability to reduce the Mtb payloads in infected macrophages.

Results

Biodegradable PLGA NPs

PLGA NPs containing VCM have been successfully developed by adapting a double emulsion solvent evaporation method ($w_1/o/w_2$) schematized in Figure 1. A concentrated VCM aqueous solution was poured into a dichloromethane (DCM) organic phase containing PLGA. After sonication, a w_1/o emulsion was formed. A second aqueous phase containing a salt (NaCl) and a surfactant (PVA) was added to this emulsion, followed by a second sonication step. At this point, a $w_1/o/w_2$ was created, where VCM was dispersed in aqueous droplets located inside the organic phase droplets. After solvent removal

under gentle stirring, NPs were formed with characteristics gathered in Table 1. The morphology of the drug-loaded NPs was investigated by cryo-TEM, a method with the advantage of gaining insights into the inner structure of the NPs. Of note, in all VCM-PLGA NP samples, the inner aqueous compartments could be clearly observed (Figure 1). The structure of the VCM-PLGA NPs is typical of a $w_1/o/w_2$ emulsion, after polymer solidification. The size of the inner aqueous inclusions (light regions as compared to the dark PLGA matrix) is relatively large, making that they are separated from the outer NP surfaces by only a 10-40 nm thick polymer layer.

According to cryo-TEM investigations, the NPs had mean diameters in the range of 200-400 nm. This was in agreement with the DLS data showing mean diameters of 310-320 nm and polydispersities of around 0.2 (Table 1). An extensive study has been carried on to optimize the preparation procedure to maximise the VCM loading. Drug loading was determined by two methods: i) a direct one, consisting in dissolving the NPs and quantifying the extracted drug and ii) dosing the non-incorporated drug in the supernatants after NP centrifugation. Both methods were consistent with less than 5% differences.

The best strategy to efficiently incorporate VCM was to use a salt, NaCl, in the emulsification process (Figure 1). The addition of only 1% NaCl had a tremendous benefit upon VCM incorporation, while it did not modify the mean diameter of the NPs (Table 1). Drug loadings (DL) increased from 9.6 to 14.5 wt% without and with 1% NaCl, respectively. Moreover, loading efficiencies increased from 24 to 36.6 % when NaCl was added.

The NP formulation was stored at 4°C for 3 months. Their mean diameter remained unchanged (less than 5% variation) indicating a good stability. Of note, less than 4% of the incorporated VCM was released over this time (Table 1).

Drug release studies were performed after NP dilution in PBS or in the cell culture media (Figure 2). VCM release was less than 10 % in PBS or cell culture media, at pH 7.4 (red and blue curves; Figure 2). In contrast, around 60% of the entrapped VCM was released within 30 min after incubation at pH 5.5.

Intracellular accumulation of PLGA-Rhodamine NPs

The ability of empty PLGA NPs to be taken up by infected cells was investigated by automated confocal fluorescence microscopy. RAW264.7 murine macrophages, previously infected with Mtb H37Rv-GFP were incubated with PLGA-Rho for different times (0.5, 2 and 24 hours) and stained with DAPI. This allowed gaining information about the location of both NPs (red signal) and Mtb (green signal) in cells (blue signal). A continuous accumulation of the NPs in the cells was observed in the first 24 hours of incubation (Figures 3A and 3B). After 0.5 hours, only 7% of the cells contained NPs. This amount was dramatically increased after 2 and 24 h incubation, reaching 73% and 99% of cells including NPs, respectively. These data highlight the efficacy of the PLGA NPs to be internalized.

In order to ascertain that the NPs were indeed located inside the cells and not only attached to their surface or present in the suspension media, a complementary study was undertaken by confocal microscopy allowing to observe with high resolution each individual macrophage. Z-stack images of infected cells incubated with PLGA-Rho and labelled with nuclei and F-actin specific stains were performed. A typical orthogonal view is presented in Figure 3C, clearly showing that several PLGA-Rho NPs were clearly located inside the cell cytoplasm and were not just surrounding the cell or attached to their membranes. It was also possible to observe that several NPs inside the cell were larger (micron-size particles) than the size previously determined by PCS (320 nm), probably due to clustering effects.

Efficacy of the PLGA containing VCM NPs against intracellular Mtb replication

After confirmation of the ability of PLGA NPs to enter in RAW264.7 cells, we investigated the activity of these VCM-loaded NPs against intracellular Mtb replication. Briefly, compound dilutions and bacteria were prepared, cells were infected for 2 hours and extracellular bacteria were removed by successive washings and 1 hour incubation with amikacin. After 5 days incubation with the compounds at 37°C, the amount of bacteria was quantified using two different methods: confocal fluorescence microscopy and Colony-Forming Unit (CFU) counting (Figure 4A).

For the image-based assay, the analysis of the intracellular bacteria area was used as a correlate of intracellular growth. For both methods, dose-response curves were

generated after normalization on water-negative and INH-positive control, (Figures 4B and Fig. 4C).

As expected, in both methods, free VCM doesn't reach complete bacterial replication inhibition. On the contrary, PLGA-encapsulated VCM reached MIC at 40 µg/mL, indicating that the intracellular drug release was critical to the antibacterial activity in Mtb infected macrophages. In terms of IC_{50}, PLGA-encapsulated VCM showed 4 to 5 times improved efficacy comparing with the free VCM in both methods (IC_{50} decreased from 5.7 to 1.3 µg/mL in the first method and from 9.7 to 5.1 µg/mL in the second method), clearly demonstrating that the encapsulation of VCM is beneficial for its intracellular activity.

Discussion

PLGA NPs of around 320 nm containing VCM have been successfully developed using a double emulsion solvent. In contrast to previously reported studies where up to four ingredients were added to efficiently load VCM in NPs (28) the VCM DL reached 14.5 wt% use just one polymer (PLGA) and by adding a salt (NaCl). The salt plays a key role in favouring the precipitation of PLGA, thus efficiently trapping the inner droplets containing VCM by avoiding their leakage during the evaporation step. CryoTEM images clearly showed NP structures with large cavities, presumably loaded with VCM. The stability of the VCM-loaded NPs (no release of the incorporated drug upon storage) and simplicity of their preparation method could be assets for applications and scale-up. The NP formulation prepared in the presence of NaCl appears as particularly promising, overcoming the DL and encapsulation efficiencies reported so far for VCM incorporation in NPs or liposomes.

Noteworthy, VCM was rapidly released at pH 5.5 and not at pH 7.4 (Figure 2). This interesting and unexpected result might be due to the peculiar structure of the VCM-PLGA NPs (cryoTEM image, Figure 1). They typically possess a thin PLGA shell delimiting aqueous internal compartments presumably containing the VCM payload. When the pH decreases, the solubility of the entrapped VCM increases (29) leading to the fast release of the entrapped drug. As such, 60% of the entrapped VCM was released within the first 30 min of incubation at pH 5.5 (Figure 2). This particular behaviour could be of interest

for a pH triggered release if the NPs are taken up in endosomes with a slightly acidic pH (around 4.8) (31).

For a long time, the use of VCM has been restricted to the treatment of critically ill patients, with drug-resistant infectious agents, particularly MRSA, in the tentative to avoid the development of resistant strains to this important antibiotic. Nowadays, the lack of effective alternatives for the treatment of TB makes the repurpose of known drugs such as VCM an attractive strategy. The Mtb strain used here was indeed sensitive to VCM, with a MIC of 40 μg/mL, in agreement with previously reported data (9-11).

Mtb is a facultative intracellular pathogen, able to survive and multiply inside phagocytes such as macrophages by subverting the effector functions of these important innate immune cells. Mtb can persist in the host in a dormant state and there is a risk of reactivation, even decades after infection (30). For a good efficacy, drugs must reach both extra-and intracellular Mtb.

Encapsulation of VCM in the developed PLGA NPs resulted in 5 times activity improvement compared to free VCM against intracellular Mtb growth. This supports the fact that VCM has low membrane permeability as previously reported (13–16). It can be hypothesized that the observed intracellular antibacterial activity was driven by VCM released in the cells rather than the drug released prior to macrophage uptake. Possibly, VCM was readily released from the internalized NPs if these were located in compartments with low pH such as endosomes. The presumed intracellular release of the drug could be responsible of the antibacterial activity. Indeed, VCM-PLGA NPs are readily engulfed in infected cells and after 24 h incubation, practically all the macrophages contained NPs.

In a nutshell, PLGA NPs acted as “Trojan” horses to deliver VCM inside the macrophages.

These data the ability of PLGA to entrap high drug payloads. Further studies will be dedicated to the encapsulations of synergic VCM/drug combinations to further improve the capacity of the NPs to kill intracellular Mtb. The combination of VCM and mycobacterial lipids synthesis inhibitors are among potential synergic combinations (10-11).

Hopefully, this and subsequent work will contribute to the development of new effective anti-TB therapies and to improve current treatment for many other infection diseases caused by gram-positive bacteria.

Materials and methods

Chemicals

Poly (D,L-lactide-co-glycolide) (PLGA 50:50 acid terminated (MW: 5–20 KDa, 10P019) was kindly provided by PCAS (Expansorb, Aramon, France). Vancomycin hydrochloride (VCM) was kindly provided by the Centre International de Recherche en Infectiologie (Lyon, France). Poly (vinyl alcohol) (PVA) (88% hydrolyzed), Rhodamine B (Rho), 4-Dimethylaminopyridine (DMAP), 1-Ethyl-3-(3-dimethylaminopropyl) carbodiimide (EDC), piperazine, trimethyl aluminium ($AlMe_3$), sodium chloride, dichloromethane, trifluoracetic acid, hydrochloric acid, potassium chloride, sodium chloride, sodium hydrogen phosphate, potassium dihydrogen phosphate and endotoxin-free water were all obtained from Sigma-Aldrich. Dichloromethane (DCM-Analar Normapur) was from Prolabo. Injectable water was purchased from Cooper (Melun, France). The solvents were analytical grade.

Rho-PLA conjugate synthesis

Rho-PLA was synthesised according to a previously reported method (32). Briefly, Rho was reacted with piperazine to allow its grafting to the terminal carboxylic group of PLA through an amide bond. To do so, 11.3 mL of a 2M solution of $AlMe_3$ in toluene were added to 17.5 mL of a 0.22 mg/mL solution of piperazine in DCM. After completion of the gas evolution, the reaction mixture was refluxed for 24 h at 50°C in the presence of 0.5 mg/mL Rho under N_2 atmosphere. After quenching with a 1 M solution of aqueous HCl, the resulting Rho-piperazine amide was extracted, dried and purified by silica gel chromatography. Then, 5 mg Rho-piperazine amide was added to 50 mg of PLA acid-terminated in 0.5 mL DCM in the presence of 1 mg of DMAP as catalyst and 2 mg EDC as coupling agent. The obtained Rho-PLA was then extracted, purified by precipitation and dried. It was used in blends (1 wt%) with PLGA to form the NPs.

Preparation of PLGA NPs containing VCM

VCM-loaded PLGA NPs were prepared by an optimized w/o/w solvent evaporation method. Briefly, 0.2 mL of an aqueous internal phase containing VCM at 150 mg/mL was emulsified for 15 s in 1 mL of DCM (containing 75 mg of PLGA) using a probe sonicator at 40% of power (Sonopuls HD 2070, BANDELIN electronic GmbH & Co, Berlin, Germany). To this primary emulsion, 5 mL of 0.5% wt PVA solution containing or not NaCl (1 % in weight) were poured and sonicated for 30 sec at 40% of power to create a w/o/w emulsion. This emulsion was left at room temperature under gentle stirring overnight to allow the organic solvent to evaporate. Control plain NPs (without VCM) were prepared similarly. All formulations were prepared in triplicate.

NP size measurement and cryoTEM analysis.

The average hydrodynamic diameter of the NPs was determined at 25 °C with an equilibration time of 60 s using a Malvern Zetasizer® (Nano ZS90, Malvern Instruments S.A., Worcestershire, UK). Dilutions with injectable water were done according to ISO 22412 and experiments were performed in triplicate. Mean diameters were reported as Z Average (nm) ± SE (Standard Error - with a PdI lower than 0.1). The NPs mean diameters were monitored up to three months of storage at 25 °C. For cryoTEM analysis, 5 µL of NPs suspensions were deposited onto a 200 mesh copper grid and flash-frozen in liquid ethane cooled down at liquid nitrogen temperature. Cryo-TEM images were acquired on a JEOL 2200FS energy-filtered (20 eV) field emission gun electron microscope operating at 200 kV.

VCM drug loading

PLGA NPs were formulated with 6 mg/mL of initial VCM. Drug encapsulation was determined by quantifying both: i) the amount of non-encapsulated drug present in the supernatant obtained after centrifugation at 10,000 rpm for 10 min and ii) the drug extracted from the NPs by dissolving them in DMSO. All the samples were dosed by reverse-phase HPLC (RP-HPLC). The RP-HPLC analysis were performed after dilution with deionized and filtered water using a Agilent HPLC system (Agilent 1100 Series) equipped with a C18 column (Kinetex 5u C18, 100 A, Phenomenex), and UV detector at λ = 280 nm. The chromatographic conditions were as follows: solvent A 0.1% Trifluoroacetic Acid

(TFA) in water and solvent B 0.1% TFA in acetonitrile; 0–2 min: 0%–20% B, 2–6 min: 20%–45% B, 6–10 min: 45%- 75% B, 10–15 min: 75%–0%. Flow rate: 1.0 mL/min at room temperature.

In all cases, R2 values for VCM was higher than 0.99.

The DL is defined as the mass fraction of a NP that is composed of drug, while the EE can be considered as the fraction of drug effectively encapsulated into the NPs compared with the amount that was used to prepare the NPs.

The DL and EE were calculated as shown in equations 1 and 2, respectively.

(1) $$DL(\%) = \frac{(mg\ of\ encapsulated\ drug^{**})}{(mg\ of\ polymer)} \times 100$$

(2) $$EE(\%) = \frac{(mg\ of\ encapsulated\ drug^{**})}{(mg\ of\ drug\ initially\ added\ to\ the\ formulation)} \times 100$$

Release studies

To estimate VCM release, PLGA VCM NPs 1% NaCl were diluted 10 times in serum containing media, PBS pH 7.4 and PBS pH 5.5 and incubated at 37 °C with constant agitation. At different time points, the suspension was centrifuged at 10,000 rpm for 10 min at room temperature (RT), and the supernatant was analysed by HPLC.

Bacteria and macrophages

A recombinant strain of Mtb H37Rv constitutively expressing the green fluorescent protein (H37Rv-GFP) was cultured at 37°C for 16 days in Middlebrook 7H9 medium (Difco) supplemented with 10% Middlebrook oleic acid-albumin-dextrose-catalase (OADC, Difco), 0.5% glycerol (Sigma-Aldrich), 0.05% Tween 80 (Sigma-Aldrich) and 50 µg/mL hygromycin B (Invitrogen). Mycobacteria were washed three times with Dulbecco's Phosphate-Buffered Saline (DPBS free from $MgCl_2$ and $CaCl_2$, Gibco) and re-suspended in RPMI-1640 Glutamax medium (Difco) containing 10% heat-inactivated Fetal Bovine Serum (FBS, Life Technologies). Clumped mycobacteria were pelleted by centrifugation at 700 rpm for 2 min and homogeneous supernatants were used for infection. Bacterial titre was determined by measuring the optical density at 600 nm and by measuring EGFP fluorescence on a Victor Multilabel Counter (Perkin Elmer). The

bacterial suspension was diluted at the required titre in RPMI 1640 supplemented with 10% FBS (RPMI-FBS) prior to infection.

RAW264.7 murine macrophages (ATCC TIB-71) were maintained at 37°C in RPMI-FBS. Macrophages were harvested by using Versene (LifeTechnologies).

Assay plate preparation

VCM dissolved in H_2O to 5 mg/mL was diluted to 0.4 mg/mL and VCM-loaded PLGA NPs were diluted in water to 0.4 mg/mL of VCM.

Eight 2-fold serial dilutions of the mother solution in a final volume of 100 µL were performed in sterile MilliQ water in a 384 deep well "diamond plate" (Axygen) in order to obtain a dose-response curve. Posteriorly, 5 µL of each concentration of the NPs or VCM were dispensed in 384-well clear-bottom polystyrene assay plates (Greiner Bio-One).

A standard anti-TB drug, such as isoniazid (INH, Sigma-Aldrich) was used as positive control. INH was dissolved in DMSO (Sigma-Aldrich) to 10 mg/mL and diluted to 0.1 mg/mL in H_2O prior to be added in 384-well assay plates to reach the final concentration of 10 µg/mL. Water was used as negative control.

Intracellular bacterial growth assay

RAW264.7 macrophages suspension at 5×10^5 cells/mL were infected with H37Rv-GFP at a MOI of 2 in RPMI-FBS under mild stirring (120 rpm). At 2 h post-infection, infected cells were washed with RPMI-FBS and treated with 50 µg/mL amikacin (Sigma-Aldrich) for 1 h, to kill the remaining extracellular bacilli. Cells were washed twice with RPMI-FBS and 45 µL of cell suspension was added per well, in 384-well assay plates. After 2 h, supernatants were removed and fresh RPMI-FBS was added. Plates were incubated for 5 days at 37°C with 5% CO_2. RAW264.7 cells were stained with 5 µM Syto 60 Invitrogen) for 1 h at 37°C before imaging.

After image-acquisition, 5 selected wells, corresponding to different concentrations of VCM (40, 10, 2.5, 0.6 and 0.2 µg/mL), and containing infected cells, were washed and lysed with DPBS-0.1% Triton X-100 buffer for 1 min. The lysates were tested for CFU determination.

CFU determination.

5-fold serial dilutions were performed in DPBS and plated onto Middlebrook 7H11 (Difco) agar plates, supplemented with 0.5% glycerol, 10% OADC and 50 µg/mL hygromycin B. After 3-weeks incubation at 37°C with 5% CO_2, CFUs were calculated.

Study of intracellular PLGA-Rho NPs accumulation

RAW264.7 macrophages suspension were seeded in 384-well plates at a density of 2×10^4 cells per well. After overnight incubation at 37°C with 5% CO_2 cells were, infected with H37Rv-GFP at a MOI of 2. At 2 h post-infection, extracellular bacilli were removed by washing three times with D-PBS and 50 µg/mL amikacin treatment for 1 h. Cells were washed twice with RPMI-FBS. 100 µg/mL PLGA-Rho were added by well and incubated for 0.5 h, 2 h or 24 h. Cells were washed, fixed using 10% neutral buffered formalin solution (Sigma-Aldrich) for 30 min. Fixed cells were washed twice with DPBS and then nucleus were stained with 2.5 µg/ml DAPI for 10 min. Cells were finally washed twice with DPBS before imaging.

In parallel, RAW264.7 macrophages were seeded in 12-well plates, containing coverslips, infected and treated with 100 µg/mL PLGA-Rho NPs for 2 h, as described above. Cells were fixed formalin solution for 24h and permeabilized using DPBS-0.1% Triton X-100 for 5 min at room temperature. Cells were then stained with 5 µg/mL DAPI and Alexa Fluor 660 phalloidin dye (ThermoFisher) for 30 min at room temperature. After three washing with DPBS, coverslips were placed in mounting medium before image acquisition.

Image acquisition and Image-based analysis

For intracellular assays performed in 384-well plates, image acquisitions were performed on an automated fluorescent confocal microscope (Opera, PerkinElmer), using a 20X-water objective (NA 0.70). The confocal microscope was equipped with 405, 488, 561 and 640 nm excitation lasers. The emitted fluorescence was captured using 3 cameras associated with a set of filters covering a detection wavelength ranging from 450 to 690 nm. A series of 6 images was taken by well and each one was analysed using the image-analysis software Columbus system (version 2.5.1, PerkinElmer). For the quantification of Mtb intracellular growth, cells (nuclei and cytoplasm) were detected by an intensity detection algorithm applied on the SYTO60 channel. A spot detection algorithm based on the GFP channel was applied for the detection of Mtb-GFP in cells and the bacterial

intensity and area in pixels were measured. The intracellular bacterial growth was quantified by the total intracellular bacterial area (pixel) per well. For the study of intracellular PLGA-Rho NPs accumulation, cells were detected by an intensity detection algorithm applied on the DAPI (blue signal) channel. Spot detection algorithms based on the GFP (green signal) and PLGA-Rho (red signal) channels were used for the detection of Mtb-GFP and NPs, respectively, in cells. Images were analysed to determine the percentage of infected cells containing NPs in the cytoplasm area.

For the intracellular assays performed in 12-well plates to study the intracellular PLGA-Rho NPs accumulation, confocal images were acquired using a confocal microscope Zeiss LSM880 equipped with a 63x objective (NA 1.4), and Zen imaging software (Zeiss). Image analysis and generation of maximum projections of z-stacks was carried out by Fiji software (33).

Results analysis for intracellular bacterial replication assay

The read-outs, intracellular bacterial area and CFU, were normalized in comparison with the values obtained for the negative control (water value corresponding to 0% inhibition) and the positive control (INH value corresponding to 100% inhibition) and could be converted into a percentage of bacterial replication inhibition (% inhibition). % inhibition was calculated by the formula:

$$\%\ inhibition = (1 - \frac{\text{Sample value} - \text{INH value}}{\text{DMSO value} - \text{INH value}}) \times 100$$

A plot of % inhibition versus the VCM concentration was determined using GraphPad Prism 5.0 software. The concentration required to inhibit 50% of the bacterial replication (IC_{50}) was calculated by nonlinear regression analysis using the equation for a sigmoidal dose-response curve with variable slope.

Acknowledgments

We gratefully acknowledge Ok-Ryul Song, Isabelle Ricard, Alexandre Vandeputte, Rosangela Frita, Xue Li, Alexandra Pastor, Sabrina Brown, Grant Kiely and Alain Baulard for technical assistance and helpful discussions. We acknowledge the PICT-IBiSA and

Frank Lafont from BiCEL for providing access to microscopy equipment. We are grateful to Sylvain Trepout for cryoTEM experiments.

Financial support for this work was provided by the European Community (CycloN Hit n° 608407, ERC-STG INTRACELLTB n° 260901, MM4TB n°260872), the Agence Nationale de la Recherche (ANR-10-EQPX-04-01, ANR-14-CE08-0017, ANR-16-CE35-0009), the Feder (12001407 (D-AL) Equipex Imaginex BioMed) and the Région Nord Pas de Calais (convention n° 12000080). This work was supported by a public grant overseen by the French National Research Agency (ANR) as part of the "Investissements d'Avenir" program (Labex NanoSaclay, ANR-10-LABX-0035).

References

1. WHO. 2016. Global Tuberculosis Report 2016. Cdc 2016 214.

2. Dheda K, Barry CE, Maartens G. 2016. Tuberculosis. Lancet 387:1211–1226.

3. Chua K, Howden BP. 2009. Treating Gram-positive infections: vancomycin update and the whys, wherefores and evidence base for continuous infusion of anti-Gram-positive antibiotics. Curr Opin Infect Dis 22:525–534.

4. Van Hal SJ, Fowler VG. 2013. Is it time to replace vancomycin in the treatment of methicillin-resistant staphylococcus aureus infections? Clin Infect Dis 56:1779–1788.

5. McGuinness WA, Malachowa N, DeLeo FR. 2017. Vancomycin Resistance in Staphylococcus aureus . Yale J Biol Med 90:269–281.

6. Collins CH, Uttley AHC. 1988. In-vitro activity of seventeen antimicrobial compounds against seven species of mycobactena. J Antimicrob Chemother 22:857–861.

7. Provvedi R, Boldrin F, Falciani F, Palù G, Manganelli R. 2009. Global transcriptional response to vancomycin in Mycobacterium tuberculosis. Microbiology 155:1093–1102.

8. Dinesh N, Sharma S, Balganesh M. 2013. Involvement of efflux pumps in the

resistance to peptidoglycan synthesis inhibitors in Mycobacterium tuberculosis. Antimicrob Agents Chemother 57:1941–1943.

9. Schoonmaker MK, Bishai WR, Lamichhanea G. 2014. Nonclassical transpeptidases of Mycobacterium tuberculosis alter cell size, morphology, the cytosolic matrix, protein localization, virulence, and resistance to β-lactams. J Bacteriol 196:1394–1402.

10. Soetaert K, Rens C, Wang XM, De Bruyn J, Lanéelle MA, Laval F, Lemassu A, Daffé M, Bifani P, Fontaine V, Lefèvre P. 2015. Increased vancomycin susceptibility in mycobacteria: A new approach to identify synergistic activity against multidrug-resistant mycobacteria. Antimicrob Agents Chemother 59:5057–5060.

11. Rens C, Laval F, Daffé M, Denis O, Frita R, Baulard A, Wattiez R, Lefèvre P, Fontaine V. 2016. Effects of lipid-lowering drugs on vancomycin susceptibility of mycobacteria. Antimicrob Agents Chemother 60:6193–6199.

12. Rybak MJ. 2006. The Pharmacokinetic and Pharmacodynamic Properties of Vancomycin. Clin Infect Dis 42:S35–S39.

13. Cruciani M, Gatti G, Lazzarini L, Furlan G, Broccali G, Malena M, Franchini C, Concia E. 1996. Penetration of vancomycin into human lung tissue. J Antimicrob Chemother 38:865–869.

14. Lamer C, De Beco V, Soler P, Calvat S, Fagon JY, Dombret - MC, Farinotti R, Chastre J, Gibert C. 1993. Analysis of vancomycin entry into pulmonary lining fluid by bronchoalveolar lavage in critically ill patients. Antimicrob Agents Chemother 37:281–286.

15. Kollef MH. 2007. Limitations of vancomycin in the management of resistant staphylococcal infections. Clin Infect Dis 45 Suppl 3:S191–S195.

16. Lehar SM, Pillow T, Xu M, Staben L, Kajihara KK, Vandlen R, DePalatis L, Raab H, Hazenbos WL, Hiroshi Morisaki J, Kim J, Park S, Darwish M, Lee B-C, Hernandez H, Loyet KM, Lupardus P, Fong R, Yan D, Chalouni C, Luis E, Khalfin Y, Plise E, Cheong J, Lyssikatos JP, Strandh M, Koefoed K, Andersen PS, Flygare JA, Wah Tan M, Brown

EJ, Mariathasan S. 2015. Novel antibody–antibiotic conjugate eliminates intracellular S. aureus. Nature 527:323–328.

17. Costa-Gouveia J, Pancani E, Jouny S, Machelart A, Delorme V, Salzano G, Iantomasi R, Piveteau C, Queval CJ, Song O-R, Flipo M, Deprez B, Saint-André J-P, Hureaux J, Majlessi L, Willand N, Baulard A, Brodin P, Gref R. 2017. Combination therapy for tuberculosis treatment: pulmonary administration of ethionamide and booster co-loaded nanoparticles. Sci Rep 7:5390.

18. Pelgrift RY, Friedman AJ. 2013. Nanotechnology as a therapeutic tool to combat microbial resistance. Adv Drug Deliv Rev 65:1803–1815.

19. Ladavière C, Gref R. 2015. Toward an Optimized Treatment of Intracellular Bacterial Infections: Input of Nanoparticulate Drug Delivery Systems. Nanomedicine 10:3033–3055.

20. Costa-Gouveia J, Aínsa JA, Brodin P, Lucía A. 2017. How can nanoparticles contribute to antituberculosis therapy? Drug Discov Today 22:600–607.

21. Pumerantz A, Muppidi K, Agnihotri S, Guerra C, Venketaraman V, Wang J, Betageri G. 2011. Preparation of liposomal vancomycin and intracellular killing of meticillin-resistant Staphylococcus aureus (MRSA). Int J Antimicrob Agents 37:140–144.

22. Ma T, Shang B-C, Tang H, Zhou T-H, Xu G-L, Li H-L, Chen Q-H, Xu Y-Q. 2011. Nano-hydroxyapatite/chitosan/konjac glucomannan scaffolds loaded with cationic liposomal vancomycin: preparation, *in vitro* release and activity against Staphylococcus aureus biofilms. J Biomater Sci Polym Ed 22:1669–81.

23. Sande L, Sanchez M, Montes J, Wolf AJ, Morgan MA, Omri A, Liu GY. 2012. Liposomal encapsulation of vancomycin improves killing of methicillin-resistant Staphylococcus aureus in a murine infection model. J Antimicrob Chemother 67:2191–2194.

24. Surewaard BGJ, Deniset JF, Zemp FJ, Amrein M, Otto M, Conly J, Omri A, Yates RM, Kubes P. 2016. Identification and treatment of the *Staphylococcus aureus* reservoir in vivo. J Exp Med 213:1141–1151.

25. Hu C-MJ, Fang RH, Wang K-C, Luk BT, Thamphiwatana S, Dehaini D, Nguyen P, Angsantikul P, Wen CH, Kroll A V., Carpenter C, Ramesh M, Qu V, Patel SH, Zhu J, Shi W, Hofman FM, Chen TC, Gao W, Zhang K, Chien S, Zhang L. 2015. Nanoparticle biointerfacing by platelet membrane cloaking. Nature 526:118–121.

26. Xu J, Xu B, Shou D, Xia X, Hu Y. 2015. Preparation and evaluation of vancomycin-loaded N-trimethyl chitosan nanoparticles. Polymers (Basel) 7:1850–1870.

27. Radovic-Moreno AF, Lu TK, Puscasu VA, Yoon CJ, Langer R, Farokhzad OC. 2012. Surface charge-switching polymeric nanoparticles for bacterial cell wall-targeted delivery of antibiotics. ACS Nano 6:4279–4287.

28. Pei Y, Mohamed MF, Seleem MN, Yeo Y. 2017. Particle engineering for intracellular delivery of vancomycin to methicillin-resistant Staphylococcus aureus (MRSA)-infected macrophages. J Control Release 0–1.

29. Pfeiffer RR. 1981. Structural Features of Vancomycin. Rev Infect Dis 3:S205–S209.

30. O'Garra A, Redford PS, McNab FW, Bloom CI, Wilkinson RJ, Berry MPR. 2013. The Immune Response in TuberculosisAnnual Review of Immunology.

31. Tan S, Russell DG. 2015. Trans-species communication in the *Mycobacterium tuberculosis*- infected macrophage. Immunol Rev 264:233–248.

32. Nguyen T, Francis MB, Science M, Di V, Berkeley L, Labs N. 2003. Practical Synthetic Route to Functionalized Rhodamine Dyes 300.

33. Schindelin J, Arganda-Carreras I, Frise E, Kaynig V, Longair M, Pietzsch T, Preibisch S, Rueden C, Saalfeld S, Schmid B, Tinevez J-Y, White DJ, Hartenstein V, Eliceiri K, Tomancak P, Cardona A. 2012. Fiji: an open-source platform for biological-image analysis. Nat Methods 9:676–682.

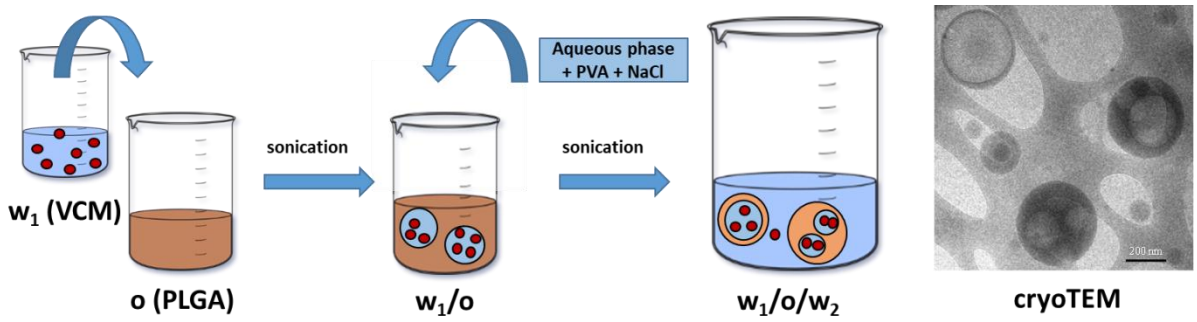

Figure 1. Schematic representation of the preparation of VCM-loaded PLGA NPs using a double emulsion (w1/o/w2) method. CryoTEM images of PLGA NPs loaded with VCM (14.5 wt%).

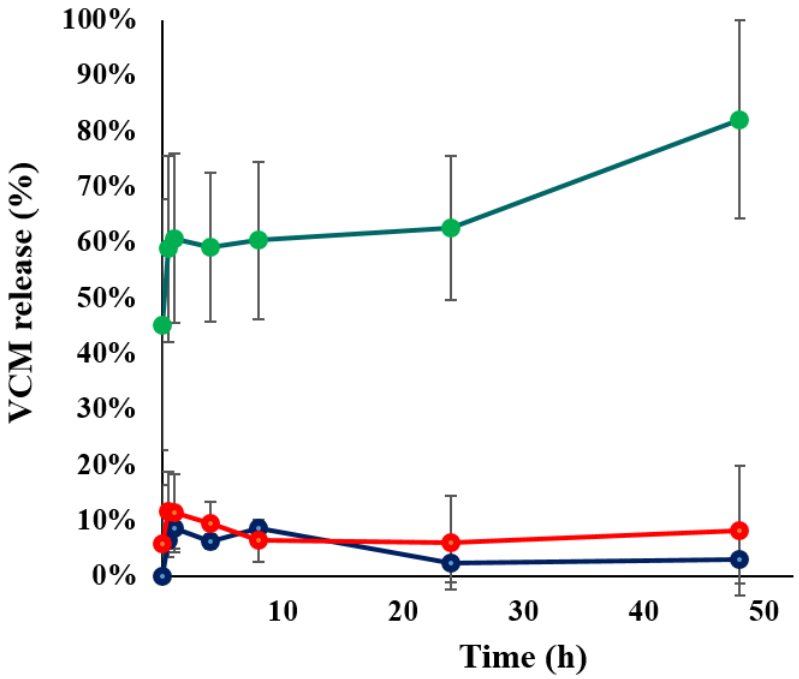

Figure 2. **Release of VCM from PLGA NPs containing 14.5 wt% VCM, prepared in the presence of NaCl.** The NPs were diluted 10 times in PBS at pH 7.4 (blue), PBS at pH 5.5 (green) and in cell culture total media (containing serum) (red). All the samples were incubated at 37°C degree under gentle stirring.

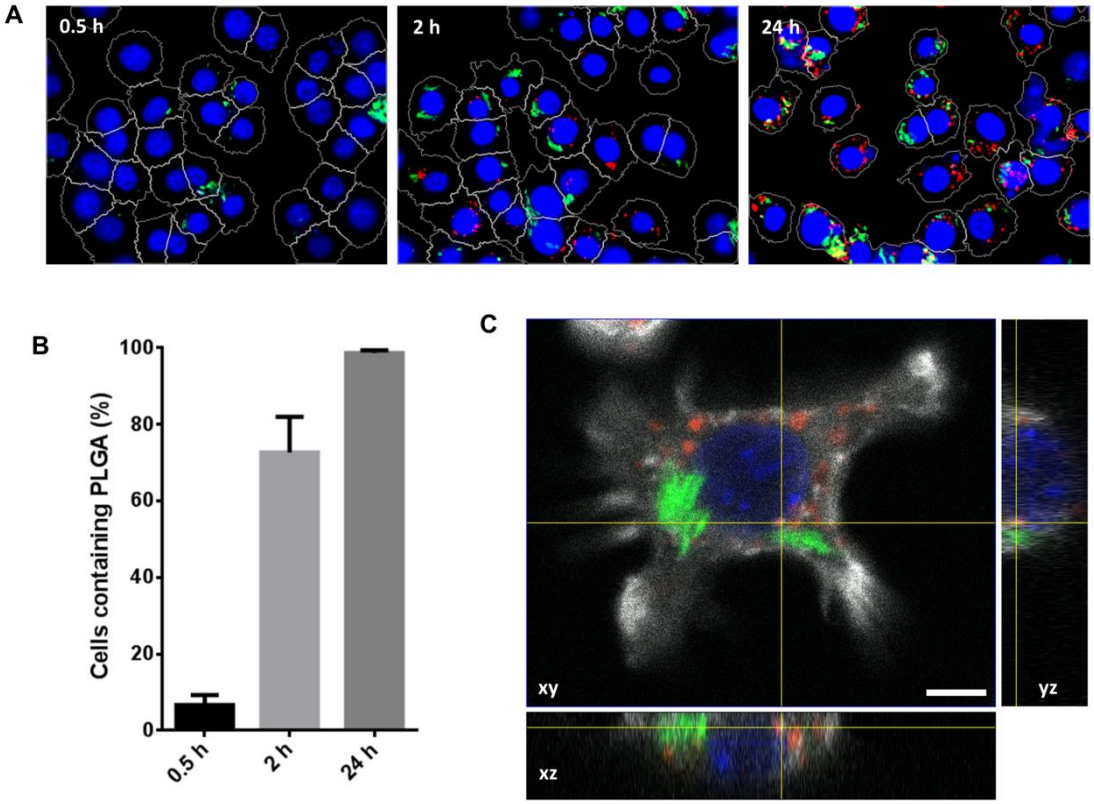

Figure 3. PLGA-Rho NPs inside RAW264.7 macrophages infected with Mtb H37Rv-GFP. (A) Representative images of cells containing PLGA-Rho NPs (red) and Mtb H37Rv-GFP (green), at the indicated time points, obtained by image acquisition using an automated confocal microscope. (B) % of cells containing PLGA-Rho NPs after RAW264.7 macrophages infection with Mtb H37Rv-GFP calculated by image analysis using the software Columbus. Data are presented as mean ± SEM. (C) Orthogonal view of an infected RAW264.7 cell imaged by confocal microscopy. F-actin was labelled by phalloidin (gray), and nuclei were stained by DAPI (blue). Shown is one z-stack in xy, xz and yz dimension. Scale bar = 5 µm.

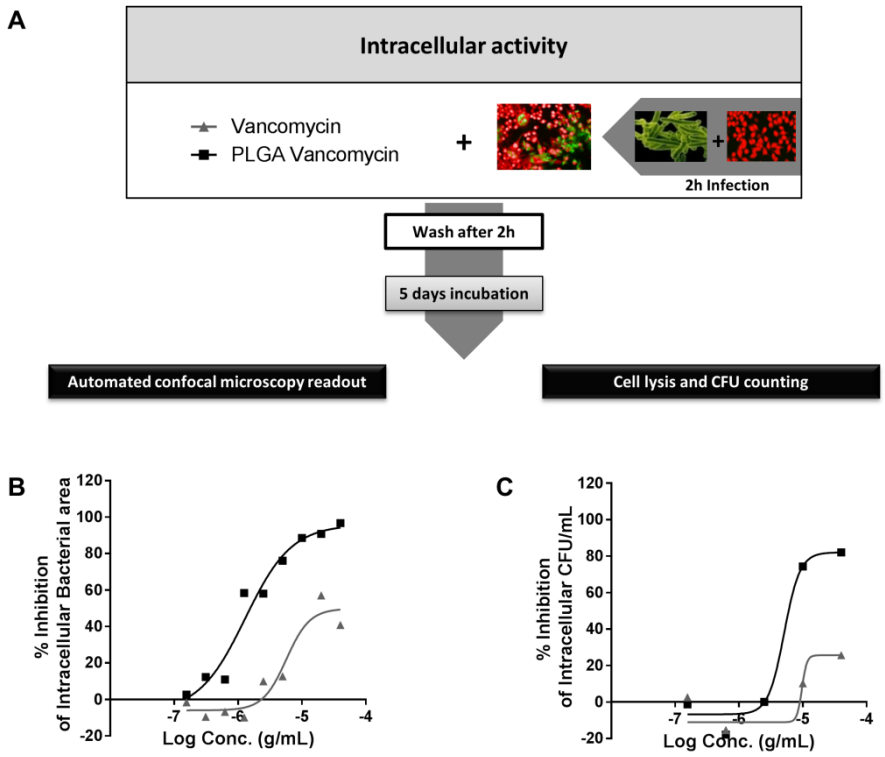

Figure 4. Intracellular antitubercular activity. (A) Scheme representing the steps performed to analyse activity of VCM (grey triangle) and PLGA VCM (black square) against Mtb H37Rv-GFP inside RAW264.7 macrophages. (B) % of inhibition on intracellular bacterial area detected by automated confocal microscopy and measured by the image-analysis software Columbus. (C) % of inhibition on intracellular bacterial growth measured by CFU counting.

Table 1. **Main characteristics of VCM-loaded PLGA NPs. Effect of NaCl on the incorporation of VCM.** Stability upon storage at 4°C.

NaCl (wt%)	DL (wt% ± SD)	Loading efficiency (% ± SD)	Mean diameter (nm) ± SD	PdI ± SD	VCM release 3 month storage 4°C (% ± SD)
0%	9.6 ± 0.9	24.0 ± 2.4	320 ± 30	0.190 ± 0.05	4.1 ± 1.4
1%	14.5 ± 0.5	36.6 ± 1.6	310 ± 59	0.226 ± 0.08	2.0 ± 0.9

Table 1. Main characteristics of VCM-loaded PLGA NPs. Effect of NaCl on the incorporation of VCM. Stability upon storage at 4°C.

NaCl (wt%)	DL (wt% ± SD)	Loading efficiency (% ± SD)	Mean diameter (nm) ± SD	PdI ± SD	VCM release 3 month storage 4°C (%± SD)
0%	9.6 ± 0.9	24.0 ± 2.4	320 ± 30	0.190 ± 0.05	4.1 ± 1.4
1%	14.5 ± 0.5	36.6 ± 1.6	310 ± 59	0.226 ± 0.08	2.0 ± 0.9

6. CHAPTER IV

Intrinsic antimycobacterial activity of NPs

Activité antimycobactérienne intrinsèque des NPs

As part of the CycloNHit consortium, different compounds and nanoparticles (NPs) synthesised by our partners were tested during this PhD, both against extracellular and intracellular bacteria using the fluorescent assays mentioned in the previous chapters.

6.1. Cyclodextrins

Cyclodextrins (CDs) were by far the most representative, with 89 CDs tested.

Due to the relatively high number of compounds tested simultaneously, a high throughput screening (HTS) platform available at the BioImaging Center of Lille was initially used. This platform contains different liquid dispensers, and plate handlers that allow a more precise and faster distribution of the compounds. In particular, the Echo liquid handler 550 (LabCyte) uses the technology ADE (Acoustic Droplet Ejection) that uses sound energy to transfer 2.5 nL droplets from source plates to destination plates, without using tips. The transfer is more accurate and precise than traditional dispensers, reduces the compound consumption and the final solvent concentration, which is a great advantage for cell assays with compounds dissolved in dimethyl sulfoxide (DMSO)). However, for the dispensing of NPs I noticed many inconsistencies in the results, leading me to prefer doing all the serial dilutions of NPs manually.

From the total CDs tested 24 were neutral, 21 cationic, 32 anionic and 12 polymeric. The structure of each one is confidential thus they are here named with code identification. From the 89 CDs tested, only 5 (6 % of the total) presented an IC50 bellow 1×10^{-4} M, against extracellular Mtb. (**Figure 15, first column**). All of them were cationic. The compound with the best extracellular efficacy was 3K with an IC50 of 1×10^{-5} M, followed by 2G with 2×10^{-5} M, 1G and 3G with 3×10^{-5} M and 1K with 7×10^{-5} M. Compound 1K and 3K presented also a slight inhibition of intracellular Mtb replication (**Figure 15, second column**). Compound 2G and 3G didn't present any clear effect against intracellular Mtb replication, while compound 1G had a negative effect, by stimulating intracellular replication. All the compounds presented cytotoxicity (**Figure 15, third column**).

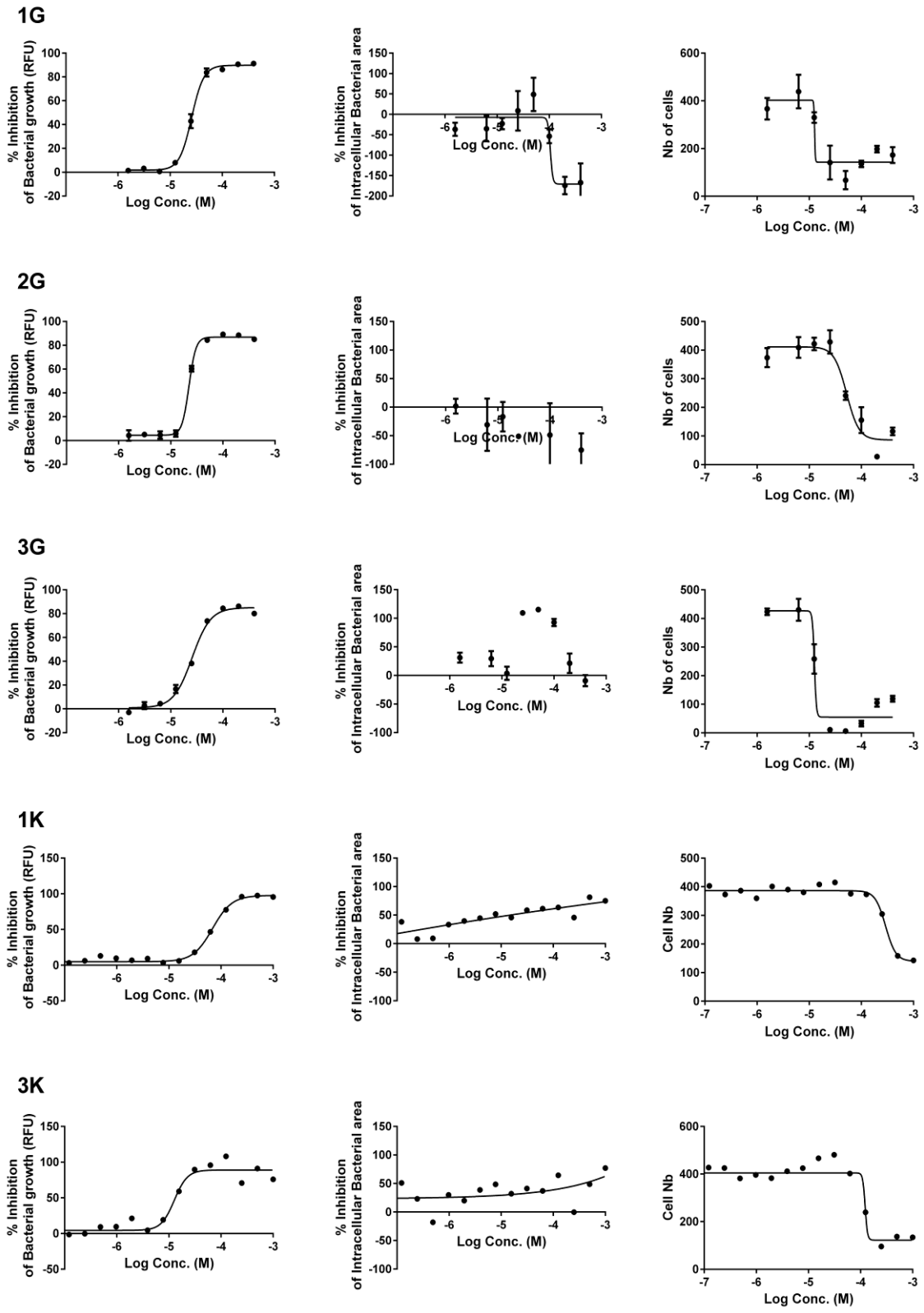

Figure 15 - Extracellular and intracellular activity of the compounds with best antitubercular activity tested. First column: % of inhibition on bacterial RFU; Second column: % inhibition of intracellular bacteria area; Third column: Number of cells in the intracellular assay.

6.2. Silver Nanoparticles

One core-shell silver NP was also tested against extracellular Mtb. Silver NPs are well known for their antimicrobial activity. However, the tested particle presented no effect on bacterial growth at concentrations bellow 30 mM (data not shown).

6.3. Nanoporous Metal-Organic Frameworks

Nanoporous Metal-Organic Frameworks (NanoMOFs) were also tested. Studies performed by Laleh Majlessi's group at Institut Pasteur Paris revealed that NanoMOFs induce significantly the autophagic marker light chain 3 (LC3) expression, with no significant toxicity found at the tested conditions. Results were obtained from flow cytometric analysis of the autophagy bio-marker LC3-II in bone marrow-derived dendritic cells (BM-DC) from C57BL/6 mice treated with NanoMOFs for 16 h. We confirmed this LC3 increased expression by fluorescence microscopy in non-infected RAW 264.7 macrophages after 16 h incubation with NanoMOF (same condition as our partner). Using the LC3 marker, but also the polyubiquitin-binding protein P62/SQSTM1, another autophagy marker (**Figure 16**). We observed that incubation with NanoMOFs increase the number of LC3 positive cells and P62 positive cells, from 6 to 40 % and form 2 to 50 %, respectively (**Figure 17 A**). We could also see that LC3 and P62 spots colocalize (see arrows, **Figure 16**). **Figure 17 B** shows an example image of how the LC3 spots detection was performed.

These results lead us to hipothesize that NanoMOFs could induce autophagy, an immune defense mechanism that has been associated with increased Mtb killing (Gutierrez, Master et al. 2004; Lam, Prabhu et al. 2017). Moreover, induction of autophagy has been claimed as a promising host-directed chemotherapeutic intervention in TB (Gupta, Misra et al. 2016). Consequently, we decided to test the effect of NanoMOFs against intracellular Mtb replication in our intracellular *in vitro* assay.

In this case, the incubation of NanoMOFs with the cells occurred during 5 days, the time necessary to obtain significant difference between the compounds active and non-active in terms of Mtb replication. The increase of incubation time resulted in dose-dependent cytotoxicity, which increased Mtb replication, both in the infected and non-infected cells (**Figure 18**).

Identification of the mechanisms and pathways of NanoMOF-induced cytotoxicity is out of scope in this thesis. However, we believe that autophagic cell death may be involved.

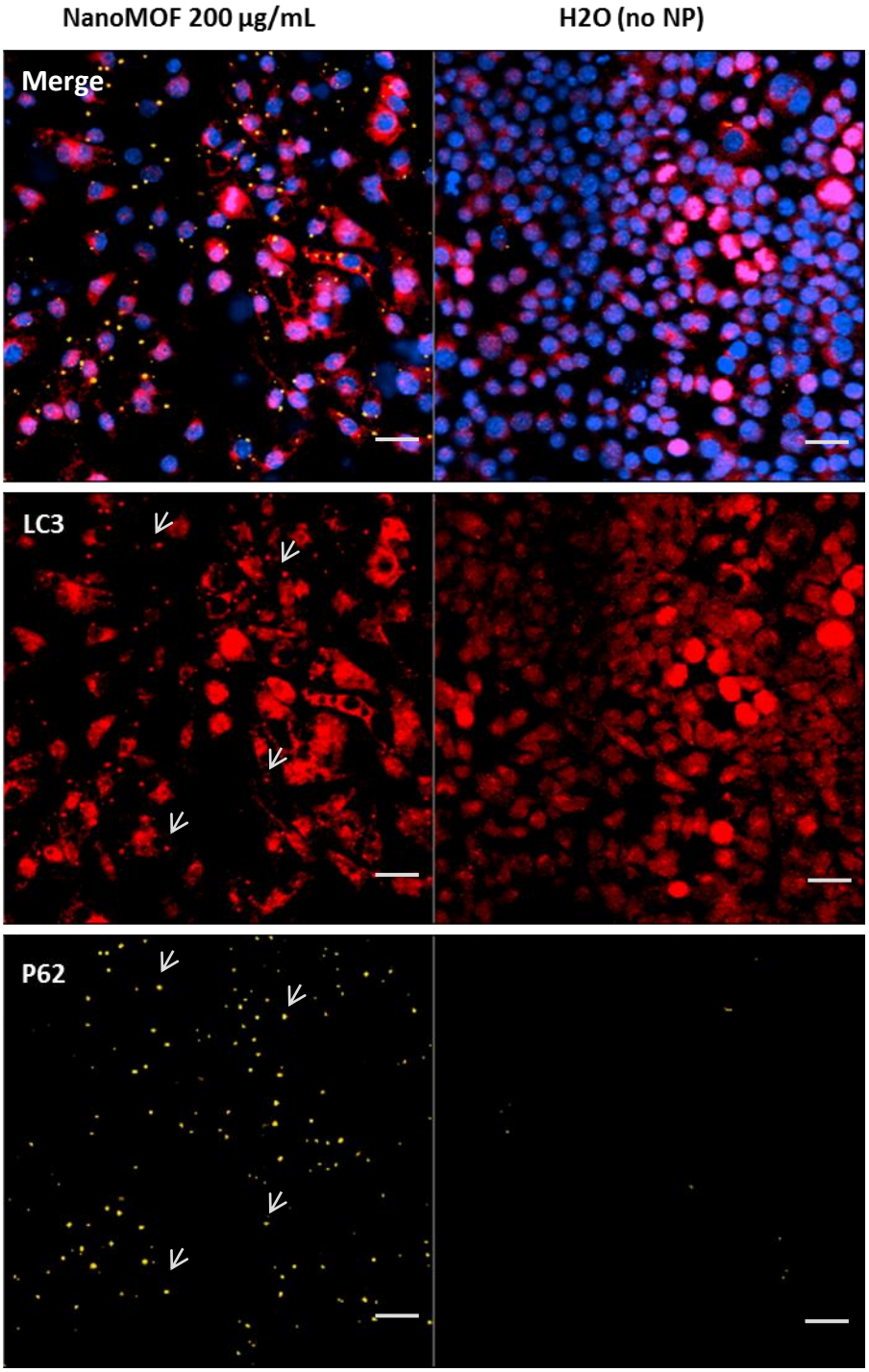

Figure 16 – Fluorescence microscopy. RAW 264.7 cells were plated 24 h before addition of NPs. After incubation with the NPs during 16 h, cells were fixed, stained with DAPI (blue) and immunostained with LC3 (red) and P62 (yellow). Arrows indicate colocalization in LC3 and P62 spots. Scale bars: 20 µm.

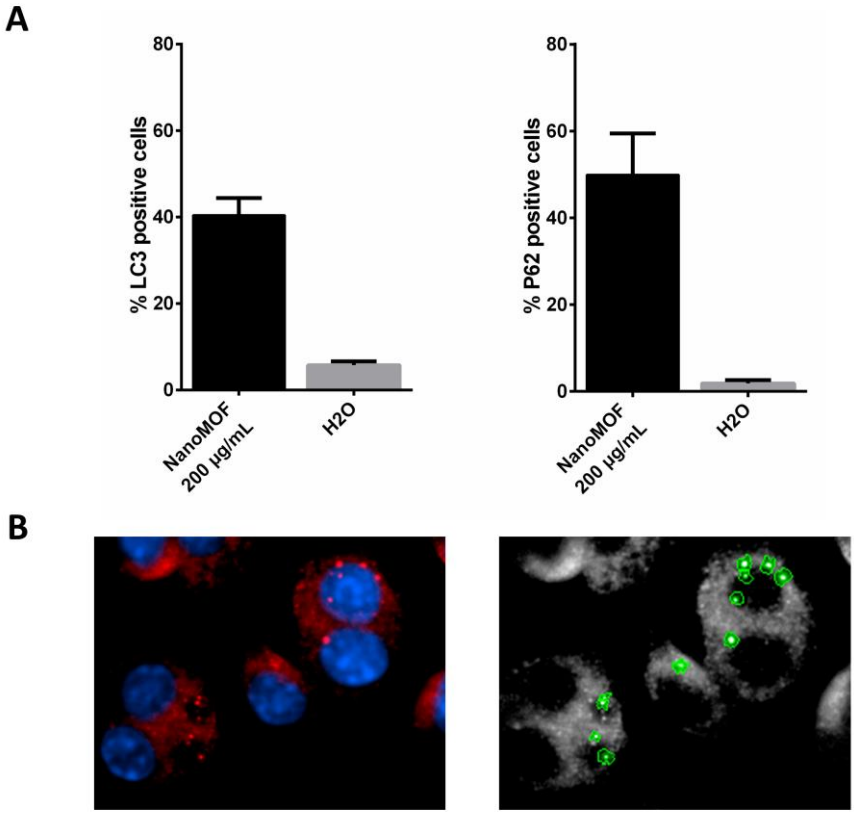

Figure 17 - LC3 and P62 quantification. A: % LC3 and P62 positive cells after 16 h incubation with NanoMOFs or water (negative control); **B**: Example of LC3 quantification using the image-analysis software Columbus. In the left is the output image with the nucleus in blue and LC3 in red, and in the right image is the LC3 in grey and the selected LC3 spots highlighted in green.

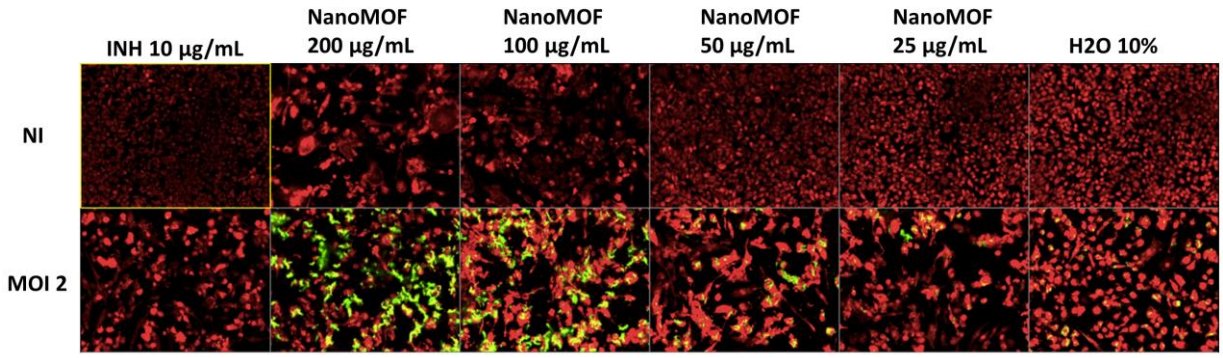

Figure 18 - Dose-response induction of cytotoxicity in non-infected cells (NI) and in cells infected with Mtb H37Rv-GFP (green) with MOI 2. Cells were stained with Syto 60 (red). INH was used as positive control and H2O was used as negative control.

7. DISCUSSION & PERSPECTIVES/DISCUSSION & PROSPECTS

The development of the world's first antibiotic, penicillin, in 1943, was one of the most important advances in the history of medical science. Antibiotics have revolutionised modern medicine by making previously incurable infections treatable and protecting patients undergoing common surgical procedures from bacterial infections. As a result, countless lives have been saved over the last 70 years.

However, despite the development of modern medicine, tuberculosis (TB) is now the world's most deadly infectious disease and is on the top 10 causes of death worldwide. *Mycobacterium tuberculosis*, the main etiological agent of TB, is one of the most successful human pathogens in history Mtb is an ancient and obligate human pathogen. Contrarily to zoonotic infections, human infection and disease is essential for the evolutionary survival of Mtb, which, therefore, evolved complex strategies for persistence in the human host. Instead of classical virulence factors such as toxins and enzymes to poison host cells and to compete with other bacteria, Mtb initiates infection in the lower lung, which harbours few commensals and thus, can deal just with its host. Mtb is able to survive and multiply inside host macrophages by subverting the effector functions of these important innate immune cells and can persist in the host in a dormant state for decades prior to progressing to active disease.

TB is a complex and dynamic disease that includes a wide spectrum of pathologies. To treat this disease, multiple antituberculosis drugs with unpleasant side-effects must be taken for long periods, which discourage patients' adherence to treatment. Currently, the co-infection with human immunodeficiency virus (HIV) and the emergence of multidrug-resistant (MDR) and extensively drug-resistant (XDR) infections have further complicated TB treatment. Therefore, it is crucial to find faster, less harmful and more-efficient alternative therapies for both drug-susceptible TB (DS-TB) and drug-resistant TB (DR-TB), in order to improve the quality of life of TB patients and to tackle the TB burden.

Despite the increasing awareness to this threat, no major new types of antibiotics have been developed by pharmaceutical companies, over the last 50 years, mainly due to the high cost and time consumed to develop new drugs and low profitability expected. In recent years, only bedaquiline and delamanid have been conditionally approved. Even if only limited clinical trial data exist for these drugs and adverse events have been noted, they are already used when no other treatment options exist.

Combining the decline in efficacy of known active agents with the difficulty associated with the development of new drugs, we have reached a point where a "postantibiotic" era is a real possibility.

Considering this, it is worthwhile to investigate the development of new regimens using old TB drugs and to repurpose drugs used to treat other infectious diseases, for antituberculosis treatment. Many of these drugs present limited antituberculosis activity due to their solubility characteristics, low intracellular permeability, instability, low bioavailability, fast metabolism and excretion, etc. The use of nanoparticles (NPs) to reformulate existing antibiotic drugs may be a solution to overpass the unfavourable characteristics of some old drugs and enhance their efficacy, thus speeding up the entrance of alternatives to the market.

In this thesis, different antibiotics reformulated using NPs were evaluated for their ability to inhibit extracellular and/or intracellular Mtb replication.

The strain used in this thesis, Mtb H37Rv, is the most studied strain of Mtb in research laboratories and is the standard for TB studies. The drawbacks of using a virulent Mtb strain include the danger of manipulating a biosafety level three (BSL3) pathogen, which demands specific research facilities and extensive personal training, and the low growth rates of these strains, which slows down investigation progress. Among alternative models, the most popular are the attenuated *M. bovis* BCG and the avirulent *M. smegmatis* and *M. marinum* (Shiloh and Champion 2010). *M. bovis* belongs to the MTBC, has similar growth rates compared to Mtb, yet is a biosafety level two (BSL2) pathogen. *M. smegmatis* exhibits much faster growth rates, but it is evolutionary different and lacks pathogenicity. *M. marinum* is a BSL2 pathogen with relatively fast growth and close evolutionary proximity to the MTBC and TB-like pathogenesis in ectotherms (Cosma, Swaim et al. 2006). Nevertheless, *M. marinum* has a lower temperature for optimal growth than Mtb. Therefore, Mtb is the most phenotypically accurate choice.

Antimycobacterial activity in axenic liquid cultures, here called extracellular activity, is a crucial characteristic that is frequently used in antitubercular drug discovery. Colony Forming Units (CFU) enumeration on specialized mycobacterial agar medium continues to be the "gold standard" for evaluating the effectiveness of antituberculosis compounds. However, this technic is laborious, involves long incubation periods (3 to 4 weeks) and is

prone to contamination. Several alternative *in vitro* assays are currently available for the quantification of bacteria replication. Among them is the resazurin reduction assay, the measurement of ATP levels using the BacTitre-Glo™ microbial cell viability assay, the measurement of oxygen consumption using the BD BACTEC™ or the MGIT™ and the spectrophotometric measurement of optical density (OD) (Blanco-Ruano, Roberts et al. 2015). However, none of these methodologies is suitable for assessing the drug activity inside macrophages. In contrast, reporter strains that express either a fluorescent protein or a luciferase can be used for drug testing both in extracellular and intracellular assays.

Here, Mtb H37Rv strain constitutively expressing the green fluorescent protein (H37Rv-GFP) was used as a reporter for the replication assays. The amount of bacteria was quantified by acquisition of the GFP-fluorescence signal on a multimode reader for the extracellular assay.

Despite the relevance of extracellular antimycobacterial activity, successful chemotherapy against Mtb must also eradicate the bacterium within the context of its host cell, a key subpopulation of bacteria that are less readily eliminated by therapy. However, several drugs with high extracellular activity show insignificant intracellular activity.

The reasons for this include low drug concentration achieved inside the phagosome where the bacteria reside, due to low membrane permeability, host metabolism and/or activities of molecular pumps (Hartkoorn, Chandler et al. 2007). Moreover, the host environment may have impact on drug action. During infection, the host cell imposes multiple pressures on intracellular *M. tuberculosis*, such as acidic stress, restricted nutrient availability, microbicidal peptides, and toxic reactive nitrogen and oxygen species (Warner and Mizrahi 2007; Liu, Tan et al. 2016). Thus intracellular survival requires metabolic and physiological adaptations relative to extracellular growth. Transcriptome analyses revealed that *M. tuberculosis*'s response inside macrophages differs from that observed in standard broth culture, suggesting that, inside phagosome, *M. tuberculosis* switches its carbon source from glucose and glycerol to fatty acids, activate DNA and cell envelope repair and induce the production of secreted siderophores to facilitate the acquisition of iron, among other adaptations (Schnappinger, Ehrt et al. 2003). Host-derived stresses negatively affect *M. tuberculosis* drug susceptibility (Liu, Tan et al. 2016) (Aljayyoussi, Jenkins et al. 2017).

Thus, to improve the efficiency of drug discovery process and to reduce identification of false positive hits that have poor translation to *in vivo* models, it is important to test also the efficacy of the drugs against intracellular *M. tuberculosis,* an environment that better *reflects* the common niche of this pathogen.

Usually, studies of *M. tuberculosis* growth within host cells *in vitro* rely on time consuming and labor intensive techniques, such as determination of CFUs or RLU titration, that are complicated by the long incubation periods required for forming a colony on solid media from a single *M. tuberculosis* (Delorme, Song et al. 2015). The readouts from these methods measure the intracellular bacterial load but don't rigorously control the host cell viability *in vitro*. However, some infection conditions, such as the multiplicity of infection (MOI), can lead to intense replication resulting in severe host cell death. This condition results in low intracellular CFU counts and leads to the wrong conclusion of low *M. tuberculosis* replication, whereas in reality, much replication occurred.

Here, a phenotypic cell-based assay, developed in 2009 by Priscille Brodin's team (Christophe, Jackson et al. 2009; Brodin, Poquet et al. 2010; Queval, Song et al. 2014), was used for the screening of drugs and NPs that interfere with the replication of *M. tuberculosis* within macrophages. Advantageously, with this method it is also possible to follow the accumulation of NPs inside cells, (see chapter III) and to obtain additional information, such as the cytotoxicity of the studied compounds, (see chapter I, II and IV). However, discrimination between bacteriostatic and bactericidal effects can only be achieved by determining CFUs.

Christophe *et al.* have demonstrated that the total pixels of green areas per field correspond to the quantity of the recombinant strain *M. tuberculosis* H37Rv-GFP and showed a linear relationship between the total green area and the actual number of bacteria by CFU counting (Christophe, Jackson et al. 2009). More recently, the team reported the same validation study showing the correlation between mycobacteria fluorescence and the CFUs (Queval, Song et al. 2016).

Similar high content imaging methods have now been successfully implemented in several laboratories for drug discovery purpose and there is more and more consensus that this technique is as reliable as CFUs for the quantification of bacterial load (Stanley,

Barczak et al. 2014; Sorrentino, Gonzalez del Rio et al. 2015; Manning, Ovechkina et al. 2017).

Nonetheless, it is still often that, during manuscript revision, reviewers ask validation of this phenotypic assay and to compare the results obtained with different parameters. The correlation between bacterial area versus bacterial area × fluorescence pixel intensity versus volume was done using a reference compound (rifampicin) (**Supplementary Figure 3)**. The IC50 values were very similar and in the range of the values previously published for the three imaging measurements. Therefore, we consider that bacteria area is a valid parameter for the quantification of *M. tuberculosis* and determination of the IC50 of an antimycobacterial compound. Moreover, the comparison between the results obtained with the image-based method with the classical CFU counting method resulted in similar dose-response curves, confirming once again the reliability of this image-based method. Additionally, it was also demonstrated here that the 1 hour amikacin treatment step, present in the protocol since 2009, does not impact on the extracellular bacteria viability (**Supplementary Figure 4)**. We concluded that the critical point to eliminate the extracellular bacteria is the repetition of washings while the 1 h incubation with amikacin could be avoided.

The present thesis showed that NPs may play different roles in different antituberculosis therapies.

In the chapter I of this thesis, biodegradable polymeric β-cyclodextrins (pCD), PLA and PLGA were studied as pulmonary delivery carrier for Ethionamide (ETH), an old second line antituberculosis drug, simultaneously with its booster BDM41906, here called Booster. The aim was to circumvent the bottlenecks related to the limited water solubility of the booster, the strong ETH tendency to crystalize and the difficulty to find a common solvent for ETH and Booster compatible with pulmonary administration.

In vitro studies on *M. tuberculosis* H37Rv in axenic conditions as well as in infected RAW 264.7 macrophages showed that the treatment with the developed NPs containing [ETH:Booster] pair was as potent as that with free [ETH:Booster] pair solubilized in organic solvents. Among tested formulations, the pCD NPs displayed the best physicochemical characteristics and were thus selected for *in vivo* studies.

The mouse model was chosen in this study because it is currently the most commonly used (Cooper, 2014) and considered by almost every scientist in the TB field as an essential model for investigating novel TB drug regimen prior to clinical trials.

No major modification of the composition of lungs immune cell subsets was observed after administration of the vehicle (water) or NPs formulations to uninfected mice. These results suggest that the endotracheal administration of particles in the lungs using a Microsprayer device does not cause any major irritation effects.

Then developed pCD NPs loaded with [ETH:Booster] were administered via the endotracheal route to the lungs of *M. tuberculosis*-infected mice. The formulation was able to reduce the mycobacterial load using subtherapeutic doses in a short course of infection model. The recommended dosage of ETH is 15 - 20 mg/kg daily. Here a lower dose was tested, 10 mg/kg, 3 times per week, due to limitations on: a) frequency of administrations using a Microsprayer that mice can tolerate; b) encapsulation efficiency. However, even using a lower dose and lower frequency, a significant decrease of the pulmonary bacterial load was observed as compared to untreated mice, using just 3 doses of the [ETH:Booster] pair within a 1 week administration. Increasing the treatment to 6 doses within 2 weeks resulted in an impressive decreased by 3-logs in the mycobacterial load in the lungs, as compared to the non-treated animals. In the future, it would therefore be interesting to investigate whether a longer course of treatment could lead to a greater efficacy. It would also be interesting to investigate the effect of this treatment in a mouse model of chronic TB.

Noteworthy, when the formulation containing [ETH:Booster] was given by oral gavage using the same regimen the mycobacterial load in the lungs was similar as the one from non-treated controls, clearly demonstrating the benefit of using the pulmonary route for ETH and Booster co-loaded nanoparticles delivery.

Our observations are in line with previous studies that reported that pulmonary administration increase the drug concentration in the lungs, with less systemic side effects and less administrations required to reach the same antituberculosis effect as oral route (Pandey, Sharma et al. 2003; Ahmad, Sharma et al. 2005; Bivas-Benita, Ottenhoff et al. 2005). By oral route, the stability and bioavailability of the compounds may be decreased due to numerous gastrointestinal limitations such as acidic pH in the stomach, high degree of enzymatic degradation, reduced passage of the intestinal barrier, hepatic

first-pass effect and transit time between the place of administration and the place of infection (Morales, Fathe et al. 2017).

Because the present approach drastically reduces the dose and the frequency of the treatment, it has the potential to diminish the systemic side effects of ETH. In humans, the instrument used for pulmonary delivery is usually self-administered without stress or pain, thus the effect of this formulation may potentially be greater because the administrations frequency can be higher.

In the future, this strategy could be used as a supplement to the standard treatment to contain the *M. tuberculosis* pulmonary manifestations and to prevent its dissemination. Therefore, this study opens new therapeutic perspectives for TB patients.

Moreover, given the fact that the current regimen for TB consists in a cocktail of four drugs, the approach used here could be extended to the encapsulation of more than two drugs, simplifying the treatment, decreasing the systemic side effects and increasing the patients' compliance to limit drug misuse.

In the chapter II, several types of Nanoporous Silica Particles (NSP), with different pore size, surface area and geometry, were studied as oral delivery carrier for Clofazimine (CLZ). CLZ is an extremely lipophilic antibiotic used today in a combination therapy for the treatment of leprosy. Due to its poor solubility in the gastro intestinal tract (GIT), the intestinal adsorption of CLZ is low, resulting in unfavourable oral pharmacokinetics. Nonetheless the promising *in vitro* data against MDR/XDR strains make CLZ a candidate for the treatment of human TB (Cholo, Steel et al. 2012).

Encapsulation in the NSP particles stabilized the amorphous form of CLZ, which resulted in a significant increase in the dissolution rate in simulated gastric fluid and a dramatic increase in the intestinal permeation in comparison to the CLZ as free drug. These results provided strong support that, *in vivo,* CLZ oral bioavailability can be enhanced by encapsulation in NSP.

When incubated with *M. tuberculosis* infected macrophages, CLZ released from NSP formulation in aqueous conditions matched the same antibacterial effect obtained from a fully dissolved concentration in organic solvent.

The concentration of CLZ dissolved from NSP, after permeation through Caco-2 monolayer was up to an order of magnitude higher than the MIC, indicating that the formulation of CLZ in NSP can lead to an enhanced permeation of CLZ to achieve the MIC after a single dose. Moreover, the NSP carrier, already generally recognized as safe for oral administration, was demonstrated here to show no cell cytotoxicity.

Encapsulation of CLZ in NSP presents a new and simple refurbishment of a well-known marketed antibiotic with bioavailability issues, for a new indication in the treatment of antibiotic-resistant *M. tuberculosis* infections.

In the chapter III of this thesis, vancomycin (VCM), the gold-standard treatment of methicillin-resistant *staphylococcus aureus* (MRSA), was encapsulated in PLGA engineered polymeric NPs. Though already demonstrated active against extracellular *M. tuberculosis*, this antibiotic has long been restricted to the treatment of critically ill patients, with drug-resistant infectious agents, particularly MRSA, in the tentative to avoid the development of resistant strains to this important antibiotic. Nowadays, the new options available for the treatment of MRSA and the lack of effective alternatives for the treatment of TB, makes the repurpose of VCM a valid strategy.

Some factors affect VCM clinical activity, namely its poor intracellular penetration (Lamer, de Beco et al. 1993; Kollef 2007; Lehar, Pillow et al. 2015) . In contrast, phagocyte cells are well known for their ability to internalize drug-loaded NPs (Pelgrift and Friedman 2013; Ladaviere and Gref 2015; Costa-Gouveia, Ainsa et al. 2017; Costa-Gouveia, Pancani et al. 2017). Thus, encapsulation in PLGA NPs acted as “Trojan” horses to deliver VCM inside the macrophages.

Interestingly, the release of the drug could be controlled and was found to be pH-dependent, with almost no release at neutral pH and fast delivery at pH 5.5. This behaviour is particularly interesting for the selective release of VCM in acidic compartments, such as when the NPs are taken up in endosomes with a slightly acidic pH (around 4.8) (Tan and Russell 2015).

Encapsulation of VCM in the developed PLGA NPs resulted in 5 times activity improvement compared to free VCM against intracellular *M. tuberculosis* growth. This supports the fact that VCM has low membrane permeability as previously reported (Lamer, de Beco et al. 1993; Cruciani, Gatti et al. 1996; Kollef 2007; Lehar, Pillow et al.

2015). It can be hypothesized that the observed intracellular antibacterial activity was driven by VCM released in the cells, from internalized NPs located in low pH endosomes, rather than the drug released prior to macrophage uptake. Indeed, NPs were readily taken up by infected cells and after 24 h incubation, practically all the macrophages contained NPs.

Besides more efficient, this “smart” drug delivery of VCM might also be less toxic than conventional drug delivery.

Over 100 years have passed since Paul Ehrlich postulate of creating “magic bullets” for a highly targeted medical treatment. Today, nanotechnology brings this idea closer to reality.

Another trend in the field of antituberculosis drugs is the search for synergic drug combinations, which can increase treatment efficacy and decrease drug dosage to avoid toxicity. Further studies will be dedicated to the encapsulations of synergic VCM/drug combinations to further improve the capacity of the NPs to kill intracellular Mtb. The combination of VCM and mycobacterial lipids synthesis inhibitors are among potential synergic combinations (Soetaert, Rens et al. 2015; Rens, Laval et al. 2016).

In the chapter IV, the intrinsic antimycobacterial activity of different compounds and NPs was investigated. From 89 Cyclodextrins (CDs) tested, 5 were active against extracellular activity, with IC50 between 10 and 70 µM. However, no significant activity was observed against intracellular Mtb and all the compounds presented cytotoxicity. One silver NP was also tested against extracellular Mtb without success.

Moreover, NanoMOFs called our attention because of the observed induction of the autophagy marker LC3 expression, without signs of cytotoxicity, upon 16 h incubation with NanoMOFs. This led us to investigate if NanoMOFs could induce autophagy in host cells and if that plays a beneficial role against Mtb intracellular replication. However, after the 5 days of incubation necessary for the intracellular Mtb replication assay, NanoMOFs presented a cytotoxic effect. These results show the importance of varying incubation times while accessing toxicity of any NP.

Altogether, this thesis show that NPs engineered with distinctive compositions, sizes, shapes, and surface chemistries to enable a wide range of biological applications. In particular, the use of NPs as drug carriers may: i) allow alternative administration routes

that wouldn’t otherwise be possible; ii) change the physicochemical properties of the drugs, such as solubility, stability and consequent bioavailability and iii) allow controlled release of drugs under specific environmental conditions.

Though much work is still needed to fully understand the long-term effects of human exposure to NPs, the information that we already possess suggest that NPs may open new perspectives in antituberculosis therapy and improve the life quality of the patients.

8. REFERENCES

. "http://www.smartglobalhealth.org/issues/entry/infectious-diseases." from http://www.smartglobalhealth.org/issues/entry/infectious-diseases.

(2016). WHO Treatment Guidelines for Drug-Resistant Tuberculosis, 2016 Update. Geneva.

Abed, N. and P. Couvreur (2014). "Nanocarriers for antibiotics: a promising solution to treat intracellular bacterial infections." Int J Antimicrob Agents **43**(6): 485-496.

Achtman, M. (2012). "Insights from genomic comparisons of genetically monomorphic bacterial pathogens." Philos Trans R Soc Lond B Biol Sci **367**(1590): 860-867.

Agency, U. S. E. P. (September 1991). "Pesticides And Toxic Substances (7508W)." (738-F-9 1-107).

Ahmad, Z., S. Sharma, et al. (2005). "Inhalable alginate nanoparticles as antitubercular drug carriers against experimental tuberculosis." Int J Antimicrob Agents **26**(4): 298-303.

Aljayyoussi, G., V. A. Jenkins, et al. (2017). "Pharmacokinetic-Pharmacodynamic modelling of intracellular Mycobacterium tuberculosis growth and kill rates is predictive of clinical treatment duration." Sci Rep **7**(1): 502.

Andries, K., P. Verhasselt, et al. (2005). "A diarylquinoline drug active on the ATP synthase of Mycobacterium tuberculosis." Science **307**(5707): 223-227.

Ankrum, J. A., O. R. Miranda, et al. (2014). "Engineering cells with intracellular agent–loaded microparticles to control cell phenotype." Nat. Protocols **9**(2): 233-245.

Antoine, D., Y. Pellequer, et al. (2015). "Biorelevant media resistant co-culture model mimicking permeability of human intestine." Int J Pharm **481**(1-2): 27-36.

Atluri, R., N. Hedin, et al. (2009). "Nonsurfactant supramolecular synthesis of ordered mesoporous silica." J Am Chem Soc **131**(9): 3189-3191.

Barberis, I., N. L. Bragazzi, et al. (2017). "The history of tuberculosis: from the first historical records to the isolation of Koch's bacillus." J Prev Med Hyg **58**(1): E9-E12.

Baulard, A. R., J. C. Betts, et al. (2000). "Activation of the pro-drug ethionamide is regulated in mycobacteria." J Biol Chem **275**(36): 28326-28331.

Bawa, R. (2013). FDA and Nanotech: Baby Steps Lead to Regulatory Uncertainty. Bio-Nanotechnology, Blackwell Publishing Ltd.**:** 720-732.

Behar, S. M., C. J. Martin, et al. (2011). "Apoptosis is an innate defense function of macrophages against Mycobacterium tuberculosis." Mucosal Immunol **4**(3): 279-287.

Bergstrom, C. A., R. Holm, et al. (2014). "Early pharmaceutical profiling to predict oral drug absorption: current status and unmet needs." Eur J Pharm Sci **57**: 173-199.

Bilati, U., E. Allémann, et al. (2005). "Nanoprecipitation versus emulsion-based techniques for the encapsulation of proteins into biodegradable nanoparticles and process-related stability issues." Aaps Pharmscitech **6**(4): E594-E604.

Bivas-Benita, M., T. H. Ottenhoff, et al. (2005). "Pulmonary DNA vaccination: concepts, possibilities and perspectives." J Control Release **107**(1): 1-29.

Bivas-Benita, M., R. Zwier, et al. (2005). "Non-invasive pulmonary aerosol delivery in mice by the endotracheal route." Eur J Pharm Biopharm **61**(3): 214-218.

Blair, J. M., M. A. Webber, et al. (2015). "Molecular mechanisms of antibiotic resistance." Nat Rev Microbiol **13**(1): 42-51.

Blanco-Ruano, D., D. M. Roberts, et al. (2015). "Antimicrobial susceptibility testing for Mycobacterium sp." Methods Mol Biol **1285**: 257-268.

Blondiaux, N., M. Moune, et al. (2017). "Reversion of antibiotic resistance in Mycobacterium tuberculosis by spiroisoxazoline SMARt-420." Science **355**(6330): 1206-1211.

Boshoff, H. I. and C. E. Barry (2006). "Is the mycobacterial cell wall a hopeless drug target for latent tuberculosis?" Drug Discovery Today: Disease Mechanisms **3**(2): 237-245.

Brauner, A., O. Fridman, et al. (2016). "Distinguishing between resistance, tolerance and persistence to antibiotic treatment." Nat Rev Microbiol **14**(5): 320-330.

Brites, D. and S. Gagneux (2015). "Co-evolution of Mycobacterium tuberculosis and Homo sapiens." Immunol Rev **264**(1): 6-24.

Brodin, P., Y. Poquet, et al. (2010). "High content phenotypic cell-based visual screen identifies Mycobacterium tuberculosis acyltrehalose-containing glycolipids involved in phagosome remodeling." PLoS Pathog **6**(9): e1001100.

Brown, L., J. M. Wolf, et al. (2015). "Through the wall: extracellular vesicles in Gram-positive bacteria, mycobacteria and fungi." Nat Rev Microbiol **13**(10): 620-630.

Browne, S. G., D. J. Harman, et al. (1981). "Clofazimine (Lamprene, B663) in the treatment of lepromatous leprosy in the United Kingdom. A 12 year review of 31 cases, 1966-1978." Int J Lepr Other Mycobact Dis **49**(2): 167-176.

Cambier, C. J., S. Falkow, et al. (2014). "Host evasion and exploitation schemes of Mycobacterium tuberculosis." Cell **159**(7): 1497-1509.

Carmona, J., A. Cruz, et al. (2013). "Differential TLR recognition of Mycobacterium tuberculosis strains modulates innate immune responses with an impact on the outcome of infection." PloS Pathogens.

Caulfield, A. J. and N. L. Wengenack "Diagnosis of active tuberculosis disease: From microscopy to molecular techniques." Journal of Clinical Tuberculosis and Other Mycobacterial Diseases **4**: 33-43.

Chakraborty, S. and K. Y. Rhee (2015). "Tuberculosis Drug Development: History and Evolution of the Mechanism-Based Paradigm." Cold Spring Harb Perspect Med **5**(8): a021147.

Chen, X., H. Hashizume, et al. (2017). "Delamanid Kills Dormant Mycobacteria In Vitro and in a Guinea Pig Model of Tuberculosis." Antimicrob Agents Chemother **61**(6).

Cholo, M. C., H. C. Steel, et al. (2012). "Clofazimine: current status and future prospects." J Antimicrob Chemother **67**(2): 290-298.

Christophe, T., M. Jackson, et al. (2009). "High content screening identifies decaprenyl-phosphoribose 2' epimerase as a target for intracellular antimycobacterial inhibitors." PLoS Pathog **5**(10): e1000645.

Chua, K. and B. P. Howden (2009). "Treating Gram-positive infections: vancomycin update and the whys, wherefores and evidence base for continuous infusion of anti-Gram-positive antibiotics." Curr Opin Infect Dis **22**(6): 525-534.

Collins, C. H. and A. H. Uttley (1988). "In-vitro activity of seventeen antimicrobial compounds against seven species of mycobacteria." J Antimicrob Chemother **22**(6): 857-861.

Comas, I., J. Chakravartti, et al. (2010). "Human T cell epitopes of Mycobacterium tuberculosis are evolutionarily hyperconserved." Nat Genet **42**(6): 498-503.

Comas, I., M. Coscolla, et al. (2013). "Out-of-Africa migration and Neolithic coexpansion of Mycobacterium tuberculosis with modern humans." Nat Genet **45**(10): 1176-1182.

Cook, G. M., M. Berney, et al. (2009). "Physiology of mycobacteria." Adv Microb Physiol **55**: 81-182, 318-189.

Cooper, A. M. (2009). "Cell-mediated immune responses in tuberculosis." Annu Rev Immunol **27**: 393-422.

Cooper, A. M. (2014). "Mouse model of tuberculosis." Cold Spring Harb Perspect Med **5**(2): a018556.

Cosma, C. L., D. R. Sherman, et al. (2003). "The secret lives of the pathogenic mycobacteria." Annu Rev Microbiol **57**: 641-676.

Cosma, C. L., L. E. Swaim, et al. (2006). "Zebrafish and frog models of Mycobacterium marinum infection." Curr Protoc Microbiol **Chapter 10**: Unit 10B 12.

Costa-Gouveia, J., J. A. Ainsa, et al. (2017). "How can nanoparticles contribute to antituberculosis therapy?" Drug Discov Today **22**(3): 600-607.

Costa-Gouveia, J., E. Pancani, et al. (2017). "Combination therapy for tuberculosis treatment: pulmonary administration of ethionamide and booster co-loaded nanoparticles." Sci Rep **7**(1): 5390.

Costa, A., M. Pinheiro, et al. (2016). "The formulation of nanomedicines for treating tuberculosis." Adv Drug Deliv Rev **102**: 102-115.

Cox, H. and N. Ford (2012). "Linezolid for the treatment of complicated drug-resistant tuberculosis: a systematic review and meta-analysis." Int J Tuberc Lung Dis **16**(4): 447-454.

Crist, R. M., J. H. Grossman, et al. (2013). "Common pitfalls in nanotechnology: lessons learned from NCI's Nanotechnology Characterization Laboratory." Integrative Biology **5**(1): 66-73.

Crist, R. M., J. H. Grossman, et al. (2013). "Common pitfalls in nanotechnology: lessons learned from NCI's Nanotechnology Characterization Laboratory." Integr Biol (Camb) **5**(1): 66-73.

Cruciani, M., G. Gatti, et al. (1996). "Penetration of vancomycin into human lung tissue." J Antimicrob Chemother **38**(5): 865-869.

Daniel, T. M. (2006). "The history of tuberculosis." Respir Med **100**(11): 1862-1870.

Davis, J. M. and L. Ramakrishnan (2009). "The role of the granuloma in expansion and dissemination of early tuberculous infection." Cell **136**(1): 37-49.

de Jong, B. C., P. C. Hill, et al. (2008). "Progression to active tuberculosis, but not transmission, varies by Mycobacterium tuberculosis lineage in The Gambia." J Infect Dis **198**(7): 1037-1043.

DeBarber, A. E., K. Mdluli, et al. (2000). "Ethionamide activation and sensitivity in multidrug-resistant Mycobacterium tuberculosis." Proc Natl Acad Sci U S A **97**(17): 9677-9682.

Delogu, G., M. Sali, et al. (2013). "The biology of mycobacterium tuberculosis infection." Mediterr J Hematol Infect Dis **5**(1): e2013070.

Delorme, V., O. R. Song, et al. (2015). "Testing chemical and genetic Modulators in Mycobacterium tuberculosis infected cells using phenotypic assays." Methods Mol Biol **1285**: 387-411.

Dheda, K., C. E. Barry, 3rd, et al. (2016). "Tuberculosis." Lancet **387**(10024): 1211-1226.

Dheda, K., T. Gumbo, et al. (2017). "The epidemiology, pathogenesis, transmission, diagnosis, and management of multidrug-resistant, extensively drug-resistant, and incurable tuberculosis." Lancet Respir Med.

Diacon, A. H., L. van der Merwe, et al. (2016). "beta-Lactams against Tuberculosis--New Trick for an Old Dog?" N Engl J Med **375**(4): 393-394.

Dinesh, N., S. Sharma, et al. (2013). "Involvement of efflux pumps in the resistance to peptidoglycan synthesis inhibitors in Mycobacterium tuberculosis." Antimicrob Agents Chemother **57**(4): 1941-1943.

Dobbs, T. E. and R. M. Webb (2017). "Chemotherapy of Tuberculosis." Microbiol Spectr **5**(2).

Donoghue, H. D. (2017). "Insights gained from ancient biomolecules into past and present tuberculosis-a personal perspective." Int J Infect Dis **56**: 176-180.

Dorman, S. (2015). "Advances in the diagnosis of tuberculosis: current status and future prospects." Int J Tuberc Lung Dis **19**(5): 504-516.

drugbank. from http://www.drugbank.ca/drugs/DB00845.

Engohang-Ndong, J., D. Baillat, et al. (2004). "EthR, a repressor of the TetR/CamR family implicated in ethionamide resistance in mycobacteria, octamerizes cooperatively on its operator." Mol Microbiol **51**(1): 175-188.

Ernst, J. D. (2012). "The immunological life cycle of tuberculosis." Nat Rev Immunol **12**(8): 581-591.

FDA. (05/25/2017). "The Drug Development Process." Retrieved July 2017, from https://www.fda.gov/ForPatients/Approvals/Drugs/ucm405622.htm.

Flipo, M., M. Desroses, et al. (2011). "Ethionamide boosters. 2. Combining bioisosteric replacement and structure-based drug design to solve pharmacokinetic issues in a series of potent 1, 2, 4-oxadiazole EthR inhibitors." Journal of medicinal chemistry **55**(1): 68-83.

Flipo, M., M. Desroses, et al. (2012). "Ethionamide boosters. 2. Combining bioisosteric replacement and structure-based drug design to solve pharmacokinetic issues in a series of potent 1,2,4-oxadiazole EthR inhibitors." J Med Chem **55**(1): 68-83.

Florence, A. T. (2005). "Nanoparticle uptake by the oral route: Fulfilling its potential?" Drug Discov Today Technol **2**(1): 75-81.

Fogel, N. (2015). "Tuberculosis: a disease without boundaries." Tuberculosis (Edinb) **95**(5): 527-531.

Fossati, L., R. Dechaume, et al. (2008). "Use of simulated intestinal fluid for Caco-2 permeability assay of lipophilic drugs." International Journal of Pharmaceutics **360**(1–2): 148-155.

Gagneux, S., K. DeRiemer, et al. (2006). "Variable host-pathogen compatibility in Mycobacterium tuberculosis." Proc Natl Acad Sci U S A **103**(8): 2869-2873.

Galagan, J. E. (2014). "Genomic insights into tuberculosis." Nat Rev Genet **15**(5): 307-320.

Gaumet, M., R. Gurny, et al. (2009). "Localization and quantification of biodegradable particles in an intestinal cell model: the influence of particle size." Eur J Pharm Sci **36**(4-5): 465-473.

Gideon, H. P. and J. L. Flynn (2011). "Latent tuberculosis: what the host "sees"?" Immunol Res **50**(2-3): 202-212.

Gillespie, S. H., A. M. Crook, et al. (2014). "Four-month moxifloxacin-based regimens for drug-sensitive tuberculosis." N Engl J Med **371**(17): 1577-1587.

Gonzalo, X. and F. Drobniewski (2013). "Is there a place for beta-lactams in the treatment of multidrug-resistant/extensively drug-resistant tuberculosis? Synergy between meropenem and amoxicillin/clavulanate." J Antimicrob Chemother **68**(2): 366-369.

Gref, R., C. Amiel, et al. (2006). "New self-assembled nanogels based on host-guest interactions: characterization and drug loading." J Control Release **111**(3): 316-324.

Grosset, J. H., S. Tyagi, et al. (2013). "Assessment of clofazimine activity in a second-line regimen for tuberculosis in mice." Am J Respir Crit Care Med **188**(5): 608-612.

Group, T. A. (2017). "An activist's guide to Tuberculosis Diagnostic Tools." Retrieved June 2017, from http://www.treatmentactiongroup.org/sites/default/files/TB%20Diagnostics%20Guide.pdf.

Guirado, E. and L. S. Schlesinger (2013). "Modeling the Mycobacterium tuberculosis Granuloma - the Critical Battlefield in Host Immunity and Disease." Front Immunol **4**: 98.

Gupta, A., A. Misra, et al. (2016). "Targeted pulmonary delivery of inducers of host macrophage autophagy as a potential host-directed chemotherapy of tuberculosis." Adv Drug Deliv Rev **102**: 10-20.

Gutierrez, M. G., S. S. Master, et al. (2004). "Autophagy is a defense mechanism inhibiting BCG and Mycobacterium tuberculosis survival in infected macrophages." Cell **119**(6): 753-766.

Hartkoorn, R. C., B. Chandler, et al. (2007). "Differential drug susceptibility of intracellular and extracellular tuberculosis, and the impact of P-glycoprotein." Tuberculosis (Edinb) **87**(3): 248-255.

Hershkovitz, I., H. D. Donoghue, et al. (2008). "Detection and molecular characterization of 9,000-year-old Mycobacterium tuberculosis from a Neolithic settlement in the Eastern Mediterranean." PLoS One **3**(10): e3426.

Hoagland, D. T., J. Liu, et al. (2016). "New agents for the treatment of drug-resistant Mycobacterium tuberculosis." Adv Drug Deliv Rev **102**: 55-72.

Hofman, S., M. M. Segers, et al. (2016). "Emerging drugs and alternative possibilities in the treatment of tuberculosis." Expert Opin Emerg Drugs **21**(1): 103-116.

Hu, C. M., R. H. Fang, et al. (2015). "Nanoparticle biointerfacing by platelet membrane cloaking." Nature **526**(7571): 118-121.

Hugonnet, J. E. and J. S. Blanchard (2007). "Irreversible inhibition of the Mycobacterium tuberculosis beta-lactamase by clavulanate." Biochemistry **46**(43): 11998-12004.

Hugonnet, J. E., L. W. Tremblay, et al. (2009). "Meropenem-clavulanate is effective against extensively drug-resistant Mycobacterium tuberculosis." Science **323**(5918): 1215-1218.

Huh, A. J. and Y. J. Kwon (2011). ""Nanoantibiotics": a new paradigm for treating infectious diseases using nanomaterials in the antibiotics resistant era." J Control Release **156**(2): 128-145.

Ingels, F., S. Deferme, et al. (2002). "Simulated intestinal fluid as transport medium in the Caco-2 cell culture model." Int J Pharm **232**(1-2): 183-192.

Jankute, M., J. A. Cox, et al. (2015). "Assembly of the Mycobacterial Cell Wall." Annu Rev Microbiol **69**: 405-423.

Janulionis, E., C. Sofer, et al. (2004). "Lack of Activity of Orally Administered Clofazimine against Intracellular Mycobacterium tuberculosis in Whole-Blood Culture." Antimicrobial Agents and Chemotherapy **48**(8): 3133-3135.

Janulionis, E., C. Sofer, et al. (2004). "Lack of activity of orally administered clofazimine against intracellular Mycobacterium tuberculosis in whole-blood culture." Antimicrob Agents Chemother **48**(8): 3133-3135.

Jindani, A., T. S. Harrison, et al. (2014). "High-dose rifapentine with moxifloxacin for pulmonary tuberculosis." N Engl J Med **371**(17): 1599-1608.

Kamholz, S. L. (1996). "Resurgence of tuberculosis: the perspective a dozen years later." J Assoc Acad Minor Phys **7**(3): 83-86.

Kaniga, K., D. M. Cirillo, et al. (2016). "A Multi-Laboratory, Multi-Country Study to Determine Minimal Inhibitory Concentration Quality Control Ranges for PhenotypicDrug-Susceptibility Testing of Selected First-Line Anti-TB Drugs, Second-Line Injectables, Fluoroquinolones, Clofazimine and Linezolid." J Clin Microbiol.

Kerantzas, C. A. and W. R. Jacobs, Jr. (2017). "Origins of Combination Therapy for Tuberculosis: Lessons for Future Antimicrobial Development and Application." MBio **8**(2).

Kester, J. C. and S. M. Fortune (2014). "Persisters and beyond: mechanisms of phenotypic drug resistance and drug tolerance in bacteria." Crit Rev Biochem Mol Biol **49**(2): 91-101.

Keswani, R. K., J. Baik, et al. (2015). "Chemical Analysis of Drug Biocrystals: A Role for Counterion Transport Pathways in Intracellular Drug Disposition." Mol Pharm **12**(7): 2528-2536.

Kieser, K. J. and E. J. Rubin (2014). "How sisters grow apart: mycobacterial growth and division." Nat Rev Microbiol **12**(8): 550-562.

Kjellman, T., X. Xia, et al. (2014). "Influence of microporosity in SBA-15 on the release properties of anticancer drug dasatinib." Journal of Materials Chemistry B **2**(32): 5265-5271.

Kleinnijenhuis, J., M. Oosting, et al. (2011). "Innate immune recognition of Mycobacterium tuberculosis." Clin Dev Immunol **2011**: 405310.

Kollef, M. H. (2007). "Limitations of vancomycin in the management of resistant staphylococcal infections." Clin Infect Dis **45 Suppl 3**: S191-195.

Kumar, G., S. Malhotra, et al. (2011). "In vitro physicochemical characterization and short term in vivo tolerability study of ethionamide loaded PLGA nanoparticles: potentially effective agent for multidrug resistant tuberculosis." J Microencapsul **28**(8): 717-728.

Laborde, J., C. Deraeve, et al. (2016). "Ethionamide biomimetic activation and an unprecedented mechanism for its conversion into active and non-active metabolites." Org Biomol Chem **14**(37): 8848-8858.

Ladaviere, C. and R. Gref (2015). "Toward an optimized treatment of intracellular bacterial infections: input of nanoparticulate drug delivery systems." Nanomedicine (Lond) **10**(19): 3033-3055.

Lakhtakia, R. (2014). "The Legacy of Robert Koch: Surmise, search, substantiate." Sultan Qaboos Univ Med J **14**(1): e37-41.

Lam, A., R. Prabhu, et al. (2017). "Role of apoptosis and autophagy in tuberculosis." Am J Physiol Lung Cell Mol Physiol **313**(2): L218-L229.

Lamer, C., V. de Beco, et al. (1993). "Analysis of vancomycin entry into pulmonary lining fluid by bronchoalveolar lavage in critically ill patients." Antimicrob Agents Chemother **37**(2): 281-286.

Lechartier, B. and S. T. Cole (2015). "Mode of Action of Clofazimine and Combination Therapy with Benzothiazinones against Mycobacterium tuberculosis." Antimicrob Agents Chemother **59**(8): 4457-4463.

Lee, M., J. Lee, et al. (2012). "Linezolid for treatment of chronic extensively drug-resistant tuberculosis." N Engl J Med **367**(16): 1508-1518.

Lehar, S. M., T. Pillow, et al. (2015). "Novel antibody-antibiotic conjugate eliminates intracellular S. aureus." Nature **527**(7578): 323-328.

Lenaerts, A., C. E. Barry, 3rd, et al. (2015). "Heterogeneity in tuberculosis pathology, microenvironments and therapeutic responses." Immunol Rev **264**(1): 288-307.

Lévy-Bruhl D, P. M., Antoine D, Bessette D. . (2007). "Recent changes in tuberculosis control and BCG vaccination policy in France " Retrieved July 2017, from http://www.eurosurveillance.org/ViewArticle.aspx?ArticleId=3268.

Lienhardt, C., P. Glaziou, et al. (2012). "Global tuberculosis control: lessons learnt and future prospects." Nat Rev Microbiol **10**(6): 407-416.

Lin, P. L. and J. L. Flynn (2010). "Understanding latent tuberculosis: a moving target." J Immunol **185**(1): 15-22.

Lind, M. L., J. Jacobsen, et al. (2007). "Development of simulated intestinal fluids containing nutrients as transport media in the Caco-2 cell culture model: assessment of cell viability, monolayer integrity and transport of a poorly aqueous soluble drug and a substrate of efflux mechanisms." Eur J Pharm Sci **32**(4-5): 261-270.

Liu, Y., S. Tan, et al. (2016). "Immune activation of the host cell induces drug tolerance in Mycobacterium tuberculosis both in vitro and in vivo." J Exp Med **213**(5): 809-825.

Luca, S. and T. Mihaescu (2013). "History of BCG Vaccine." Maedica (Buchar) **8**(1): 53-58.

Ma, T., B. C. Shang, et al. (2011). "Nano-hydroxyapatite/chitosan/konjac glucomannan scaffolds loaded with cationic liposomal vancomycin: preparation, in vitro release and activity against Staphylococcus aureus biofilms." J Biomater Sci Polym Ed **22**(12): 1669-1681.

Ma, Z., C. Lienhardt, et al. (2010). "Global tuberculosis drug development pipeline: the need and the reality." Lancet **375**(9731): 2100-2109.

Mamaeva, V., C. Sahlgren, et al. (2013). "Mesoporous silica nanoparticles in medicine--recent advances." Adv Drug Deliv Rev **65**(5): 689-702.

Manjunatha, U. H., H. Boshoff, et al. (2006). "Identification of a nitroimidazo-oxazine-specific protein involved in PA-824 resistance in Mycobacterium tuberculosis." Proc Natl Acad Sci U S A **103**(2): 431-436.

Manning, A. J., Y. Ovechkina, et al. (2017). "A high content microscopy assay to determine drug activity against intracellular Mycobacterium tuberculosis." Methods **127**: 3-11.

Markopoulos, C., F. Thoenen, et al. (2014). "Biorelevant media for transport experiments in the Caco-2 model to evaluate drug absorption in the fasted and the fed state and their usefulness." Eur J Pharm Biopharm **86**(3): 438-448.

Mathys, V., R. Wintjens, et al. (2009). "Molecular genetics of para-aminosalicylic acid resistance in clinical isolates and spontaneous mutants of Mycobacterium tuberculosis." Antimicrob Agents Chemother **53**(5): 2100-2109.

Matsumoto, M., H. Hashizume, et al. (2006). "OPC-67683, a nitro-dihydro-imidazooxazole derivative with promising action against tuberculosis in vitro and in mice." PLoS Med **3**(11): e466.

Merle, C. S., K. Fielding, et al. (2014). "A four-month gatifloxacin-containing regimen for treating tuberculosis." N Engl J Med **371**(17): 1588-1598.

Morales, J. O., K. R. Fathe, et al. (2017). "Challenges and Future Prospects for the Delivery of Biologics: Oral Mucosal, Pulmonary, and Transdermal Routes." AAPS J **19**(3): 652-668.

Mukherjee, J. S., M. L. Rich, et al. (2004). "Programmes and principles in treatment of multidrug-resistant tuberculosis." Lancet **363**(9407): 474-481.

Murray, J. F., D. E. Schraufnagel, et al. (2015). "Treatment of Tuberculosis. A Historical Perspective." Ann Am Thorac Soc **12**(12): 1749-1759.

Nasiri, M. J., M. Haeili, et al. (2017). "New Insights in to the Intrinsic and Acquired Drug Resistance Mechanisms in Mycobacteria." Front Microbiol **8**: 681.

Nathan, C. (2004). "Antibiotics at the crossroads." Nature **431**(7011): 899-902.

Nathan , C. and O. Cars (2014). "Antibiotic Resistance — Problems, Progress, and Prospects." New England Journal of Medicine **371**(19): 1761-1763.

Nuermberger, E. L., T. Yoshimatsu, et al. (2004). "Moxifloxacin-containing regimen greatly reduces time to culture conversion in murine tuberculosis." Am J Respir Crit Care Med **169**(3): 421-426.

O'Connor, R., J. F. O'Sullivan, et al. (1995). "The pharmacology, metabolism, and chemistry of clofazimine." Drug Metab Rev **27**(4): 591-614.

O'Garra, A., P. S. Redford, et al. (2013). "The immune response in tuberculosis." Annu Rev Immunol **31**: 475-527.

Othman, M., K. Bouchemal, et al. (2011). "A comprehensive study of the spontaneous formation of nanoassemblies in water by a "lock-and-key" interaction between two associative polymers." J Colloid Interface Sci **354**(2): 517-527.

Ottenhoff, T. H. and S. H. Kaufmann (2012). "Vaccines against tuberculosis: where are we and where do we need to go?" PLoS Pathog **8**(5): e1002607.

Pai, M., M. A. Behr, et al. (2016). "Tuberculosis." Nat Rev Dis Primers **2**: 16076.

Pai, M., C. M. Denkinger, et al. (2014). "Gamma interferon release assays for detection of Mycobacterium tuberculosis infection." Clin Microbiol Rev **27**(1): 3-20.

Pandey, R., A. Sharma, et al. (2003). "Poly (DL-lactide-co-glycolide) nanoparticle-based inhalable sustained drug delivery system for experimental tuberculosis." J Antimicrob Chemother **52**(6): 981-986.

Paramasivan, C. N., S. Sulochana, et al. (2005). "Bactericidal action of gatifloxacin, rifampin, and isoniazid on logarithmic- and stationary-phase cultures of Mycobacterium tuberculosis." Antimicrob Agents Chemother **49**(2): 627-631.

Paulson, T. (2013). "Epidemiology: A mortal foe." Nature **502**(7470): S2-S3.

Pei, Y., M. F. Mohamed, et al. (2017). "Particle engineering for intracellular delivery of vancomycin to methicillin-resistant Staphylococcus aureus (MRSA)-infected macrophages." J Control Release.

Pelgrift, R. Y. and A. J. Friedman (2013). "Nanotechnology as a therapeutic tool to combat microbial resistance." Adv Drug Deliv Rev **65**(13-14): 1803-1815.

Petersen, E., M. Maeurer, et al. (2017). "World TB Day 2017: Advances, Challenges and Opportunities in the "End-TB" Era." Int J Infect Dis **56**: 1-5.

Porter, C. J., N. L. Trevaskis, et al. (2007). "Lipids and lipid-based formulations: optimizing the oral delivery of lipophilic drugs." Nat Rev Drug Discov **6**(3): 231-248.

Portevin, D., S. Gagneux, et al. (2011). "Human macrophage responses to clinical isolates from the Mycobacterium tuberculosis complex discriminate between ancient and modern lineages." PLoS Pathog **7**(3): e1001307.

Prasad, B. R. and S. Lele (1994). "Stabilization of the amorphous phase inside carbon nanotubes: Solidification in a constrained geometry." Philosophical Magazine Letters **70**(6): 357-361.

Provvedi, R., F. Boldrin, et al. (2009). "Global transcriptional response to vancomycin in Mycobacterium tuberculosis." Microbiology **155**(Pt 4): 1093-1102.

Pumerantz, A., K. Muppidi, et al. (2011). "Preparation of liposomal vancomycin and intracellular killing of meticillin-resistant Staphylococcus aureus (MRSA)." Int J Antimicrob Agents **37**(2): 140-144.

Pym, A. S., P. Brodin, et al. (2002). "Loss of RD1 contributed to the attenuation of the live tuberculosis vaccines Mycobacterium bovis BCG and Mycobacterium microti." Mol Microbiol **46**(3): 709-717.

Queval, C. J., O. R. Song, et al. (2016). "STAT3 Represses Nitric Oxide Synthesis in Human Macrophages upon Mycobacterium tuberculosis Infection." Sci Rep **6**: 29297.

Queval, C. J., O. R. Song, et al. (2014). "A microscopic phenotypic assay for the quantification of intracellular mycobacteria adapted for high-throughput/high-content screening." J Vis Exp(83): e51114.

Ramakrishnan, L. (2012). "Revisiting the role of the granuloma in tuberculosis." Nat Rev Immunol **12**(5): 352-366.

Ramaswamy, S. V., A. G. Amin, et al. (2000). "Molecular genetic analysis of nucleotide polymorphisms associated with ethambutol resistance in human isolates of Mycobacterium tuberculosis." Antimicrob Agents Chemother **44**(2): 326-336.

Reddy, V. M., G. Nadadhur, et al. (1996). "Antituberculosis activities of clofazimine and its new analogs B4154 and B4157." Antimicrob Agents Chemother **40**(3): 633-636.

Reddy, V. M., J. F. O'Sullivan, et al. (1999). "Antimycobacterial activities of riminophenazines." J Antimicrob Chemother **43**(5): 615-623.

Rengarajan, G. T., D. Enke, et al. (2008). "Stabilization of the amorphous state of pharmaceuticals in nanopores." Journal of Materials Chemistry **18**(22): 2537-2539.

Rens, C., F. Laval, et al. (2016). "Effects of Lipid-Lowering Drugs on Vancomycin Susceptibility of Mycobacteria." Antimicrob Agents Chemother **60**(10): 6193-6199.

Riva, M. A. (2014). "From milk to rifampicin and back again: history of failures and successes in the treatment for tuberculosis." J Antibiot (Tokyo) **67**(9): 661-665.

Rubin, E. J. (2017). "Reviving a Drug for Tuberculosis?" N Engl J Med **376**(23): 2292-2294.

Ryu, Y. J. (2015). "Diagnosis of pulmonary tuberculosis: recent advances and diagnostic algorithms." Tuberc Respir Dis (Seoul) **78**(2): 64-71.

Said, G. Z. (2014). "Orthopaedics in the dawn of civilisation, practices in ancient Egypt." Int Orthop **38**(4): 905-909.

Salgame, P., C. Geadas, et al. (2015). "Latent tuberculosis infection--Revisiting and revising concepts." Tuberculosis (Edinb) **95**(4): 373-384.

Sande, L., M. Sanchez, et al. (2012). "Liposomal encapsulation of vancomycin improves killing of methicillin-resistant Staphylococcus aureus in a murine infection model." J Antimicrob Chemother **67**(9): 2191-2194.

Schito, M., D. Hanna, et al. (2017). "Tuberculosis eradication versus control." Int J Infect Dis **56**: 10-13.

Schnappinger, D., S. Ehrt, et al. (2003). "Transcriptional Adaptation of Mycobacterium tuberculosis within Macrophages: Insights into the Phagosomal Environment." J Exp Med **198**(5): 693-704.

Schoonmaker, M. K., W. R. Bishai, et al. (2014). "Nonclassical transpeptidases of Mycobacterium tuberculosis alter cell size, morphology, the cytosolic matrix, protein localization, virulence, and resistance to beta-lactams." J Bacteriol **196**(7): 1394-1402.

Scorpio, A. and Y. Zhang (1996). "Mutations in pncA, a gene encoding pyrazinamidase/nicotinamidase, cause resistance to the antituberculous drug pyrazinamide in tubercle bacillus." Nat Med **2**(6): 662-667.

Semiramoth, N., C. Di Meo, et al. (2012). "Self-assembled squalenoylated penicillin bioconjugates: an original approach for the treatment of intracellular infections." ACS Nano **6**(5): 3820-3831.

Serajuddin, A. T. (1999). "Solid dispersion of poorly water-soluble drugs: early promises, subsequent problems, and recent breakthroughs." J Pharm Sci **88**(10): 1058-1066.

Shiloh, M. U. and P. A. Champion (2010). "To catch a killer. What can mycobacterial models teach us about Mycobacterium tuberculosis pathogenesis?" Curr Opin Microbiol **13**(1): 86-92.

Simeone, R., A. Bobard, et al. (2012). "Phagosomal rupture by Mycobacterium tuberculosis results in toxicity and host cell death." PLoS Pathog **8**(2): e1002507.

Simeone, R., F. Sayes, et al. (2015). "Cytosolic access of Mycobacterium tuberculosis: critical impact of phagosomal acidification control and demonstration of occurrence in vivo." PLoS Pathog **11**(2): e1004650.

Singh, R., U. Manjunatha, et al. (2008). "PA-824 kills nonreplicating Mycobacterium tuberculosis by intracellular NO release." Science **322**(5906): 1392-1395.

Soetaert, K., C. Rens, et al. (2015). "Increased Vancomycin Susceptibility in Mycobacteria: a New Approach To Identify Synergistic Activity against Multidrug-Resistant Mycobacteria." Antimicrob Agents Chemother **59**(8): 5057-5060.

Song, H., Y. Ahmad Nor, et al. (2016). "Silica Nanopollens Enhance Adhesion for Long-Term Bacterial Inhibition." J Am Chem Soc **138**(20): 6455-6462.

Sorrentino, F., R. Gonzalez del Rio, et al. (2015). "Development of an Intracellular Screen for New Compounds Able To Inhibit Mycobacterium tuberculosis Growth in Human Macrophages." Antimicrob Agents Chemother **60**(1): 640-645.

Sotgiu, G., R. Centis, et al. (2012). "Efficacy, safety and tolerability of linezolid containing regimens in treating MDR-TB and XDR-TB: systematic review and meta-analysis." Eur Respir J **40**(6): 1430-1442.

Sotgiu, G., L. D'Ambrosio, et al. (2016). "Carbapenems to Treat Multidrug and Extensively Drug-Resistant Tuberculosis: A Systematic Review." Int J Mol Sci **17**(3): 373.

Sotgiu, G., G. Sulis, et al. (2017). "Tuberculosis-a World Health Organization Perspective." Microbiol Spectr **5**(1).

Sreevatsan, S., X. Pan, et al. (1997). "Restricted structural gene polymorphism in the Mycobacterium tuberculosis complex indicates evolutionarily recent global dissemination." Proc Natl Acad Sci U S A **94**(18): 9869-9874.

Stanley, S. A., A. K. Barczak, et al. (2014). "Identification of host-targeted small molecules that restrict intracellular Mycobacterium tuberculosis growth." PLoS Pathog **10**(2): e1003946.

Stover, C. K., P. Warrener, et al. (2000). "A small-molecule nitroimidazopyran drug candidate for the treatment of tuberculosis." Nature **405**(6789): 962-966.

Surewaard, B. G., J. F. Deniset, et al. (2016). "Identification and treatment of the Staphylococcus aureus reservoir in vivo." J Exp Med **213**(7): 1141-1151.

T.A.G. (2016). 2016 Report on Tuberculosis Research Funding Trends, 2005–2015: No Time to Lose.

Tan, S. and D. G. Russell (2015). "Trans-species communication in the Mycobacterium tuberculosis-infected macrophage." Immunol Rev **264**(1): 233-248.

Tang, S., L. Yao, et al. (2015). "Efficacy, safety and tolerability of linezolid for the treatment of XDR-TB: a study in China." Eur Respir J **45**(1): 161-170.

Tiberi, S., A. C. Carvalho, et al. (2017). "The cursed duet today: Tuberculosis and HIV-coinfection." Presse Med **46**(2 Pt 2): e23-e39.

Tyagi, S., N. C. Ammerman, et al. (2015). "Clofazimine shortens the duration of the first-line treatment regimen for experimental chemotherapy of tuberculosis." Proc Natl Acad Sci U S A **112**(3): 869-874.

UNAIDS (2017). Financing the Response to HIV in Low- and Middle-Income Countries in 2016.

Van Deun, A., A. K. Maug, et al. (2010). "Short, highly effective, and inexpensive standardized treatment of multidrug-resistant tuberculosis." Am J Respir Crit Care Med **182**(5): 684-692.

van Ingen, J., S. Simons, et al. (2010). "Comparative study on genotypic and phenotypic second-line drug resistance testing of Mycobacterium tuberculosis complex isolates." J Clin Microbiol **48**(8): 2749-2753.

Van Rensburg, C. E., R. Anderson, et al. (1997). "Riminophenazine compounds: pharmacology and anti-neoplastic potential." Crit Rev Oncol Hematol **25**(1): 55-67.

VanderVen, B. C., L. Huang, et al. (2016). "The Minimal Unit of Infection: Mycobacterium tuberculosis in the Macrophage." Microbiol Spectr **4**(6).

Vannelli, T. A., A. Dykman, et al. (2002). "The antituberculosis drug ethionamide is activated by a flavoprotein monooxygenase." J Biol Chem **277**(15): 12824-12829.

Vasanthakumari (2009). Practical Microbiology, B.I. Publications Pvt. Limited.

Veziris, N., C. Truffot, et al. (2011). "Activity of carbapenems combined with clavulanate against murine tuberculosis." Antimicrob Agents Chemother **55**(6): 2597-2600.

W.H.O (2016). "World Malaria Report 2016."

W.H.O. (2014). Definitions and reporting framework for tuberculosis – 2013 revision (updated December 2014)

W.H.O. (2016). Global tuberculosis report 2016.

Wang, J., Y. Wang, et al. (2016). "Rational Design of Multifunctional Dendritic Mesoporous Silica Nanoparticles to Load Curcumin and Enhance Efficacy for Breast Cancer Therapy." ACS Appl Mater Interfaces **8**(40): 26511-26523.

Warner, D. F. and V. Mizrahi (2007). "The survival kit of Mycobacterium tuberculosis." Nat Med **13**(3): 282-284.

WHO. (March 2017). "Tuberculosis-Fact sheet." Retrieved June 2016, from http://www.who.int/mediacentre/factsheets/fs104/en/.

WHO. (2015). "Fact sheet N°194 - Antimicrobial resistance." from http://www.who.int/entity/mediacentre/factsheets/fs194/en/index.html.

WHO. (2017). "The End TB Strategy." Retrieved 16/06/2017, 2017, from http://www.who.int/tb/strategy/end-tb/en/.

Willand, N., B. Dirie, et al. (2009). "Synthetic EthR inhibitors boost antituberculous activity of ethionamide." Nat Med **15**(5): 537-544.

Wolf, A. J., L. Desvignes, et al. (2008). "Initiation of the adaptive immune response to Mycobacterium tuberculosis depends on antigen production in the local lymph node, not the lungs." J Exp Med **205**(1): 105-115.

Wolf, A. J., B. Linas, et al. (2007). "Mycobacterium tuberculosis infects dendritic cells with high frequency and impairs their function in vivo." J Immunol **179**(4): 2509-2519.

Xia, X., K. Pethe, et al. (2014). "Encapsulation of Anti-Tuberculosis Drugs within Mesoporous Silica and Intracellular Antibacterial Activities." Nanomaterials **4**(3): 813.

Xia, X., K. Pethe, et al. (2014). "Encapsulation of Anti-Tuberculosis Drugs within Mesoporous Silica and Intracellular Antibacterial Activities." Nanomaterials (Basel) **4**(3): 813-826.

Xia, X., C. Zhou, et al. (2012). "In vivo enhancement in bioavailability of atazanavir in the presence of proton-pump inhibitors using mesoporous materials." ChemMedChem **7**(1): 43-48.

Xu, J., Y. Lu, et al. (2012). "In vitro and in vivo activity of clofazimine against Mycobacterium tuberculosis persisters." Int J Tuberc Lung Dis **16**(8): 1119-1125.

Yawalkar, S. J. and W. Vischer (1979). "Lamprene (clofazimine) in leprosy. Basic information." Lepr Rev **50**(2): 135-144.

Z Ahmad, N. M., J Grosset (2011). History of drug discovery: early evaluation studies and lessons learnt from them. In Antituberculosis chemotherapy. Antituberculosis Chemotherapy, S. Karger AG. **10:** 2-9.

Zhang, M., C. Sala, et al. (2012). "Streptomycin-starved Mycobacterium tuberculosis 18b, a drug discovery tool for latent tuberculosis." Antimicrob Agents Chemother **56**(11): 5782-5789.

Zhang, Y., B. Heym, et al. (1992). "The catalase-peroxidase gene and isoniazid resistance of Mycobacterium tuberculosis." Nature **358**(6387): 591-593.

Zhang, Y. and D. Mitchison (2003). "The curious characteristics of pyrazinamide: a review." Int J Tuberc Lung Dis **7**(1): 6-21.

Zheng, J., E. J. Rubin, et al. (2013). "para-Aminosalicylic acid is a prodrug targeting dihydrofolate reductase in Mycobacterium tuberculosis." J Biol Chem **288**(32): 23447-23456.

Zink, A., C. J. Haas, et al. (2001). "Molecular analysis of skeletal tuberculosis in an ancient Egyptian population." J Med Microbiol **50**(4): 355-366.

Zuckerman, J. E., I. Gritli, et al. (2014). "Correlating animal and human phase Ia/Ib clinical data with CALAA-01, a targeted, polymer-based nanoparticle containing siRNA." Proc Natl Acad Sci U S A **111**(31): 11449-11454.

Zumla, A., P. Mwaba, et al. (2009). "Reflections on the white plague." Lancet Infect Dis **9**(3): 197-202.

9. SUPPLEMENTARY INFORMATION / INFORMATION SUPPLÉMENTAIRE

9.1. Bacterial quantification methods: 2D versus 3D

Using the same intracellular assay described before, we incubated RAW 264.7 cells infected with *M. tuberculosis* H37Rv-GFP with different concentrations of rifampicin, during 5 days at 37°C, 5 % CO_2. Macrophages were then stained and images from 4 fields at the center of each well were recorded by an automated fluorescent ultra-high-throughput microscope Opera (Perkin Elmer). A double laser excitation (488-nm and 640-nm) and dedicated dichroic mirrors were used to record green fluorescence of mycobacteria and red fluorescence of the macrophages on two different cameras, respectively. For the 2D analysis, pictures of the focal plane were recorded and then analysed using Columbus system version 2.5.1 to extract the intracellular bacterial area and the mean fluorescence intensity (**Supplementary Figure 1**).

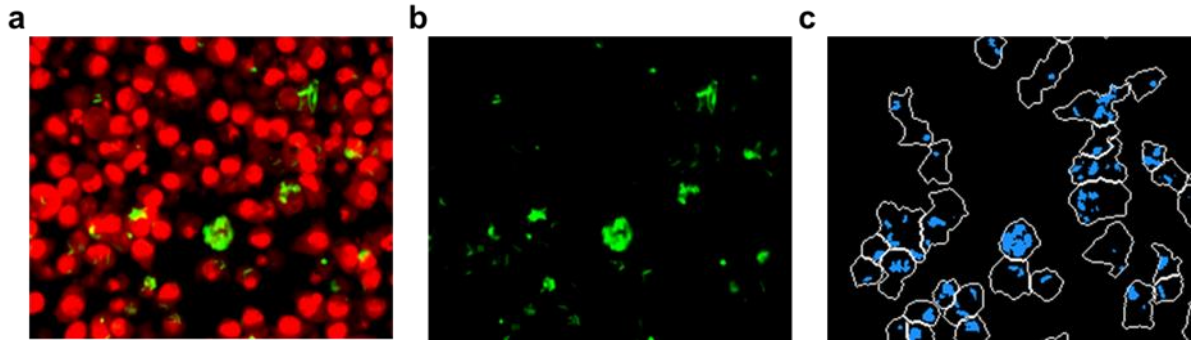

Supplemetary Figure 1 - Image-based analysis of bacterial area and fluorescence intensity performed with the image-analysis software Columbus 2.5.1 (PerkinElmer). (a) Input 2D confocal image: cell nuclei were detected in the red channel and *M. tuberculosis* H37Rv-GFP was detected in the red channel. **(b)** *M. tuberculosis* H37Rv-GFP detected in the green channel. (c) Bacteria area detected is represented in blue.

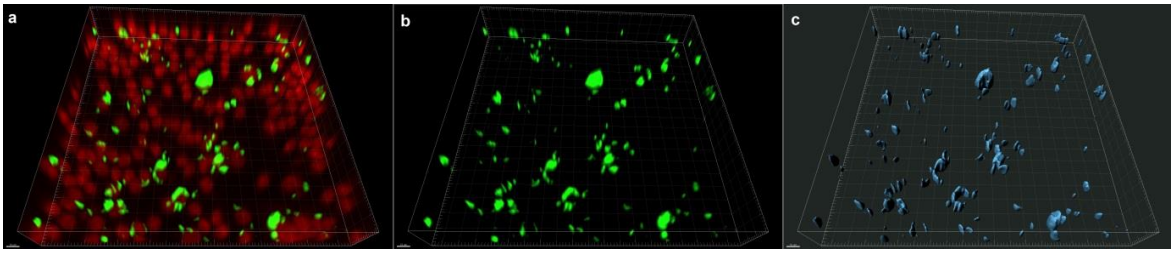

Supplemetary Figure 2 - Image-based analysis of bacterial volume performed with the image-analysis software Imaris. (a) Input 3D confocal image: cell nuclei were detected in the red channel and *M. tuberculosis* H37Rv-GFP was detected in the green channel. (b) *M. tuberculosis* H37Rv-GFP detected in the green channel. **(c)** Bacteria volume detected is represented in blue**.**

For the 3D analysis, pictures of 65 sequential z-stacks interspaced by 0.5 µm were recorded and analysed using the Imaris software. This allowed quantification of the bacterial volume (**Supplementary Figure 2**).

Bacterial area or bacterial area × mean fluorescence intensity or bacterial volume versus the rifampicin concentration (Log10. Scale) was plotted with GraphPad Prism 5.0 software and the IC50 was calculated by nonlinear regression analysis using the equation for a sigmoidal dose-response curve with variable slope (**Supplementary Figure 3**).

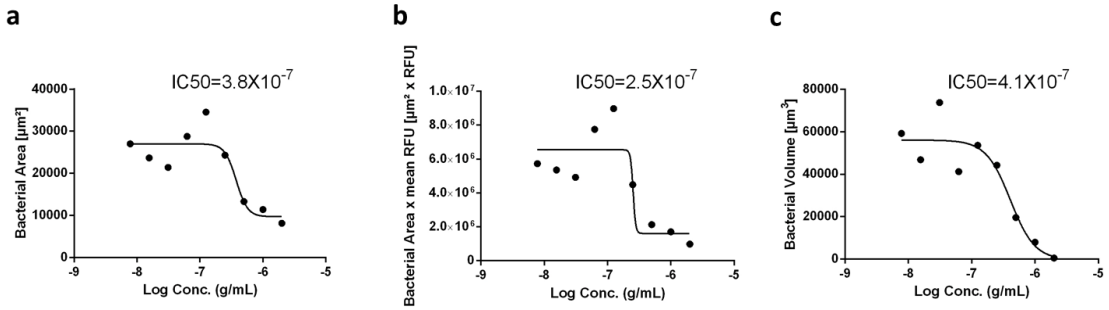

Supplemetary Figure 3 - Comparison of IC50 obtained for a reference compound (rifampicin) by using image-based analysis of 2D and 3D confocal images of RAW 264.7 cells infected with *M. tuberculosis* H37Rv-GFP. (a) Dose-response curve obtained with bacterial area analysis performed on the 2D images. **(b)** Dose-response curve obtained with bacterial area x mean RFU analysis performed on the 2D images. **(c)** Dose-response curve obtained with bacterial volume analysis performed on the 3D images.

The IC50 obtained with the analysis of bacterial area, bacterial area × mean fluorescence intensity and bacterial volume was, respectively, 3.8×10^{-7}, 2.5×10^{-7}, 4.1×10^{-7} g/mL. These IC50 values are very similar and in the range of the values previously published. Therefore, we consider that the three imaging measurements are valid for the quantification of *M. tuberculosis* and determination of the IC50 of an antimycobacterial compound.

It is clear that the 3D-analysis is currently time-consuming due to the limitation of the Imaris software. Indeed the quantification of the bacterial load in the 3D-pictures have to be done field by field, whereas that on the 2D-images can be done on multiple plates, thus for drug discovery purposes we consider that analysis of 2D-images is a better option.

9.2. Amikacin Treatment: Is it necessary?

The combination of judicious centrifugations and amikacin treatment was introduced in the protocol in 2009 due to a reviewer request to allow optimal removal of extracellular bacteria. The correct elimination of extracellular bacteria was confirmed when we subcultured the supernatant of the last wash observing the absence of all mycobacteria that were not internalized during the infection step (Christophe et al., 2010). However, we are fully aware that the amikacin alone is not sufficient for killing the extracellular bacteria. To answer to this question, we incubated a suspension of 2×10^6 bacteria/mL with 50 µg/mL amikacin during 1h in the same conditions as the assay (37°C, 120 rpm) and ten-fold serial dilutions were plated onto 7H11 agar plates supplemented with 10 % OADC. We did not observe any differences in the CFU of treated and non-treated bacteria (**Supplementary Figure 3**).

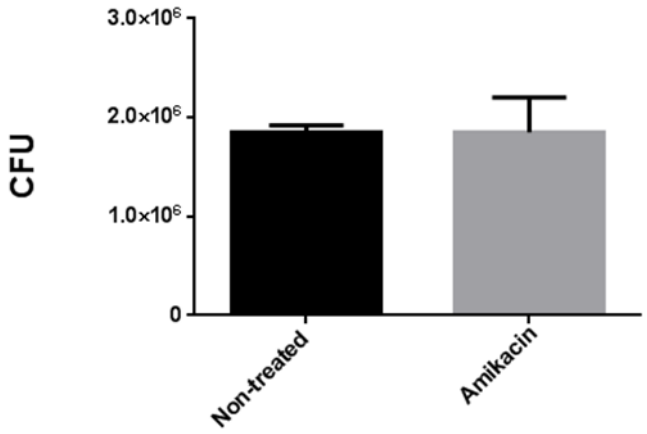

Supplemetary Figure 4 - Effect of 1 h treatment of 2×10^6 H37RV-GFP/mL with 50 µg/mL amikacin.

We conclude that the critical point to eliminate the extracellular bacteria is the repetition of washings, 3 washings in total, and that the 1 h incubation with amikacin could be avoided. Nevertheless, we kept this step in the procedure since it is generally considered as an important step for the standardization of HTS/HCS phenotypic assays related to *M. tuberculosis* infected cells, which was published in Mycobacteria Protocols book (Delorme et al., 2015).